# MODELLING PERINATAL STROKE AND STEM CELL GRAFTING IN A NEONATAL RAT;

## MODELLING AND TREATING PERINATAL STROKE IN AN ANIMAL MODEL

Reem Mohammed A Basuodan

Thesis submitted in partial fulfilment of the requirements of the regulations for the degree of Doctor of Philosophy

Newcastle University

Faculty of Medical Sciences

Institute of Neuroscience

September 2017

# Abstract

Perinatal ischemic stroke (PIS) in humans occurs mostly at full term and is a significant cause of hemiplegic cerebral palsy. A suitable animal model is needed to test early intervention therapies. Firstly, we developed and compared two PIS Models; middle cerebral artery occlusion (MCAO) at the level of the temporal bone, and the injection of reversible vasoconstrictor endothelin-1 (ET-1) into the sensorimotor cortex (SMC), at postnatal day (P) 12. Appropriate sham procedures were performed. Animals underwent behavioural testing (cylinder and grid walking tests) at P35-40 followed by immunohistological examination of the brain for markers of inflammation and hypoxia. We found that MCAO is a poor stroke model in P12 rat pups with minimal involvement of the SMC, a major site of damage in human neonates, however ET-1 models did induce focal ischemia in the SMC. However, no significant behavioural deficits were detected in either model although there was a trend towards a deficit in the ET-1 animals.

In a second study, ET-1 or sham treated animals received a unilateral injection of retrograde tracer into the contralesional cervical spinal cord at P40. There was depletion of corticospinal (CS) neurons in the ipsilesional hemisphere but an increase in labelled CS neurons in the contralesional cortex. An upregulated ipsilateral corticospinal pathway is a feature of human hemiplegic CP again suggesting that ET-1 model is an appropriate model. We found preliminary evidence that this nervous system plasticity could rescue behavioural performance.

Finally, we attempted an intervention therapy to repair the corticospinal tract by grafting human neural stem cells into the SMC of ET-1 lesioned animals. Cells were dispersed in a semi-synthetic extracellular matrix ($1x10^6$ cells per µl) and either cultured in vitro or transplanted in vivo to the lesioned SMC at P14. Rosettes of cells resembling cerebral organoids and expressing human specific NCAM were observed in vivo at the graft site after a month but not in *in vitro* cultures. The organoids comprised a dense cellular layer expressing neural progenitor cell markers arranged around a small lumen surrounded by more loosely packed cells with neurites expressing markers for post-mitotic neurons. Some host cells and blood vessels infiltrated the graft and after three months the organoids had broken down and very few transplanted neurons had integrated with host tissue.

Animal modelling of hemiplegic cerebral palsy continues to present a significant challenge but some progress has been made. The feasibility of using neural stem cells for perinatal brain repair has been tested with unexpected results.

# Acknowledgment

This research would not have been possible without the invaluable support of many people. I would like to acknowledge my main supervisor, Dr. Gavin Clowry, for his inspiration, continuous help, knowledge, patience and constructive comments throughout this work. I would also like to thank my second supervisor, Dr. Anna Basu, for her advice, wise counsel and for being supportive. I am grateful for their enthusiastic approach to solve practical problems that have contributed invaluably throughout my PhD study period.

I would like to express my sincere thanks to my family. My warm and special thanks go to my husband Osama for his love, encouragement and endless support. I am deeply and forever grateful for my parents, Mohammed and Fatimah, who always believed in my ability to be a successful person. Mother, you are gone but your belief in me has made this journey possible. Thank you also to my brothers, sisters, parents-in-law for their continuous love and encouragement throughout my studies. To my precious "little angels", Layan, Rakan, Kareem, and Yasmeen, thank you for giving me love, happiness and joy. Thank you to my dearest son Kareem, who lives with cerebral palsy condition, for inspiring me to explore his condition. I dedicate this work to him and all children who came into this world with cerebral palsy.

My gratitude goes also to the Saudi Arabian Cultural Bureau and the Ministry of Higher Education both of Saudi Arabia for financially supporting my studies and for their cooperation. Many thanks go to all the members in the institute of neuroscience in Newcastle University who supported me. I would like to thank my office colleagues, in particular Dr. Bas and Dr. Caroline, for sharing the good, bad and difficult times with me and for their encouragement and friendship. Also thank you to Dr. Elizabeth for her cooperation and guidance in the stem cell lab. My appreciation also goes to all the many other persons, too numerous to mention individually, who have provided support throughout this study.

# Table of Content

# List of Figures

# List of Tables

# List of Abbreviations

| | |
|---|---|
| β-TUB | Beta-III-Tubulin |
| BBB | Blood-brain barrier |
| BDNF | Brain-derived neurotrophic factor |
| bfSSC | Barrel field somatosensory cortex |
| C | Cervical level |
| CCA | Common carotid artery |
| CH | Contralesional hemisphere |
| CNS | Central nervous system |
| CP | Cortical plate |
| CS | Corticospinal |
| CST | Corticospinal tract |
| D | Dimension |
| DAB | 3,3-Diaminobenzidine |
| DAPI | 4',6-diamidino-2-phenylindole |
| ECM | Extracellular matrix |
| EEG | Electroencephalography |
| ESCs | Embryonic stem cells |
| ET-1 | Endothelin-1 |
| FG | Fluorogold |
| FL | Forelimb |

| | |
|---|---|
| FLF | Forelimb fault |
| GABA | Gamma-aminobutyric acid |
| g | Gram |
| HA | Hyaluronan |
| HIF-1 | Hypoxia-inducible factor-1 |
| hiPSCs | Human induced pluripotent stem cells |
| HL | Hindlimb |
| HLF | Hindlimb fault |
| HRP | Horseradish peroxidase |
| ICC | Immunocytochemistry |
| IHC | Immunohistochemistry |
| IH | Ipsilesional hemisphere |
| kg | Kilogram |
| lSMC | Limb sensorimotor cortex |
| MC | Motor cortex |
| MCA | Middle cerebral artery |
| MCAO | Middle cerebral artery occlusion |
| µg | Microgram |
| µl | Microliter |
| MRI | Magnetic resonance imaging |
| NaCL | Sodium chloride |

| | |
|---|---|
| NCL | Neural cellular layer |
| NGF | Nerve growth factor |
| NPCs | Neuroprogenitor cells |
| NPNF | Non-phosphorylated neurofilaments |
| NSCs | Neural stem cells |
| P | Postnatal age |
| PBS | Phosphate buffered saline |
| PCL | Progenitor cellular layer |
| PCW | Postconceptional weeks |
| PEGDA | Polyethylene (glycol) Diacrylate |
| PFA | Paraformaldehyde |
| PIS | Perinatal ischemic stroke |
| Pmol | Picomole |
| PV | Parvalbumin |
| S2 | Secondary somatosensory cortex |
| SMC | Sensorimotor cortex |
| SSC | Somatosensory cortex |
| SVZ | Subventricular zone |
| T | Thoracic level |
| TMS | Transcranial magnetic stimulation |
| TPBS | Triton phosphate buffered saline |

| | |
|---|---|
| UCB | Umbilical cord blood |
| VZ | Ventricular zone |

# Chapter 1. Introduction

Stroke during the perinatal period of life is a leading cause of cerebral palsy (Kirton et al., 2011) and holds second place in terms of incidence after elderly stroke (Raju et al., 2007). Up to sixty-eight percent (68%) of children who experience perinatal stroke develop cerebral palsy, of whom hemiplegic cerebral palsy occurs in 87% (Golomb et al., 2008). It affects 1/2300 full term neonates and 7/1000 preterm infants (Benders et al., 2008, Schulzke et al., 2005). It is therefore a common condition that causes disability throughout life.

In fact, the perinatal stroke led to hemiplegic cerebral palsy that is progressive in its nature. In cerebral palsy children, there is a progressive loss of corticospinal projections from the affected cortex two years after the stroke resulting in progressive appearance of hemiplegic cerebral palsy sign and symptoms over the first two years of life (Eyre et al., 2007). Thus, perinatal stroke results in a major health condition that requires an effective therapy. Such a therapy, however, remains unavailable.

Although there are no current recommended treatments for PIS (Basu, 2014), there are some experimental approaches such as applying hypothermia at the time of the stroke. Hypothermia decreases the risk of disability in neonates with hypoxic ischemic encephalopathy (Jacobs et al., 2013) and reduces the lesion size by 44% in neonates with ischemic stroke (van der Worp et al., 2007). However, this approach has side effects such as bradycardia and thrombocytopenia. Also it has some limitations: treatment should be administered within around 6 hours after the onset of the stroke and more randomized clinical trials are needed in the acute stage of the ischemic stroke (Jacobs et al., 2013, van der Worp et al., 2007) . Another experimental approach is the systematic administration of Erythropoietin which is a cytokine that contributes to immunomodulation, angiogenesis and cell death inhibition (Xiong et al., 2011). As yet there are insufficient experimental investigations to judge the safety of erythropoietin treatment and its effectiveness in treating stroke (Souvenir et al., 2015).

Experimental models have been developed to mimic human perinatal stroke under specific criteria (Hsu, 1993). Such models vary in terms of the techniques used to develop perinatal stroke and the age of the animal.

In order to test potential therapies, extensive research has been carried out with animal models of adult stroke, but such studies in neonatal animals are far more limited. In this introduction I will describe in more detail the effects of perinatal arterial stroke in humans, how we might model the condition in rodents. Then I will go onto describe the rationale for using stem cell grafts as a therapy for treating perinatal brain injury and how this might be approached in an animal model.

### 1.1 Perinatal arterial ischemic stroke (PIS)

As proposed by participants in the perinatal stroke workshop of the United States National Institutes of Health in 2006, perinatal ischemic stroke is defined as 'a vascular event causing focal interruption of blood supply, occurring between 20 weeks of foetal life through 28th postnatal day (P28), and confirmed by neuroimaging or neuropathology studies,' and it involves either arterial or venous occlusion (Raju et al., 2007). PIS is one of five subcategories of neonatal stroke: PIS, Neonatal arterial ischemic stroke, cerebral sinovenous thrombosis, intracerebral hemorrhage, and periventricular venous infarction (Kirton and Deveber, 2013). Focal ischemia in human neonates has higher incidence than global cerebral ischemia resulting from hypoxia (Lynch, 2009), and PIS occurs mainly at, or close to, full term (Kirton and Deveber, 2013). The arterial injury most involved in PIS, based on diffusion-weighted imaging, is left middle cerebral artery occlusion (MCAO) with focal injury or multi focal injury at cortical and sub-cortical regions, leading to long-term disabilities (Kirton and Deveber, 2013) and limitations in hand use (Golomb et al., 2008).

Clinical diagnosis is usually based on cranial imaging triggered by the presence of seizures and/or encephalopathy during the first few days of life, yet it is not a symptom for all PIS victims' especially preterm infants

The mechanisms underlying neuronal death in PIS is complex. The activation of the apoptotic pathways depends on intrinsic factor, mitochondria, and extrinsic factors, cell death receptor such as caspases, after the neonatal stroke (Fernandez-Lopez et al., 2014). Neuronal apoptosis or caspase-3 activation is a crucial mechanism in focal ischemia occurred after the necrosis in the infarction core and decreases with brain maturation (Hu et al., 2000, Manabat et al., 2003). The Coexistence of these mechanisms resulted in continuum cell death that occurs only in neonatal stroke (Northington et al., 2011). Although microglia activation after neonatal stroke shows harm effect in term of producing inflammatory and toxic mediators, they contribute to

endogenous brain defences in acute stage, reduces infarction size and apoptotic debris removal size (Faustino et al., 2011, Woo et al., 2012).

Permanent MCA occlusion results in severe ischemic injury, as indicated by caspase-3 activity, transient occlusion can produce lower injury severity, depending on occlusion duration with apoptosis (Derugin et al., 2000, Manabat et al., 2003). Apoptosis-like cell death also occurs during the first 24 hours in permanent occlusion models (Wen et al., 2004).

In many children with cerebral palsy, the descending pathways, including the corticospinal tract (CST), is affected (Eyre et al., 2007). Although it has often been proposed that the developing motor system has increased plasticity with which to compensate for these deficits (Choi et al., 2010, Kennard, 1938) there is also abundant evidence that aberrant plasticity leads to the increased and different symptoms seen in cerebral palsy compared to similar lesions in adults (Kolb and Gibb, 2007). The human situation only provides opportunities for observational and non-invasive research, highlighting the need for an animal model. In neonatal stroke models, although rodents do not suffer spasticity or severe locomotor impairment in response to SMC lesions, there is evidence of subtle, CST dependent sensorimotor deficits that can be quantified (Clowry et al., 2014).

It is important to know that differences between human and rodent CST exist (Clowry et al., 2014). One difference is the number of decussating CST fibers. The CST fibers descend from the cortical level of the brain and decussate at the level of the medulla oblongata before descending to the spinal cord (Kuypers, 1981). In rodents, only 2-3% of these descending axons do not decussate, whereas in human and primates, non-crossing fibers make up 13% (Kuypers, 1981, Rouiller et al., 1991). Another difference is the anatomical location of the descending CST in the spinal cord. In human, the CST descends in the white matter laterally whereas in rodent it descends in the dorsal funiculus (Figure 1.1A) (Armand, 1982). Despite these differences there are similarities that make rats a good species to model PIS. For example, in both humans and rodents, the CST projects the full length of the spinal cord (Armand, 1982, Bareyre et al., 2005, Lemon, 2008) whereas in other animals such as sheep the CST fails to project below the upper cervical level (Nieuwenhuys et al., 2014).

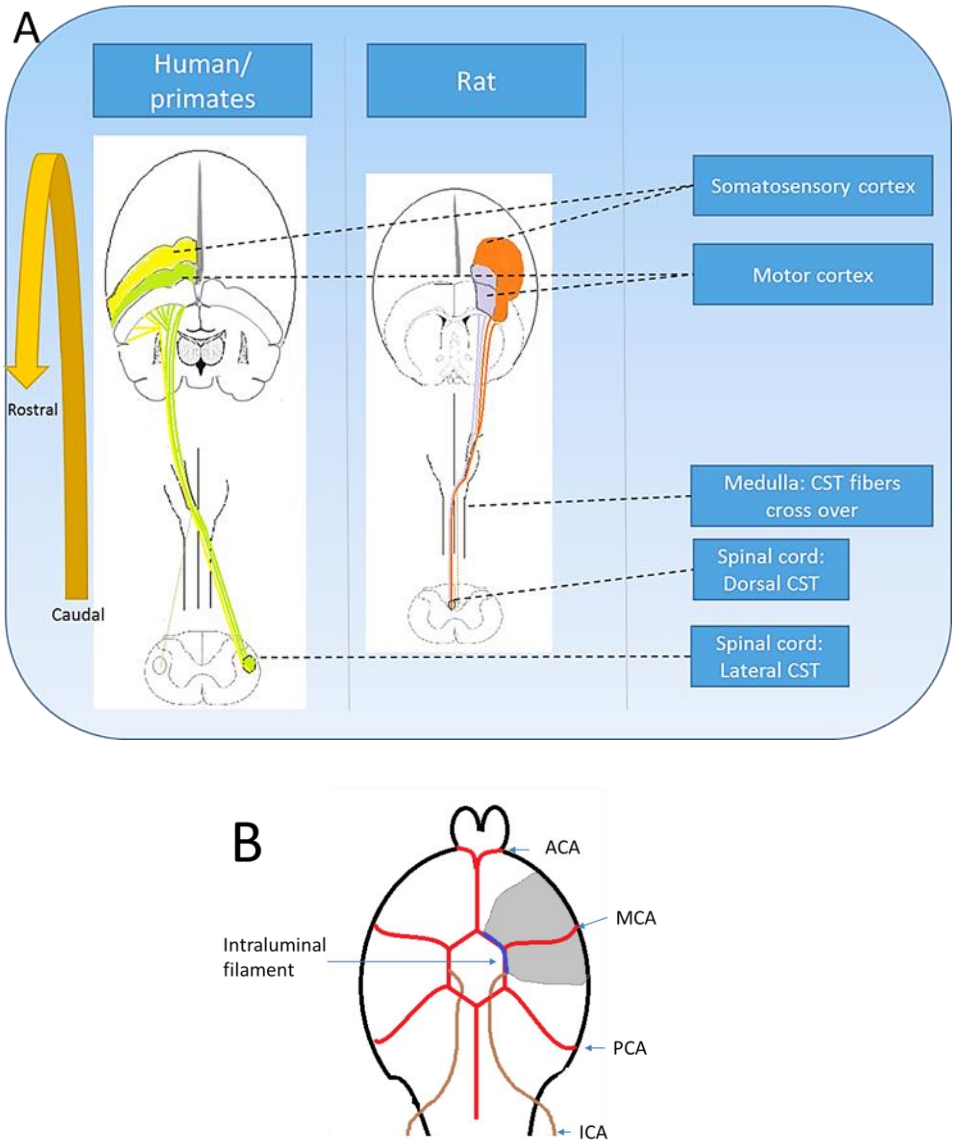


**Figure 0.1 corticospinal tract and cerebral arteries schematic diagrams.**

(A) Simplified illustration of the SMC, motor cortex, and CST pathway in human/primate and rat central nervous system (CNS). (B) View of ventral surface of brain. Intraluminal filament MCAO. The cerebral arteries forming the circle of Willis: Anterior circulation consists of internal carotid artery (ICA), posterior cerebral artery (PCA), middle cerebral artery (MCA), and anterior cerebral artery (ACA).

## 1.2 PIS model via MCAO

In human neonates, PIS events occur mostly in the middle cerebral artery (MCA), while occlusion of the cortical branch occurs in preterm infants (Kirton and Deveber, 2013, Lee et al., 2005b). Focal MCAO models reflect the vascular distribution seen in human neonates that experience ischemic stroke, in contrast to other ischemic-hypoxia models, such as Rice-Vannucci's model (Hagberg et al., 2002, Rice et al., 1981), of unilateral carotid ligation and hypoxia (Ashwal et al., 2007), where the injury distribution extends beyond the MCA territory. Furthermore, ischemic-hypoxia models lead to injuries in both cerebral hemispheres, since these models involve global hypoxia in addition to arterial occlusion (Ashwal et al., 2007). This leads to a massive injured area that includes the striatum, hippocampus, cortex, and white matter (Ashwal et al., 2007, Derugin et al., 2000). As such, the pathophysiological and histological events that occur with focal MCAO infarcts are different from those in a hypoxic-ischemia model (Derugin et al., 2000, Tsuji et al., 2013).

Unilateral infarction in perinatal stroke occurs on the left MCA by (63%) and on the right MCA by (61%) whereas bilateral arterial distribution infarcts occurs only by (7-8%) in both term and preterm infants. The MCA is involved in 91% of PIS term neonates and 81% in preterm infants and only few have another cerebral artery territory (Husson et al., 2010, Lee et al., 2005a).

### *1.2.1 Transient and permanent MCAO*

The heterogeneous nature of PIS in humans leads to two types of studies. Some investigators use permanent focal MCAO in animal models, while others apply transient occlusion that allows for reperfusion of occluded vessels; the decision about which to use is based on the study's purpose. The pathology in both types is similar, as both involve neuronal cell death. Conversely, injury pattern and severity of brain injury differ between the types. Whereas permanent occlusion results in severe ischemic injury, as indicated by caspase-3 activity and Apoptosis-like cell death (Wen et al., 2004) , transient occlusion produces lower injury severity, depending on occlusion duration (Derugin et al., 2000, Manabat et al., 2003).

Two zones of ischemic injury are present after introducing transient MCAO lesion in rat pups. The most severe injury zone, with little possibility of recovery, is at the center of the injured area and involves necrosis. The zone with less severity is at the periphery and involves apoptosis; it is called a penumbra. It is vulnerable but has some scope for recovery in the right

environment (Bouet et al., 2010, Derugin et al., 2000, Manabat et al., 2003, Renolleau et al., 1998)

Studies using transient MCAO (Ashwal et al., 1995, Ashwal et al., 2007, Derugin et al., 1998, Derugin et al., 2000) have claimed that the model reflects neonatal PIS, since reperfusion mimics what happens to neonates when collateral circulation is permitted to the penumbral part of the ischemic lesion (Kahvecİ et al., Liebeskind, 2003). On the other hand, studies not using reperfusion in their MCAO model have argued that either the reperfusion timing or the chance of reperfusion occurrence itself differs among patients (Tsuji et al., 2013). Since the nature of PIS is heterogeneous in neonates, both transient and permanent MCAO methods can be utilized according to the study aim.

Different techniques that utilize either permanent or transient occlusion of the left MCA to produce focal ischemic injury will be reviewed here (Kirton and Deveber, 2013, Lee et al., 2005b). One method is intraluminal MCAO. In this technique, the internal carotid artery is catheterized by monofilament suture to occlude the MCA permanently by retaining the filament, or temporarily by removing the filament at the desired time (Belayev et al., 2010) (Figure 1.1B). This model was developed by Koizumi in 1986 in adult rats (Koizumi, 1986).

Another method is transient MCAO via the carotid artery. This approach was first applied in 1995 on young P14-18 rats (Ashwal et al., 1995), with transient occlusion at the proximal MCA induced by inserting a nylon filament through the external carotid artery into the internal carotid artery, followed by reperfusion. Cytotoxic edema occurred in the ischemic region immediately after occlusion, and severe injury occurred in a similar region after perfusion (Derugin et al., 2000). Regarding infarction volume, one study that used high-field magnetic resonance imaging (MRI) in neonatal animals over a 28-day period demonstrated that transient filament MCAO models induce infarction with maximum volume at days 1-3 (Ashwal et al., 2007). Using this technique for a period of 3 hours yielded infarct volumes of around 38-54% and may resemble human stroke in terms of injury type and necrosis located in the caudate and putamen(Ashwal et al., 1995). When MCAO induced via transient (60-90 min) occlusion of the carotid artery was combined with permanent ligation of the middle cerebral artery, only neocortical injury occurred (Renolleau et al., 1998). Using transient MCAO for 3 hours via external carotid artery yielded infarct volumes around 38 to 54% and it may resemble human stroke; injury type and location necrosis in the caudate and putamen (Ashwal et al., 1995).

Mechanical damage to the blood vessels and hemorrhage during insertion of the nylon filament is one complication that can occur (Ashwal et al., 1995). Also, reliability of the infarction is questionable since it is measured 24 hours after injury; many events can happen within this period of time, such as decreased edema size after 24 hours (Dirnagl, 2010). Using this model for a longer period yields a high mortality rate. Only 21% of rat pups survived for 28 days using this model (Ashwal et al., 2007).

Another study was conducted on 7-day-old rats (Derugin et al., 1998). A suture with a silicone-coated tip was used to cause transient occlusion of the MCA (through insertion into internal carotid artery via the external carotid artery) followed by reperfusion. This technique was developed to decrease the perfusion complications that occurred in (Ashwal et al., 1995) transient MCAO model by measuring insertion length to increase infarction reliability. The model might be avoided by other researchers, however, because of the difficulty of inserting the size 7-0 suture into the tiny external carotid artery of P7 rat pups. Furthermore, vessel sizes vary within similar species at certain ages, leading to incomplete perfusion of the occluded artery when using a fixed-size inserted suture (Belayev et al., 2010, Li et al., 1999).

In both Ashwal *et al*. (1995) and Renolleau et al. (1998), perfusion complications may occur due to the skills needed to perform the procedure. The time required to perform such a surgery results in issues with temperature control, which is important for reducing the variability of the lesion size. In addition, direct damage to the vascular endothelium occurs. The mortality rate may reach 7% (Belayev et al., 2010, Derugin et al., 2000).

### *1.2.2 Transient MCAO by transient common carotid artery (CCA) ligation and permanent MCA ligation*

After Ashwal *et al*. (1995) developed their transient focal ischemia model in rats aged between P14 and P18, Renolleau et al. (1998) claimed to have overcome the difficulty of applying Ashawl's model on P7 rats by developing another model for transient focal ischemia. The model involves a permanent electroligation of the left MCA at its distal part, combined with transient CCA occlusion (Renolleau et al., 1998). Rennollau et al. (1998) occluded both arteries because they found that permanent ligation of only the MCA resulted in no ischemic lesion.

The resulting infarction volume is less than that from intraluminal MCAO via the carotid artery (Ashwal et al., 1995, Renolleau et al., 1998), and the ischemic area involves neocortical

infarction and small variability at the level of the striatum (Renolleau et al., 1998). This model can lead to sensorimotor and cognitive impairments in early adulthood, including postural asymmetry, motor coordination, cognitive impairments, and a cone shape ischemic lesion that contains only glial cells and no neurons and macrophages at P40 (Bouet et al., 2010).

Although Renolleau *et al*. (1998) intended to develop a model for transient unilateral ischemia that included perfusion and could mimic what happens to the human neonate in the intensive care unit, the perfusion was not complete due to permanent MCAO. In addition, ligation of an extra cranial vessel to reflect events that occur in humans is a questionable practice. Similar to the intraluminal MCAO technique, Renolleau et al.'s model requires considerable time to perform, leading to a high mortality rate.

### *1.2.3 Permanent MCAO by carotid artery ligation*

The MCA was occluded permanently when the carotid artery in rat pups by inserting an embolus into the external carotid artery and then advancing it to the internal carotid artery until it reached the MCA (Derugin et al., 2000). The technique was improved by Wen *et al*. (2004), who inserted silicon-coated suture emboli into the CCA to occlude the middle cerebral artery. The authors claimed that the infarction pattern in their model mimics that of the MRI pattern in the human neonate (Govaert et al., 2000). Infarcts in this model are located in the cortex and the striatum, and the cortical infarcted area is 51-56% of the ipsilateral hemisphere in the forebrain, with apoptosis-like cell death occurring during the first 24 hours (Wen et al., 2004).

Variation in the cerebrovascular structures within the same rat species leads to varied histological outcomes in term of anatomical location after inducing ischemic lesion in stroke models. Wen *et al*. (2004) claimed that their model overcomes the complications experienced in previous studies (Ashwal et al., 1995, Derugin et al., 1998, Renolleau et al., 1998) by demonstrating a 0% mortality rate. In Wen et al.'s study, the inserted suture embolus was individualized to the rat's size. It was inserted into the left CCA instead of the external carotid artery in order to make the procedure easier. Although the infarction was noted in all rats with no mortality, bleeding occurred in 9% of the animals in this model, indicating that such an invasive technique requires skills that may affect the selection of this model. Also, the study only showed MCAO outcomes for 24 hours; a longer period is needed to observe outcomes.

### *1.2.4 Direct occlusion of the middle cerebral artery*

Direct occlusion of the MCA is performed by occluding the MCA by inserting intraluminal filament or by electrocauterization to produce permanent MCAO. In immature rats, occlusion of the left MCA leads to no ischemic lesion (Coyle, 1982, Renolleau et al., 1998). Recently, the technique was applied in neonatal CB-17 mice (Tsuji et al., 2013), where the distal part of the left MCA was electrocauterized, resulting in an infarction volume of 73±3.2 $mm^3$. In this model, selective and consistent cortical injury, mild corpus callosum atrophy, and mild thalamic injury were reported, all of which also occur in infant stroke (Tsuji et al., 2013). Behaviourally, this model leads to significant sensorimotor defects, such as in rotarod and open-field tests (Tsuji et al., 2013).

Variation in the cerebrovascular structures within the same rat species leads to varied histological outcomes in term of anatomical location after inducing ischemic lesion in stroke models. For example, Wistar rats exhibited no infarction after receiving a similar injury to CD-17 mice because of a different vascular distribution that provides collateral supply to the injured area (Kahvecİ et al., Liebeskind, 2003).

In CB-17 mice, the advantages of this model include high reproducibility, less needed time to perform (e.g. 15 minutes), and high survival rate (100%) (Tsuji et al., 2013). However, the reproducibility is due to using the CB-17 strain, which has little variation in cerebrovascular structure (Taguchi et al., 2010). This limitation could be reduced by avoiding the use of strains with high collateral blood supply (Macrae, 2010). Furthermore, infarction volume cannot be increased or decreased, since the occlusion is permanent.

### *1.2.5 MCAO via the photo thrombotic technique*

The photothrombotic technique was developed in 1985 by Watson et al; it produces thrombosis by injecting the animal with a photosensitive dye and exposing it to a laser, resulting in permanent focal ischemia(Watson et al., 1985). When the photosensitive dye is exposed to a green laser light, a photochemical reaction occurs that leads to brain infarction (Witte, 2010). Permanent MCAO was achieved by Kuluz *et al*. (2007), who exposed the MCAto a laser beam over 15 minutes and 4 hours (Kuluz et al., 2007). Their aim was to develop a new model of ischemic stroke in infant piglets. Severe reduction in cerebral blood flow and grey and white matter injury with a 7.1-12.3% infarction volume of ipsilateral hemisphere occurred in this piglet model. Recently, a 7-day-old rat model was developed by directly injuring the SMC via application of a green laser beam over 30 seconds and 5 minutes (Brima et al., 2013). As laser

exposure duration increased, the severity and size of injury increased, as did the deficit in motor performance (Brima et al., 2013).

## 1.3 PIS model via Endothelin-1 (ET-1)

The potent vasoconstriction peptide ET-1 was first used in 1990 (Robinson et al., 1990) to produce an ischemic lesion in the brain by temporally reducing the cerebral blood flow. This reduction was followed by a gradual return over 3 days when ET-1 was injected intrastriatally into juvenile rat brains (Saggu, 2013). The ET-1 application method is being increasingly used because of its advantages over other methods. When ET-1 was injected into P1 rat hippocampus, it caused a temporary reduction in oxygen saturation 10 minutes post injection, before ET-1 produced a significant reduction in oxygen saturation and cerebral blood flow lasting one and a half hours (Tsenov et al., 2015).

### *1.3.1 ET-1 application adjacent to the MCA*

To occlude the MCA and at the same time avoid manipulating the cerebral vessels, which complicates the surgical procedure, researchers injected ET-1 adjacent to the MCA in adult models of stroke (Sharkey and Butcher, 1995, Sharkey et al., 1994, Windle et al., 2006, Yager et al., 2006). Yager et al. (2006) aimed to produce ischemic lesions at three different ages (P10, P63, P180) by injecting ET-1 intracerebrally adjacent to the MCA. Windle et al. (2006) tested 4 methods for delivering ET-1 to produce focal cerebral ischemia: topical, intracortical, adjacent to MCA, and intracortical plus intrastriatal application. They concluded that the last method is most effective in terms of inducing focal ischemia.

### *1.3.2 ET-1 application into specific brain regions*

ET-1 can be applied topically on the cortical surface. For example, applying ET-1 on the surface of the SMC produces dorsal ischemic lesions (Adkins et al., 2004, Fuxe et al., 1992, Hsu and Jones, 2005, Windle et al., 2006). However, topical application leads to diffuse non-focal ischemic lesions. To produce more focal ischemia, ET-1 was injected via stereotaxic injection into several brain regions (Frost et al., 2006, Fuxe et al., 1992, Gilmour et al., 2004, Windle et al., 2006).

In addition to the use of topical ET-1 in ischemia studies, ET-1 has been also used intracerebrally in adult stroke models. Intracerebral injection of ET-1 resulted in focal ischemia in adult and aged rat brains (Soleman et al., 2010, Windle et al., 2006).

Only very recently has a model of cerebral ischemia in neonates been developed. Neonatal focal stroke was produced via intracerebral injections of ET-1 into the motor cortical region of P14 rat pups (Gennaro et al., 2017). ET-1 has also been delivered intracerebrally into the hippocampus of P12 and P25 rats, with greater damage seen in the younger group (Mateffyova et al., 2006, Tsenov et al., 2015).

### *1.3.3 Advantages of using ET-1*

Endotheline-1 overcame some challenges that are present in other stroke modelling methods. For example, infarction volume cannot be increased or decreased after permanent MCAO by electroligation while the infarction size is dose-dependent when using ET-1 (Tsenov et al., 2015). Also, the ET-1 method avoids the invasive technique that requires skills when inserting an embolus into the external carotid artery and then advancing it to the internal carotid artery until it reached the MCA in rat pups by (Derugin et al., 2000). The various uses of ET-1, in addition to the quick and less invasive procedure because there is no need to manipulate the cerebral vessels, make ET-1 a compelling tool for stroke modelling studies (Windle et al., 2006).

Another important advantage of using ET-1 is that the gradual reperfusion induced by the ET-1 is more related to the PIS pathology (Mecca et al., 2009, O'Neill and Clemens, 2001, Saggu, 2013, Sharkey et al., 1993). The use of apparent diffusion coefficient MRI to investigate the ischemic pathology induced by intrastriatal microinjection of ET-1 in 3-week-old and adult rats showed a reduction in blood flow in the younger rat group at 2.5 h, followed by recovery by 72 hours, yet persisted in the adults (Saggu, 2013). However, variability in the resulting infarction between animals was observed using this method.

## 1.4 Age-dependent patterns of injury

Events of perinatal ischemia in human are suggested to occur anytime over a period of 20 weeks during the foetal or neonatal periods (Raju 2008). Clinicians and scientists thus adopt human perinatal stroke subtypes according to the infant age when the diagnosis is made, and according to radiological readings, which detail patterns of injury (Kirton and Deveber, 2013, Raju et al., 2007). The first week of life is the most common period of PIS occurrence (Kirton and Deveber, 2013).

The use of animal models, mainly rodent, to reflect ischemic stroke during the perinatal human period, requires matching the ages between human neonate and animal based on neuronal events that occur during maturation in both species. Correlating the human full term infant age P0 to animal postnatal age is an area of conflict in the literature. Based on different criteria, authors have claimed that the human P0 corresponds to either P7 (Hagberg et al., 1997) or P8-14 in rat age (Hagberg et al., 2002, Romijn et al., 1991, Tucker et al., 2009).

Animal models developed to mimic PIS show different responses according to the animal age (Comi et al., 2008). For example, injury severity within the ipsilateral hemisphere is 35% at P7 and 49% at P14-18 (Ashwal et al., 1995, Derugin et al., 1998). Knowing that immature models, mainly rats, exhibit different vascular maturation patterns, such as in local cerebral blood flow (Nehlig et al., 1989), different injury responses and PIS events can occur during the period of immaturity (Comi et al., 2008). Considering differences in brain maturation, usage of models of different ages to reflect PIS is open to debate. Therefore, knowing the animal age that best reflects human P0 is crucial for developing a valid PIS animal model.

Studies used different neonatal age and rodent strains to model stroke (Table 0.1). Several studies have used P7 rats (Bouet et al., 2010, Brima et al., 2013, Derugin et al., 1998, Derugin et al., 2000, Renolleau et al., 1998, Wen et al., 2004) (Table 0.1). Some of those studies were based on Hagberg *et al.*'s (1997) study, which suggested that rats P7-P14 is comparable to term human neonates in terms of brain development. However in a later study, Hagberg *et al*. (2002) used P7 rat pups for a model of preterm white matter injury, and reported rat/mouse P8-12 as the age reflecting a full-term human neonate. Other studies (Ashwal et al., 1995, Ashwal et al., 2007) have used rats older than P7 due to the difficulty of performing occlusion techniques in younger animals. Similarly, other studies (Gennaro et al., 2017, Tsuji et al., 2013, Yager et al., 2006) have used rats/mice aged beyond P7 to model neonatal stroke.

| Author | Rodent age | Rodent type | Modelling method | Perfusion time | Histological assessment |
|---|---|---|---|---|---|
| Ashwal et al., 1995, Ashwal et al., 2007 | P>7 | Spontaneously hypertensive rats | Intrafilament+ Hypoxia 2-3 h | 24h<br>Over 28 days | mitochondrial stain, TTC |
| Derugin et al., 1998, | P7 | Sprague–Dawley rats | Intrafilament | 24h | TTC |
| Derugin et al., 2000 | P7 | Sprague–Dawley rats | Intrafilament | 4, 8, 24, and 72 h | TTC<br>MRI before and 20 minutes after reperfusion, GFAP, ED-1, cresyl violet |
| Gennaro et al., 2017, | P>7 | Wistar rats | intracerebral injection of ET-1 | | propidium iodide. anterograde dye Biotinylated Dextran Amine, DAB staining |
| Yager et al., 2006 | P>7 | Wistar rats | | 60 | hematoxylin and eosin, GFAP |
| Wen et al., 2004 | P7 | SD rats | Intrafilament | 24h | TTC, TUNEL |
| Tsuji et al., 2013 | P>7 | CB-17 mice | Intrafilament | 48 h, 8 weeks | TTC, hematoxylin–eosin |
| Bouet et al., 2010, | P7 | Wistar rats | Intrafilament CCA 1 h +MCA electroligation | 33days | Astrocytic and neuronal pattern |

| | | | | | |
|---|---|---|---|---|---|
| Brima et al., 2013, | P7 | Wistar rats | photothrombotic | 67 days | cresyl violet |
| Renolleau et al., 1998 | P7 | Wistar rats | Intrafilament | 48 h<br>4 to 96 hours, 7 and 14 days, 1 and 3 months | TTC, cresyl violet, Silver Staining, TUNEL |

**Table 0.1 Rodents in PIS models**

Studies matching neuronal maturation are needed to confirm which rodent age is the most appropriate for a PIS model. Many studies have adopted rodent age P7 to model humans at 32-34 weeks of gestation, and rodent P12-13 as the equivalent of full-term human infant, based on histological findings such as cerebral layering of cortical neurons (Rice et al., 1981). More recent studies have considered rodent P8-12 as the age that reflects the timing of P0 human PIS in terms of cortical maturation events(Romijn et al., 1991) and electrophysiological readings (Tucker et al., 2009).

Since radiographic methods are considered the gold standard for differentiating between PIS subtypes in human neonates, studies using these methods to determine the animal age that matches the human neonate at term are important to consider. Hagberg *et al*. (2002) claimed that human term is comparable to P8-12 in the rat/mouse, while human 24-30 weeks gestational age is comparable to rat/mouse P4 in terms of white matter maturation. Electroencephalography (EEG) background activity strongly correlates with human (Burdjalov et al., 2003) and rat age (Tucker et al., 2009). In a study correlating human brain maturity with rat pups aged from P0 to P21 using a "gold standard" method, EEG, human term P0 neonates were found to be equivalent to P10-12 rats pups in terms of their longest interval of burst activity and voltage (Tucker et al., 2009). The authors suggested that cortical EEG activity in P1 rat pups corresponds to 23 weeks gestational age in human neonates, P7 corresponds to 30-32 weeks, and P10 corresponds to 40-42 weeks.

Rats are common stroke model in term of using the ET-1 because it induces a reproducible focal cerebral lesion in their brains (Frost et al., 2006, Fuxe et al., 1992, Gilmour et al., 2004, Sharkey and Butcher, 1995, Windle et al., 2006) but this is not the case in mice. Different mice strains show no cerebral lesion after using the ET-1 and this is due to the less potent effect of ET-1 on the injected brain area in mice. When the ability of the ET-1 to induce ischemic infarction in rat and mice strains, all tested mice strains showed no ischemic lesion unlike rat models that showed focal cerebral ischemia (Wang et al., 2007). Even when higher ET-1 dose were given to mice to induce cerebral ischemic lesion, only mortality rate increased but no ischemic lesion was found (Horie et al., 2008).

Rodent strain is another factor that can affect the PIS models. Comi et al. (2009) found that the strain strongly influences the ischemic injury pattern in mice. For instance, following post-carotid-ligation at P12, CD1 mice are more vulnerable to epilepsy than C57Bl/6 mice (Comi et

al., 2008). Also, differences exist between rats and mice. For example, the consistency of infarct size observed in Tsuji et al.'s (2013) study is due to the use of CD-17 mice, which are known for their similarity between individuals in terms of vascular distribution. When using other strains, differences in blood cerebral flow and vascular distribution lead to different infarction patterns.

Rats provide a common stroke model when using ET-1 because it induces a reproducible focal cerebral lesion in their brains (Frost et al., 2006, Fuxe et al., 1992, Gilmour et al., 2004, Sharkey and Butcher, 1995, Windle et al., 2006) but this is not the case in mice. Different mice strains show no cerebral lesion after using the ET-1 and this is due to the less potent effect of ET-1 on the injected brain area in mice. When the ability of the ET-1 to induce ischemic infarction in rat and mice strains was tested, all tested mice strains showed no ischemic lesion unlike rat models that showed focal cerebral ischemia (Wang et al., 2007). Even when a higher ET-1 dose were given to mice to induce cerebral ischemic lesion, only the mortality rate increased but no ischemic lesion was found (Horie et al., 2008).

Many factors can strongly influence PIS models, including technique, age, and strain. Both the techniques used to develop these models and the age at which the injury is induced yield PIS models with different outcomes, as does the animal and strain used. The pathogenesis in some models is vastly different from the human clinical situation. The electroligation and photothrombotic techniques have the lowest mortality rate and shorter surgery duration, while the intraluminal and CCA/MCAO methods have higher mortality rates and longer duration. The day on which the injury is induced in the animal is crucial; the most recent and reliable studies confirm that the most widely-used PIS models use P10-12 rats/mice to reflect human neonates at full term.

### 1.5 Stem cells in stroke repair

There are some interventional trials for neonatal hypoxic ischemia that could reduce the lesion size but also produces some side effects and their safety is questionable such as Erythropoietin (Jacobs et al., 2013, Souvenir et al., 2015, van der Worp et al., 2007, Xiong et al., 2011). Early interventions such as hypothermia during the acute stage of the ischemic stroke in neonate decreases the ischemic infraction but lead to bradycardia and thrombocytopenia (van der Worp et al., 2007). Another effective early intervention that could provide therapeutic effects in neonatal stroke is the use of the stem cell (Kiasatdolatabadi et al., 2017).

Stem cell therapy is a compelling current approach that is being investigated extensively in neurological disorder research due to its therapeutic effects. Interventional experiments for cerebral palsy were covered in a recent review (Kiasatdolatabadi et al., 2017), which showed that stem cells have the ability to reduce neurological symptoms. For example, transplanted stem cells secrete trophic factors that help in brain plasticity, attenuate the inflammatory response to brain lesions, stimulate endogenous neuroprotection, neurogenesis, angiogenesis, axonal sprouting, and synaptogenesis, and most importantly, replace damaged cells (Castillo-Melendez et al., 2013, Englund et al., 2002, Jablonska et al., 2010).

Neural stem cells (NSCs) are multipotent cells that are able to self-renew and ultimately produce neurons, astrocytes, and oligodendrocytes. NSCs can be derived from foetal or adult brain, such as from the subventricular zone (Alvarez-Buylla and Temple, 1998). NSCs can also be derived from pluripotent stem cells such as human embryonic stem cells (ESCs) and human induced pluripotent stem cells (hiPSCs) (Figure 0.2).

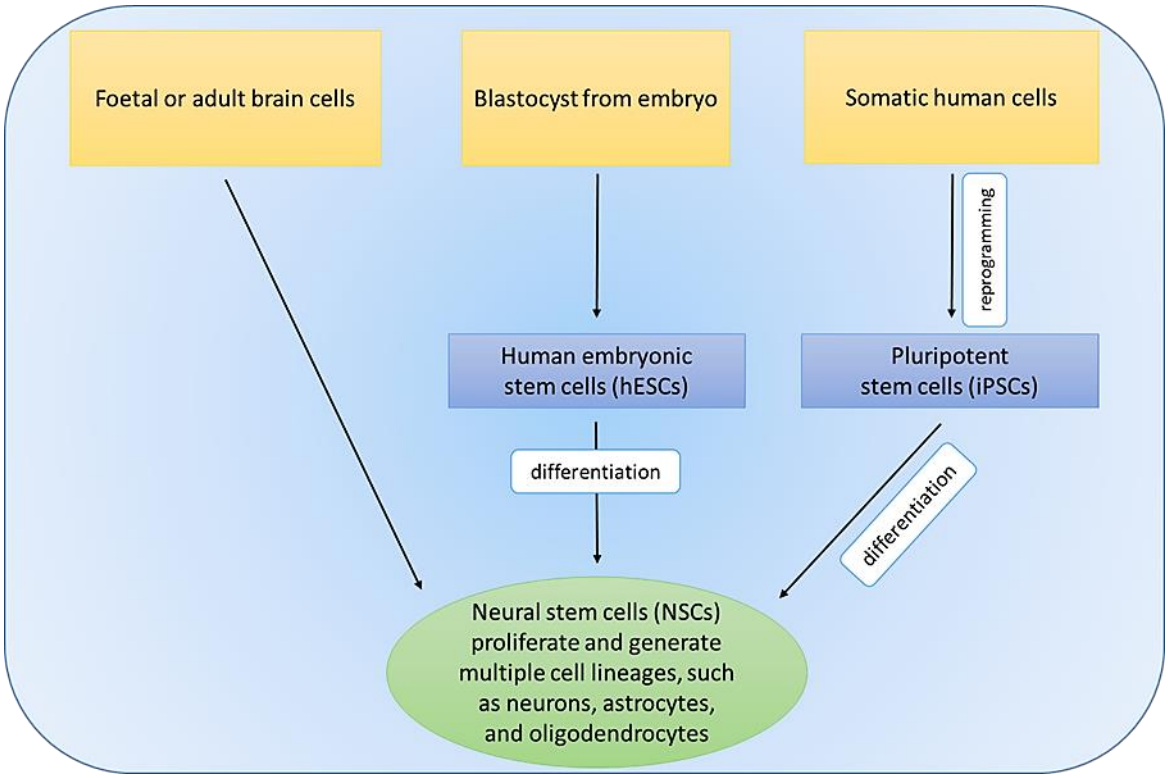


**Figure 0.2 Sources of NSCs.**

NSCs derived from human ESCs have the ability to differentiate and to provide a functional circuit with the host cell, and they display healthy cellular electrophysiological characteristics when transplanted directly into normal P1-P2 rat cortex or hippocampus (Englund et al., 2002). Furthermore, embryonic NSCs have been found to reduce brain atrophy when transplanted into the neonatal stroke animal model (Comi et al., 2008). The P12 stroke mouse model was induced via unilateral carotid ligation. ESCs derived NSCs were injected intrastriatally 2 days after inducing the ischemic lesion and brain atrophy was assessed 4 weeks later. The authors found that embryonic NSCs attenuated brain atrophy, although 30% of the treated animals developed a local tumour (Comi et al., 2008). In addition to tumour formation, the use of the human ESCs have some associated obstacles, such as the immune reaction of the host body as well as ethical issues (Lo and Parham, 2009). These drawbacks make the use of the NSCs derived from human ESCs less attractive.

The recent revolution in stem cell studies has made the production of NSCs from autologous hiPSCs (iPSCs-NSCs) possible (Takahashi et al., 2007). NSCs derived from autologous hiPSCs are generated by reprogramming autologous somatic cells using specific transcription factors delivered by a viral vector, thus providing promising personalized stem cell therapy in the clinic. An additional advantage is the ability to generate iPSCs directly and more safely by direct delivery of reprogramming proteins and without even the use of the viral vector (Ban et al., 2011, Kim et al., 2009), making hiPSCs a compelling source to use in cell replacement therapies.

In neonatal brain injury studies, hiPSCs are considered a non-tumourigenic alternative source of NSCs (Gruen and Grabel, 2006, Hess, 2009, Lepore et al., 2006, Low et al., 2008). One source of iPSC-NSC cell lines is umbilical cord blood (UCB) (Ali et al., 2009, Bużańska et al., 2002, Kögler et al., 2004, McGuckin et al., 2004, Sanchez-Ramos et al., 2001). An NSC cell line derived from hiPSCs originating in human UCB (Bużańska et al., 2002, Jablonska et al., 2010) was found to be safe and reliable in interventional studies using *in vitro* and *in vivo* adult and neonatal models of neurological disorders. hiPSCs-NSCs transplanted into neonates showed their ability to survive, migrate, and differentiate into neuronal cells, with no signs of tumour formation in normal rat neonates (Jablonska et al., 2010).

In stroke studies, stem cells can be delivered via many methods but they have been mainly used for mesenchymal stem cells. intravenous and intranasal delivery are examples of these delivery

routes however most of stem cell engraftments die after being delivered *in vivo* (Bliss et al., 2007). Although intravenous delivery of stem cells is a common systemic administration method in stroke research, it requires a vast amount of cells to be administered because only few of them reach the brain, possibly due to the non-permeability of the blood-brain barrier (BBB) (Detante et al., 2009, Gonzales-Portillo et al., 2014). Yet, these stem cells delivery routes have been mainly used for mesenchymal stem cells.

Alternatively, injecting stem cells directly into the stroke infarction or pre-infarction, the location of neuroplasticity in stroke (Carmichael, 2006), leads to cells that are located in the target area and that survive (Comi et al., 2008). However, the stroke infarction is a hostile environment for transplanted cells, often leading to grafted cell death (Bakshi et al., 2005). The absence of trophic factors in the infarction cavity, a damaged BBB and the loss of extracellular matrix (ECM) proteins due to stroke lead to the accumulation of extracellular fluid and the leakage of plasma proteins into the infarction cavity (Baeten and Akassoglou, 2011). For these reasons, the use of compatible biomaterials that fill the infarction cavity to provide the grafted cells with a stimulatory environment for survival and enhance the efficacy of stem cell therapy is a crucial aim in treating stroke (Wang et al., 2014).

### *1.5.1 ECM and stem cells*

The ECM in the CNS has three main components: the basement membrane, the perineuronal net, and the neural interstitial matrix. First, the basement membrane or basal lamina components, such as laminin, fibronectin and heparin sulphate proteoglycan, serve as a sheath that surrounds the cerebral blood vessels and separates it from the brain parenchymal tissue. The second component is a condensed mesh-like layer called the perineuronal net; it surrounds the neuronal cell bodies and dendrites and contains hyaluronic acid. It is believed that this layer is crucial for maintaining neuronal health and synaptic plasticity (Ethell and Ethell, 2007, Kwok et al., 2011, Murphy et al., 2017a). The third layer, the neural interstitial matrix, consists of a network of ECM components in the parenchyma located furthest away from the first and the second layers; it contains a dense network primarily composed of hyaluronic acid and link proteins.

Natural biomaterials such as hyaluronan (HA) (which is a crucial component in ECM in the developing brain), chitosan, and collagen are able to be utilized clinically (Pakulska et al., 2012, Rauch et al., 2004, Van Zelst et al., 2006). However, synthetic biomaterials such as Puramax

are more advantageous because their components mirror the characteristics of natural ECM while provoking a milder immune reaction, and they confer the ability to modify the biocompatibility of the hydrogel to suit the application purposes (Aurand et al., 2012).

Biomaterials such as hydrogels have recently become common for use as vehicles of neural cell delivery in neurological disorder research. A hydrogel is a polymer that has chemical properties such as high water content (>90% water); its physical characteristics can be tuned and controlled to produce a variety of textures ranging from rigid to soft (Aurand et al., 2012).

The hydrogel matrices used in interventional studies can be natural, synthetic, or semi-synthetic (Zarembinski et al., 2011). Figure 0.3 provides an example of available hydrogel matrices that are commonly used in research. Zhong et al. (2010) used the semi-synthetic hydrogel (HyStem-HP) that was constructed by modifying purified natural biopolymers (HA) (Zhong et al., 2010). The authors' results demonstrated a focal presence of the graft with a high survival rate and less immune reaction in the host brain cells.

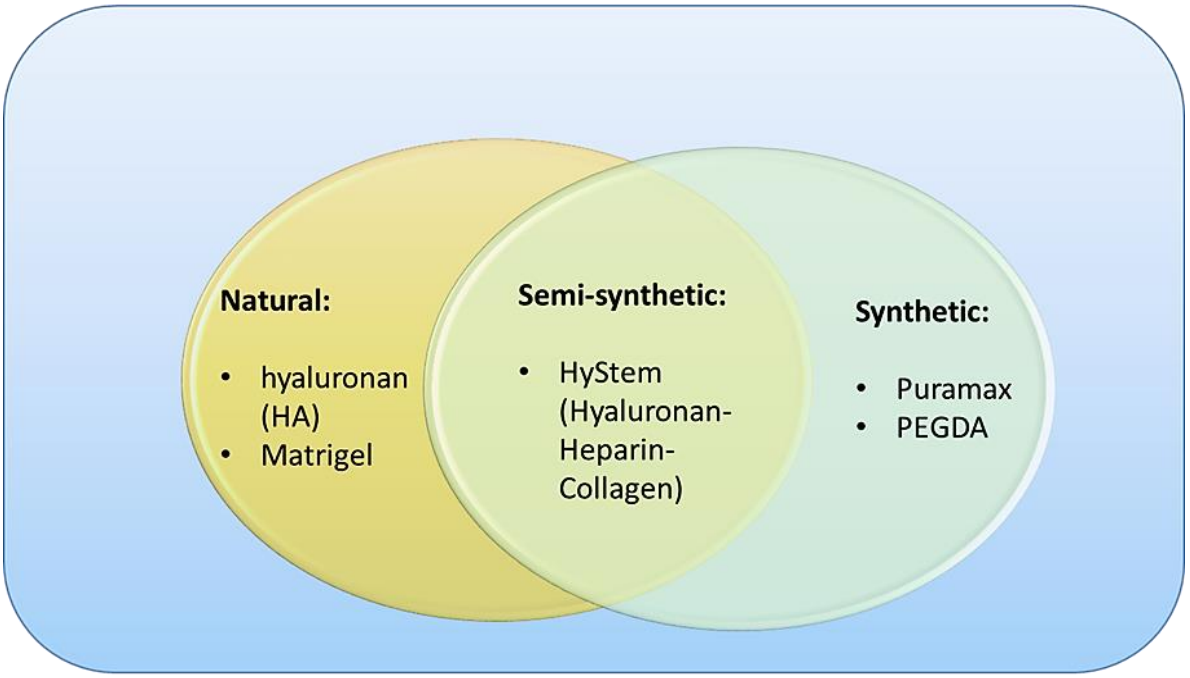


**Figure 0.3 Types of hydrogel matrices.**

*In vitro* and *in vivo* neuro-regeneration studies using stroke models have shown that hydrogel application is feasible when used as scaffold for the transplanted stem cells (Bible et al., 2012, Burdick and Prestwich, 2011, Liang et al., 2013, Thonhoff et al., 2008, Zhong et al., 2010). An *in vitro* study compared human NSCs incubated in two-dimensional (2D) standard culture and in 3D ECM culture. After seven days, the 3D culture demonstrated an advantage over the 2D in terms of NSC differentiation assessed by axonal outgrowth (Stevanato et al., 2015).

Recent advances in tissue engineering research have shown that biomaterials can function as compatible ECM *in vivo* and support transplanted stem cell viability in experimental adult stroke models.

Transplanting a hydrogel such as Matrigel *in vivo* into a focal ischemic model in rat showed efficient results. Jin et al.'s (2010) study showed cellular survival and differentiation, reduction in infarction volume and improved functional outcomes after transplanting a combination of Matrigel and human ESC neuronal precursor cells 3 weeks post induction of an ischemic lesion in rats (Jin et al., 2010). However, a downside to Matrigel, which is derived from mouse sarcoma, is that its components are poorly defined.

HyStem (HA-Heparin-Collagen) contains HA and collagen that bio-mimics the brain microenvironment and stimulates angiogenesis, host cell infiltration, and synaptic plasticity, and reduces the innate immune response of the host when delivered *in vivo* in rat models, indicating its feasibility in stem cell transplantation therapy (Fraser et al., 1997, Hou et al., 2005).

HA hydrogel is a good choice for stem cell transplantation experiments because it has the ability to co-exist with no inflammatory response of the transplanted stem cells in the brain (Nih et al., 2017). Administration of HA alone immediately following removal of the SMC of adult rat brains led to significant reduction in the glial scar, as indicated by a decreased number of GFAP positive cells in immunohistological analysis (Lin et al., 2009). Similarly, Yu et al (2010) demonstrated that NSC transplanted with collagen type-I in a transient ischemia rat model resulted in new synapse formation and led to better functional outcomes 30 days post implantation, a time when collagen was completely degraded (Yu et al., 2010).

HA causes the encapsulated neural progenitor cells derived from iPSCs to differentiate into neuroblasts one week after transplantation into the infarct cavity of stroke model mice (Lam et al., 2014).

A study using HyStem hydrogel, with neural progenitor cells transplanted intracerebrally into the infarction cavity 7 days after inducing ischemic stroke in rats, demonstrated beneficial effects, including improved stem cell survival and a reduced number of inflammatory cells infiltrating the infarction (Zhong et al., 2010). Injecting HyStem with NSCs resulted in a significant increase in the number of the viable cells in mice brains at day 7 post transplantation. This study highlighted the importance of gelling time in the success of intracerebral NSC transplantation, suggesting that a 25-minute delay prior to injecting the cells-ECM will allow the mixture to maintain its shape *in vivo* and not be absorbed by the brain tissue (Jiang et al., 2005). However, biodegradation of the hydrogel is difficult to control and the weak mechanical structure prevented the transplanted cells from migrating out of the graft (Kai et al., 2012, Skop et al., 2014). This indicates the importance of performing further investigations to overcome these weaknesses.

## 1.6 Research project

### *1.6.1 Rationale of the study*

In human neonates, PIS is a significant cause of hemiplegic cerebral palsy (Golomb et al., 2008, Kirton et al., 2011). The diagnosis of hemiplegia reaches 87% in children with PIS (Golomb et al., 2008). Early interventions using stem cell therapy can provide support to the infarcted motor cortex, or perhaps even replace lost cortical cells. However, the invasive nature of our proposed interventions requires that they first be tested in a rodent model.

Although MCAO is a common method for inducing neonatal stroke (Ashwal et al., 1995, Ashwal et al., 2007, Derugin et al., 1998, Derugin et al., 2000, Tsuji et al., 2013), intracerebral injection of reversible vasoconstrictor ET-1 has advantages over the MCAO method, such as gradual reperfusion that mimics the clinical symptoms in human neonates (Saggu, 2013, Tsenov et al., 2015) and the reliability of using a CST disturbance to produce an interventional model in developing rats (Gennaro et al., 2017).

Interventional stroke studies have shown the ability of stem cells to improve neurological outcomes post stroke and promote endogenous neuroprotection, neurogenesis,

neovascularization, axonal sprouting, and synaptogenesis (Castillo-Melendez et al., 2013, Englund et al., 2002, Jablonska et al., 2010).

Several types of stem cells have been used for cerebral palsy treatment in previous studies (Kiasatdolatabadi et al., 2017). One of these stem cell types is NSCs, which are multipotent, able to self-renew, and ultimately produce neurons, astrocytes, and oligodendrocytes, and most importantly, replace damaged cells (Jendelová et al., 2016). NSCs derived from ESCs have the ability to reduce brain atrophy when transplanted into a neonatal stroke model, although they also generate tumourigenic cells (Comi et al., 2008). A non-tumourigenic alternative source of NSCs is iPSCs (Gruen and Grabel, 2006, Hess, 2009, Lepore et al., 2006, Low et al., 2008).

Among in vivo stem cell administration methods, intracerebral transplantation is considered one of the most convenient routes. Grafted cells have been found to survive in the lesion site, usually the infarction cavity, after intracerebral transplantation. Yet most of these engraftments die due to the hostile environment of the infarction site (Bliss et al., 2007).

In fact, stem cell transplantation studies have failed to fill the infarction site or produce a well-developed, organised formation of regenerated cerebral cells in vivo due to the accumulation of extracellular fluid and proteins in the local post-stroke lesion site (Baeten and Akassoglou, 2011). This indicates the need to administer an additional supporting component that works as a scaffold for the transplanted stem cells. Recent advances in tissue engineering have shown that hydrogel works as a compatible ECM in vivo and supports transplanted stem cell survival in the infarction cavity in adult stroke models (Zhong et al., 2010).

### *1.6.2 Aims of the study*

The objectives of the present study are as follows:

(1) To develop a model of focal sensorimotor cortical stroke in P12 rats using MCAO or ET-1 injection at specific coordinates to ensure high reproducibility with a low mortality rate.

(2) To induce acute and chronic histological responses that resemble the SMC in the PIS brain.

(3) To produce chronic functional disabilities that resemble the sensorimotor deficits associated with PIS.

(4) To compare between the survival and development hNSCs-ECM *in vitro* and following grafting to a rat model of perinatal infarction damaging SMC at P14.

# Chapter 2 Materials and Methods

## 2.1 Overview

This chapter describes the methods used in the three main experiments performed to achieve our research aims (Figure 2.1). The respective methods used for the first and the second experiments were middle cerebral artery occlusion (MCAO) and intracerebral injection of Endothelin-1 (ET-1).

The first experiment involved methods that were applied in order to develop a model of perinatal ischemic stroke (PIS) in postnatal age 12 (P12) rats with cortical ischemic lesion to the sensorimotor cortex (SMC) and resulting behavioural dysfunction. The results and discussion of these experiments will be presented in chapter three.

The second experiment consisted of an additional surgery to inject Fluorogold (FG) retrograde tracer into the contralesional side of the cervical spinal cord at P45 to investigate the possible anatomical reorganisation of the corticospinal tract (CST) after intracerebral injection of ET-1 at P12. The results and discussion of these experiments will be presented in chapter four.

The third experiment's methods included culturing neural stem cells (NSCs) in a 2-dimensional (2D) monolayer or in a 3D semi-synthetic extracellular matrix (ECM) in vitro to test for spontaneous differentiation into neuronal lineages. Then, in vivo NSCs-ECM transplantation into the ET-1-ischemic SMC was performed in P14 rats to investigate the potential therapeutic effects of the transplanted complex. The results and discussion of these experiments will be presented in chapter five.

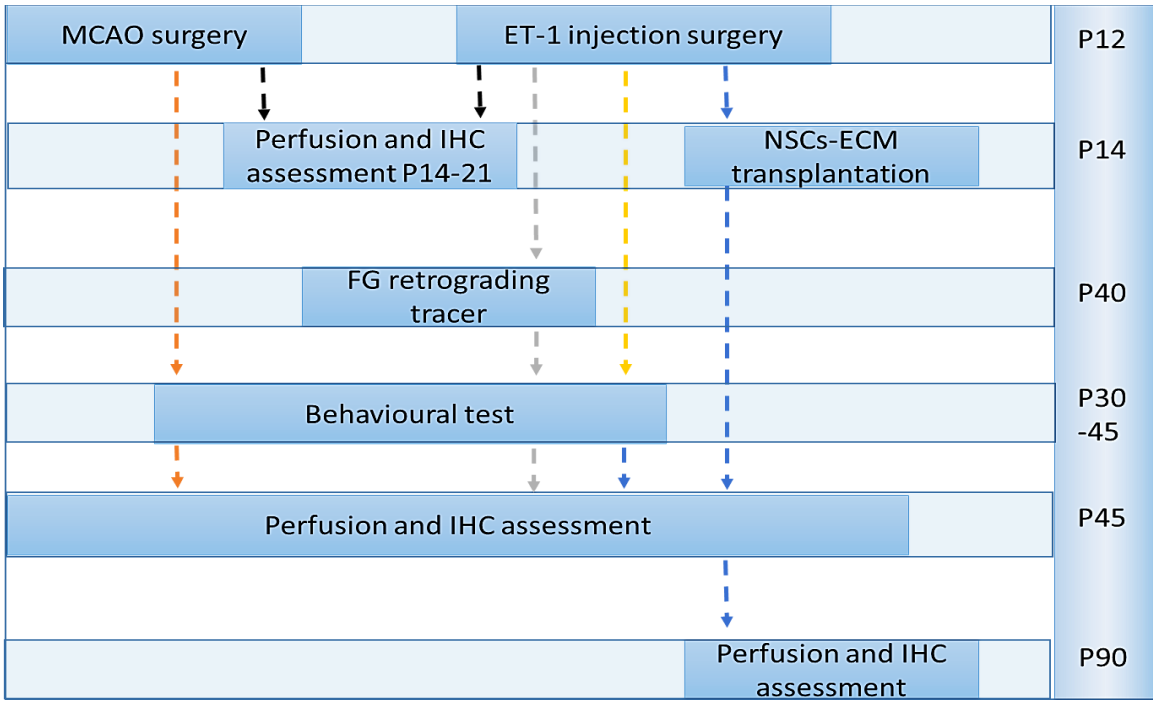


**Figure 2.1 Main structures of the project methodology.**

## 2.2 Animals

The Wistar rats used in all experiments were purchased from Charles River Laboratories and were housed in the Newcastle Comparative Biology Centre at Newcastle University. All animal procedures were performed with the approval of the Newcastle University Animal Welfare and Ethics Review Board and under project license number 60/4266 from the UK Government Home Office.

All rat neonates were kept with their mother in the same cage until weaning at around P21, and were then separated into two cages according to gender. All rats shared the same room with the same care routine and light/dark cycle. Surgeries were carried out in the Newcastle Comparative Biology Centre theatres at Newcastle University under aseptic conditions.

## 2.3 PIS model methodology

Two main experiments were performed: a MCAO experiment and an ET-1 experiment. In both experiments, 29 male and female P12 immature Wistar rats were used in each experiment to conduct the PIS modelling surgery, with P0 being the day of birth.

### *2.3.1 MCAO surgical procedure*

Three surgeries were performed on three groups of rats. The first group underwent one-spot electroligation proximal to the middle cerebral artery (MCA) bifurcation. However, this method was discontinued due to a lack of brain injury observed in histological sections. The second group received a modified method consisting of electroligation along the MCA between the inferior cerebral vein and the olfactory tract. The third group was the sham group and only received craniectomy. All three groups were assessed histologically and behaviourally. A decision was made not to occlude the MCA by inserting a filament through the external carotid artery for two reasons. Firstly, we wished only to lesion the cortex as the eventual plan was to graft stem cells programmed to become cortical neurons. Occluding the MCA via the external carotid will cause damage to the striatum as well and so any repair strategy would become more complicated. Secondly, occlusion via the external carotid with reperfusion requires the filament to remain in situ for 2 hours before it is removed. This reduces the number of animals that can be operated on in one day and so if all animals are to be operated on at the same age more litters have to be used.

Two main experiments were performed: a MCAO experiment and an ET-1 experiment. In both experiments, 29 male and 29 female P12 immature Wistar rats were used to conduct the PIS modelling surgery, with P0 being the day of birth.

**One-spot electroligation for MCAO surgery**

Eight P12 rat pups received a subcutaneous injection of the anaesthetic agent Hypnorm (Janssen, UK; 0.3 ml/kg body weight 0.126 mg/kg body weight fentanyl citrate and 4 mg/kg body weight fluanisone) injected subcutaneously. After testing the depth of anaesthesia by pinching the tail and paws, each rat was positioned on its side and a skin incision was made between the left eye and the left ear to expose the temporal muscle, which then underwent careful blunt dissection using a surgical microscope. Attempts were made to observe the MCA before peeling the semi-transparent fragile skull, and then a craniectomy just above the expected area of the MCA route was performed with fine forceps. Electroligation proximal to where the MCA bifurcates into parietal and frontal branches was performed once (Figure 2.2A), and then the cranial bone was returned and the skin was sutured (Tsuji et al., 2013).

Post-surgical care was given to each rat. Anaesthesia was reversed but analgesia maintained by injecting 1% butorphanol (Torbugesic) (10mg/ml) subcutaneously, and the rat pups were kept in a thermal incubator and observed until they woke up. P12 rats usually need to stay for a few hours in the warm incubator. After checking the rat pups, they were taken to their mother's cage in the rodent area. There was no need to give soft food because they were suckling. On the next day, observations were made of any signs of pain or stress; if present, the animals received a subcutaneous analgesic such as buprenorphine. The rats were checked daily for possible complications from surgery, such as infection or severe pain.

We needed to modify our surgical procedure because the one-spot electroligation method was not sufficient to occlude the MCA in P12 rat pups.

**Extended electroligation for MCAO surgery**

Thirteen P12 rat pups underwent a similar surgery to the one-spot MCAO group, but with a modification guided by the results of the MCAO model performed previously. The ligation area was increased by ligating along the MCA trunk, proximally from the olfactory tract level and distally to the inferior cerebral vein level as far as possible to prevent the collateral cerebral

arteries from supplying the sensorimotor area (Taguchi et al., 2010) in order to produce cortical ischemia (Figure 2.2B).

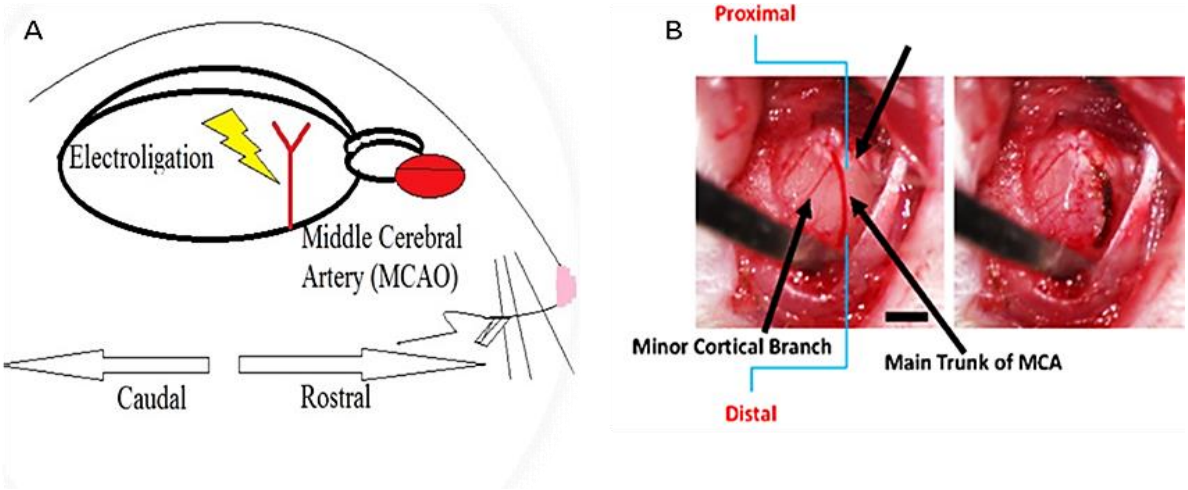


**Figure 2.2 MCAO surgery via electroligation.**

(A) Cartoon diagram of lateral view of the rat brain and the location of the electroligation. (B) Extended method of MCAO from distal to proximal MCAO rats, main and minor MCA branches are indicated by arrows and in the right photo is the MCAO along the MCA trunk(Tsuji et al., 2013).

**Sham surgery**

Sixteen rat pups were assigned to the sham group. The rats underwent a similar protocol under similar conditions as the experimental group, up to the point of craniectomy. After craniectomy was performed, the cranial bone was returned and the skin was sutured. The rats did not receive electroligation. Animals also received the same post-operative care and analgesia.

### *2.3.2 ET-1 intracerebral injection surgical procedure*

In this study, total of 29 of P12 immature Wistar rats were assigned into ET-1 experimental group and sham operated group.

A total of 17 rats were assigned to the experimental group and received ET-1 injections intracerebrally into the SMC. We employed a stereotactic frame with inset and ear bars designed for rat pups and a special nosepiece to allow the administration of gaseous anaesthetic. We therefore anesthetised the animals with isoflurane, and injected 0.03 mg/kg buprenorphine to provide long term analgesia.

ET-1 dose was 400 Picomole (Pmol) (0.1mg Endothelin-1, Human and Porcine, 117399-94-7 – Calbiochem) dissolved into 0.9% Sodium chloride (NaCL) at each site (Soleman et al., 2010). Three direct intracerebral ET-1 injections were done to cause infarction in the sensorimotor area. A syringe pump and a narrow needle Hamilton syringe (neuros$^{TM}$ Hamilton syringe 7000, 33 gauge) that attached to the stereotactic frame was used over a period of about 20 minutes (Figure 2.3A, B and C). Injections were made following the sequence of slowly injecting half the ET-1 (0.5µL), waiting a minute, and then injecting the rest (0.5µL) using an Ultra micropump with microcontroller (World Precision Instruments, Sarasota, FL, USA) (Figure 2.3 D). Under anaesthesia, a flap in the skull bones was cut and hinged at the midline over the right hemisphere and three injections were made into the exposed cortex (Figure 2.3E) at the following co-ordinates, +2.00 mm anterior of bregma and +2.00 mm lateral of the midline, +0.75 mm anterior and +2.00 mm lateral, and -0.50 mm posterior of bregma and +1.00 mm lateral, all to a depth of 1 mm. Each rat received 3µL of ET-1 solution, 1 µL for each cortical injection co-ordinate. A careful injecting protocol using an electronic timer/stopwatch and following a precise checklist (Table 2.1) was performed.

Then, the skull and scalp was repaired and the animals allowed to recover before returning to their mother's cage for 24 hours. Post-surgery care was carried out as described in the MCAO surgical procedures.

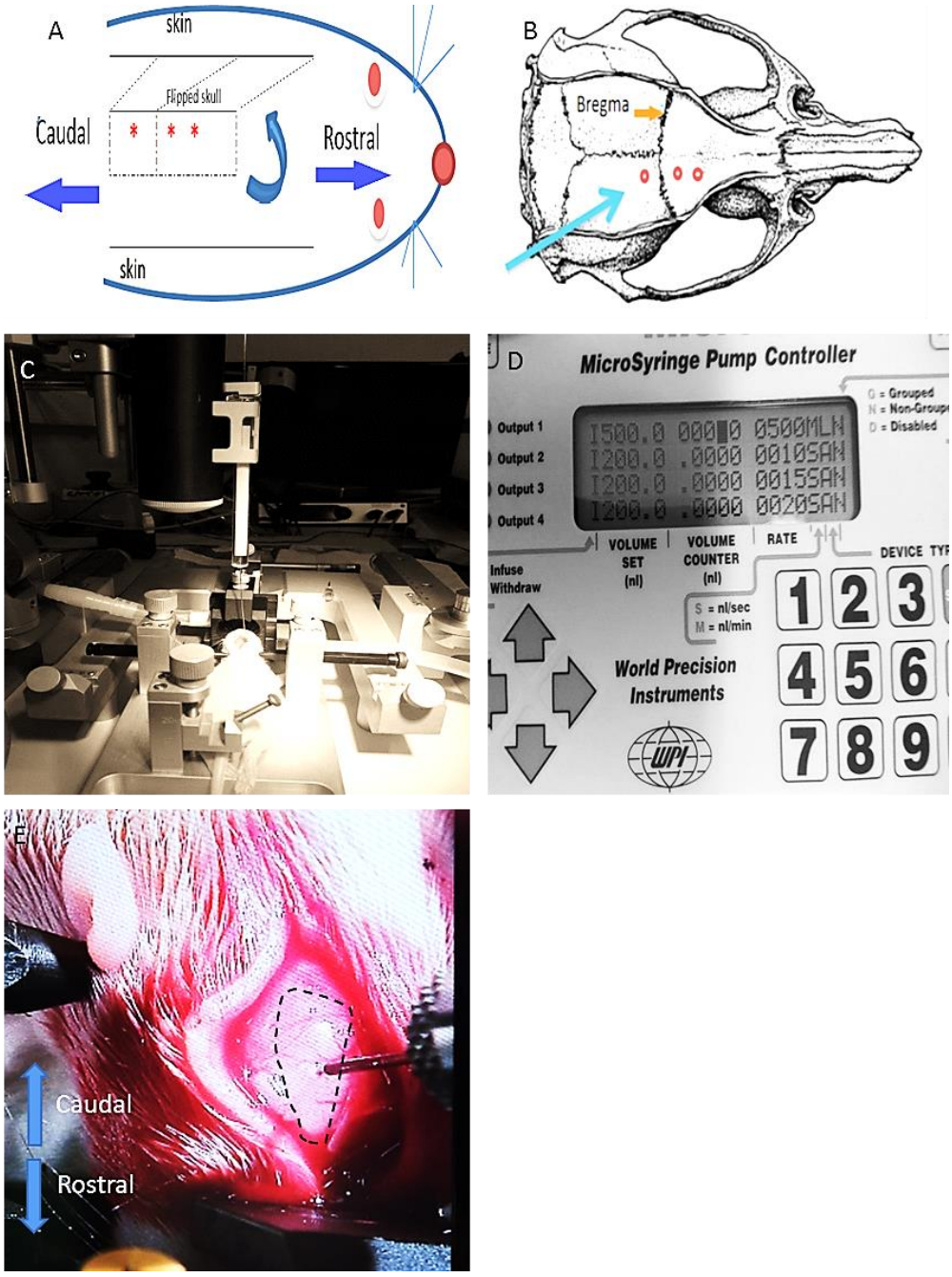


**Figure 2.3 Surgical procedures of the intracerebral ET-1 injection.**

(A) Three injection sites (asterisks) (B) at three coordinates (blue arrow) two of them are anterior to the bregma (orange arrow) and one posterior to the bregma. (C) ET-1 intracerebral injection surgical setting with and a rat lay down in stereotactic frame with Hamilton syringe attached to it. (D) Ultra Micropump with microcontroller to inject1µL of ET-1 per injection site. (E) The needle is inserted in the SMC (surrounded by dashed line) during the first minute of injecting ET-1.

| Intracranial injections | Rats | | | | | | | |
|---|---|---|---|---|---|---|---|---|
| | 1 | 2 | 3 | 4 | 5 | 6 | 7 | 8 |
| First intracranial injection (1µL) at AP +2.00mm, ML 2.00mm, DV +1mm | | | | | | | | |
| 1st 0.5µL of ET-1 | ✓ | | | | | | | |
| pause 1 min | | | | | | | | |
| 2nd 0.5µL of ET-1 | | | | | | | | |
| pause 3 min | | | | | | | | |
| remove the needle up | | | | | | | | |
| Second intracranial injection (1µL) AP +0.75mm, ML 2.00mm, DV +1mm | | | | | | | | |
| 1st 0.5µL of ET-1 | | | | | | | | |
| pause 1 min | | | | | | | | |
| 2nd 0.5µL of ET-1 | | | | | | | | |
| pause 3 min | | | | | | | | |
| remove the needle up | | | | | | | | |
| Third intracranial injection (1µL): AP (-0.5)mm, ML +1.00mm, DV +1mm | | | | | | | | |
| 1st 0.5µL of ET-1 | | | | | | | | |
| pause 1 min | | | | | | | | |
| 2nd 0.5µL of ET-1 | | | | | | | | |
| pause 3 min | | | | | | | | |
| move the needle up | | | | | | | | |

**Table 2.1 ET-1 injection check list**

To investigate the effects of ET-1 injection at P12 on normal growth in the PIS model, body weight was recorded at regular intervals starting from the day of surgery until the perfusion day. The relative body weight was calculated and expressed as a percentage as follows: (body weight at the end of the experiment P45 ⁄ body weight on surgery day P12) x 100 (Mateffyova et al., 2006).

**Sham surgery**

Twelve rats were assigned to the sham group and received saline injections intracerebrally into the SMC. The rats underwent a similar protocol under similar conditions as the experimental group up to the point of craniectomy. Then, instead of injecting ET-1 intracerebrally into the SMC, saline was injected using the same ET-1 surgical and post-surgical protocol.

### *2.3.3 Retrograde tracing surgical procedure*

Rats in both ET-1 and sham groups were tested behaviourally after P30 and then a random subgroup of them were assigned to be injected with the FG for CST retrograde tracing at the spinal cord level of cervical (C)7-8 contralateral to the lesion at P40.

Previous studies used a retrograde tracer to investigate the CST projection from the spinal cord to the cortical level of the brain. The use of an injectable tracer that has unique immunofluorescence properties, such as FG, is one of the most useful methods in central nervous system (CNS) tracing studies (Willenberg and Steward, 2015, Yoshikawa et al., 2011). Once tracers/dyes are injected, they accumulate in the neural cells bodies and express intense fluorescence under ultraviolet illumination that is resistant to bleaching or fading over time. The use of available commercial antibodies to label stained FG cells adds another advantage to using FG as a retrograde tracer (Lanciego and Wouterlood, 2011).

In this surgery different anesthetic regime was given to the Juvenile rats at P40 than all other surgeries that were done at a neonatal age. Fifteen PIS model rats were anaesthetized by intraperitoneal injection (dose 0.3 ml/100g) with a mixture of Hypnorm and midazolam (1.25 mg/ml midazolam, 2.5 mg/ml fluanisone and 0.079 mg/ml fentanyl citrate) at P40. Oxygen was given throughout the surgery at 500ml/min to avoid hypoxia. Opticare was applied to protect the rats' eyes (eye lube and hyaluran 155g/0.53 oz.)

FG (3% dissolved in 0.9% saline, Sigma,) was injected using Hamilton syringe which was driven by a micromanipulator with two axis (Figure 2.4A). Each rat was placed prone with a

flexed neck. The most prominent vertebra at thoracic level (T) 1, was palpated as a guide to the location of the injection site which was made between C6 and C7 vertebrae. Under the microscope, the skin, fat, and muscles overlying the cervical spinal cord were retracted and ligaments between the sixth and seventh vertebrae were removed to expose the spinal cord unilaterally. To inject the FG, a Hamilton syringe (26 gauge) was driven into the dorsal horn of the cervical spinal cord contralateral to the cortical lesion and inserted diagonally away from the midline to a depth of 1.00 mm. Cautions were taken to avoid crossing the midline. The syringe was attached into a manipulator stand. FG solution (0.5 µL per rat) was slowly injected over three minutes then the needle was left for 5 minutes before withdrawing to avoid fluid drawback (Figure 2.4B). Then, muscles and skin were sutured. Antibiotic (Calmoxyl 150mg/ml) was given (dose 0.1 ml/g) subcutaneously and subcutaneous injection of the pain killer Buprenorphine (0.1mg/100g) were given post-surgery.

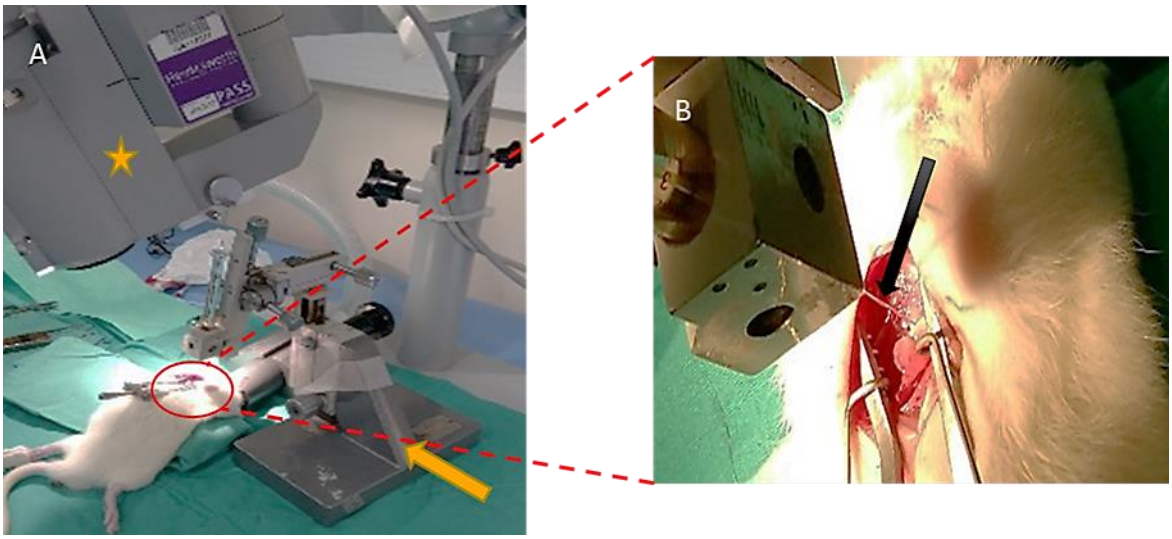


**Figure 2.4. FG surgical settings.**

(A) The manipulator stand (arrow), Hamilton syringe, and the microscope (star). (B) Magnified image of the surgical site the exposed spinal cord and the needle (arrow) is inserted in it.

### *2.3.4 Behavioural outcome assessments*

The behavioural tests for all animals started on P30, and continued until about 2-3 weeks after MCAO induction or ET-1 injection. This age was chosen because weaning has already occurred, as well as maturation of the sensorimotor system. Rats can perform skilled reaching before one month of age and can walk on a grid with few errors after P21 (Schallert and Woodlee, 2005b). All rats were tested under similar conditions to ensure comparability. The tester was the same for all tests and was blind to whether the animals had received an ischemic lesion or sham. Assessments involved four tests: reaching test, grid walk test, asymmetry placement test, and pasta test. Each animal was tested and placed in the assessment apparatus individually and tests were done at approximately the same time each day. All experimental and sham groups in the MCAO and ET-1 PIS models followed the same behavioural test protocol.

**Reaching test**

The reaching test was used to assess skilled forepaw usage and motor function (Chen et al., 2010, Schaar et al., 2010). Food was withdrawn 12 hours prior to the beginning the test. The rat was placed in a transparent Plexiglas box and reached through a small window to get food (single pellets) presented on an external shelf (Figure 2.5A). A successful attempt was counted when the rat reached, grasped, and brought food to its mouth. If the food piece dropped during this process, the attempt was counted as failed. The test ended when the number of trials reached 40 or when 30 minutes had passed; testing was conducted at P30, P35, P40, and P45.

**The asymmetry placement (cylinder) test**

This test is reliable for assessing limb asymmetry in neonatal and adult rodent models using ischemic brain lesions (Adkins et al., 2004, Grow et al., 2003). It was undertaken at P34 (Schallert et al., 2000). The cylinder test was used to assess forelimb use and neglect. The rat was placed in a transparent cylinder box and allowed to explore the box (Figure 2.5B). The number of times each forelimb was placed on the cylinder wall as the rat explored its environment was observed using a Samsung Camera at 2.6 zoom positioned above the cylinder at the centre of the opening (Figure 2.5C) and recorded using a slow motion video player over 2 minutes.

The number of placements and contacts of single and both limbs on the cylinder wall were counted. The asymmetry score for the contralesional limb was calculated as follows: contra-limb contacts + ½ both-limb contacts ÷ (total limb contacts) x 100 (Schallert and Woodlee, 2005a). Normal animals score near 50%; a lower percentage indicates diminished usage of independent contralateral paw movement relative to the ipsilateral paw usage and co-usage.

**Grid walk test**

This test was done 35 days after inducing the cortical lesion to evaluate motor coordination and placing deficits during locomotion (Gold et al., 2013). Using a webcam attached to a laptop, we counted the steps taken on the grid (Figure 2.5D) and the number of foot or hindlimb faults (Schaar et al., 2010) occurring when the whole limb fell in between the grid (Figure 2.5E), but not when the limb hung on with one or two digits. After 5 minutes, the test was ended and the counting was done visually by watching the video recording. Calculation of the footfault ratio was performed by dividing the total number of foot faults by the number of steps. The forelimb fault (FLF) percentage was calculated by dividing the contralesional FLF by the number of total steps, multiplied by 100%. The hindlimb fault (HLF) percentage was calculated correspondingly.

**Pasta test**

The pasta test described by (Whishaw and Coles, 1996) is a useful test for assessing the manual dexterity symmetry in the fine motor movements used in gripping and manipulating a piece of thin dry pasta in models of upper extremity impairment (Allred et al., 2008). Food was withdrawn 12 hours prior to the beginning of the test. In the test, the rat was placed in a transparent cylinder box and given four pieces of pasta, one piece at a time (4.0 cm strands of dry thin spaghetti), and was filmed using the same apparatus used in the asymmetry placement test. The rat holds the pasta with both paws symmetrically then uses coordinated asymmetrical paw movements to eat the pasta (Figure 2.5F). One paw, called the grasp paw, is placed further away from the rat's mouth, whereas the paw that is closer to the rat's mouth is called the guide paw. As the pasta is eaten, the rat moves the paws in a symmetrical holding pattern by adjusting one paw on top of the other. This symmetry is expressed as a percentage by counting the number of adjustments made with the forepaw ipsilateral to the lesion for each pasta piece, dividing it by the total adjustments, and then multiplying it by 100. Also, the amount of time that the rat

took to eat the pasta was recorded. Following unilateral hemisphere injury, one paw should be used less or not at all during this process (Allred et al., 2008).


**Figure 2.5. Behavioural tests started at P30 in PIS models.**

(A) A rat performing the reaching test task of reaching for a food pellet (arrow) on an external tray attached to the test box. (B) Exploratory activity of a rat while being tested in a cylinder box with the asymmetry placement test. (C) Videotape setting was prepared prior commencing the test. (D) A rat walking in the grid walk test. (E) An example of hindlimb fault (arrow). (F) A normal rat holds the pasta with both paws.

### *2.3.5 Transcardial perfusion*

Rats were perfused transcardially with a fixative (4% paraformaldehyde (PFA) in phosphate buffered saline (PBS)) for histological assessment. Perfusion was done at P45 for long-term histological analysis in all animal groups. For acute stage analysis, perfusion was done at P2 - 9. Following perfusion, all fixed brains were sectioned. First, the rats were anesthetized deeply with Euthatal (0.3 ml for P12-20 pups) and placed in a fume hood or specific perfusion table. Then, 50 ml of 0.1 M PBS (Sigma-Aldrich) at pH 7.4 was flushed in via cannula attached to a blunt needle inserted into the left ventricle of the animal heart (Figure 2.6A). Following the PBS, buffered fixative consisting of 4% PFA in 0.1 PBS, (pH 7.4) was infused gradually via the cannula using an electrical pump (Figure 2.6 B and C). The rat brain and spinal cord were then gently extracted. The rat tissue was preserved in the same PFA used for perfusion at 4ºC overnight, followed by washing three times with PBS and preservation in PBS containing 30% sucrose.


**Figure 2.6. Transcranial perfusion protocol.**

(A) A blunt needle (arrow) injecting the 4% fixative into the left ventricle of the animal heart. (B) The perfusion setting, including the table fume hood, solutions, and electrical pump. (C) The electrical pump used in the perfusion procedure.

### *2.3.6 Immunohistological outcome assessments*

Parallel sets of coronal brain sections (50µm) from fixed brains were collected from the frontal two-thirds of the brain (using a freezing sliding microtome) as free-floating sections. Eight coronal sections per brain were made serially from the two-thirds of the forebrain for immunohistochemistry (IHC) procedures. This was done for all animals in all animal groups. For FG+ and (Parvalbumin) PV+ cell counting, eight brain sections were collected from locations +2.50, +2.00,+1.50, +1.00, +0.50, 0.00, -0.50, -1,00 mm from the bregma according to the Paxinos and Watson atlas (Paxinos and Watson, 1998).

The sections were then either stained with cresyl violet or underwent IHC. For Nissl staining, the sections were mounted on gelatine-coated glass slides and incubated in cresyl violet solution for 5-20 minutes. They were then rinsed with distilled water before being dehydrated in a series of diluted ethanol in water and were finally dipped in Histoclear twice for 10 minutes each and coverslipped.

For IHC, sections were incubated at 4$^{o}$C overnight with gentle agitation in a cocktail containing PBS, 0.3% Triton X-100 (TPBS) for permeabilization, 3% appropriate blocking serum (Vector Laboratories, UK) and primary antibody (Table 2.2). The sections were then washed 3 times with PBS for 10 minutes each and were incubated in biotinylated secondary antibody (1:200 Vector Laboratories, UK) for 2 hours at room temperature with gentle agitation following by 3 washes with PBS for 10 minutes each. Next, the sections were incubated in streptavidin horseradish peroxidase (HRP) (1:200, Vector Laboratories, UK), for one hour with gentle agitation and then washed with PBS as above. Following this, the sections were incubated with 3, 3-Diaminobenzidine (DAB) and peroxide for 5 to 10 min which reacts with HRP to produce a colour reaction. Then, the sections were washed with PBS as described above. Finally, the sections were mounted on slides, dehydrated in gradual ethanol (Table 2.3), dried and then coverslipped for light microscopy.

| Primary antibodies | Antibody dilution | Company |
|---|---|---|
| HIF-1 | 1:1000 | Abcam |
| IBA1 | 1:500 | Abcam |
| GFAP | 1:1000 | Sigma |
| PV | 1:2000 | Sigma |
| FG | 1:50 | Merck Millipore |
| SMI-32 | 1:1000 | Biolegend |
| Pax6 | 1:500 | Covance |
| DCX | 1:1000 | Abcam |
| TUJ1 | 1:500 | Merck Millipore |

**Table 2.2. Names and dilutions of primary antibodies used in IHC research assessments.**

| Solution | IHC and lectin histochemistry dehydration protocol |
|---|---|
| 70% ethanol | 5 minutes |
| 90% ethanol | 5 minutes |
| 100% ethanol | 10 minutes |
| 100% ethanol | 10 minutes |
| histoclear | 10 minutes |
| histoclear | 10 minutes |

**Table 2.3. Dehydration protocol of the coronal brain sections.**

The following primary antibodies were used for the IHC assessments: hypoxia-inducible transcription factor (HIF-1) for hypoxia reaction (Sharp et al., 2001), a marker for microglia (ionized calcium-binding adapter molecule 1) (IBA1), which recognizes microglia in both normal (Ito et al., 1998) and ischemic perinatal rat brain; a marker for astrocytes (glial fibrillary acidic protein) (GFAP) to detect any inflammatory reaction (Burtrum and Silverstein, 1994), a marker for calcium-binding protein and inhibitory interneuron marker (PV) to detect functional interneurons (Araki et al., 1994) and a marker for non-phosphorylated neurofilaments (SMI-32) to identify neuronal cell bodies, thick axons, and dendrites (Merigo et al., 2005). To detect the traced CST neurons in the cortex (Sarkar et al., 2014), anti-fluorescent gold antibody was used (FG). A separate set of sections was incubated overnight following the same primary antibody incubation protocol described above, but using biotinylated B4-isolectin (1:1000, Vector Laboratories) to detect microglia (Genade and Lang, 2011). Primary antibody details are listed in Table 2.2.

All sections were visualized under light microscopy at different magnifications to study the morphological changes in the cortex in both brain hemispheres in all animal groups.

**Histological Quantification of FG+ cell**

All FG+ neurones were counted after Immunoperoxidase staining using an anti-fluorogold antibody. Scanned images of sections immunostained with anti-FG antibody were processed in ImageJ software (v 1.48r, Wayne Rasband, National Institute of Health, USA). The cyto-architectural landmarks at the borders of the cortical regions were detected to outline the following regions: medial, motor, somatosensory, and lateral cortex.

Only animals with FG immunopositivity confined to the spinal cord contralateral to the brain lesion were included for cell counting. Lines separating cortical regions in both hemispheres were drawn in each coronal brain section, and automated quantifications of FG+ neurons were done using ImageJ software. Each cortical region was processed individually for all experimental and sham rat brains. Then, the cells were automatically detected by the software and counted (Figure 2.7). These analyses were conducted blind for both the experimental and sham groups.

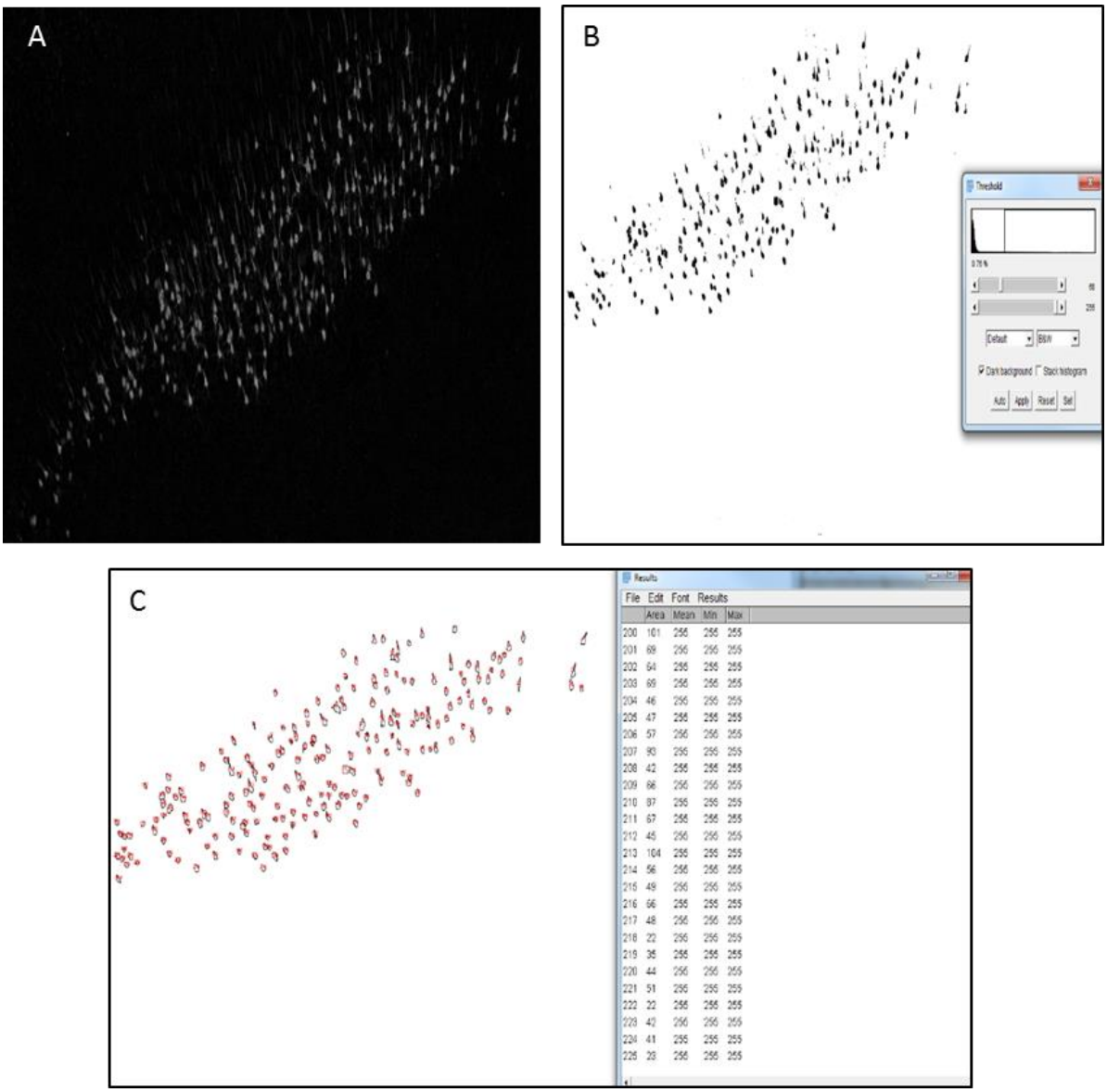


**Figure 2.7 Quantification of FG+ cells using ImageJ.**

(A) A coronal section with FG+ cells in grey scale before (B) subtracting the background and adjusting the threshold. (C) An example of the cell counting processes.

**Histological Quantification PV+ cell**

Following the same protocol as for FG+ cell counting, all sections were immunostained with anti-PV antibody, imaged and processed to automatically quantify PV+ neurons. The cortical regions that were assigned to count PV+ cells were the medial, motor, and lateral cortices.

### *2.3.7 Statistical analyses*

Behavioural and histological quantitative data were analysed using IBM SPSS Statistics version 24. The groups were first analysed for a normal distribution using a normality test, and then parametric or non-parametric statistical tests were performed as appropriate. For the normally distributed data, parametric tests were conducted to compare between means, with independent sample t-test used for non-paired groups and dependent sample t-test used for paired groups. For the non-normally distributed data, the Mann Whitney U non-parametric test was used to compare between two non-related pairs of experimental groups. A non-parametric paired test, the Wilcoxon signed ranks test, was used to compare between two related groups. Significance was defined as $P \leq 0.05$.

## 2.4 Stem cell experiment methodology

### *2.4.1 Experimental design*

We first tested the viability and number of hNPCs after culturing them overnight in preparation for cell encapsulation for *in vitro* and *in vivo* experiments the next day. We then characterized the cells after an *in vitro* differentiation experiment in 2 dimensions (D) versus 3D culture at three time points using immunocytochemistry. Biosafety hazard and contamination regulations were followed strictly, according to the protocols of the stem cell laboratory at Newcastle University.

In parallel to the i*n vitro* experiment, two *in vivo* experiments were performed to study the transplanted NSCs/ECM and the host's cellular behaviour at two time points: one and three months. The sham group received only ECM transplantation and underwent a similar procedure as the NSC/ECM groups for the one-month time point. Behavioural tests were then performed at P33, before the animals were perfused transcardially. All brains were cryopreserved and microsectioned for immunohistochemical characterization by fluorescence microscopy (Figure 2.8).

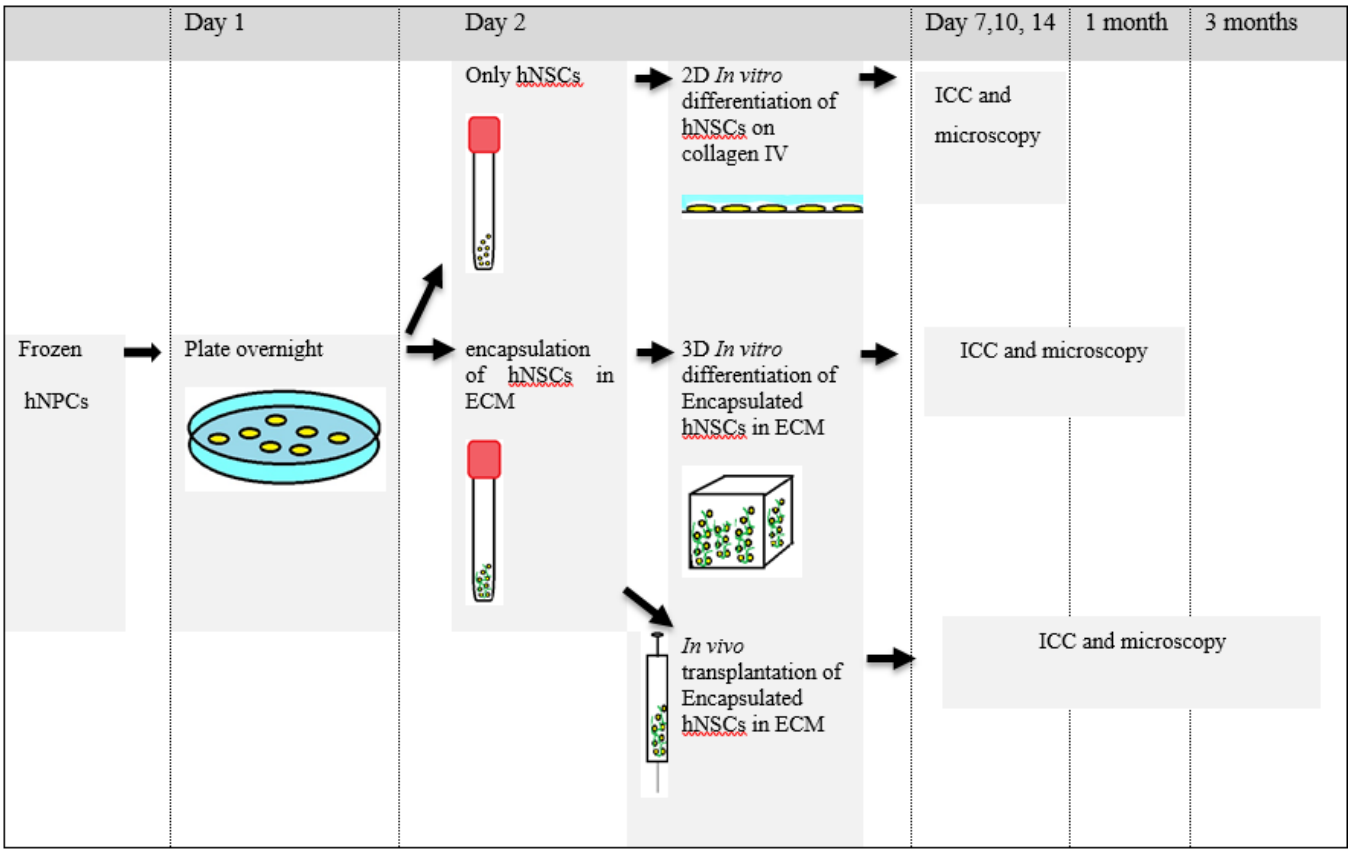


**Figure 2.8. Experimental design diagram of the stem cell experiment.**

### *2.4.2 Cells culturing and encapsulation for in vitro and in vivo experiments*

One vial containing 1.5 million frozen human induced pluripotent stem cells (hiPSCs) derived neural stem cells (iPSC-NSCs, ax0015) was purchased from Axol Bioscience (Cambridge, UK). The hiPSC derived NSCs were obtained from a male newborn cord blood donor (CD34+) and reprogrammed. More information about the donors is readily available online (https://www.axolbio.com/). The NSCs were derived from hiPSC under fully defined neural induction conditions.

Procedures for thawing and plating cells for the first 24 hours and then 2D differentiation into the neural lineage, and the details of all reagents used, were as stated by the manufacturer (Axol Bioscience, Cambridge, UK) and available online (https://www.axolbio.com). The 3D *in vitro* differentiation and the transplantation protocol were adopted and modified from the Axol Bioscience protocol by Melissa R Andrews that is available online https://www.axolbio.com) and (Liang et al., 2013, Zhong et al., 2010). Frozen hiPSC -NSCs ($1.5 \times 10^6$) were quickly thawed in a 37ºC water bath and transferred into a 50 mL sterile conical tube in a sterilized biological safety cabinet. Then, 10 mL of pre-warmed, 37ºC, Neural Plating–XF Medium (Axol Bioscience, ax0033) was added to the conical tube before the tube was centrifuged at 200 x g for 5 minutes at room temperature. After centrifuging, the supernatant was aspirated and the cell pellet was re-suspended in the Neural Plating–XF to achieve a density of 200,000 cells/cm2. Finally, the NSCs were plated on a 6cm petri dish (Sigma) coated overnight at 37ºC, 5% CO2 with SureBond (Axol Bioscience, ax0041) at a volume of 200 µl per cm2. The plated cells were then checked under the light microscope in the lab to ensure cell adherence to the substrate and even cellular distribution in the culture plate (Figure 2.9A).

On the following day, NSC viability and general conditions were observed under the lab microscope to check that the cells reached 70-80% of confluency. Figure 2.9B shows an example of 80% confluency. The cells were then rinsed once with Dulbecco's-PBS without calcium or magnesium (BSS-1005-A , MilliTrace), 2 mL D-PBS per 10 cm2 culture surface area, and 1 mL per 10cm2 of detachment solution Unlock-XF (Axol Bioscience, ax0044XF) at room temperature was added immediately and kept for 5 minutes at 37ºC. The Unlock-XF solution was then diluted by adding four volumes of pre-warmed, 37ºC, Neural Expansion-XF Medium followed by centrifugation at 200 x g for 5 minutes at room temperature. After centrifuging, the supernatant was aspirated and the cell pellet was re-suspended.

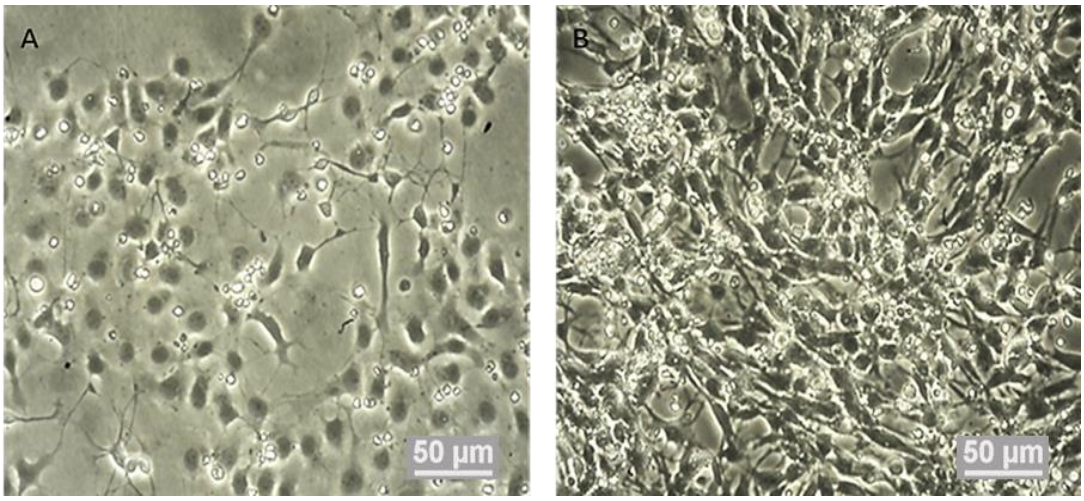


**Figure 2.9 Routine lab check-up for the cultured hNSCs prior to *in vitro* culture and *in vivo* transplantation.**

Examples of NSC check-up on (A) plating day, to check for adherence and (B) after 24 h, to check for 80% confluency.

For the 2D *in vitro* experiment, the cell pellet was re-suspended with Neural Plating–XF Medium (Axol Bioscience, ax0033), Axol Sure GrowthX Recombinant Human FGF2 (Axol Bioscience, ax0047X) and EFG (Axol Bioscience, ax0047) at appropriate concentrations to achieve a seeding density of 200 µl per $cm^2$.

For the 3D *in vitro* experiment and transplantation surgery, the NSC/ECM complex was prepared. The cell pellet was re-suspended with freshly prepared HyStem-C hydrogel from a HyStem®-C cell culture scaffold kit containing three vials of hyaluronan, gelatine, and cross-linker (HYSC020, Sigma Aldrich) at a concentration of 100,000 NSCs. To achieve this concentration, hiPSC-NSCs ($1.5 \times 10^6$) were resuspended in a mixture of 12.5 µl hyaluronan, 12.5 µl gelatine, and 7µL cross-linker to form a NSC/ECM complex (H:G:P=2:2:1). This complex was used for both the *in vitro* 3D differentiation and *in vivo* grafting. A similar mixture was used immediately after in preparation for the transplantation surgery.

### *2.4.3 The in vitro 2D differentiation protocol*

Collagen IV (C6745, SIGMA) coated, 12-chamber, sterilized glass microscopy slides (81201, IBIDI), and with well dimensions of 7.5 × 7.5 × 8 mm were used. 100 µL of the re-suspended NSC pellet was plated in each chamber at a seeding density of 70,000 cells/$cm^2$ and incubated in at 37ºC, 5% CO2. On the next day, the medium was replaced with fresh, pre-warmed, 37ºC, Neural Maintenance-XF Medium without growth factors FGF2 or EFG, and after a further 24 hours, only two-thirds of the medium was replaced. Then, half of the medium was replaced every two days. A daily microscopic observation routine was performed to check cell viability and differentiation (Figure 2.10). Contamination-free culture was maintained throughout the experiment by using sterile procedures and performing a daily microscopic inspection in the lab.

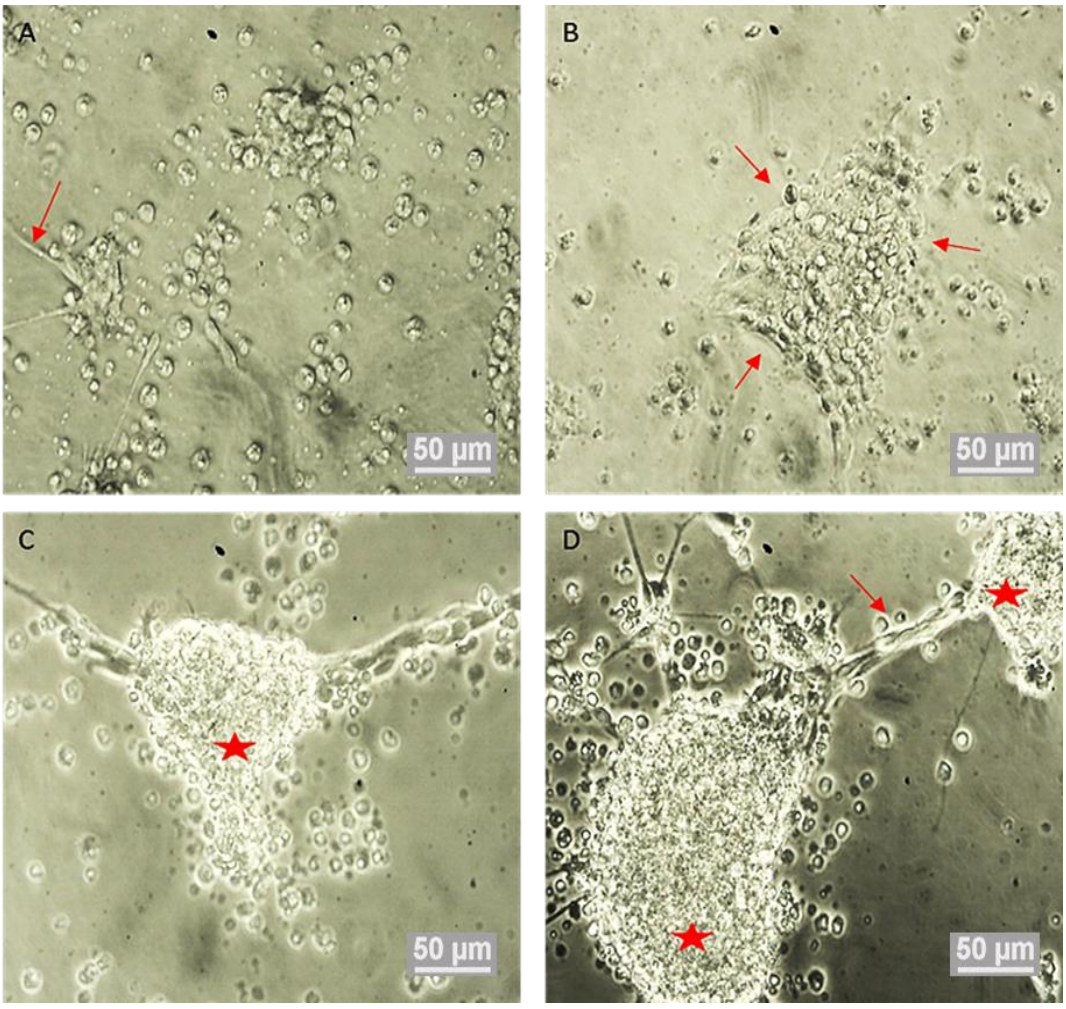


**Figure 2.10 Routine observation of NSCs in 2D culture.**

Examples of the NSC observation routine under the microscope to ensure cell differentiation and check morphology. (A) NSCs attaching to the 2D substrate and extending short processes (arrow) after 24 hours, (B) NSCs starting to gather in clusters (arrows) after 48 hours, and (C) NSCs form large clusters (starts) that are (D) connected (arrow) by 10 days after the start of differentiation.

The NSCs in 2D culture were then fixed and immunostained at three time points: 10, 14, and 17 days after initiation of differentiation. For fixation, NSCs in the 12-chamber slide were rinsed twice with PBS, and then incubated with 4% PFA in PBS (pH 7.4) for 15 minutes at room temperature with gentle agitation followed by two PBS rinsing steps. The slides were kept at $4C^0$ until immunofluorescence assessment.

### *2.4.4 The in vitro 3D differentiation protocol*

The NSC/ECM complex was plated in four micro-inserts (Culture-Insert 4-Well, ibidi, 80409) that were placed in a 2-chamber slide (80281, ibidi) in a 100 mL petri dish. The NSC pellet was re-suspended in HyStem-C hydrogel at a concentration of $1\times10^5$ cells/5 µl. Next, 5 µL of the NSC/ECM complex was plated in each micro-insert (Figure 2.11A and B) and incubated at 37ºC, 5% CO2 for one hour to ensure a successful gelling process. Once the appropriate gel texture was achieved, 140 µL of pre-warmed, 37ºC, Neural Maintenance-XF Medium with growth factors FGF2 and EFG was added into each insert and the dish was returned to the warm incubator. The same protocols for changing the medium and performing microscopic observations were followed as described in the section on 2D differentiation. Figure 2.11C-F shows examples of the routine for observing NSCs under the microscope to ensure cell differentiation and check morphology in the ECM.

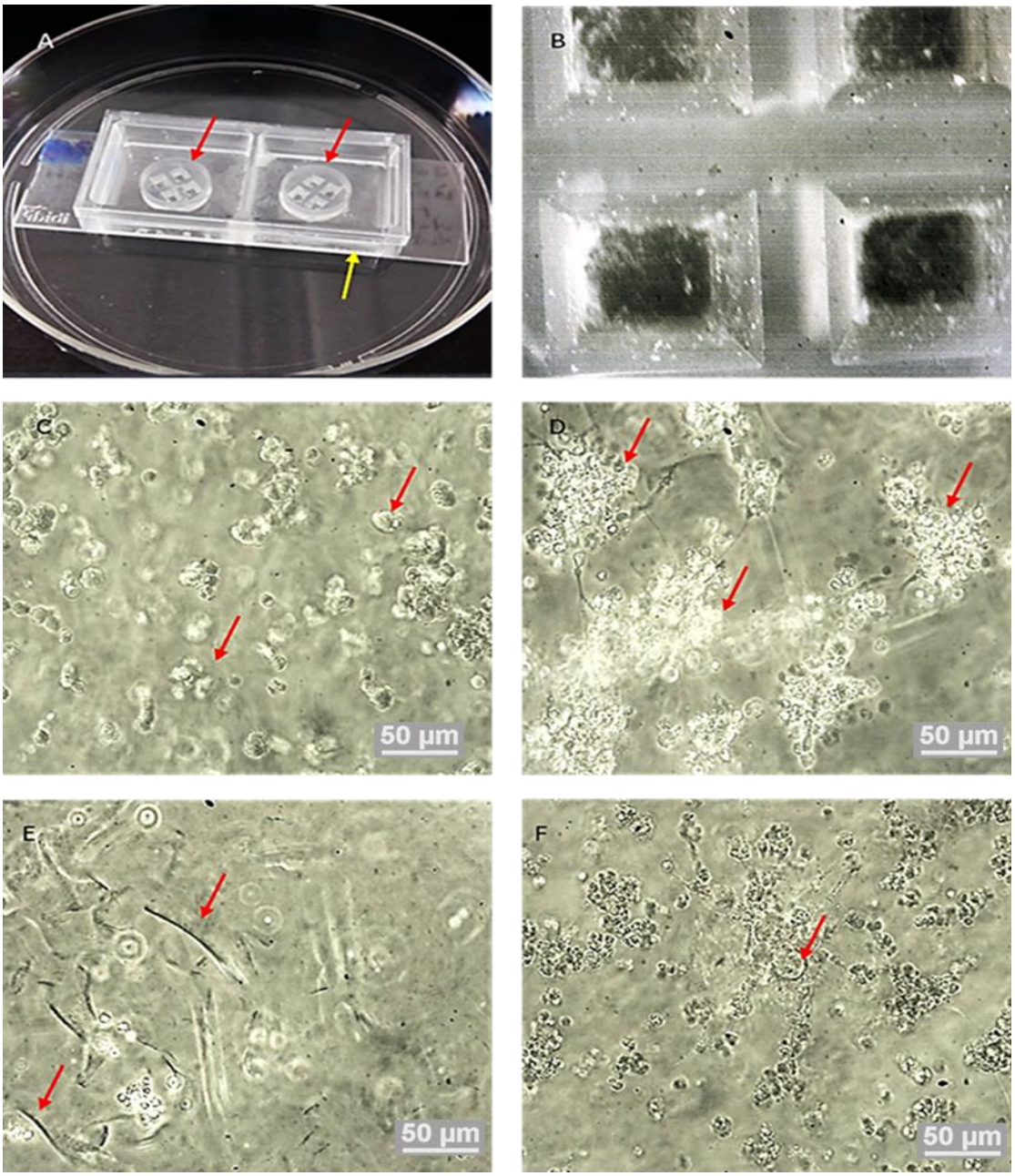


**Figure 2.11 Observation routine for NSCs in 3D culture.**

Examples of the NSC observation routine under the microscope to ensure cell differentiation and check morphology in the ECM. (A) Low magnification image of the 2 sets of 4 micro-insert (red arrows) placed in two chambers slide (yellow arrow), including NSCs-ECM. (B) Magnified image of the 4 micro-insert with NSCs-ECM. (C) NSCs with a rounded shape and no extended processes (arrows) after 24 hours. (D) NSCs starting to gather in clusters (arrows) after 6 days. (E) NSCs extend long processes (arrows). (D) Larger cell bodies within the clusters 14 days after start of differentiation.

Cell fixation was done as described in the 2D differentiation section at 4 time points; 10, 14, 17, and 43 days after initiation of differentiation. However, the rinsing steps were longer, 30 minutes, to ensure PBS penetration into the hydrogel.

### *2.4.5 The NSCs/ECM transplantation protocol*

NSCs/ECM complex was transplanted into the lesioned SMC of the PIS model at P14. Only the hyaluronan and gelatine hydrogel components were mixed and added to the NSC cell pellet. Samples were aliquot into 8 sterilized vials then taken out of the sterilized hood in an ice container to the surgery room. The cross-linker was added just before transplantation due to the small time window for gelling (20 minutes for the hydrogel ratio that we used). Next, 2 µl of the NSC/ECM complex was injected into the SMC (AP1.3, MD2, and DV1.8) at a rate of 0.5 µ/min. Each rat received a 100,000 cells in 2µl of NSC/ECM complex (Table 2.4).

| Intracranial injection at AP1.3, MD2, DV1.8 | Rats | | | | | | | |
|---|---|---|---|---|---|---|---|---|
| | 1 | 2 | 3 | 4 | 5 | 6 | 7 | 8 |
| 2 µl of hNSCs-ECM/ or ECM for 4 min | | | | | | | | |
| Pause 1 min | | | | | | | | |
| remove the needle up | | | | | | | | |

**Table 2.4. Stem cells injection check list.**

Six sham operated animals received ECM only with no NSCs following the same surgical procedure as the experimental group. The experimental group included fifteen P14 rat pups. Rats in both groups received the NSCs/ECM intracerebral injections two days after receiving the ET-1 injections. Each animal was anesthetised by nasal inhalation of isoflurane and underwent the same surgery procedure described in the ET-1 surgery (section 2.3.2). For furthered gelling time confirmation, a quick simple test was performed just prior to starting the surgery. The gelling time of a drop of the hydrogel was tested by turning on a timer once the cross-linker was added. A pipette tip (Volume 1,000 µL) was taken and inserted into the drop allowing the fluid to get inside the tip via capillary action. Once gelling started, the hydrogel was no longer taken up by the tip and the timer was stopped to set this point of time. Gelling time was found to be 12 minutes after adding the cross linker in our hands (Figure 2.12).

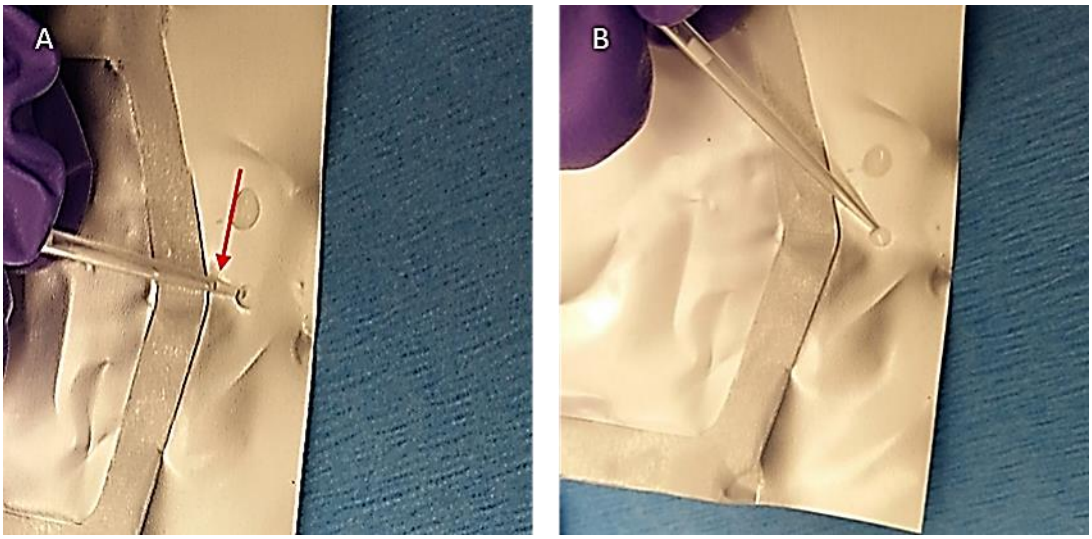


**Figure 2.12 ECM gelling time test prior to grafting.**

(A)The hydrogel in a fluid state being taken up into the pipette tip (arrow) 4 minutes after the cross-linker was added. (B) Hydrogel is in gel form at 12 minutes after adding the cross-linker, as indicated by no fluid inside the pipette tip.

The size of the autoclaved Hamilton syringes used in the surgery to deliver the NSCs/ECM while in liquid form were 26 gauge to allow for the flow of the suspension. Prior to injection, the cross-linker agent of the HyStem-C was added to one of the eight NSC/ECM vials and the timer was started. The needle was lowered after breaking the dura with fine tip needle. Injection of the NSCs/ECM began 4 minutes after adding the cross-linker and continued for 6 minutes. Then, the needle was kept in its place for an additional minute to prevent flow back and was then withdrawn slowly. The Hamilton syringes were cleaned with sterilized saline and 70% ethanol after each injection. Suturing and post-surgical care were conducted as described in the ET-1 surgical protocol (Section 2.3.2).

We did not use immunosuppression to ameliorate the immune reaction, that occurs due to the immediate reaction of microglia after grafting (Glezer et al., 2007), as some studies have argued that using immunosuppression will prevent neural repair, or lead to deterioration in the underlying disorder and prevent the beneficial role of microglia in the repair of the lesioned brain tissue (Glezer et al., 2007, Kulbatski, 2010). Furthermore, the immune system is too immature and less able to mount an immunogenic response to xenogeneic transplants in neonate rodents (Coenen et al., 2005, Englund et al., 2002, Jablonska et al., 2010).

### *2.4.6 Immunohistological assessments*

Parallel sets of coronal brain sections (50μm) from fixed brains were collected serially and stained with cresyl violet or Immunoperoxidase following the same protocol described before for the immunohistological outcome assessments in the PIS model (Section 2.3.6). In addition, immunofluorescent staining for IHC and immunocytochemistry (ICC) was done by incubating the sections or cells with one or two primary antibodies (double labelling) in a blocking buffer at 4°C overnight. The sections or cells were then washed and incubated for two hours in the dark with one (or two, if performing double labelling) of the secondary antibodies: Alexa Fluor 488-conjugated goat anti mouse IgG and Alexa Fluor 594-conjugated goat anti- rabbit (1:200–500; Abcam). Nuclei were counterstained with 4',6-diamidino-2-phenylindole (DAPI) using a hard set of mounting medium with DAPI (Vectashield). Fluorescence signals were detected with a Nikon (Melville, NY) PCM-2000 laser-scanning confocal microscope at excitation/emission wavelengths of 650/668 nm (Alexa Fluor 647, far red), 590/617 nm (Alexa Fluor 594, red), 495/519 nm (Alexa Fluor 488, green), or 360/400 nm (DAPI, blue). Sections or cells were subjected to imaging.

The primary antibodies described for IHC assessments in the PIS model (Section 2.3.6) were used in this experiment as well. These primary antibodies were for IBA1, GFAP, PV (Nodari et al., 2010), and biotinylated B4-isolectin (1:1000 for IHC, 1:200 for ICC, Vector Laboratories) to observe neovascular formation (Benton et al., 2008). Additional primary antibodies used in this experiment included antibodies to neural cell adhesion molecules (NCAMs)(Smith et al., 2017b); markers for human cell cytoplasm but not rodent or non-human primate cells (STEM121); markers for Ku80 Protein located in human cell nucleus only (STEM101) (Guzman et al., 2007, Sareen et al., 2014, Tornero et al., 2013); a marker for human GFAP, a marker for astrocytes and radial glial cells, but not rodent GFAP (STEM123) (STEM123) (Sareen et al., 2014); paired box protein (PAX6), a marker for proliferating cortical progenitor cells including radial glia (Bayatti et al., 2008); doublecortin (DCX), a marker for migrating neuroblasts and neurogenesis (Lam et al., 2014); Beta-III-Tubulin (TUJ1), a marker for neuron-specific class III β-tubulin in post-mitotic neuroblasts and neurons (Stevanato et al., 2015); MAP2, which has neuron-specific expression in dendrites and soma (Guzman et al., 2007); neural synaptic vesicle marker (synaptophysin) (Smith et al., 2017b); TBR1, an early post-mitotic cortical glutamatergic neuron marker (Ali et al., 2012, Bayatti et al., 2008); and CTIP2, a marker for deep layer cortical neurons (Ip et al., 2011). Details for the primary antibodies are listed in Table 2.5.

| Primary antibodies | Antibody dilution | | Company |
|---|---|---|---|
| | IHC | ICC | |
| IBA1 | 1:500 | - | Abcam |
| GFAP | 1:1000 | 1:200 | Sigma |
| PV | 1:2000 | - | Sigma |
| Pax6 | 1:500 | 1:100 | Covance |
| NCAM | 1:1000 | 1:100 | Santa Cruz Biotechnology |
| STEM121 | 1:3000 | 1:500 | Stem Cells, Inc. |
| STEM101 | 1:1000 | 1:50 | Stem Cells, Inc. |
| STEM123 | 1:2000 | 1:250 | Stem Cells, Inc. |
| DCX | 1:1000 | 1:250 | Abcam |
| TUJ1 | 1:500 | 1:100 | Merck Millipore |
| Map2 | 1:500 | 1:200 | Abcam |
| Synaptophysin | 1:5000 | 1:200 | sigma |
| TBR1 | - | 1:100 | Abcam |
| CTIP2 | 1:300 | - | Abcam |

**Table 2.5 Names and dilutions of primary antibodies used in IHC and ICC research assessments.**

## 2.5 Image acquisition

Coronal brain sections with Immunoperoxidase staining were imaged using upright light microscopy (Olympus, BX6) and an attached colour digital camera (Axiocam Zeiss). Images were viewed in Axiovision 4.8 software. For quantitative analyses, images of FG-traced, anti-PV, and cresyl violet stained sections were scanned using the Leica SCN400 Slide Scanner (Newcastle Biomedicine Biobank Imaging facility) at 20x magnification and 3.08 zoom.

The facilities of the Bio-Imaging Unit at Newcastle University were used for fluorescent image acquisition. Images of coronal brain sections were captured using the upright fluorescent microscope Zeiss AxioImager with an automated stage. Ultraviolet incident light was used to visualize FG+ cells in the spinal cord and validate the success of unilateral FG injections.

To obtain 3D fluorescence images of the double-labelled sections, a fully motorized, confocal-based upright Nikon Ni was used. Inverted light and fluorescent confocal microscopy (Nikon A1R) was used to capture images of fluorescent double-labelled cells cultured *in vitro*. Both microscopes had a colour digital camera (Nikon, DS-Fi1 2560 x 1920) that was used to image the *in vitro* cultured cells.

Image acquisition was done at 4, 10, 20, 40, 100 (Oil) magnification and viewed and produced in NIS-Elements Viewer 4.2. Adobe Photoshop CS6 was used to prepare figures, with resolution set at 300 pixels per inch.

# Chapter 3 .Perinatal Ischemic Stroke Model: MCAO and ET-1

## 3.1 Introduction

In rodents, inducing focal ischemia utilizing the middle cerebral artery occlusion (MCAO) or application of endothlin-1 (ET-1) methods results in vascular distribution of the SMC. The MCAO method involves permanent occlusion that results in severe ischemic injury, as indicated by caspase-3 activity where apoptosis-like cell death also occurs during the first 24 hours (Manabat et al., 2003, Wen et al., 2004). PIS can be modeled by the intracerebral ET-1 using the stereotaxic frame to produce focal ischemia in adult and aged rat brains (Gennaro et al., 2017, Soleman et al., 2010, Windle et al., 2006).

It is widely accepted that research with animal models is crucial to developing and testing new therapies. Different methods have been utilized to model perinatal ischemic stroke in rodents considering the extent the animal model reflects humans in terms of the way the nervous system functions and develops.

The aim of this experiment was to develop and compare two separate models of perinatal ischemic stroke (PIS) capable of causing anatomical lesion to the limb sensorimotor cortex (lSMC) and sensorimotor behavioural dysfunction in P12 Wistar rat neonates: 1) MCAO at the level of the temporal bone, and 2) injection of reversible vasoconstrictor ET-1 directly into the lSMC. Sham operations were performed for each model.

## 3.2 Results

All animals underwent three behavioural tests. Firstly, a weekly reaching test was done at four time points: postnatal (P) P31, P38, P45, and P51. Then, cylinder and grid walking tests were performed on experimental and sham animals at P35-40 before they were perfused at P40-45. Finally, all brains were sectioned coronally prior to being processed histologically for assessment by immunohistochemistry (IHC).

### *3.2.1 MCAO Model*

**Animal numbers**

P12 Wistar rats underwent three separate MCAO/sham surgeries; the total number and the subcategory values of the participating rats are detailed in Table 3.1. The MCAO surgery involved craniectomy at the level of the temporal bone and electroligation of the distal middle

cerebral artery (MCA) on the left side of the brain; 13 P12 rats underwent this surgery. One died during the MCAO surgery and two were excluded due to surgical errors during craniectomy that led to mechanical brain damage. The exclusion was done immediately after the surgery and before performing any IHC. Animals were transcardially perfused with fixative (4% buffered paraformaldehyde (PFA)) at different time points post-surgery to test for hypoxia and inflammation by IHC in the acute stage: one rat on Day 2, two rats on Day 5, one rat on Day 9, and one rat on Day 20. Five MCAO rats were perfused at P40-45 following behavioural outcome assessments and the brains processed for IHC.

The sham surgery involved only craniectomy with no MCAO; this was done to 16 P12 rats, one of which was excluded due to a technical error during craniectomy that led to mechanical brain damage. The exclusion was done immediately after the surgery and before performing any IHC. Perfusion for IHC assessment was done at time points parallel to those for the MCAO rats: two rats on day 2, two rats on day 5, one rat on day 9, one rat on day 20, and 9 rats on day 33 after surgery. Five sham rats were tested behaviourally between P40-45.

| Groups | Total number | Perfusion time points for IHC | | | | | Behavioural assessment | Number of excluded rats* |
|---|---|---|---|---|---|---|---|---|
| | P12 | 2D/P14 | 5D/P17 | 9D/P21 | 20D/P32 | 33D/P45 | P40-45 | |
| MCAO | 13 | 1 | 2 | 1 | 1 | 5 | 5 | 3 |
| Sham | 16 | 2 | 2 | 1 | 1 | 9 | 5 | 1 |

**Table 3.1 The number of animals included and excluded in each time point of the MCAO model and sham groups.**
* Exclusion reasons were described in the text.
D= days post-surgery, P=postnatal age.

**Behavioural Results and the Quantitative Analyses**

A total of 10 rats (sham n=5, MCAO n=5) underwent behavioural testing. Three behavioural tests were applied using similar procedures for both the MCAO and sham group. The reaching test was performed 3 times for each group, and the asymmetry placement test and the grid walking test were done once for each group. Statistical comparisons were carried out using non-parametric tests due to the small sample size.

**Grid walk test**

Data from this test were recorded as described in Chapter Two. The forelimb fault (FLF) percentage was calculated by dividing the contralesional FLF by the number of total steps and multiplied by 100%. The hindlimb fault (HLF) percentage were calculated correspondingly. Overall, we found that MCAO did not adversely affect the placement of forelimb (FL) and the hindlimb (HL) contralateral to the lesion ($p=0.69$; Mann Whitney U test) (Figure 3.1A) and ipsilateral to the lesion ($p=0.84$; Mann Whitney U test) (Figure 3.1B) compared to the sham group.

The figure shows no detectable difference or trend between the two groups was in the percentage of FLF and HLF in the limb contralateral to the lesion (Figure 3.1A).

Interestingly, the median total steps for the forelimb and hindlimb contralateral and ipsilateral to the lesion demonstrated a similar trend between the MCAO and sham groups. The MCAO animals showed a tendency to take more steps than sham animals; this reached statistical significance for the forelimb ($p=.05$; Mann Whitney U test), but not for the hindlimb ($p=.15$; Mann Whitney U test) (Figure 3.1C).

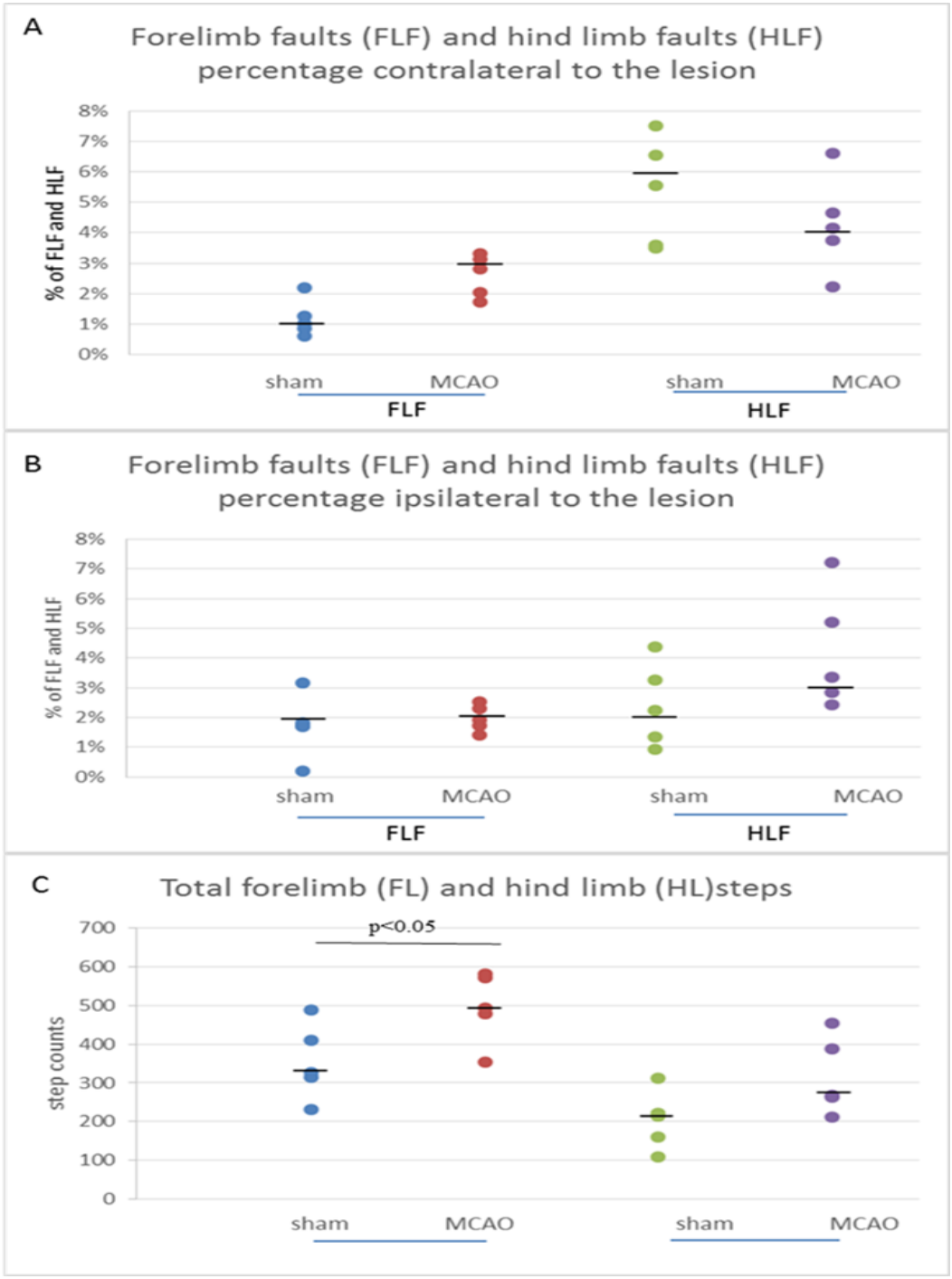


**Figure 3.1 The grid walk test outcomes in MCAO model and sham animals.** (A) MCAO caused a small but not significant increase in FLF contralateral to the lesion compared to sham animals but a small but not significant decrease in HLF. Black bars show the median values. (B) MCAO did not significantly affect footfaults ipsilateral to the lesion. (C) MCAO caused a statistically significant increase in FL steps taken ($p<0.05$) and a small but not significant increase in HL steps taken.

**The Asymmetry Placement Test**

Data from this test were recorded as described in Chapter 2. The number of placements and contacts made by single and both forelimbs on the cylinder wall was counted for both sham and MCAO animals. The asymmetry score of the contralesional limb was calculated as follows: contra-limb contacts + ½ both-limb contacts ÷ (total limbs contacts) x 100 (Schallert and Woodlee, 2005a). No significant difference was found in the median asymmetry score between groups (p=0.60; Mann Whitney U test). The typical score is around 50% (Schallert and Woodlee, 2005a), and rats in both groups mainly used both forelimbs symmetrically (Figure 3.2A).

Similarly, the number of limb contacts showed no significant differences between MCAO and sham animals for the limb ipsilateral to the lesion, the limb contralateral to the lesion, or for both limbs touching the wall (p=0.26, 0.30, 0.45 respectively; Mann Whitney U test) (**Error! Reference source not found.**) (Figure 3.2B). Non-parametric tests were used because of the small sample size in this experiment.

| Groups | Median | | | | |
|---|---|---|---|---|---|
| | Asymmetry score | Ipsilesional paw contact | Contralesional paw contact | Both paw contact | Total paw contact |
| MCAO (n= 5 ) | 53% | 28 | 35 | 6 | 67 |
| sham (n=5) | 46% | 27.5 | 25 | 5 | 56 |

**Table 3.2 The median scores of the asymmetry placement tests and the limb contacts in MCAO and sham animals.**

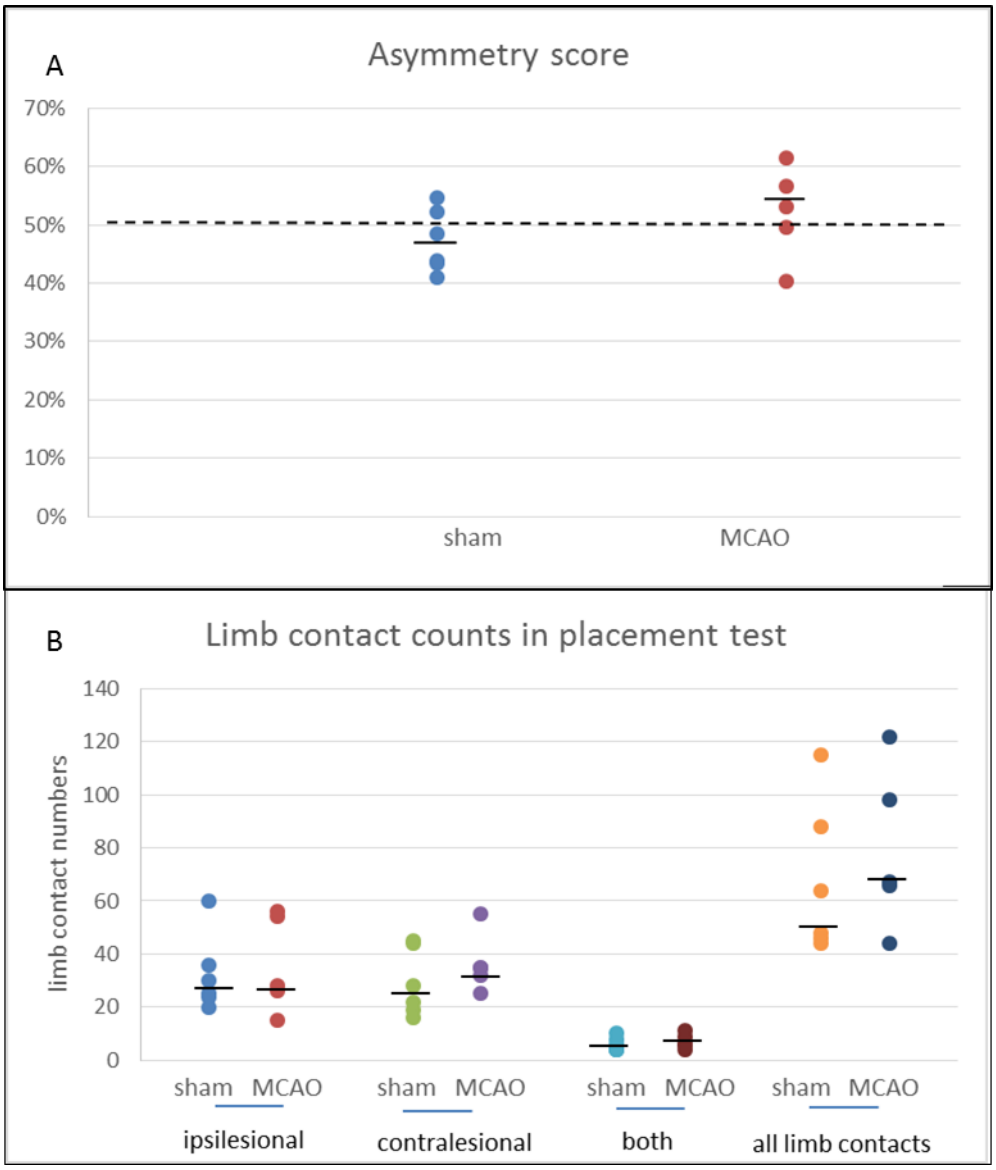


**Figure 3.2 Average of the asymmetry placement test and limb contacts in MCAO model and sham animals.**

(A) Non-significant deficit in the symmetry score for MCAO animal models compared to the sham animals, the dashed line marks 50% where the number of using both limb is equal. (B) Also, no significant difference in the number of contacts made by the forelimbs in MCAO compared to sham animals was found. Black lines are the median values.

In conclusion, is that there was no detectable difference between the MCAO and sham groups, so we decided not to pursue these experiments further. The following behavioural tests were excluded:

**Reaching test**

The reaching test was eventually omitted from our protocol due to the challenges in distinguishing the motive for limb use, as it was noticed that rats might use the limb ipsilateral to the lesion due to limb preference; animals start using one limb and continue to do so until they become accustomed to this limb choice. This bias is usually avoided in adult rat studies by training them to use only the limb contralateral to where the lesion will be made for reaching as a baseline, or by performing a baseline test prior to the lesion surgery However, these pre-surgery protocols were inapplicable in our study since our rats were newborns during the pre-surgery period. Moreover, the corticospinal tract (CST) is not myelinated until P28 and the pups aren't weaned before P21-28 so have no motivation to reach (Schallert and Woodlee, 2005a). Thus, no training or behavioural investigations could be conducted before the surgery.

Figure 3.3 shows the reaching test for the MCAO and sham groups, and an additional normal rat group added to compare the laterality index, at four time points: P31, P38, P45, and P51. To assess limb preference, the laterality index for each group was calculated as follows: (ipsilateral limb reaches - contralateral limb reaches) / (ipsilateral limb reaches + contralateral limb reaches). Scores are between 1 and -1, with 1 considered to be ipsilateral limb preference, -1 contralateral limb preference, and 0 no preference. We found a shift toward using the ipsilateral limb (left limb) that could have been a result of the lesion. However, the shift toward using the left limb was observed even in normal (unoperated) rats which might indicate a bias toward left limb usage. It also was noticed that during the tests, the rats started their reaching using both limbs, and then they chose the limb with more successful reaches as a preference.

When this preferred limb is the ipsilateral one, the lesion effect on the contralateral limb will be confounded (Allred et al. 2008). In a trial done to avoid this bias, the reaching box cage was modified by inserting a wall into the reaching test box a few mm from the window to try and force the rats to use the contralateral limb. However, this was unsuccessful since the rats, at this age, were still able to fit their small bodies against the wall and then use either limb for reaching. Thus, the bias was unavoidable, unless perhaps we were prepared to wait longer until the rats

gained more weight, and so we consequently omitted the reaching test from the behavioural tests.

**Pasta test**

The test was not found to be suitable for testing cortical asymmetry deficits. A trial for normal rats was performed and we found that non-experimental rats can use only one paw to hold the pasta independently without using the other hand which will confound the comparison to lesioned rat performance (Figure 3.4). Therefore, this test was not included in our protocol.

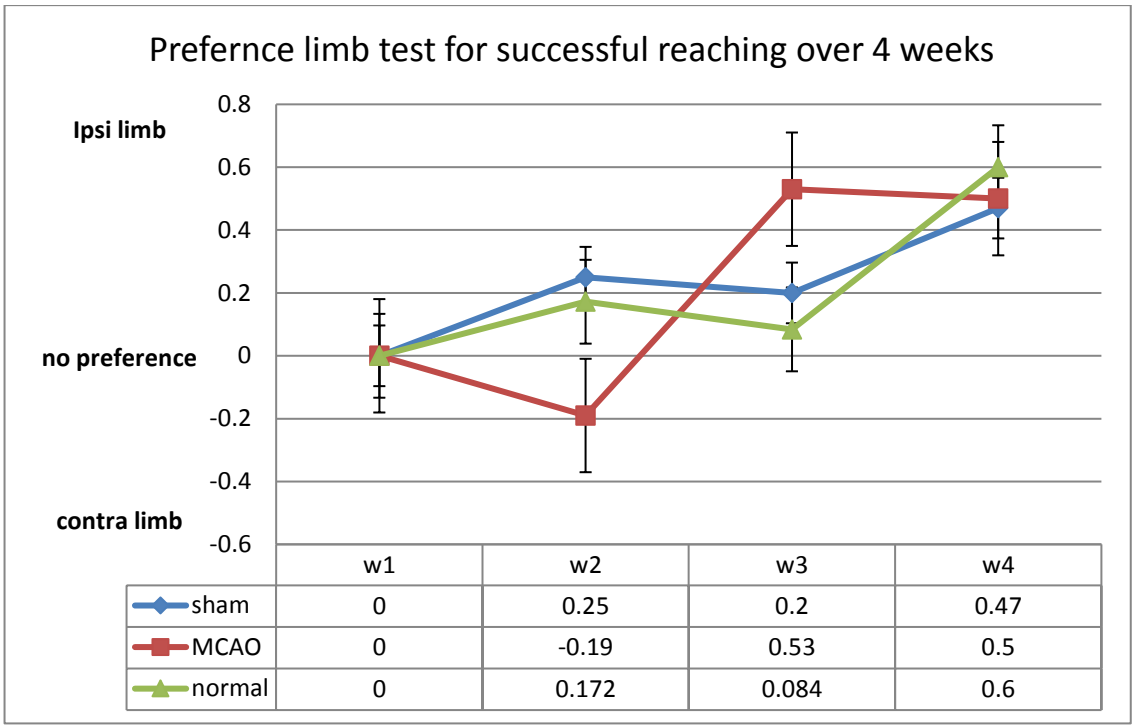


**Figure 3.3 Laterality index in MCAO, sham and normal successful reaching attempts over 4 weeks reaching tests.**

The laterality index showed the preference limb in each of the three groups.There was only one rat with right (contralateral) limb preference among five rats with left (ipsilateral) limb preference in each group. In all groups, most rats showed a preference toward using their left (ipsilateral in lesion or sham groups) limb in all reaching attempts. Error bars are standard deviation.

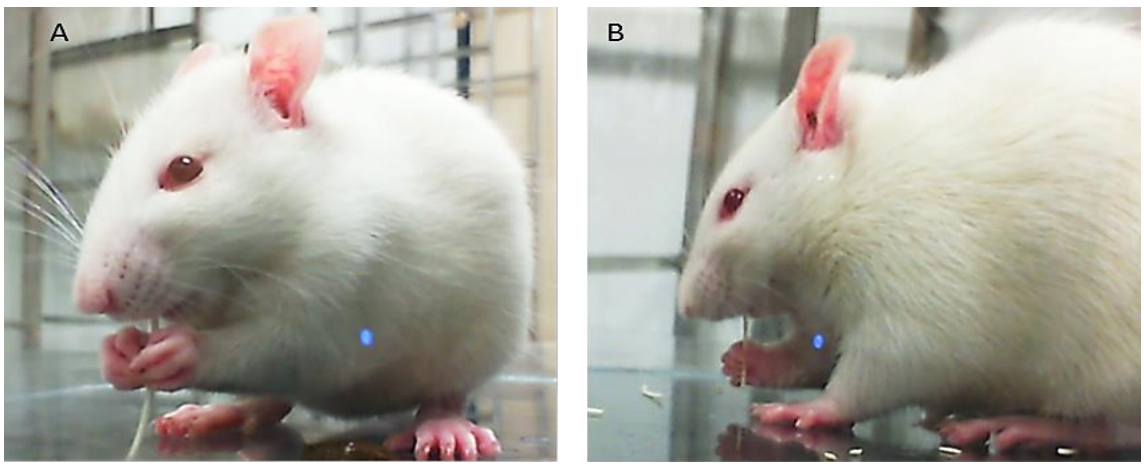


**Figure 3.4 Pasta test.**

Normal rat (A) holds the pasta with both paws, and (B) holds the pasta with one paw.

**Histological observations**

At the beginning of our experiment, no histologically detectable infarction occurred when MCAO was applied to the distal part of the MCA at one spot (Figure 3.5 A and B), which is a method adopted from (Coyle, 1982, Renolleau et al., 1998). Thus, we stopped this occluding method and excluded it.

Then, we ligated along the MCA trunk from the olfactory tract level proximally to the inferior cerebral vein level distally as much as possible to prevent collateral cerebral arteries from supplying the sensorimotor area (Taguchi et al., 2010) . At 2, 5, 9 and 20 days after occlusion, we studied the expression of a hypoxia-inducible transcription factor (HIF-1), which we predicted would show brain regions deprived of a blood supply by MCA occlusion. We also looked at expression of the microglial marker IBA1, which shows the innate inflammatory response of the host tissue due to induced hypoxia

At Days 2 and 5 post occlusion, expression of HIF-1 was increased in the lateral cortex close to the site of occlusion, including barrel field somatosensory cortex (bfSSC) and the secondary somatosensory cortex (S2), while the more dorsal primary lSMC controlling the limbs showed little or no expression (Figure 3.5C).

We also found that permanent MCAO in immature rats rapidly induced microglial activation and subsequent accumulation of activated microglia in lesioned forebrain structures. IBA1 expression in the MCAO group showed a similar pattern to HIF-1 (Figure 3.5D). These data demonstrate that perinatal ischemic brain injury induces rapid accumulation of activated microglia, as detected by IBA1.

No immunoreactivity was detected with either antibodies at Days 9 or 20 post occlusion in the MCAO group nor at any of the four time points in the sham group.

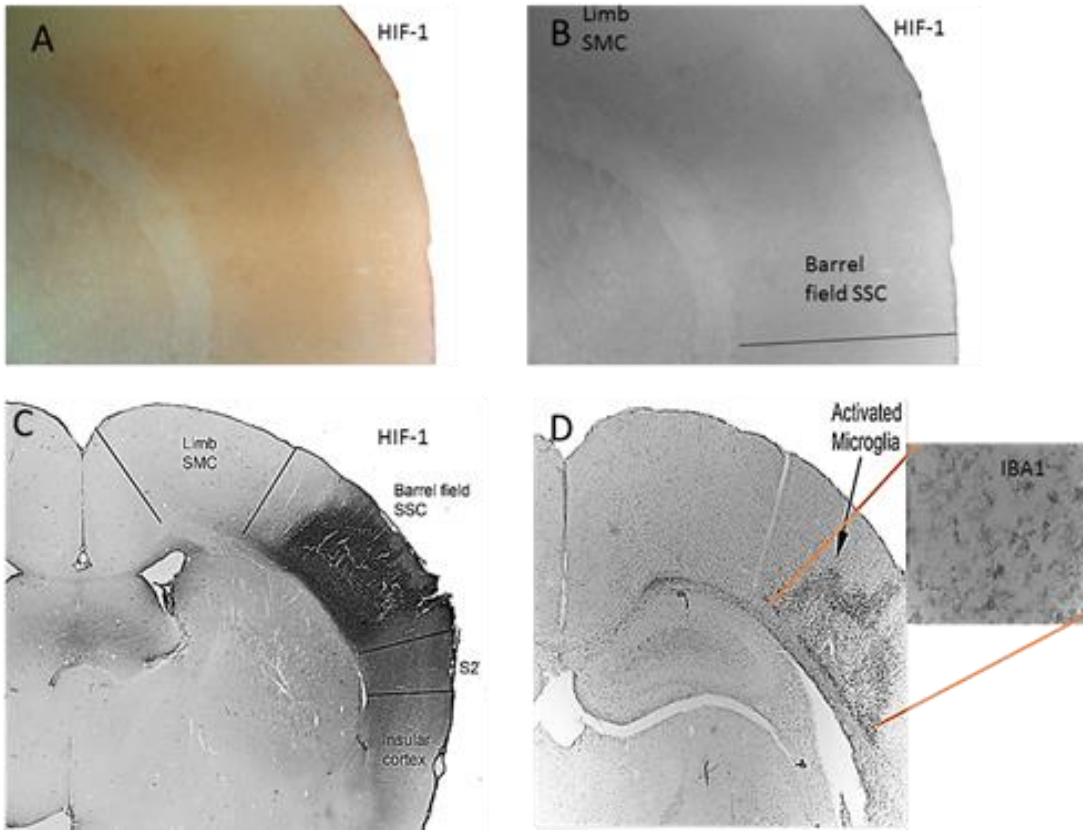


**Figure 3.5 Immunoreactivity for HIF1 and IBA1 5 days after inducing MCAO in rat pups.**

No increased expression of HIF-1 when MCAO was applied to the distal part of the MCA (A) and (B) at one spot. Increased expression of HIF-1 (C) and IBA1 (D) in the lateral cortex close to the site of occlusion in the bfSSC, but the more dorsal lSMC showed little or no expression in rat pups at P17.

At P45, animals were perfused for chronic-stage IHC assessment. Eight coronal sections through the forebrain of each animal were stained with cresyl violet, anti-calcium-binding protein (parvalbumin) antibody, and the anti-IBA1 antibody.

Cresyl violet was used to visualize the neuronal distribution. Inspections of forebrain structures in both the MCAO and sham groups revealed cortical tissue damage in the bfSSC (Figure 3.6A). However, no tissue alterations of cerebral cortex in the lSMC were seen (Figure 3.6B). In all sham brain sections, normal cell morphology was seen in the sensorimotor cortex (SMC) when using cresyl violet staining (Figure 3.6C and D).

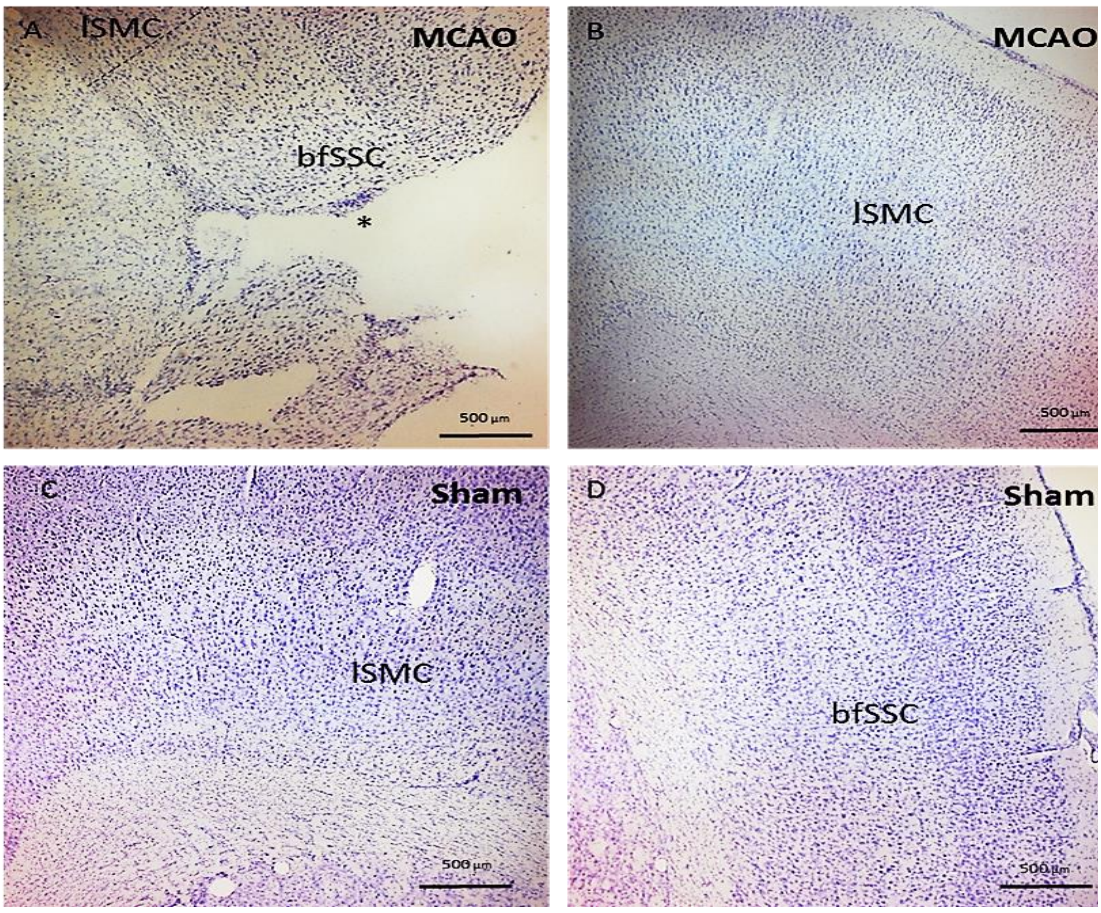


**Figure 3.6 Representative images of brain tissue in the IH using cresyl violet staining in coronal sections.**

Neuronal morphology from P45 MCAO model brains showed (A) cortical lesion (asterisk) in the bfSSC but no lesion in the lSMC. (B) No abnormal morphology in the lSMC (C) or the bfSSC (D) in sham brains.

Parvalbumin (PV) immunoreactivity was present in a normal distribution in lSMC of the in the contralateral cortex in MCAO rats, and in sham animals (Figure 3.7A and B). However, an obvious decrease in PV immunoreactivity was observed in the bfSSC of the IH after MCAO when compared to the normal PV expression in the adjacent lSMC (Figure 3.7A).

Few activated (ameboid) microglia immunopositive for IBA1 were found in the bfSSC at 33 days after MCAO (Figure 3.7C and D). However, the normal ramified phenotype of microglia with small bodies and long, thin processes were present throughout the cortical tissue of MCAO and sham animals (Figure 3.7E).

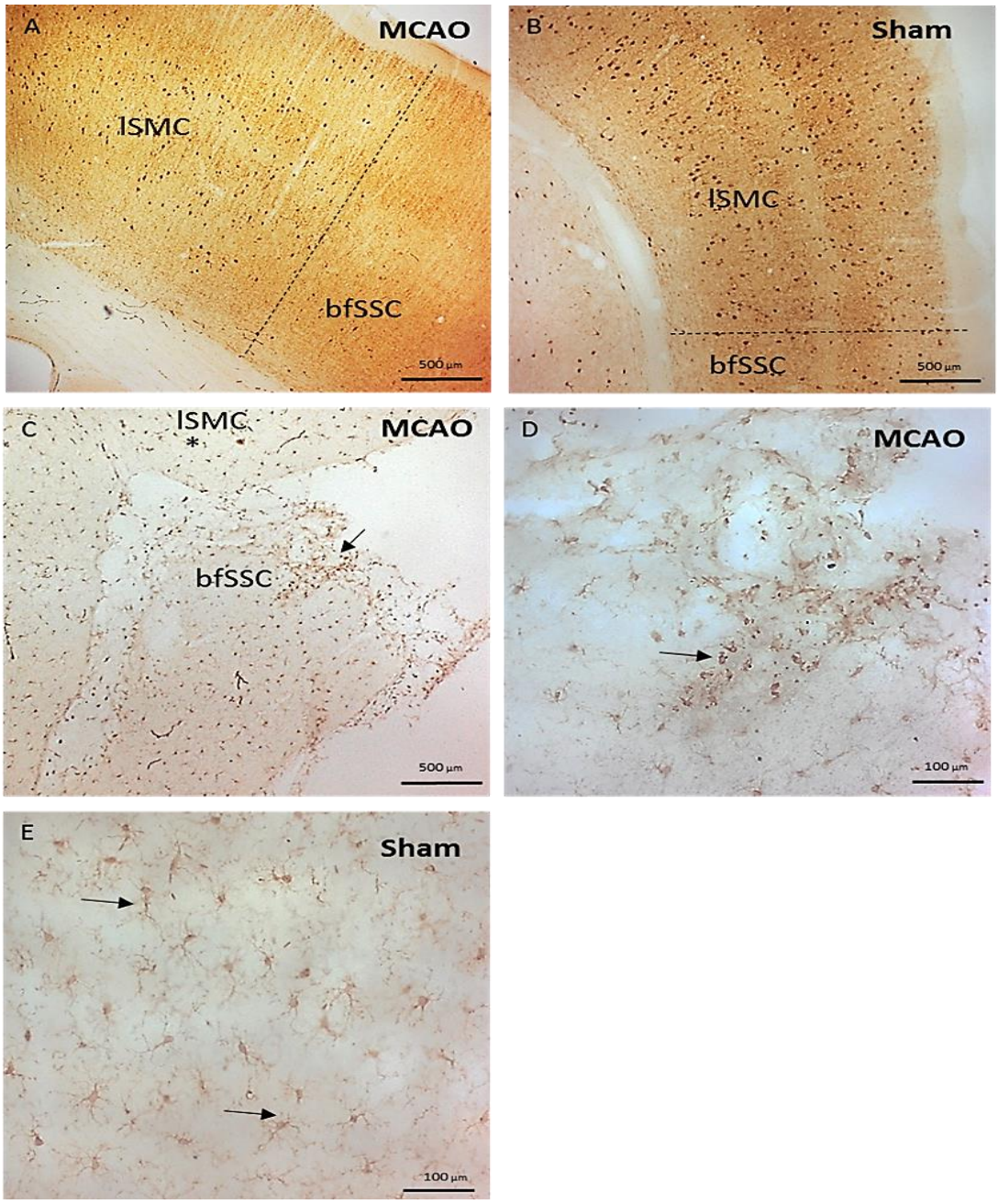


**Figure 3.7 Representative images of PV and IBA1 Immunoperoxidase reactivity at P45 of brain tissue in the IH following MCAO.**

(A)Loss of PV immunoreactivity in the bfSSC but not in the lSMC in MCAO models, the dashed line represent the border between the lSMC and the bfSSC. (B) No decrease in PV staining in sham animals' bfSSC. (C) Few activated microglia immunoreactive for IBA1 in the bfSSC (arrow) but not in the lSMC (asterisk) in MCAO models. (D) Magnified image of IBA1+ microglia (arrow) in bfSSC after MCAO and (E) in sham animals displaying ramified microglia (arrow).

### *3.2.2 ET-1 Model*

**Animal numbers**

ET-1 or saline was injected into the SMC of 37 Wistar rat pups at P12. The total number of operated rats and the subcategories of these numbers are detailed in Table 3.3. A total of 17 rats were assigned to the experimental group and received ET-1; 12 rats were assigned to the sham group and received saline injections intracerebrally into the lSMC. One rat from the ET-1 group and one rat from the sham group died during the retrograde tracer surgery due to anaesthesia-related causes. Another rat was excluded from the ET-1 group due to post-operation swelling at the incision site over the head that was fluid-filled, non-painful and superficial at P20. When the swelling did not subside after being given the anti-inflammatory Meloxicam (Metacam, 0.5mg/kg) orally, the animal was humanely terminated.

Eleven rats from the ET-1 group and 11 rats from sham group were tested behaviourally at the same time points between P40 and P45. Four days before transcardial perfusion with fixative, a retrograde tracer, fluorogold dye, was injected into the cervical spinal cord on the side contralateral to the lesioned cortex to count and record the number and location of corticospinal neurons (chapter four).

Transcardial perfusion with fixative was performed at three time points post-surgery. For IHC assessment of hypoxia and the inflammatory reaction in the acute stage, two rats in the ET-1 group were perfused on Day 2 post surgery, and one on Day 9 post surgery. Also, one rat from the sham group was perfused on Day 9 post surgery. For the chronic-stage IHC assessment, 12 rats from the ET-1 group and 10 rats from the sham group were perfused at P45.

| Groups | Total number | Perfusion time points for IHC | | | Behavioural assessment | Number of excluded rats* |
|---|---|---|---|---|---|---|
| | P12 | 2D/P14 | 9D/P21 | 33D/P45 | P40-45 | |
| ET-1 | 17 | 2 | 1 | 12 | 11 | 2*^ |
| Sham | 12 | 0 | 1 | 10 | 11 | 1* |

**Table 3.3 The number of animals included and excluded in each time point of the ET-1 model and sham groups.**

^died at P21. *died at P45 after the performing the behavioural tests and during the retrograde tracer surgery. Exclusion reasons were described in the text, and D= days post-surgery, P=postnatal age.

**Behavioural Results and the Quantitative Analyses**

A total of 22 rats (ET-1=11, sham=11) underwent behavioural testing. Two behavioural tests were applied using the same procedures for the ET-1 and sham groups. The asymmetry placement test and the grid walking test were performed once for each group. Statistical comparisons were carried out using non-parametric tests.

**Grid walk test**

When performing this test, one rat from the ET-1 group escaped from the grid walk test grid and escaped again 3 times during repeat tests before it was excluded. Thus, the total number of animals in this test was 21 rats (ET-1 =10, sham=11).

The FLF and HLF scores were calculated using the formula described in Section 3.1.2. Overall, we found that FLF and HLF scores for the limb contralateral to the lesion were slightly higher in ET-1 than in the sham group, and this more pronounced for the forelimb than for the hindlimb. However, no significant differences were found between ET-1 and shams rats in terms of the FLF (p=.86; Mann Whitney U test) or HLF scores (p=.81; Mann Whitney U test) for the limb ipsilateral to the lesion, or for the FLF (p=0.7; Mann Whitney U test) or HLF scores (p=0.8; Mann Whitney U test) for the limb contralateral to the lesion (Figure 3.8Figure 3.9A and B).

Interestingly, ET-1 animals showed a strong tendency to take fewer steps than shams; however, no statistical significance was found between the median total steps for forelimb (p=0.08; Mann Whitney U test) or hindlimb (p=0.13; Mann Whitney U test) (**Table 3.4**) (Figure 3.8C).

| Groups | Median | | | | | |
|---|---|---|---|---|---|---|
| | Contra FLF % | Contra HLF % | Ipsi FLF % | Ipsi HLF % | Total steps FL | Total steps HL |
| ET-1 (n= 10) | 6% | 4% | 3% | 2% | 143 | 54 |
| Sham (n=11) | 5% | 4% | 2% | 2% | 192 | 72 |

**Table 3.4 The median % of FLF, HLF, and FL steps and HL steps in ET-1 and sham animals.**

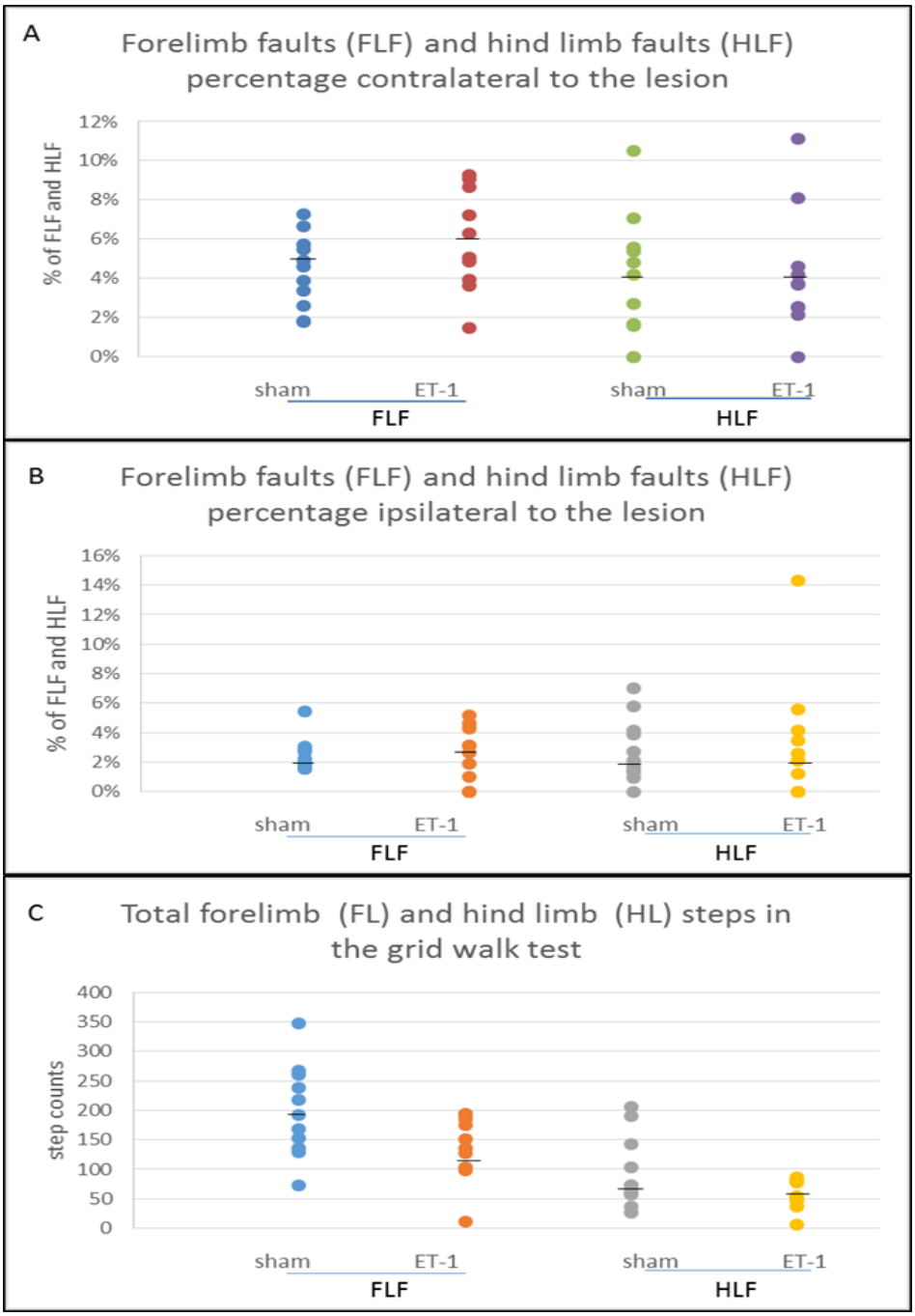


**Figure 3.8 The grid walk test outcomes in ET-1 stroke model and sham animals.**

There is a trend towards having more faults with fewer steps in ET-1 rats than sham ones with non-significant difference in the median of the FLF ratio and HLF ratio in (A) the contralateral limbs and (B) the ipsilateral limbs between ET-1 animal and sham animals. (C) Also, there was no significant difference in the median of the total step number in the ipsilateral and contralateral limbs between ET-1 and sham animals. Black lines are medians.

**Asymmetry placement test**

In this test, the asymmetry score for the contralesional forelimb was calculated using the formula described in Section 3.1.2. The number of single-limb and both-limb contacts on the cylinder wall were counted for the sham and ET-1 groups.

No significant difference was found in the number of limb contacts between groups (p=0.16.; Mann Whitney U test) and rats in both groups mainly used both forelimbs symmetrically (Figure 3.9A).

Similarly, there was no significant difference in the number of limb contacts between ET-1 and sham animals for the limb ipsilateral to the lesion, the limb contralateral to the lesion, or total wall touch counts (p=0.21, 0.26, 0.10, respectively; Mann Whitney U test). However, there was a trend towards lesioned animals making fewer contacts (Figure 3.9B).

Interestingly, the ET-1 stroke group did have significantly fewer cylinder wall contacts using both limbs than sham (p=0.01; Mann Whitney U test) (**Table 3.5**) (Figure 3.9B).

| Group | Median | | | | |
|---|---|---|---|---|---|
| | Asymmetry score | Ipsilesional paw contact | Contralesional paw contact | Both paw contact | Total paw contact |
| ET-1 (n= 11 ) | 45% | 12 | 17 | 0 | 28 |
| Sham (n=10) | 42% | 24 | 21 | 2 | 49 |

**Table 3.5 The median of the asymmetry placement tests and the limb contacts in ET-1 and sham animals.**

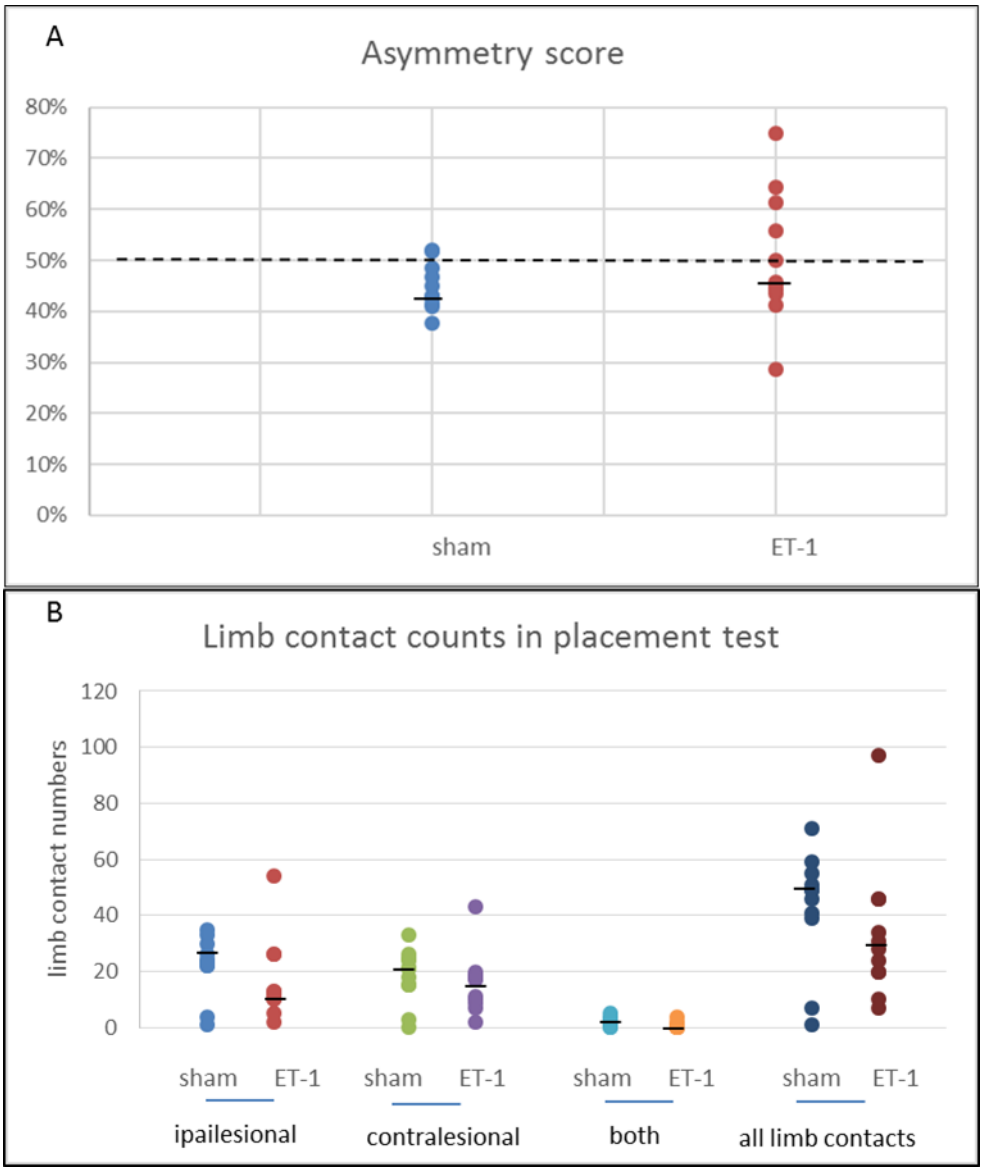


**Figure 3.9 Average of the asymmetry placement test and limb contacts in ET-1 model and sham animals.**

(A) Non-significant deficit in the symmetry score for ET-1 animals compared to the sham animals, dash line equals 50% where the use of each limb is equal. (B) Also, no significant difference in the number of contacts in ET-1 compared to sham group. Black lines mark the medians.

**Weight Results**

Throughout the experiment, the weights of 18 rats (7 sham, 11 ET-1) were monitored every 2-3 days starting from the day of surgery at P12. Generally, a significant difference in weight gain between ET-1 and sham rats was found when measured over the 22 days post-surgery. The mean weight was around 24 g on the day of surgery in both groups. The weight of rats in both groups increased with time; however, the weight of rats in the sham group increased steadily and to a greater extent than that of ET-1 rats (Figure 3.10A).

The mean weight of sham animals was significantly higher than in the ET-1 lesioned animals ($p=.02$; Independent Sample t Test). Although the weight scores calculated by dividing the final weight by the 1$^{st}$ weight were higher in sham than in ET-1 animals, no significant difference was found between the groups (Figure 3.10B).

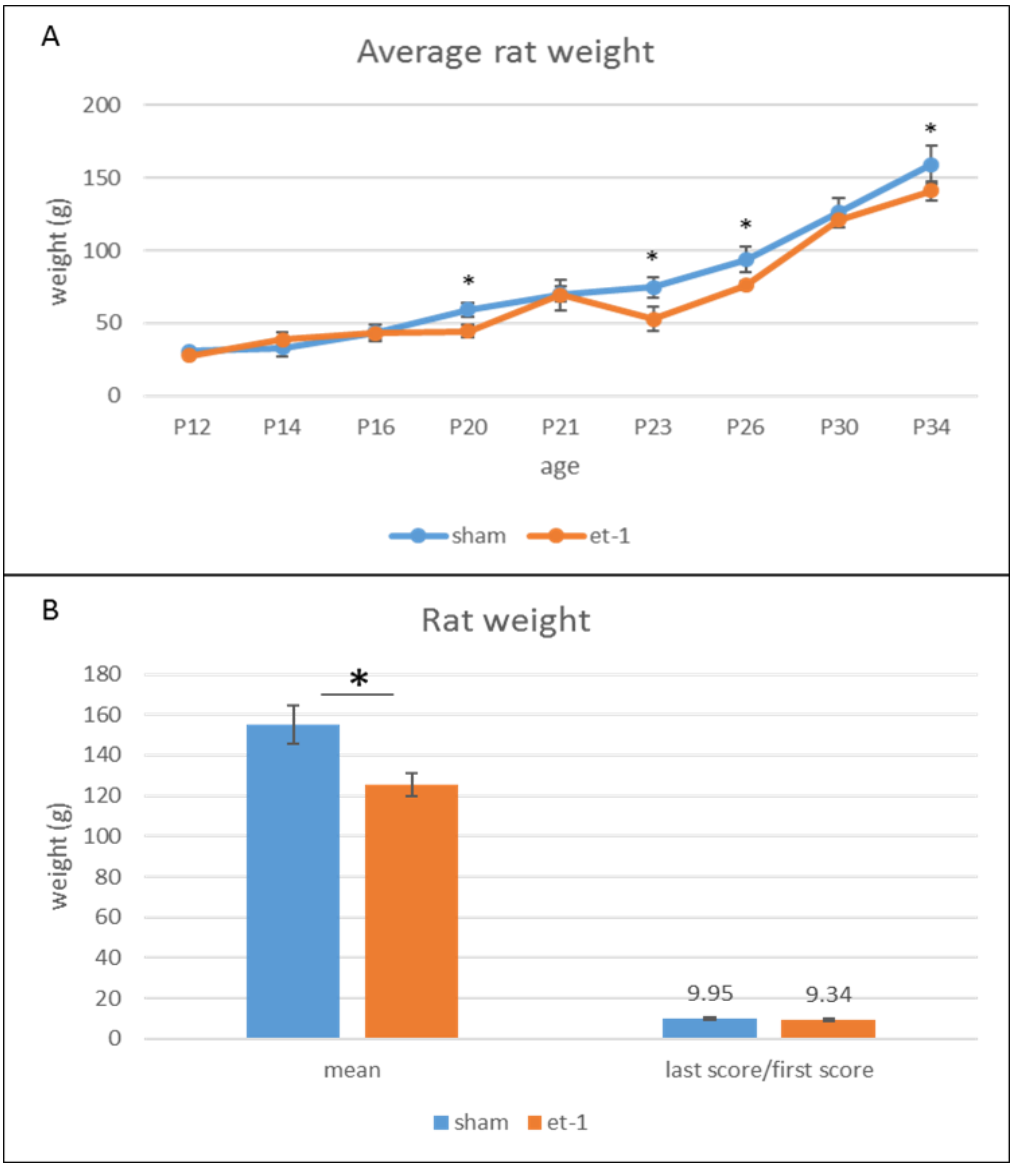


**Figure 3.10 The weight change in ET-1 and sham animals.**

(A) Effect of ET-1 injection on rat weight compared to the sham operated weight over 9 time points. (B) There was a significant difference between the mean weight of ET-1 lesioned rats and sham animals but a comparison of scores derived by dividing the weight on P34 by the weight on P12 demonstrated no significant difference.

**Histological observations**

We made precise injections of ET-1 at 3 sites in the lSMC over a period of about 20 minutes using a stereotactic frame with a syringe pump and a narrow needle Hamilton syringe. We observed an immediate whitening of the superficial area of the SMC surrounding the needle while we were injecting the ET-1 (Figure 3.11A).

In the first set of experiments performed 2 and 10 days after ET-1 injection, we studied the expression of a hypoxia-inducible transcription factor (HIF-1) and a microglia marker (IBA1) that shows the innate inflammatory response of the host tissue due to induced hypoxia. On Day 2, we observed a localised but extensive induction of hypoxic damage indicated by increased expression of HIF-1 in the lSMC and accumulation of activated microglia, indicated by IBA1 immunoreactivity. No immunoreactivity was detected with either antibody on Day 10 post ET-1 injection or in shams.

Figure 3.11B compares the use of MCAO and ET-1 for modelling PIS histologically using the anti-HIF and IBA1 antibodies as indicators of hypoxia and the inflammatory reaction two days after surgery. In immature rats injected with ET-1, we found rapidly-induced hypoxia and subsequent accumulation of activated microglia in the lSMC controlling the limbs in rats and to a lesser degree in the S2.

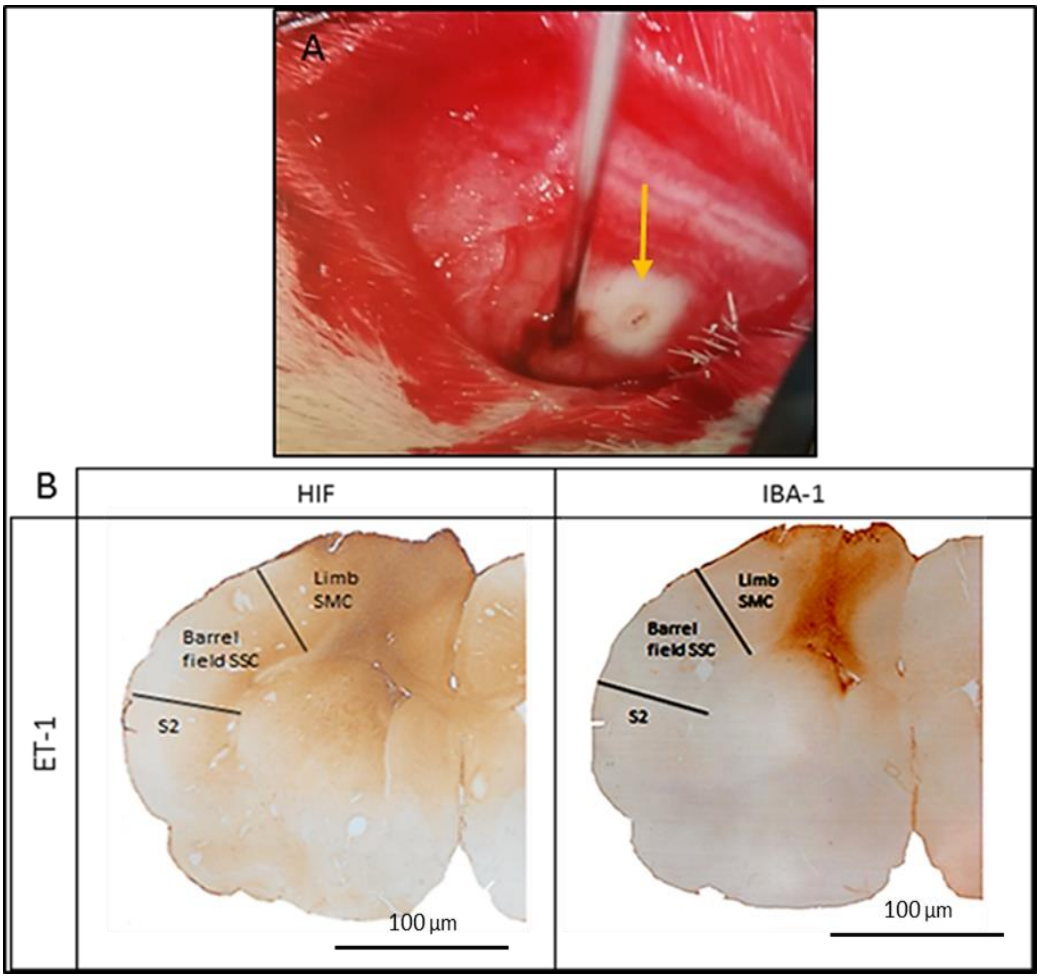


**Figure 3.11 Representative images of neonatal rat brain in PIS models.**

(A) Immediate brain discolouration around the first injection site (arrow) after injecting the ET-1 into the SMC. (B) Comparison between the Immunoperoxidase staining at P14 rat pups for HIF1 and IBA1 in MCAO and in ET-1 experimental groups. In the MCAO model, immunoreactivity for HIF-1 and IBA1 was restricted to lateral cortex close to the occlusion site including S2 but in the ET-1 model they were expressed in the lSMC.

To assess the histological changes at P45, animals were perfused and eight coronal sections through the forebrain for each animal were stained with cresyl violet. Immunoperoxidase staining was carried out using IHC with antibodies to PV (calcium-binding protein and inhibitory interneuron marker); GFAP (astrocyte marker); IBA1 (activated microglia and vascularization marker); and SMI-32 (antibody to non-phosphorylated neurofilaments).

**Effects of ET-1 on Brain tissue in PIS model**

Cresyl violet staining revealed tissue alterations in the lSMC of the ipsilesional hemisphere (IH) in ET-1 animals. Overall, a consistent lSMC lesion was observed in all experimental rats; however, the infarction size varied between the lesioned rats (**Table 3.6** ). The variation in infarction size was determine subjectively as follows: Mild to moderate infarction where a disturbance in cellular morphology occurs but with no tissue loss, Moderate to severe infarction where the cellular morphology occurs in addition to cortical tissue loss, and Ventricular dilatation where an observable dilatation in the ventricle occurs.

| Group | Mild to moderate infarction | Moderate to severe infarction | Ventricular dilatation | Subcortical lesion |
|---|---|---|---|---|
| ET-1 (n=10) | 6 | 3 | 5* | 1 |
| sham (n=9) | One rat had a small infarction. No infarction was detected in the remaining animals. | | | |

**Table 3.6 infarction types in the lSMC of the ET-1 stroke animals.**
*3 rats had moderate to severe infarction, one had mild to moderate infarction and one had subcortical lesion in addition to the ventricular dilatation.

ET-1 lesion resulted in a thinner cortex of the IH compared to the cortex of the contralesional hemisphere (CH), as well as in dilatation of the lateral ventricle (Figure 3.12A). Also, some shrunken neurons and pyknotic or fragmented nuclei were observed (Figure 3.12B), suggesting neuronal degeneration in the lSMC of the IH. By contrast, intact neuronal morphology with no tissue damage was observed in all other cortical regions in the IH and CH (Figure 3.12C) and in the lSMC of sham animals (Figure 3.12D). Variation in infarction volume and morphology was found across ET-1 injected rats. For example, Figure 3.12B shows a mild to moderate infarction in one rat while Figure 3.12E represents an example of severe cortical loss in another rat.

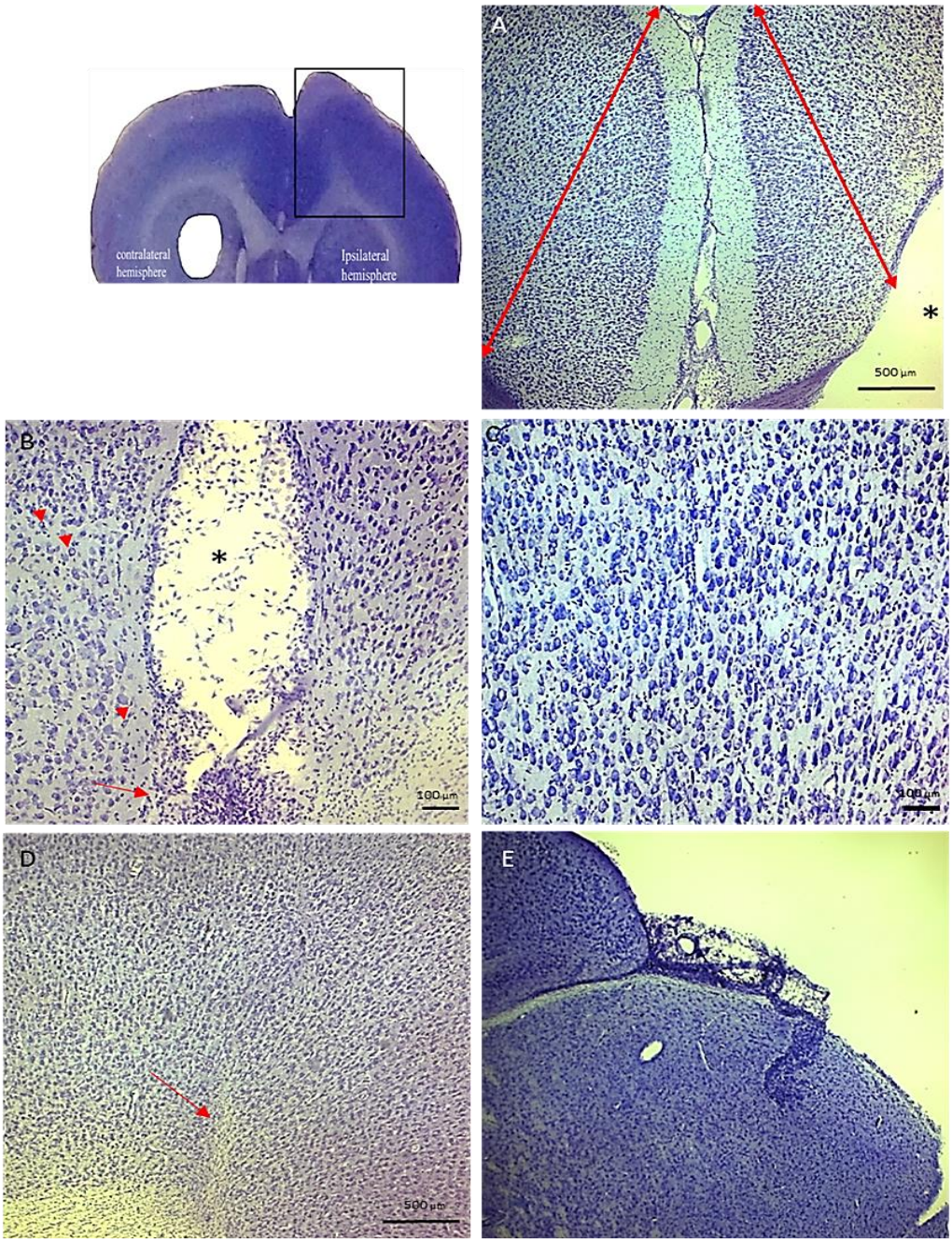


**Figure 3.12 Representative images of the neuronal changes in the lSMC of the IH in the ET-1 stroke and sham rats at P45.**

(A) Thin cortex (arrow) of the ipsilateral hemisphere (right) with ventricular dilatation (asterisk), (B) mild to moderate cortical infarction (asterisk) surrounded with pyknotic or fragmented nuclei (arrowhead) and dead cells (arrow), (C) normal appearing density in the contralateral cortex, (D) needle track in the lSMC of shams, and (E) cortical loss due to severe cortical infarction.

**Effects of ET-1 on neuronal activity in PIS model**

PV is a marker for active neural circuitry and reveals a widespread effect of lesions; thus, PV immunoreactivity was examined in both IH and CH in ET-1 stroke animals. Quantitative analysis of the effect of ET-1 injection on the number of cortical PV neurons in both IH and CH was performed in six animals. All immunopositive PV neurons were counted in eight serial coronal sections using Image hub and Image-J software. Overall, there was a reduction in immunoreactivity in the lSMC ipsilateral to ET-1 lesion.

PV counts in the IH and CH were compared using the paired test (Wilcoxon Signed Ranks Test), revealing that the ET-1 lesion caused a significant reduction in the number of PV-positive neurons in IH compared to the CH of the same animals (Figure 3.13).

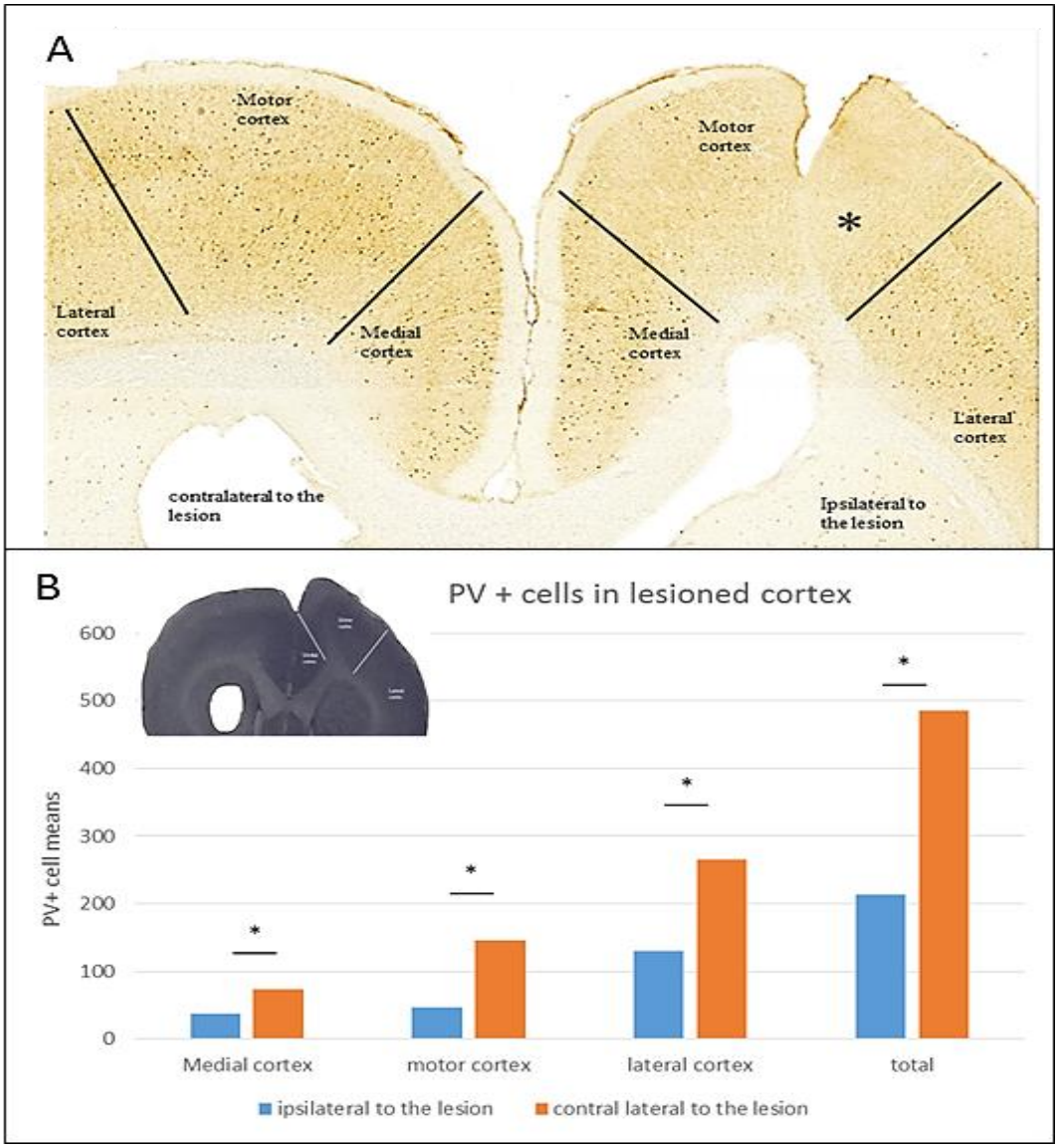


**Figure 3.13 Parvalbumin (PV) immunopositive cells quantitave analysis in ET-1 stroke model.**

ET-1 injection into the SMC resulted in a significant loss of PV expression in interneurons of the lSMC in the lesioned hemisphere compared to the contralateral side not only at the lesion site but at more distant locations (A, B).

**Effects of ET-1 on Glial and neuronal Response in PIS Model**

A few activated astrocytes and microglia immunopositive for GFAP and IBA1 were observed in the lSMC of the IH in P45 ET-1 rats. Figure 3.14A and B shows GFAP staining of astrocytes that sealed the infarction or trajectory of the injection needle in the lSMC of the IH. A few hypertrophic microglial cells were observed at the lesion site and at the needle trajectory (Figure 3.14C and D). Otherwise, the normal ramified phenotype of microglia with small bodies and long, thin processes and appeared to be present throughout the cortical regions of both the ET-1 and sham animals (Figure 3.14 D).

Neuronal immunoreactivity for non-phosphorylated neurofilaments (NPNF) showed a decrease at the ET-1 injection site. From observation of the sections, there appeared to be neuronal loss in the lSMC of the IH in ET-1 stroke animals (Figure 3.14E). Intact distribution of the lSMC cortical neurons was observed consistently throughout the cortex of sham animals (Figure 3.14F).

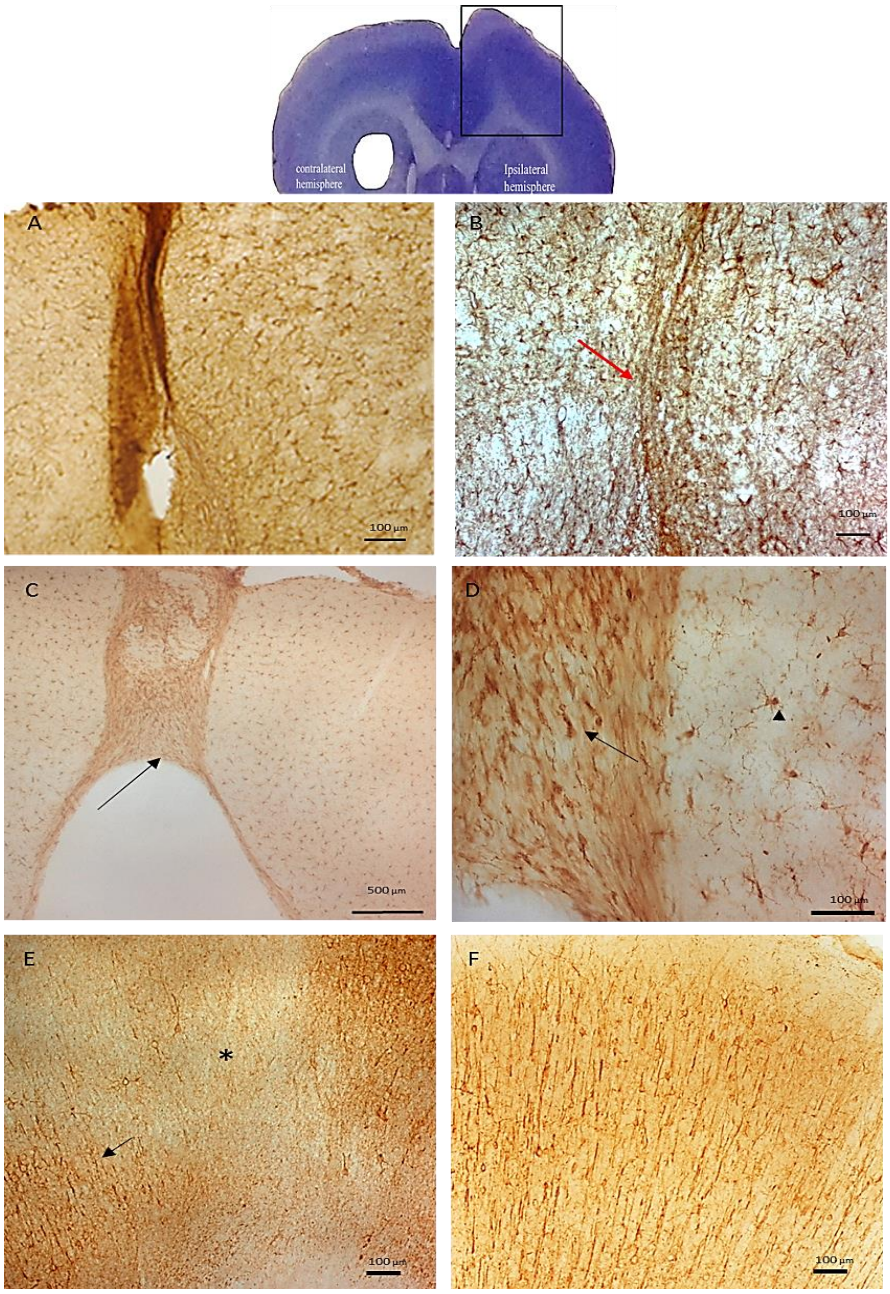


**Figure 3.14 Representative images of Effects of ET-1 on glial and neuronal response**

(A) Activated astrocyte at the injection site of ET-1, and (B) magnified image of swollen bodies of the GFAP+ astrocytes. (C) Activated microglia immunoreactive for IBA1 in the lSMC (arrow). (D) Magnified image of IBA1+ microglia in lSMC, ramified microglia (arrowhead) and activated microglia (arrow) (D). (E) Loss of NPNF+ neurons (asterisk) at the injection site in lSMC in ET-1 rat, and normal neuronal NPNF expression and morphology (arrow) adjacent to the infarcted site (F) in sham animals.

## 3.3 Conclusion

The MCAO model of PIS resulted in acute hypoxia and an inflammatory response in the brain that persisted for 5 days after occlusion and cortical tissue loss, with suppression of neuronal activity 33 days after the occlusion in the bfSSC but not in the lSMC that controls limb function. Injection of ET-1 to model PIS resulted in a similar pattern of lesion to the MCAO but instead localised to the lSMC, suggesting that ET-1 is a more appropriate model of PIS in terms of histopathology. Behavioural tests revealed no defects in either model, except in the use of both forelimbs at the same time in the asymmetry placement test in the ET-1 model. This conclusion leads us to the next chapter (chapter four), where the possible plasticity that might underlie the absence of behavioural dysfunction in the ET-1 model was explored.

## 3.4 Discussion

In this chapter, two methods by which the P12 immature brain rat pups were lesioned to model PIS were used, namely middle cerebral artery occlusion (MCAO) and ET-1 injection into the SMC. The MCAO method resulted in an ischemic cortical lesion principally in the, but not the lSMC. Thus, we utilized the second method instead. This latter method resulted in cortical ischemia in the lSMC, which controls limb movements. There was no significant loss of sensorimotor function during juvenile age P45 with either model. To our knowledge, this is the first time these two techniques that have been used to model PIS in P12 neonatal rats.

### *3.4.1 Anatomical and behavioural response to MCAO*

All animals with permanent MCAO showed acute cortical lesions at P5 and chronic cortical lesions at P40-50 that were restricted to the bfSSC but did not extend into the adjacent lSMC. HIF-1 immunopositive cells were clearly present in the bfSSC at 3 to 5 days post MCA occlusion, indicating acute hypoxia (Lai et al., 2003). Permanent MCAO occlusion studies in neonatal rodents have revealed similar lesion location (Bonnin et al., 2011, Tsuji et al., 2013, Wen et al., 2004, Yager et al., 2006)

At the beginning of our experiment, the MCA was occluded by applying one spot electroligation at the distal part of the MCA. This technique revealed no cortical infarction, suggesting that collateral blood vessels continued to supply the brain so that infarction was avoided. Studies have shown similar results when using filament ligation of the left MCA in

immature rats to induce permanent MCAO (Coyle, 1982, Renolleau et al., 1998). However, ligation along the MCA, starting from its origin or proximal to the olfactory tract and extending to the level of the inferior cerebral vein, occludes all supplying arteries from the distal to the proximal portions of the MCA (Bederson et al., 1986, Tsuji et al., 2013). For example, the MCA in neonatal CB-17 mice was permanently electroligated, resulting in cortical infarction that affected the lateral cortex with mild corpus callosum atrophy, mild thalamic injury, and sensorimotor defects in rotarod and open-field tests (Tsuji et al., 2013). Another study on permanent MCAO was conducted using suture embolus introduced into the MCA in immature rat pups (P7), resulting in a large infarcted area that was not restricted to the lSMC, affecting about 51-56% of IH in the forebrain with apoptotic-like cell death during the first 24 hours (Wen et al., 2004). Thus, to produce an infarction, we performed electroligation along the MCA from the distal part of the left MCA until the proximal part, a surgical procedure adopted from (Tsuji et al., 2013).

Immature rodent models show inconsistency in terms of the behavioural outcomes of permanent MCAO. In our study, MCAO stroke resulted in bfSSC ischemic lesion, but did not lead to significant behavioural dysfunction, similar to previous studies (Coyle, 1982, Renolleau et al., 1998, Yager et al., 2006). MCAO using ET-1 adjacent to the MCA to induce stroke in rats at three different ages; P10, 63, 180 showed no significant differences in behavioural tests such as the grid walk test in rats that were lesioned at P10, but in older groups, behavioural dysfunctions were reported (Yager et al., 2006). On the other hand, some immature stroke models using permanent MCAO have shown behavioural deficits. A neonatal stroke study showed that transient occlusion of MCA in P7 rats resulted in motor deficits during early adulthood in sensorimotor performances including asymmetries in the corner test, the staircase test, and adhesive-removal test (Bouet et al., 2010). This discrepancy among studies might be due to many factors. Possible reasons include the extent of brain damage, the involvement of subcortical regions in the lesion, and the different rodent strains and behavioural tests utilized (Tsuji et al., 2013). Also, the different procedures for inducing PIS, such as the photo thrombotic and intrafilament occlusion techniques (Brima et al., 2013), as well as the lesion type, such as transient MCAO (Ashwal et al., 1995, Ashwal et al., 2007, Bouet et al., 2010, Derugin et al., 1998, Derugin et al., 2000, Larpthaveesarp and Gonzalez, 2017) and different neonatal ages at the time of lesion induction (Tsuji et al., 2013, Wen et al., 2004) could have contributed to the different results.

Although there was increased expression of markers for hypoxia and microglial activation in the lateral cortex close to the site of occlusion, the more dorsal lSMC showed little or no expression. These results suggest that MCAO caused hypoxia and microglial activation as a result of ischemia, but that this did not occur in the lSMC; it did, however, affect the face somatosensory cortex (SSC), S2 and insular cortex. Therefore, the small but statistically non-significant differences in forelimb and hindlimb behavioural outcomes might have arisen from a lesioned S2 or neglect of the right side due to loss of whisker sensitivity, but not from a lesion of limb SMC.

MCAO proved to be a poor PIS model in P12 rat pups, as there was minimal involvement of the lSMC, a major site of damage in human neonates. Therefore, we decided to inject ET-1 directly into the lSMC in order to produce stroke damage.

### *3.4.2 Anatomical site of lesion in response to ET-1 in the acute stage*

In this experiment, the ET-1 intracerebral injection into the SMC of P12 rat pups established a disturbance of the lSMC tissue morphology in the acute and chronic stages. Although there was some evidence of functional disabilities in the ET-1 group compared to sham animals using the grid walk and the asymmetry placement test at P45, these differences were not statistically significant. The low-mortality rate following the injection of ET-1 provided another advantage to using this method to produce PIS.

For the first time, the anatomical damage in the PIS model was compared between the MCAO and ET-1 methods in the acute stage in P12 rat pups. We found that the first model revealed an ischemic lesion in the bfSSC while the second model led to ischemic damage in the lSMC. The main advantage of the use of ET-1 to model PIS over the MCAO is the appropriate lesion location.

Our result is consistent, in terms of the location of the resultant cortical ischemia, with a similar study in adult stroke models (Windle et al., 2006). In the later study, the outcomes of two methods were compared; the MCAO and direct ET-1 application into the SMC and the striatum. The MCAO method produced the PIS model with a bfSSC lateral cortex lesion whereas the ET-1 application resulted in a confined lesion in the forelimb motor region in an adult stroke model (Windle et al., 2006).

In our study, injecting ET-1 into SMC at P12 caused hypoxia and an inflammatory reaction in the lSMC for at least five days post inducing the lesion before it diminished after nine days post-lesion. The HIF-1 immunopositive cells were clearly present two to five days in the bfSSC post MCA occlusion, and in the lSMC after injecting the ET-1 indicating hypoxia and ischemia exposure in our immature rats (Lai et al., 2003). In agreement with our study, Saggu et al (2013) found the reperfusion after occlusion of the MCA using ET-1 in 3-week-old rats occurred over three days (Saggu, 2013). The Hypoxia-inducible factor-1 (HIF-1) expression was also studied in a neonatal stroke model study following interfilament advancement through the carotid arteries for 1.5 h to induce transient MCAO in immature rodents. Using IHC and Western blot analysis their results showed that HIF-1 expression peaked at 8 h post MCAO but hours but it could still have been present one or 2 days later (Mu et al., 2003). The discrepancy between the later study and ours is possibly due to the differences in the lesion-inducing techniques.

Our study revealed obvious activation of microglia in the ischemic lSMC. The highest immunoreactivity was seen within ischemic brain areas on days two to five. Consistent with previous investigations of the inflammatory response in neonatal ischemic injury, microglia with short-ramified processes progressing to round amoeboid morphology were observed in our results, suggesting a gradual activation of the local microglia (Raivich et al., 1999).

In an acute neonatal (P7) stroke study, microglia have been shown to play both beneficial and destructive roles in the neural tissue. Microglia help in the defense mechanism, but at the same time exacerbate inflammation and secrete neurotoxic factors in the lesion site, resulting in neuronal death (Faustino et al., 2011). Changes in morphology and inflammatory factor release in response to inflammation in cultured microglia from neonate rats was found to be similar to the response of microglia from older adult rats, but different to microglia from embryos or young adults, suggesting an age-dependent microglial response (Lai et al., 2003). Also, in line with adult stroke studies, our results showed that microglial activation is an indicator of the immediate inflammatory response after ischemic stroke peaking at 3–4 days (Annunziato et al., 2013, Nowicka et al., 2008). The dense expression of IBA1+ cells in the acute stage in our study suggested that microglia were participating in forming scar tissue at the lesion site. On the other hand, a beneficial role for the microglia might be present at this site (Denes et al., 2007). They work as a first barrier and to remove the cell debris at the inflammatory site to

protect the neural tissue after acute neonatal focal stroke (Denes et al., 2007, Faustino et al., 2011).

### *3.4.3 Anatomical response to the ET-1 injection in the chronic stage*

Cresyl violet staining at P45 in our study showed that injecting ET-1 into SMC of P12 rats produces cortical tissue damage in the lSMC of the coronal forebrain sections. However, an inter-animal variability in the infarction size was observed in our study. There are several possible reasons that might underlie this variability. The cerebral vascular structures differ slightly from rat to rat, which results in variable infarctions according to the affected cerebral vessels (Comi et al., 2005, Macrae, 2010). Also, different rodent strains that are used to model the stroke revealed different results. When specific rodent strains that were characterized by minor variation in the vascular distribution in the cerebral cortex, such as the mice CB-17 strain are used, a more consistent cortical lesion size is observed (Taguchi et al., 2010, Tsuji et al., 2013).

Another possible factor is the isoflurane-exposure duration. Immature rats displayed a more consistent brain lesion with shorter exposure to isoflurane in surgery to induce the ischemic lesion that lasted for 5 min rather than 20 min (Chen et al., 2011). Our 20-minute duration for the surgery protocol is inevitable because of the gradual pumping of ET-1 into the SMC to avoid any flow back. These factors might explain in our study the heterogeneity of the resultant cortical infarction after injecting ET-1.

The cellular response in our PIS after injecting ET-1 into the lSMC involved significant loss of PV expression by inhibitory interneurons with mild defects in the excitatory cortical neurons (NPNF+). However, we don't know if the interneurons have disappeared or have merely stopped expressing PV, as PV is a marker for activity in neuronal circuits. The extent of neuronal activity suppression in the ischemic lesion was revealed from counting the PV+ interneurons at P45 coronal sections of the rat forebrain. PV is a calcium binding protein that influences the excitability of nerve cells. In developing rat the first PV+ interneurons are seen at P8 in the hippocampus and at P14 in the cortex (Solbach and Celio, 1991). PV-interneurons are one of three main subtypes of the inhibitory cortical interneurons that release the neurotransmitters gamma-aminobutyric acid (GABA) and it have a crucial role in maintaining the brain circuitry and activity(Dreifuss et al., 1969, Kelsom and Lu, 2013). In previous neonatal rat studies with motor cortex lesion at P7 and under muscimol implants, a reduction

in the PV positive neurons in the cervical spinal cord contralateral to the lesion and in the cortex under the implant were reported in the contralateral side compared to the sham animals when assessed at P28 (Clowry et al., 1997) and persisted into adulthood (Gibson et al., 2000a). In agreement to our results, another study reported a persistent loss in PV+ and GABAergic interneurons in the chronic stage after inducing perinatal hypoxia in P3-10 mice (Fagel et al., 2009).

In addition to the neural activity inhibitory effect of ET-1 on the lSMC, we observed some loss of the cortical excitatory neurons SMI-32+ in lSMC of all coronal sections in our PIS model compared to the shams. Consistent with our results in the chronic stage, perinatal hypoxia in P3-10 mice revealed a 30% loss of SMI-32+ neurons that completely recovered after one month (Fagel et al., 2009). Another study in immature rats confirmed the reduction in neuronal nuclei compared to sham animals at P40 after transient MCAO (Bouet et al., 2010). On the contrary, a study in kittens to model neonatal stroke reported a decreased cortical volume due to failure of axonal and dendritic growth, but not due to neuronal loss in the SMC (Martin et al., 2000). This discrepancy in the results might be due to the distinct species used to model the neonatal stroke.

We employed anti-GFAP IHC to show that astrocytes exhibited changes in their morphology at P45 and contributed to scar formation. In pathological conditions such as stroke, astrocyte activation is considered as a sensitive indicator for astrocyte response to the brain lesion (Yang and Wang, 2015). After a stroke, astrocytes express GFAP excessively in the acute stage and seal the infarction site in the chronic stage (Kawano et al., 2012, Nowicka et al., 2008). In agreement with a previous neonatal stroke study in P7 rat, astrocytes that were immunopositive for GFAP at P40 were restricted in separating the ischemic lesion area from the normal adjacent cortical tissue in the chronic stage in our study(Bouet et al., 2010). Adult rodent stroke studies demonstrated the neuroprotective role via the inhibitory effect of GFAP+ astrocytes on recovery in the chronic stages (Li et al., 2008) , yet reactive astrocytes might not participate in the neuroprotection role. For example, no improvement was found to have no effect on reducing the infarction volume in acute or subacute stages after neonatal brain hypoxic ischemia in mice with inhibited astrocyte reaction (Järlestedt et al., 2010).Thus, we suggest that the presence of reactive astrocytes in the chronic stage might have no positive effect on reducing the resultant infarction volume in our study.

### *3.4.4 Behavioural response to the ET-1 injection in the chronic stage*

The behavioural outcomes that were assessed at P45 after injecting ET-1 were similar to the outcomes after occluding the MCA in our study. Unexpectedly, the resultant ischemic lesion in the lSMC did not lead to significant sensorimotor defects. Although the sensorimotor dysfunction was non-significant, there was a trend towards finding reduced performance in the affected contralateral limb compared with sham animals after injecting the ET-1. On the contrary, intracerebral injection of ET-1 caused ischemic lesions and behavioural defects in neonatal rats at P14 when tested in adulthood (Gennaro et al., 2017). There are several reasons that might affect the behavioural outcomes in neonatal brain lesion studies. The anatomical regions that are involved in the lesion, the animal's age when the lesion was induced and the type of the behavioural assessment used might have a role in the non-significant motor dysfunction in our neonatal stroke model.

The location of the cortical ischemia could affect the severity of the functional disability. Our resultant ischemic lesions in the lSMC after ET-1 and in the bfSSC lesion after the MCAO were cortical and did not involve subcortical structures. Compared to our purely-cortical lesion, studies that involved the cortex and the striatum in the induced focal ischemia found significant behavioural defects, as shown in neonatal and adult stroke studies (Brima et al., 2013, Windle et al., 2006)). For example, a perinatal SMC lesion in P7 rats induced by photothrombosis over 5 minutes led to cortical and subcortical structure (e.g. striatum) lesions (Brima et al., 2013). Furthermore, direct ET-1 application into the SMC and the striatum resulted in motor defects in immature rats (Windle et al., 2006). However, we had one rat with cortical and subcortical lesions in the striatum but it did not affect the asymmetry forelimb placement or the number of the footfaults in the grid-walk test, which were similar to those for other rats in the lesioned group. This involvement of the striatum in our study was due to a technical error during injection of the ET-1.

Another probable reason behind having nearly normal limb-function outcomes is the animal's age at the day of the lesion. It was found that adult rodents demonstrated normal function in the affected limb if the stroke was induced during the neonatal period, but not when the lesion was induced during adulthood (Yager et al., 2006). It was also shown that adult rodents with neonatal cortical lesions exhibited a normal tactile-placing reflex and few faults in the grid-

walk test in the contralesional forelimbs, whereas animals with a similar injury at maturity showed poor recovery (Alaverdashvili and Whishaw, 2008, Brima et al., 2013, Schallert et al., 2000, Windle et al., 2006, Yager et al., 2006). Some studies of lesioned immature rats at P12 or less showed no behavioural deficits, in contrast to rats lesioned at an older age than P13. Cortical lesioning at 7–10 days of age in immature rats has revealed nearly normal outcomes behaviourally and spontaneous filling of the lesion cavity with new cells when assessed in adulthood (Dallison and Kolb, 2003). Although we found no performance deficit, no cells were observed to be generated in the infarction in our study. Also, Yager et al (2006) found that P10 rats which received MCAO, induced by injecting ET-1 adjacent to the MCA, had recovered behaviourally when tested in adulthood. On the other hand, when adult and immature stroke models that received ET-1 intracerebral injection into the SMC were compared, the adult rats showed significant behavioural deficits but these were not present in the immature rats (Windle et al., 2006).

In a very recent study, behavioural deficits were observed after injecting ET-1 intracerebrally in P14 rat pups to produce ischemic stroke under intraperitoneal anaesthesia (Gennaro et al., 2017). In addition to the animals' age differences between this later study and our study, Gennaro et al. (2017) used intraperitoneal anaesthesia whereas we used inhalation anaesthesia in our ET-1 model surgery. It has been shown that the use of isoflurane as an inhaled anaesthetic improves the neurological outcome after the ischemic lesion (Chen et al., 2011). In contrast, another neonatal stroke study in mice used isoflurane for permanent MCAO surgery but the operated animals showed sensorimotor defects in the rotarod treadmill and open-field tests. Unlike our study, the latter study used the permanent method of inducing a stroke, different species, involvement of cortical and subcortical tissue lesion, and used different behavioural assessments (Tsuji et al., 2013).

Furthermore, the variety of the available outcome assessments is a considerable factor that leads to different behavioural results for post-ischemic lesions in many studies. In our assessment method, we utilized the grid-walk and the asymmetry-placement test because of their reliability in testing unilateral SMC damage (Rogers et al., 1997, Schallert, 2006), though not unilateral bfSSC damage (Stüttgen and Schwarz, 2010). Some studies utilized different tests to assess the behavioural outcomes in immature stroke models (Bouet et al., 2010, Brima et al., 2013). For example, applying the laser directly on the SMC in P7 led to deficits in motor performance in

the bar-holding test and in the open-field test (Brima et al., 2013). Yet, in the Brima et al (2013) study, non-significant behavioural dysfunction in the ladder-rank walking test was reported which is similar to the grid-walk test in our study. It seems that the differently utilized behavioural tests affect the assessment outcomes in immature stroke studies.

### *3.4.5 Mortality rate and body weight after the ET-1 injection at the chronic stage*

We reported a 5% accidental death rate during ET-1 injection surgery using isoflurane anaesthesia and 7% during MCAO surgery; in both surgeries rats died mainly due to anaesthesia-related causes during the surgery. We had no incidence of animal death after the surgery and all rats survived until the perfusion day, except that one animal was humanely terminated at P20 due to inflammation at the incision site that did not subside with treatment.

Comparing our animal mortality rate with other studies is inappropriate because of the lack of similar studies that inject ET-1 at P12 to produce the PIS model. A very recent, similar study injected ET-1 intracerebrally into P14 rats but did not report the mortality rate (Gennaro et al., 2017). However, in a P12 neonatal study, ET-1 was injected into the hippocampus which led to a 20% death rate that occurred only during the first 24-hours post-surgery using halothane anesthesia (Mateffyova et al., 2006). Also, injecting ET-1 at the level of MCA in P10 rats led to a 46.5% death rate, with the authors claiming that the resultant brain damage caused the high mortality rate (Yager et al., 2006). In our study, the mortality rate was much lower, and therefore, ethically, more acceptable than other studies.

Different procedures of inducing stroke are associated with different complications. Studies showed that the method we used (injecting ET-1 directly into the SMC) to induce the cortical ischemic lesion resulted in a lower mortality rate than the other methods. When MCAO is occluded, either by the direct electroligation (Renolleau et al., 1998) or by injecting ET-1 near the MCA (Ansari et al., 2011, Yager et al., 2006), the mortality rate is high. For example, in a study by (Renolleau et al (1998), a high percentage of P7 rat pups died during the MCAO with transient carotid occlusion surgery. In another more recent study mentioned above, P10 rats who underwent MCAO via ET-1 injection showed a 46.5% death rate, but not the older rats (P63 and P180) (Yager et al., 2006). However, when the induced focal ischemia was due to injecting ET-1 into the SMC in immature rodent as in our study or in an aged rodent as in a previous study (Soleman et al., 2010), a low mortality rate was recorded.

However, it is not always the case that MCAO results in high mortality. In a study that used immature mice, the mortality rate was low (15%) two days after the surgery with no animal deaths occurring during the surgery when isoflurane was used. In the previous section (3.7) we indicated that the anesthetic type used in the modelling surgery might affect the behavioural outcomes. Similarly, the mortality rate could be affected by the type of the used anesthetic. For example, Tsuji et al (2013) suggested the beneficial effect of the use of isoflurane in reducing the infarction severity (Chen et al., 2011). In our study, we used isoflurane as a gaseous anesthetic during the surgery. In agreement with our results, a low mortality rate (13.35%) was reported in an adult rat study that injected ET-1 into the SMC using isoflurane during surgery (Soleman et al., 2010). On other hand, a considerable number of rat deaths was reported after intraperitoneal injection of chloral hydrate in P7 rats during MCAO surgery (Renolleau et al., 1998). We suggest that the anesthesia used during the surgery might also have a role in this high mortality.

In our ET-1 stroke model experiment, each rat pup was weighed at the day of the ET-1 injection surgery and then weighed regularly until P34. Generally, ET-1–injected rats exhibited a significantly lower absolute weight gain than the sham-operated animals over 22 days, post insult.

There is no similar study to compare our results against. Even the very recent study that injected ET-1 in the SMC of P14 rats did not weigh their animals (Gennaro et al., 2017). In a neonatal study of rats undergoing a hippocampus lesion at P12 by ET-1, the relative and absolute body weight measured on day 65 post lesion did not differ significantly(Mateffyova et al., 2006).The low mortality rate and the weight loss suggest that our ET-1 method to produce PIS is safer than other methods though it affects the body weight adversely which is in agreement with the below average weight recorded in cerebral palsy children (Day et al., 2007, Krick et al., 1996).

## 3.5 Conclusion

The experiments in this chapter have shown that inducing an ischemic lesion in P12 neonatal rats using ET-1 or MCAO leads to histological changes in different cortical regions. We occluded the MCAO resulting in hypoxic damage to the bfSSC, but not to the lSMC that controls limb function. The MCAO model failed to show evidence of an inflammatory reaction or hypoxia in the lSMC in the acute phase, or a neuronal loss in the chronic phase. The MCAO proved to be a poor stroke model in P12 rat pups as the lSMC is, a major site of damage in

human neonates. On the other hand, injecting ET-1 directly into the SMC did result in focal, unilateral hypoxic damage to the lSMC. However no significant behavioural dysfunction resulted from either method which led us to trace the CST arising from the ET-1 lesioned hemisphere and compare it to the tract arising contralateral hemisphere. In the next chapter, the possibility of cortical plasticity of the CST in our PIS model was addressed.

# Chapter 4. Plasticity of the CST in PIS Model

## 4.1 Introduction

Perinatal ischemic stroke (PIS) leads to hemiplegia that is progressive in its nature and affects more than 80% of the infants that have CP following perinatal stroke (Golomb et al., 2008). In hemiplegic cerebral palsy, there is a progressive loss of corticospinal projections from the affected cortex for up to two years after the stroke resulting in the progressive appearance of neurological signs and symptoms (Eyre et al., 2007).

The behavioural outcome in those affected children is determined by the extent of the corticospinal projection from the infarcted cortex. The outcome of adult-onset stroke is largely determined by the extent of the initial brain injury, and motor recovery occurs if a critical portion of corticospinal system function has been spared at the time of the lesion (Hendricks et al., 2003). However, this is not the case in a perinatal stroke, and infants with a significant corticospinal projection from the infarcted cortex present soon after the stroke, as detected by transcranial magnetic stimulation, can still exhibit poor motor outcomes (Eyre et al., 2007).

Several studies showed that rat is a good model to investigate the corticospinal tract (CST) alteration in neonatal stroke studies. Despite some existing differences, crucial similarities such as CST pathway and full length projections into the spinal cord between human and rats CST attracts researcher to use rats as stroke models (Armand, 1982, Bareyre et al., 2005, Eyre et al., 2007, Kuypers, 1981, Lemon, 2008, Rouiller et al., 1991). Moreover, using rodent as a model that have short life span and mature in a matter of weeks rather than over months and years as in humans is an additional important advantage (Clowry et al., 2014).

The aims of this experiment were: firstly to look for possible anatomical re-organisation of the corticospinal tract (CST) from both the ipsilesional hemisphere (IH) and contralesional hemispheres (CH) in our perinatal ischemic stroke (PIS) model, compared to sham operated animals, after injecting the retrograde tracer Fluorogold (FG) into the left (contralesional) side of the cervical spinal cord at P45 (Juvenile age) to label both forelimb (FL) and hindlimb (HL) regions of IH and any other cortical areas projecting to the spinal cord from the IH and CH (Nielson et al., 2011), and secondly, to explore the relationship between any behavioural defect and corticospinal plasticity, in our PIS model..

## 4.2 Results

We injected 20 rats at P40 with FG and only animals in which the tracer was confined to the left side of the spinal cord were included in this study (Figure 4.1). For this reason, five animals from the sham group and 6 rats' from the ET-1 group had to be excluded. Also, two animals died during surgery (Table 4.1). For each lesioned (n=4) and sham (n=5) animal, all positive FG neurons, detected by Immunoperoxidase staining, were counted in eight serial coronal sections using the Image hub and imageJ software.

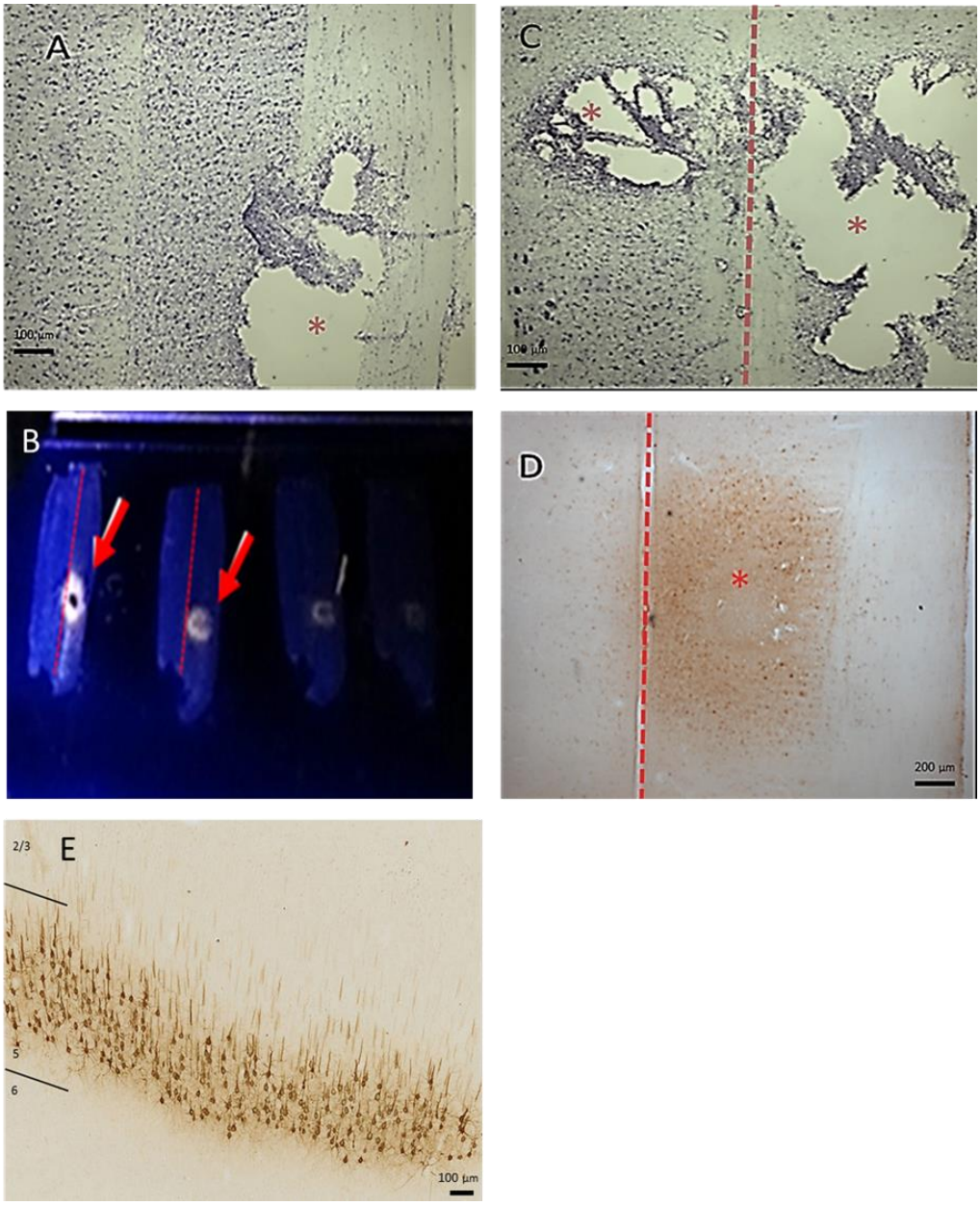


**Figure 4.1 Unilaterality of the injected FG into the spinal cord at the cervical level.** Transverse sections of the injected spinal cord. (A) Cresyl violet staining shows unilateral successful FG injection (asterisk). (B) FG fluorescence under UV light shows successful FG injection unilaterally (arrows). (C) Cresyl violet shows unsuccessful injection site crossing (asterisk) the midline (dashed red line). (D) Immunostaining for CST neurons using anti-FG antibody showing unilateral injection (asterisk). The midline of the spinal cord is marked by a dashed red line. (E) The cortex of coronal rat brain sections stained for FG in the sensorimotor cortex (SMC).

| Groups | Total Number before the surgery at P40 | Number of excluded rats | | Number of included rats |
|---|---|---|---|---|
| | | Crossed FG labelling at the spinal cord level | Died during surgery | |
| ET-1 | 10 | 6 | 1 | 4 |
| Sham | 10 | 5 | 1 | 5 |

**Table 4.1. The number of animals included and excluded after retrograde tracer surgery the in each the ET-1 model and sham groups.**

### *4.2.1 Counts of the FG+ neurons*

The number of FG+ neurons in the IH and CH for each rat in both endothelin-1 (ET-1) models and sham animals was counted. To compare between the ET-1 and the sham groups, we used non-parametric statistics because of the small size of the sham (n= 5) and ET-1 (n= 4) groups and also because the assumptions of the t-test were violated. Two comparisons were made: first the counts of FG+ neurons in the CH were compared between ET-1 and sham groups and second the numbers of FG+ neurons in the IH were compared between ET-1 and sham groups. Overall, larger numbers of FG+ neurons were found in the CH of the PIS model than in the sham animals. Although the number of FG+ neurons varied greatly between animals, the percentage of total FG+ neurons in the CH was invariably smaller than in the IH in sham animals (Figure 4.2).

The difference in numbers of FG+ neurons between sham and ET-1 groups in the CH and then in the IH was tested. Interestingly, we found a borderline significant difference in the CH between sham and ET-1 groups (p=.05; Mann Whitney U test). Conversely, no significant difference was found in the IH for FG+ neuron counts between sham and ET-1 groups.

Secondly, we compared the difference in the numbers of FG+ neurons between the CH and IH within sham group and correspondingly within the ET-1 group using paired data (Wilcoxon signed ranks test). Interestingly, we found a significant difference in the FG+ neuron counts in the sham group between CH and IH (p=.0.04) while in the ET-1 group, we correspondingly found no difference in the FG+ neuron counts between CH and IH .

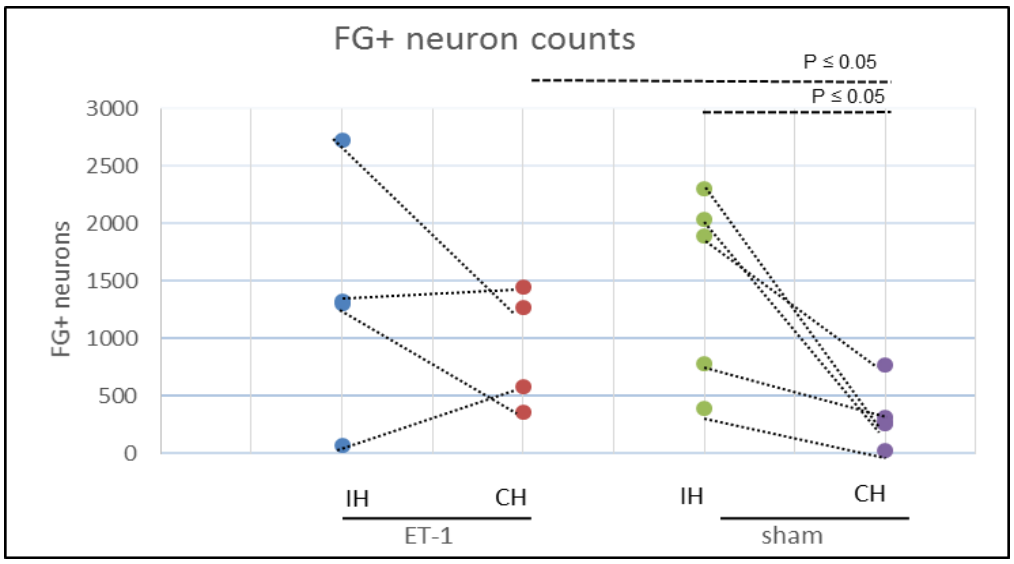


**Figure 4.2 Counts of FG+ neurons summarized in plotting charts.**

Counts of FG positive neurons in IH and CH of sections from 8 serial coronal sections of each ET-1 and sham animals. A significantly lower number of FG+ neurons was counted in CH ET-1 animals than shams (Mann Whitney U test) and in CH compared to IH within sham animals using paired data (Wilcoxon signed ranks) test).

### *4.2.2 Proportions of FG+ neurons*

The proportion of FG+ neurons in each hemisphere and each compartment of each hemisphere as a percentage of total corticospinal (CS) neurons labelled was calculated for each rat to normalize the data. Overall, a smaller proportion of FG+ neurons were found in the motor cortex (MC), somatosensory cortex (SSC), and lateral cortical regions of the IH in the PIS model than in the sham animals. Conversely, there was a three-fold increase in the percentage of FG+ neurons found in the CH of the ET-1 animals compared to sham (Figure 4.3).

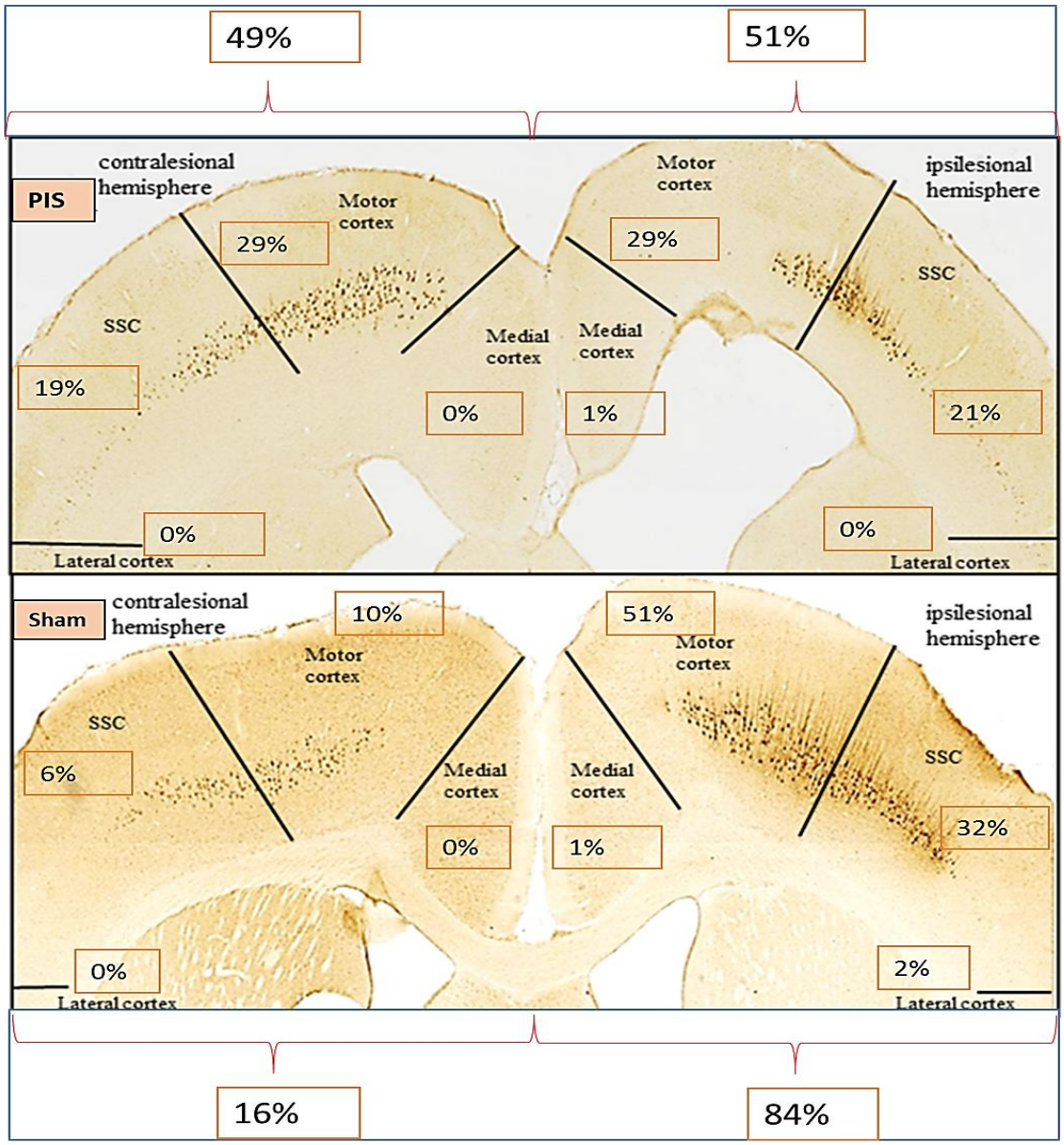


**Figure 4.3 Percentage of Immunoperoxidase stained neurons for the retrograde tracing FG for brain coronal sections in both ET-1 and sham groups.**

Lower mean percentage of FG+ neurons in the motor, somatosensory, and lateral cortex of the IH in ET-1 group but an increase in percentage of FG+ neurons in the medial IH and all regions on the CH compared to sham. The percentage of the neurons immunopositive for FG in the sham group was smaller in the non-lesioned cortex compared with lesioned one. percentage=number of FG+ neurons in one region of the cortex divided by the total number of FG+ neurons and multiplied by 100.

When the mean % of FG+ CS neurons in the CH and IH were compared between the ET-1 and sham animals, a larger proportion of FG+ neurons was found in the CH than in the IH particularly in the MC, in the ET-1 group (Figure 4.3 and Figure 4.4). The difference in proportion of FG+ neurons in each cortical compartment of the CH revealed that in shams approximately a half of FG+ CS neurons were localised to the MC whereas in the ET-1 group less than a third of total FG+ neurons were in the MC in CH. Similarly, on average, in shams a third of FG+ neurons were located in the contralesional SSC, but only a fifth in ET-1 animals (Figure 4.3).

When the mean of the FG+ neuron percentages of the CH and IH were compared within sham animals, a higher percentage was found in the IH (84%) than in the CH (16%). However, in the ET-1 group, the mean FG+ neuron percentage in the IH was (51%) and in the CH (49%) (Figure 4.3).

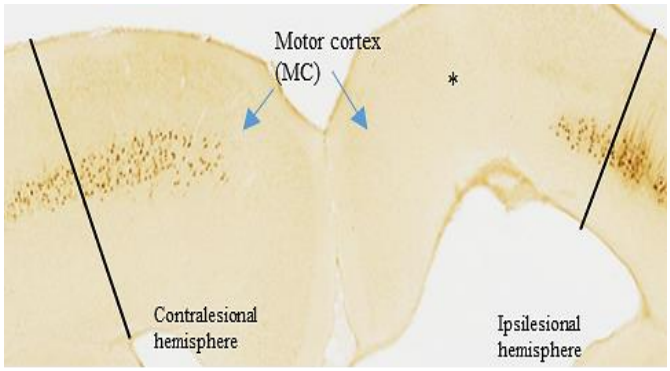


**Figure 4.4. Immunoperoxidase staining of the CST at P45 after injecting ET-1 at P12 in the PIS model in the MC**

In the motor cortex, neuronal loss indicated by the depletion of some of the FG+ neurons in the IH (asterisk) compared to the CH.

**FG+ percentage in the et-1 vs sham group**

To compare between the ET-1 and the sham groups, we used non-parametric statistics because of the small group sizes.

The proportion of FG+ cells found in the CH in ET-1 animals was statistically significantly higher than in the sham lesioned animals in total, and in the MC and SSC when considered separately ($p= 0.05$; Mann Whitney U test). In the IH, we correspondingly found a significantly smaller percentage of FG+ neurons in ET-1 animals compared to sham ($p= 0.05$) (Figure 4.5).

**FG+ percentage in the ipsilesional vs contralesional hemisphere**

We compared the percentage of the FG+ cells in the IH vs CH in the ET-1 and sham group using the paired data (Wilcoxon signed ranks test). In the ET-1 group, the percentage of FG+ cells in the CH did not differ significantly from the percentage of FG+ cells in the IH in any cortical region. However, in the sham group, the percentage of FG+ neurons in the CH was statistically significantly lower than the percentage of FG+ cells in the IH in total, and in the MC and SSC ($p= 0.04$) (Figure 4.5) as would be expected, as the normal rodent CST shows a high degree of crossover (Joosten et al., 1992, Rouiller et al., 1991).

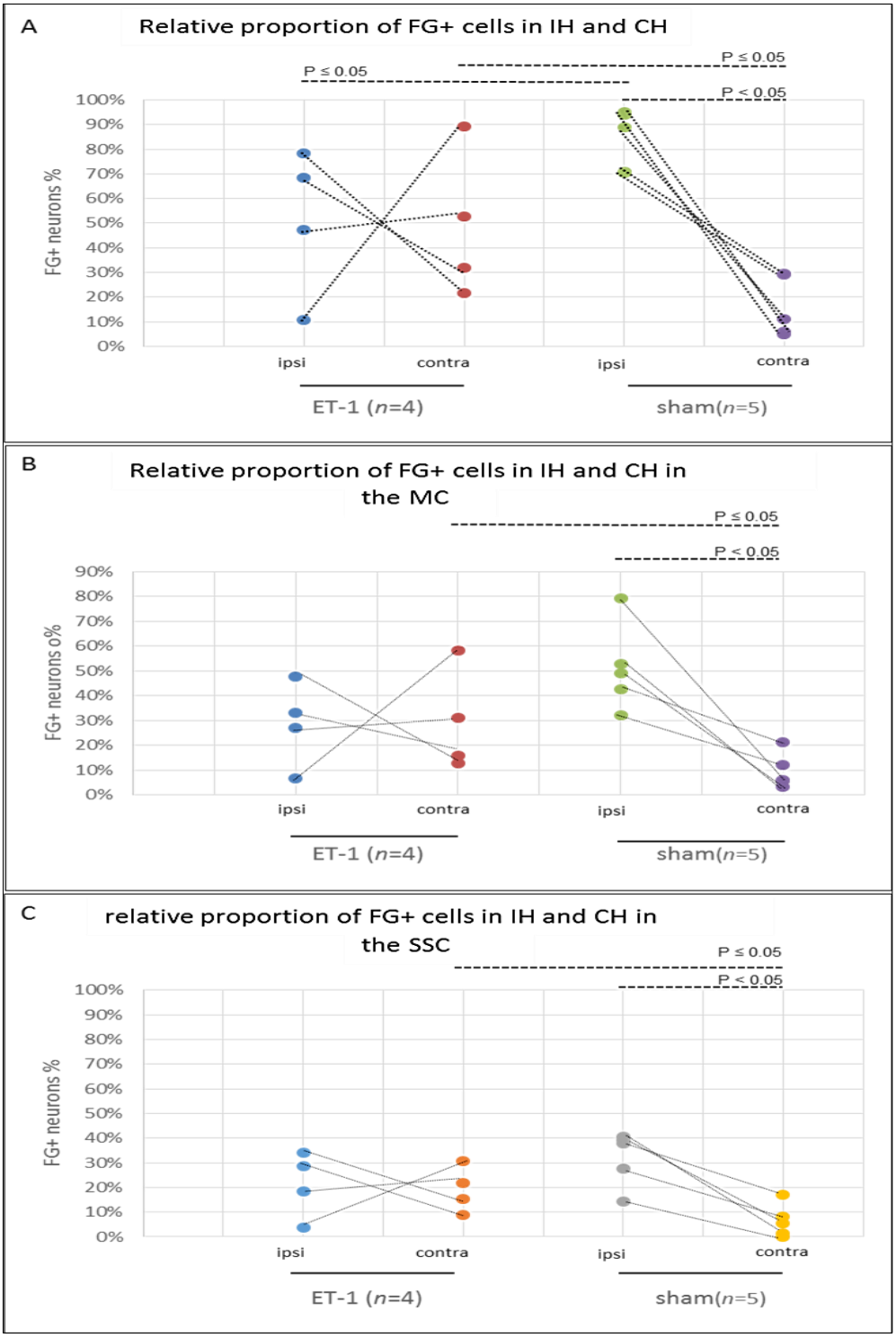
A
Relative proportion of FG+ cells in IH and CH
P ≤ 0.05
P ≤ 0.05
P < 0.05
FG+ neurons %
100%
90%
80%
70%
60%
50%
40%
30%
20%
10%
0%
ipsi
contra
ipsi
contra
ET-1 (n=4)
sham(n=5)
B
Relative proportion of FG+ cells in IH and CH in the MC
P ≤ 0.05
P < 0.05
FG+ neurons o%
90%
80%
70%
60%
50%
40%
30%
20%
10%
0%
ipsi
contra
ipsi
contra
ET-1 (n=4)
sham(n=5)
C
relative proportion of FG+ cells in IH and CH in the SSC
P ≤ 0.05
P < 0.05
FG+ neurons %
100%
90%
80%
70%
60%
50%
40%
30%
20%
10%
0%
ipsi
contra
ipsi
contra
ET-1 (n=4)
sham(n=5)

**Figure 4.5. Percentage of FG-positive neurons summarized in plotting charts.**

A summary of the % FG positive neuron in IH and CH from 8 serial coronal sections from each of the ET-1 and sham animals. A significantly lower number of FG+ neurons in IH compared to CH within sham animals in all cortical regions using paired data (Wilcoxon signed ranks test). (A) A significant lower % in IH and higher % in CH in ET-1 animals compared to shams (Mann Whitney U test). (B) and (C) a significant higher % of FG+ neuron in CH than IH in MC and SSC cortical regions (Mann Whitney U test) and a trend towards a reduction in FG+ neuron % in IH of ET-1 animals compared to shams was seen but this was not significant (Mann Whitney U test).

### *4.2.3 Correlation of the FG+ neurons in the ipsilesional and contralesional hemisphere*

The percentage of the FG+ neurons in one hemisphere and the total number in both hemispheres were plotted in Figure 4.6. Figure 4.6, shows, disregarding the one outlier that the proportion of labelled neurons in IH increased as the total number of neurons labelled increased while in CH the proportion decreased as the total number of neurons labelled increased.

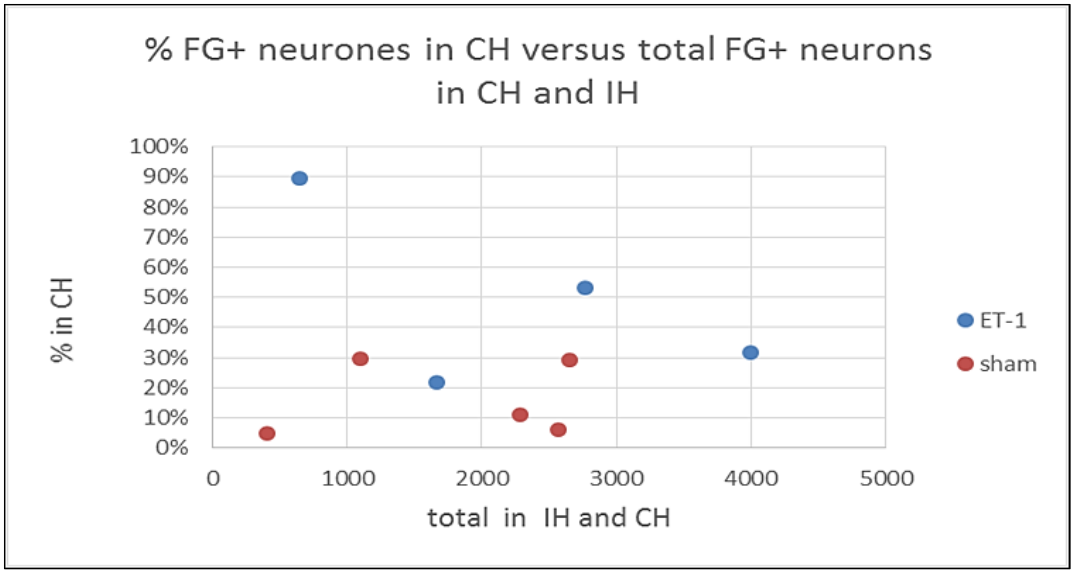


**Figure 4.6. Correlation between the total number of FG+ neurons in both hemispheres and the proportion of FG+ neurons in the CH in ET-1 and in sham groups**

There is a trend towards more labelled neurons in the CH as the total number of cells labelled increases.

### *4.2.4 The relationship between the percentage of the FG+ neurons and the behavioural outcomes*

We found above that the proportion of neurons immunopositive for FG was higher in the IH than in the CH in the sham group (Figure 4.2). Moreover, after inducing the ischemic lesion in the ET-1 group, this distribution was reorganised giving a higher proportion of neurons in the CH with a smaller proportion of FG+ neurons in the IH compared to sham (Figure 4.2). Thus, in this section we investigated whether there was a relationship between a possible relative increase in the ipsilateral tract and the smaller than behavioural deficits previously observed (see Chapter 3).

FG+ neuron percentage in each hemisphere in sham and ET-1 groups was plotted against the score for the contralesional limb performance in the cylinder and the grid walk tests. Three lesioned rats and 5 shams were included.

Generally, we found better functional performance if the FG+ neuron percentage in the CH was higher in the ET-1 model. In the sham group, there was a much higher proportion of FG+ neurons in the IH than the CH regardless of behavioural performance, as expected.

**Grid walk test**

In this test we calculated the percentage of forelimb faults (FLF) by dividing the contralesioned FLF by the number of total steps. The hindlimb faults (HLF) percentages were calculated correspondingly. Overall, we found better functional outcomes for FLF and HLF when there were higher proportions of FG+ neurons in the CH in the ET-1 model, but this was not observed in the sham group (Figure 4.7A and Figure 4.8A).

Interestingly, in the ET-1 animals, we found that the largest percentage of FG+ neurons in CH and the smallest percentage of FG+ neurons in IH was found in the rat where the FLF percentage was the smallest (i.e. the best performing) (Figure 4.7B).

In the CH of the ET-1 group, we found that the rat with the best performance had a much higher proportion of FG+ neurons in the MC compared with the SSC while the FG+ neurons in the rat with the worst performance had almost similar percentage (Figure 4.7C).

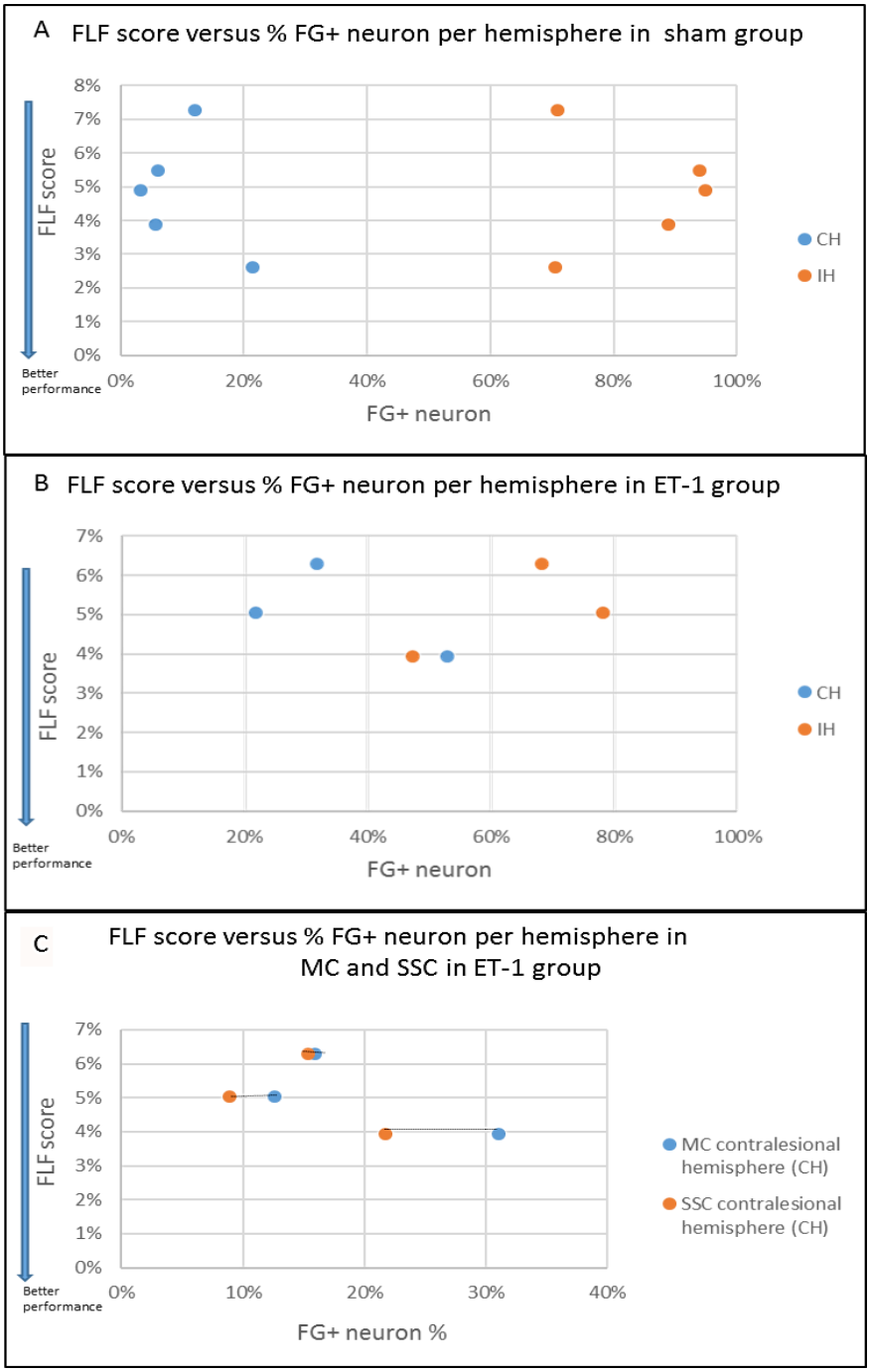


**Figure 4.7. Correlation between FLF scores and proportion of FG+ neurons in each hemisphere.**

The graph shows the relationship between the percentage of FG+ neurons in both hemispheres and the contralesional FLF score in sham (A) and ET-1 group (B). The relationship between the percentage of FG+ neurons in MC and SSC in ET-1 group and the contralesional FLF score (C).

The relationship between the distribution of FG+ neurons in the cortex and the HLF score was similar to the relationship seen for the FLF score (Figure 4.8A). In the ET-1 animals, the greater the HLF score, the smaller the percentage of FG+ neurons in CH. The rat with worst performance had the smallest proportion of FG+ neurons in the CH compared to the rats with better performance (Figure 4.8B).

In the ET-1 group, we found that better performance was associated with a greater positive difference between FG+ neurons in the MC versus SSC (Figure 4.8C).

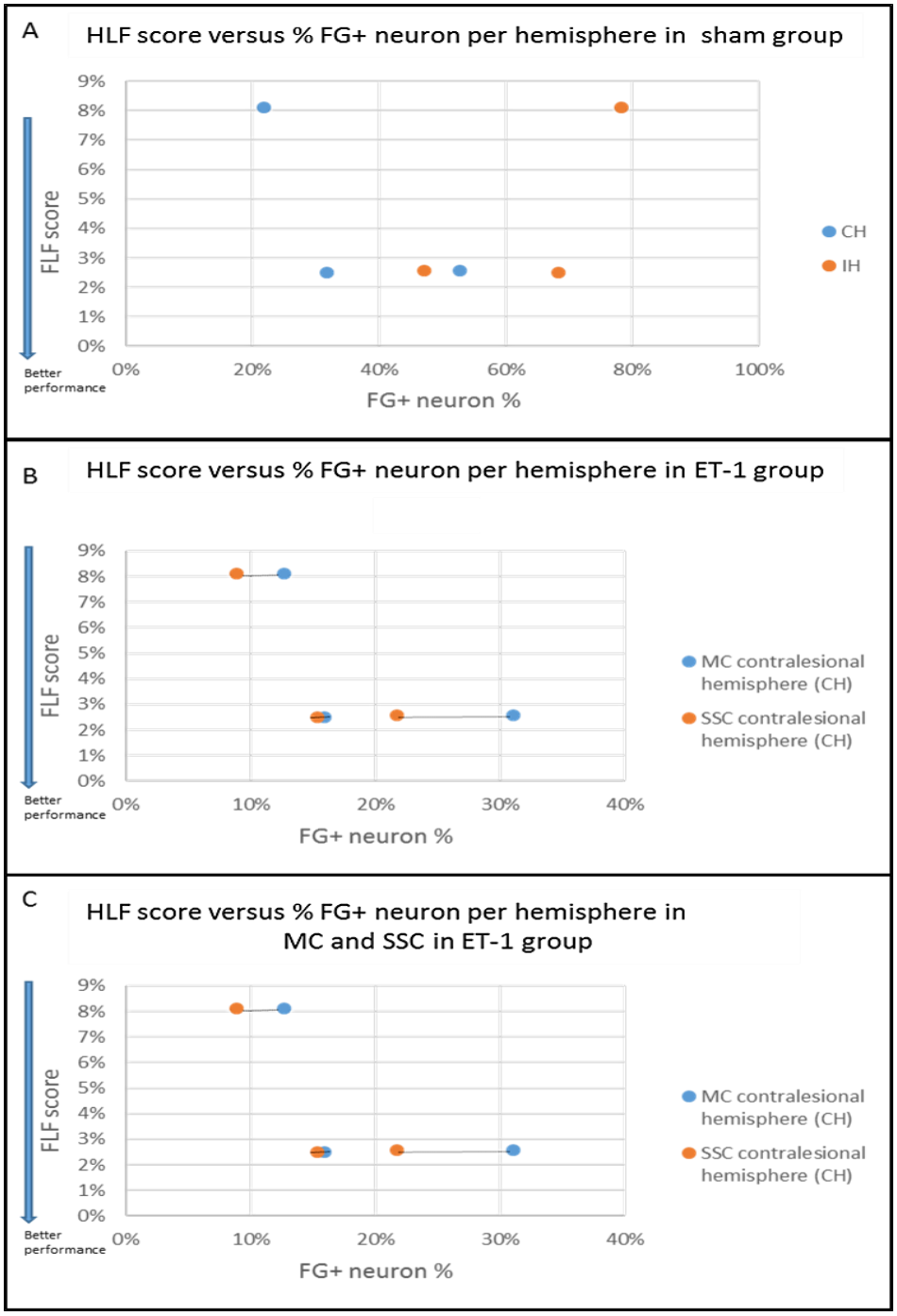


**Figure 4.8. Correlation between proportion of HLF scores and FG+ neurons in each hemisphere**

The graph shows the relationship between the percentage of FG+ neurons in both hemispheres and the contralesional HLF score in % in sham (A) and ET-1 group (B). The relationship between the percentage of FG+ neurons in MC and SSC in ET-1 group and the contralesional HLF score (C).

**Asymmetry Placement Test**

All animals tested in the grid walk were tested for forelimb placement asymmetry using the cylinder test. Generally, we found better functional outcomes for the asymmetry test with an increased proportion of FG+ neurons in the CH in the ET-1 model, while in the sham group, all rats had more FG+ neurons in the IH than the CH regardless of behavioural performance as expected (Figure 4.9A and Figure 4.9B).

We found that as the FL performance in the asymmetry test tended toward the 50% score (the point at which both lesioned and non-lesioned limbs performed equally), the percentage of FG+ neurons in the CH in the ET-1 group increased (Figure 4.9B).

The proportion of FG+ cells in the MC and in the SSC (Figure 4.9C) was studied in relation to forelimb asymmetry test performance. Interestingly, similar to the grid walking test, we found that in the rat with better performance, there were many more FG+ neurons detected in MC than in SSC (Figure 4.9C).

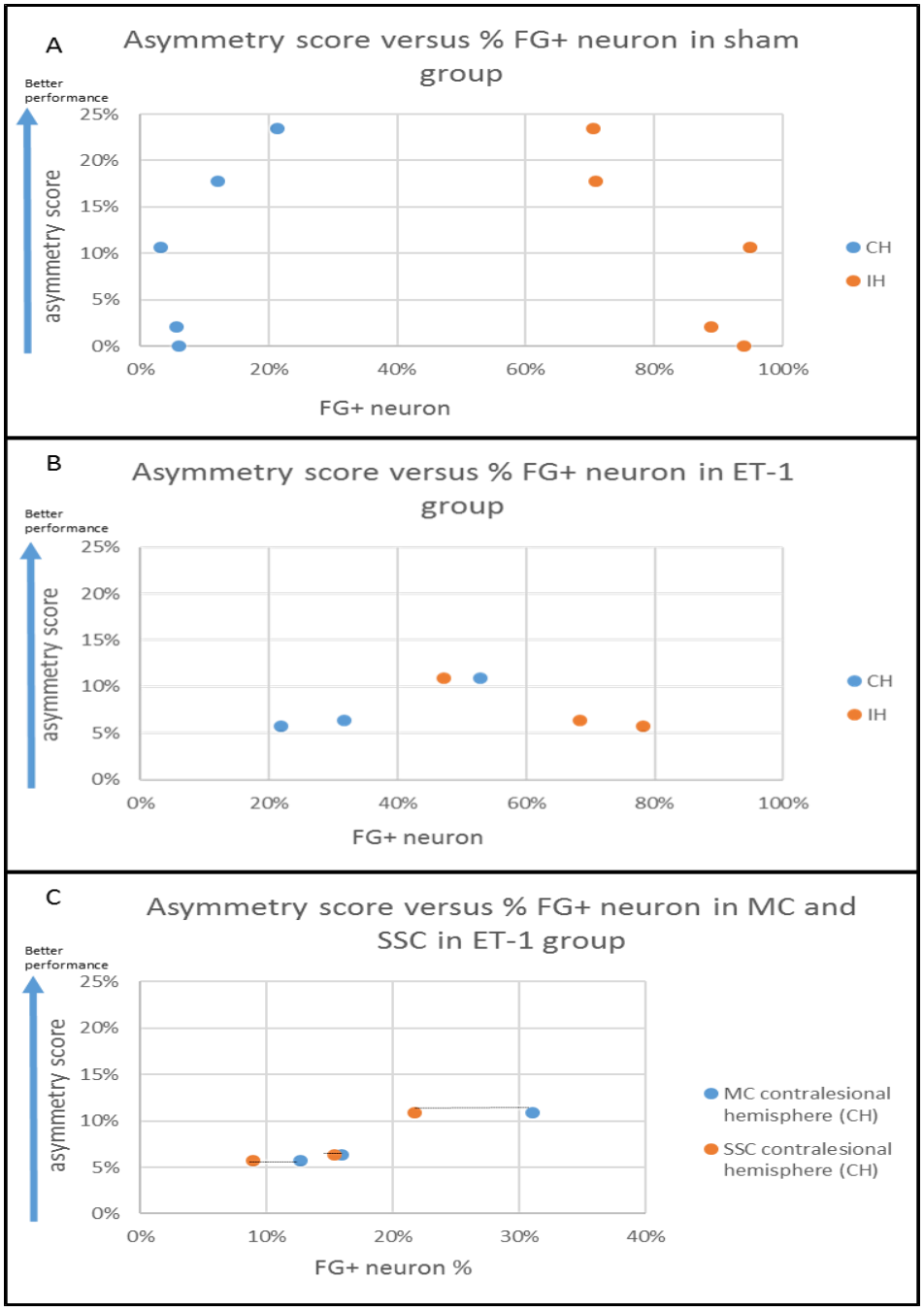


**Figure 4.9. Correlation between asymmetry placement scores and proportion FG+ neurons in each hemisphere**

The relationship between the percentage of FG+ neurons in both hemispheres and asymmetry placement scores in % in sham (A) and ET-1 group (B). The relationship between the percentage of FG+ neurons in MC and SSC in ET-1 group and the asymmetry score (C).

## 4.3 Discussion

The experiments described in this chapter and in Chapter Three have shown that inducing focal ischemic lesion in the SMC of P12 neonatal rats using ET-1 results in hypoxic damage to the limb sensorimotor cortex (lSMC) unilaterally resulting in a smaller proportion of retrogradely labelled CS neurons in the IH and a larger proportion in CH than in a sham group. To our knowledge, this is the first time retrograde tracing of the CST has been studied in a PIS model at P12 using ET-1.

Although ET-1 resulted in a smaller proportion of labelled CS neurons in the IH and larger proportion in CH than in sham, we also tended to find a higher absolute number of labelled CS neurons in both IH and CH in the ET-1 group than in the sham group. There were, on average, considerably more FG+ CS neurons in the CH of the ET-1 group than in the sham group but also more CS neurons on average in the IH in ET-1 group than in sham group. There was a tendency for a higher proportion of neurons to be labelled in the CH as the total number of CS neurons labelled increased regardless of whether it was a sham or ET-1 experiment suggesting that the number of neurons labelled in any hemisphere was to some degree dependent upon some variable to do with the experimental procedure, perhaps how close to the midline the FG was injected. Nevertheless it doesn't seem likely that this would not account for all of the very large increase in relative contralesional cortical labelling observed in these experiments; two other factors are likely to also contribute.

The smaller proportion of CS neurons in the IH of ET-1 animals could be due to a loss of some neurons in the IH because of the PIS and/or because of an increase in labelled neurons in the CH due to plasticity. Previous studies indicate that a large unilateral cortical lesion in the SMC leads to a decrease in CS neuron projections from that hemisphere. (Gibson et al., 2000b) have reported substantial loss of direct CS projections in the cervical spinal cord originating from the MC in the IH after a MC ablation in P7 neonatal rats. In our study our subtle lesion kept the SMC intact but perhaps with fewer CS neurons projecting to the spinal cord.

Corticospinal axons of developing rodents originate in cortical layer V of the SMC; 96–98% of them cross to the contralateral side of the spinal cord, while the remaining 2-3% stay on the ipsilateral side (Joosten et al., 1992, Rouiller et al., 1991). However, many experiments have found that lesioning (Jansen and Low, 1996, Joosten et al., 1992, Kartje-Tillotson et al., 1985, Kartje-Tillotson et al., 1986) or merely inactivating (Clowry et al., 2004, Staudt et al., 2004)

the SMC unilaterally during development leads to an increased ipsilateral projection to the spinal cord from the spared hemisphere. It is likely that the ET-1 induced lesion may have killed some CS neurons in the SMC but also suppressed activity in the surviving neurons. As Figure 4.10 in Chapter Three shows, parvalbumin expression is greatly reduced at the lesion site. Parvalbumin is expressed by highly active interneurons within functioning networks suggesting suppression of network activity in the lesioned cortex. It has been proposed that surviving, but not very active, CS projections may lose out, after unilateral stroke, in competition for spinal cord synaptic space, leading to these projections being withdrawn as their potential targets are taken over by more active ipsilateral CS projections from the unaffected hemisphere and also by proprioceptive muscle afferents (Clowry, 2007, Eyre, 2007, Martin, 2005). The result is a higher proportion of CS neurons projecting from the CH via the ipsilateral CS pathway, with a smaller proportion arising from the IH. However, the current study cannot address whether the loss of CS projections from IH was progressive as in human PIS or non-progressive(Eyre et al., 2007).

Our finding of a likely increased ipsilateral projection from the CH complements previous studies conducted at younger ages (P1-P7) (Chen et al., 2004, Eyre, 2007, Jansen and Low, 1996). In rat neonate study, more contralateral projections from the MC of the CH were observed after inducing hypoxia unilaterally and after unilateral SMC lesion (Jansen and Low, 1996). We have shown that this type of plasticity extends until to lesions mad at a later developmental stage (P12) than has been studied previously, although the extent of plasticity seem less than has been observed in other studies, for instance (Clowry et al., 2004) maintained the ipsilesional pathway by inhibiting the SMC pharmacologically, but induced an ipsilateral projection of the same size as the normal contralateral projection as judged by retrograde labelling. The reorganisation seen in the present study is not as dramatic and may reflect a declining plasticity with age.

After neonatal rats (P0) received a unilateral SMC lesion, no deficit was observed in the forelimb placement test at P32-43. The authors suggested that the intact contralesional SMC provided part of the behavioural recovery mechanism that could be mediated by the formation of indirect ipsilateral pathways (Barth and Stanfield, 1990) via the ipsilateral red nucleus and not via direct ipsilateral CS projections (Z'Graggen et al., 2000).

Electrophysiological studies have been conducted to confirm the finding of increased ipsilateral projections originating from the CH. Research has confirmed the functionality of this pathway formed after unilateral cortical ablation in neonate rats, via microstimulation of the SMC in the CH intracortically at abnormally low current thresholds, which resulted in movement of the lesioned limb during adulthood. These movements were abolished by medullary pyramidotomy (Kartje-Tillotson et al., 1985, Kartje-Tillotson et al., 1987). Nevertheless, the timing of the SMC lesion in humans is crucial for the functionality of the plastic CS neurons in the CH. For instance, the paretic hand in a patient with hemiparesis was found to be controlled by the CST originating from the CH only if the lesion (such as MCAO) occurred prior to the late third trimester, using transcranial magnetic stimulation (TMS) and diffusion-tensor imaging to assess the CS pathways(Staudt et al., 2004). However, our neonatal rat study showed that inducing ischemic lesion into the SMC at P12, which represents the time of birth in human newborn, can lead to an increased proportion of CS neurons projecting to the ipsilateral tract from the CH.

The mechanism of structural plasticity after early unilateral cortical lesion in the developing brain is proposed to arise from the preservation of the aberrant CS projections originating from the CH. These projections do not arise from newly generated CS neurons, but instead are transient CS pathways generated during development. Normally, these aberrant CS connections projecting from the SMC withdraw by 2 years old in humans (Eyre, 2007). In rodents, there is no much evidence for transient ipsilateral projections indicated by a retrograde labelling study (Clowry et al., 2004). However, these transient connections were detected in developing rodents recently (Gu and Kalambogias, 2017).

In humans, there is evidence for an extensive transient ipsilateral projection, where, in the newborn, TMS is as likely to produce ipsilateral contractions in arm muscles as it is contralateral muscles, only with a shorter latency, suggesting a direct projection (Eyre et al., 2007). These ipsilateral projections are down-regulated during normal post-natal development, however in patients with hemiplegia derived from a pre- or perinatal lesion, or developmental malformation, these ipsilateral connections are retained (Eyre, 2007). We propose this underlying mechanism could explain our finding. In neonatal rats, the CS axons from the CH may remain as a compensatory reaction to the lesion allowing control of the lesioned limb to be retained (Gu and Kalambogias, 2017). In our experiment, retrograde tracing of the CST in the PIS model showed more CS neurons in the SMC at P45 in the CH, especially the MC,

compared to sham animals which might correlate to the better behavioural outcomes. We observed better functional performance when the proportion of FG+ neurons in the CH was larger than in the IH in our PIS model. Our findings would suggest that the structural plasticity in the CH contributed to the functional recovery described in Chapter Three. Because the CST is involved in limb function in rodents (Whishaw and Kolb, 2004), we suggest that the CST plasticity observed in response to the ET-1 lesion might be functionally advantageous. For instance,(Jansen and Low, 1996) suggested that motor regions such as SMC and striatum in the CH that underwent compensatory hypertrophic changes in the neonatal hypoxic model might be the reason for the normal functional results on rotarod test outcomes during adulthood. Moreover, good reaching and grasping performance were achieved in a neonatal hemidecortication study (Takahashi et al., 2009) as well as in an electrophysiological study that demonstrated that aberrant CS neurons located in the SMC in CH mediated pyramidal excitation to the affected limb (Umeda et al., 2010), and in a retrograde tracing study that suggested that CH plasticity underlies the good performance in these neonatal rats (Yoshikawa et al., 2011) . In fact, rodents do not show severe locomotor impairment in response to SMC lesions, but there is evidence of subtle, CST dependent sensorimotor deficits that can be found (Clowry et al., 2014, Nathan, 1994).

Electrophysiological studies have investigated the IH control over the affected limb. Studies have suggested that such plasticity is mediated either by a direct CS pathway, as found in hemiplegic patients (Eyre et al., 2001), or by an indirect pathway via the IH red nucleus in neonate animals (Z'Graggen et al., 2000) . following hemi-decortication in rats at P5, aberrant connections were formed from the surviving MC to contralateral red nucleus, superior colliculus, pontine nuclei, and the ipsilateral dorsal column nucleus and cervical spinal cord, which preserved FL function, but no aberrant projection to reticulospinal neurons was seen (Takahashi et al., 2009).

Recently, (Zewdie et al., 2017) studied the electrophysiology characteristics of the M1in CH in PIS children aged from 8–12y. They found that poor motor function was associated with persistence of ipsilateral projections after recording the MEPs. CST originating from CH was found hypertrophy in sub-primate animals after a substantial SMC lesion (Hicks and D'Amato, 1970, Hicks and D'Amato, 1977, Uematsu et al., 1996) and there was significant increase in CST axons from the CH in PIS children detected by the MRI (Eyre, 2007, Scales and Collins,

1972). To test the functionality of these ipsilateral CST axons from the CH Eyre (2001) utilized TMS to excite the CH motor cortex in PIS children. They found that the function of the paretic hand was limited when the CST of the CH was excited (Eyre et al., 2001). This was contradictory to our result suggesting that the increase in CS projections in the ipsilateral pathway does not improve the function of the affected paw and the best outcome when the CS projection originating from IH (Staudt et al., 2004).

In our model, although no significant dysfunction in motor behaviours was found, there was a constant trend of achieving lower outcomes in PIS models than sham animals. In fact, we could not validate whether the increase in FG+ neurons in the CH was linked to the improved behavioural performance due to the small sample size. Further researches with a larger sample size are needed to validate the correlation between improved behavioural outcomes and compensatory reorganisation of CS neurons from the CH. Thus, our findings suggest with caution that greater plasticity of CST in the CH leads to more recovery of functionality.

### 4.4 Conclusion

We have been able to show a likely anatomical reorganisation of the CS projections from the IH and CH in our PIS model. There was possibly a small loss of CS neurons in the IH in response to a developmental lesion of the SMC, coupled with an increase in ipsilaterally projecting CS neurons in the CH. Some evidence was found that surviving aberrant CS projections from the CH could be related to positive behavioural outcomes in the lesioned animals.

# Chapter 5. Transplantation of NSCs/ECM into Ischemic SMC in Neonatal Rat

## 5.1 Introduction

Stem cells are multipotential cells that have the ability to renew themselves and to differentiate into mature cell types such as neurons and have been used for cerebral palsy treatment in previous studies (Kiasatdolatabadi et al., 2017). Certain stem cell types such as neural stem cells (NSCs) have shown their capability to support the tissue structure and protect neurons at the lesion site in cerebral ischemia (Jendelová et al., 2016). Furthermore, stem cells have the ability to improve neurological outcomes post stroke in rodent models and promote endogenous neuroprotection, neurogenesis, neovascularization, axonal sprouting, and synaptogenesis (Castillo-Melendez et al., 2013, Englund et al., 2002, Jablonska et al., 2010).

In stroke models, grafting stem cells within an extracellular matrix (ECM) that mimics the brain niche in adult brain resulted in better results than transplanting stem cells alone in term of cell survival and improved cells viability and differentiation selectively in vivo (Bliss et al., 2007). The use of hydrogel that works as a compatible ECM adds an additional supporting that works as a scaffold for the transplanted stem cells and reduces the hostile environment in the ischemic infarction post stroke (Baeten and Akassoglou, 2011, Zhong et al., 2010).

We hypothesise that NSC transplantation along with HyStem hydrogel will protect and repair the lesioned SMC by reducing the inflammatory process resulting from the lesion in the host brain, inducing neurogenesis and angiogenesis or neovascularization at the site of the cortical infarction. The aim of this experiment was to compare between the survival and development of human neural stem cells (hNSCs) suspended in semi-synthetic extracellular matrix (ECM) in vitro and following grafting in vivo to a P14 rodent model of perinatal infarction damaging the sensorimotor cortex (SMC).

## 5.2 Results

### *5.2.1 Overview*

In the *in vivo* experiment, we injected twenty-two P14 PIS model rats, which was developed in Chapter 3, with hNSCs-ECM/ECM-only. Fifteen rats were assigned to the hNSCs/ECM group and seven rats to the ECM-only transplants group. Three animals from the ECM-only group had to be excluded due to error in the ECM injection coordinates that led to anatomical location

error of the graft. Also, one animals died during the ECM-only surgery. All animals were transcardially perfused with fixative (4% buffered paraformaldehyde (PFA)) at different time points post-grafting to test for survival and development of the hNSCs by immunohistochemistry (IHC) at one week, one month and three months post-transplantation. The total number and the subcategory values of the participating rats are detailed in **Table 5.1**.

| Groups | Total number | Perfusion time points for IHC | | | Number of excluded rats* |
|---|---|---|---|---|---|
| | P14 | 6D/P22 | 14D/P44 | D76/P90 | |
| hNSCs-ECM | 15 | 1 | 6 | 8 | - |
| ECM-only | 7 | 1 | 2 | - | 4 |

**Table 5.1. The number of animals included and excluded in each time point of the *in vivo* hNSCs/ECM and ECM-only groups.**
* Exclusion reasons were described in the text. D= days post-surgery, P=postnatal age.

### *5.2.2 In vitro experiment*

The hNSCs were cultured in a 2D monolayer or in a 3D semi-synthetic ECM were investigated by IHC prior to the in vivo NSCs transplantation to test the ability of NSCs to spontaneously differentiate into neuronal lineages. Immunolabeling was carried with antibodies to: PAX6 (neuroprogenitor cells (NPCs) proliferation and corticogenesis marker); hNCAM (human neural cell adhesion molecule); cytoplasmic protein of human cells (STEM121): DCX (migrating neuroblasts and neurogenesis marker); GFAP (astrocyte marker); neuron-specific marker Beta-III-Tubulin (TUJ1); MAP2 (neuron specific expression in dendrites and somata); TBR1 (early post-mitotic neuron marker of the neocortex); synaptophysin (neural synaptic vesicle marker). Cells were counterstained with the fluorescent nuclear marker 4',6-diamidino-2-phenylindole (DAPI).

**2D NSCs culture**

NSCs in 2 dimension (D) culture were fixed and immunostained at three time points: 10, 14, and 17 days after initiation of differentiation. Ten days after initiation of differentiation, NSCs expanded in number to form a mixed population of neural progenitor cells that were immunopositive for PAX6 and hNCAM (Figure 5.1A), new post-mitotic neurons that co-expressed TBR1 and STEM121 (Figure 5.1B), and the astrocyte marker GFAP (Figure 5.1C).

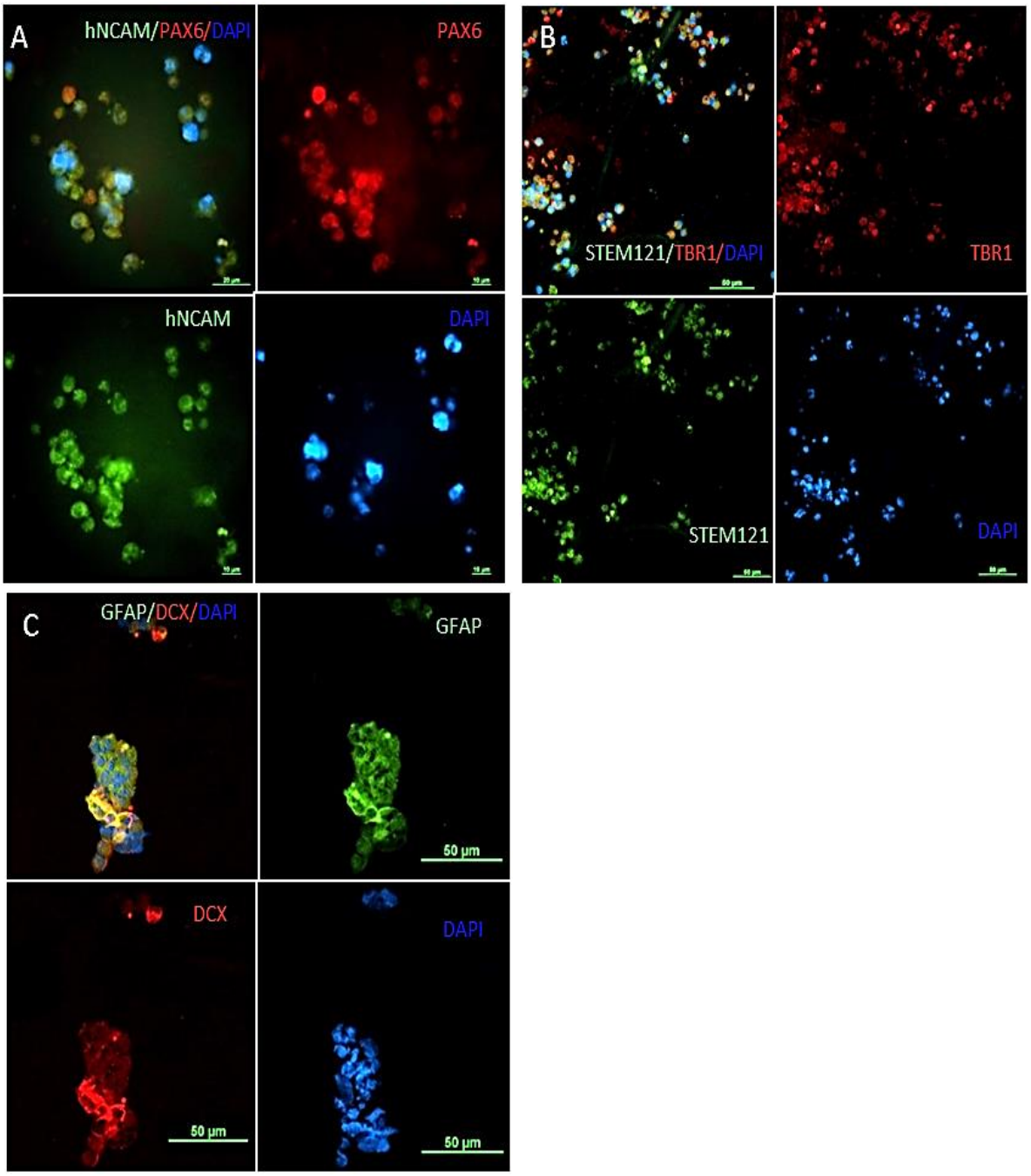


**Figure 5.1 Immunofluorescence of NSCs in 2D culture ten days after spontaneous differentiation *in vitro*.**

(A) NSCs expressed the cytoplasmic human marker hNCAM (green), and some of them co-expressed the neuronal progenitor marker PAX6 (red). (B) NSCs expressed the cytoplasmic human marker STEM121 (green), and some of them co-expressed the early post-mitotic neuron marker in the cortex TBR1 (red). (C) Few NSCs differentiated into the immature neurons DCX that co-expressed with the astrocyte marker GFAP (green).

14 Days after the initiation of differentiation PAX6/hNCAM+ progenitor cells were still observed (Figure 5.2A) in addition to post-mitotic neurons immunopositive for TBR1 (Figure 5.2B) and immature neurons immunopositive for DCX (Figure 5.2C). However, we observed more post-mitotic maturing pyramidal neurons expressing strong anti-MAP2 immunoreactivity (Figure 5.2D).

After Seventeen days of differentiation, NSCs individual cells were observed. However, cells also formed clumps close to the plate well's wall containing heterogeneous cell phenotypes. Figure 5.3A shows some cells that still stained with PAX6+ neuronal progenitors as single cells and in a sphere forming an immature neuronal clump. Furthermore, cells in the sphere expressed the marker DCX for immature neurons (Figure 5.3B) and MAP2 for more mature neurons (Figure 5.3C).PAX6 + progenitors and MAP2 + neurons were seen as single cells as well (Figure 5.3A and C). Also, cells in the sphere were immunopositive for synaptophysin suggesting that functional immature synapses may have been formed (Figure 5.3D). Finally, more pyramidal shaped TBR1 + cortical neurons presented at this time point (Figure 5.3E).

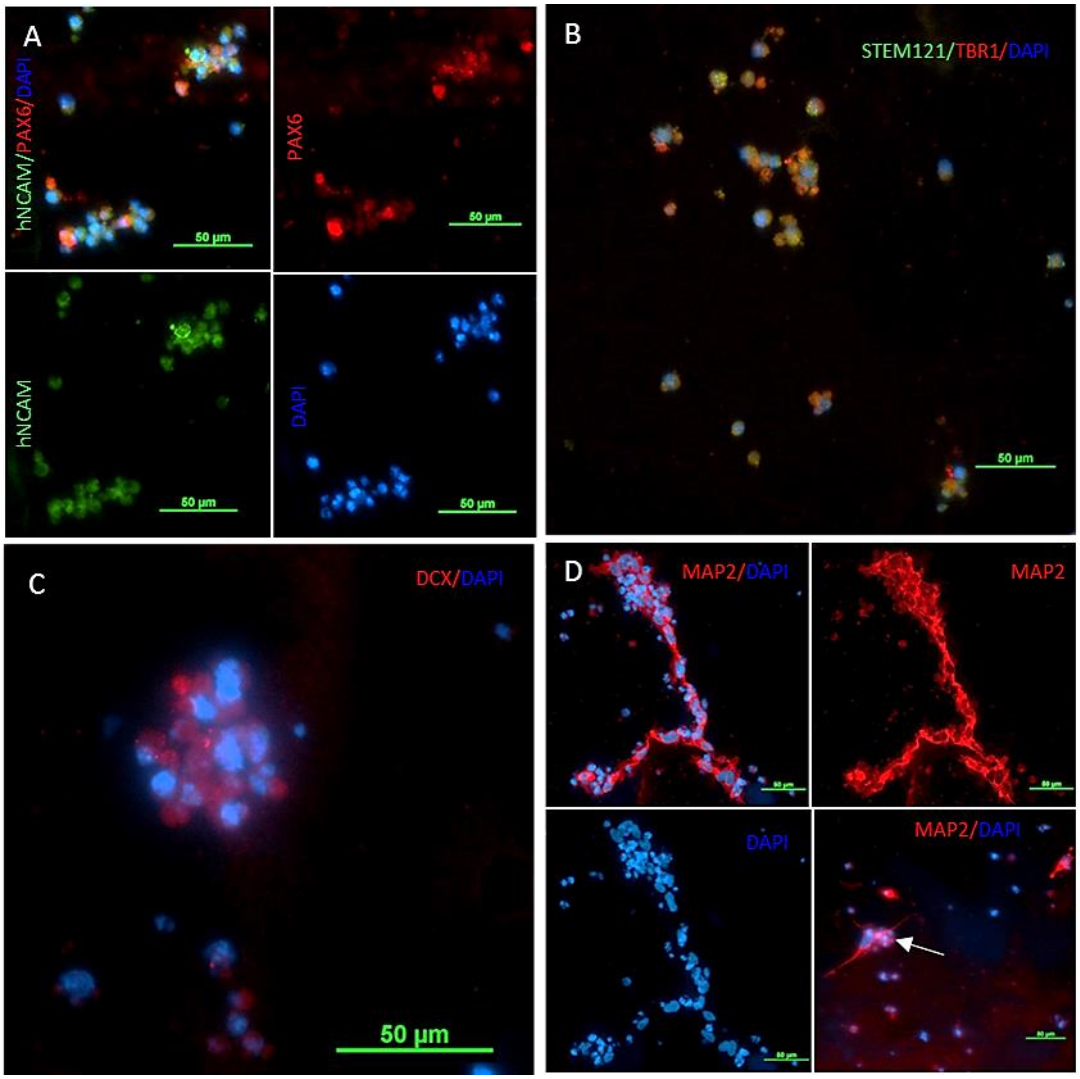


**Figure 5.2. Immunofluorescence of NSCs in 2D culture 14 days after spontaneous differentiation *in vitro*.**

(A) NSCs expressed the cytoplasmic human marker hNCAM (green), and some of them co-expressed the neuronal progenitor marker PAX6 (red). (B) NSCs expressed the cytoplasmic human marker STEM121 (green), and some of them co-expressed the early post-mitotic neuron marker in the cortex TBR1 (yellow). (C) Some NSCs differentiated into the immature neurons that expressed DCX (red). (D) NSCs differentiated into MAP2+ pyramidal neurons in chain form and single cell form (arrow). Cells were counterstained with the fluorescent nuclear marker DAPI (blue).

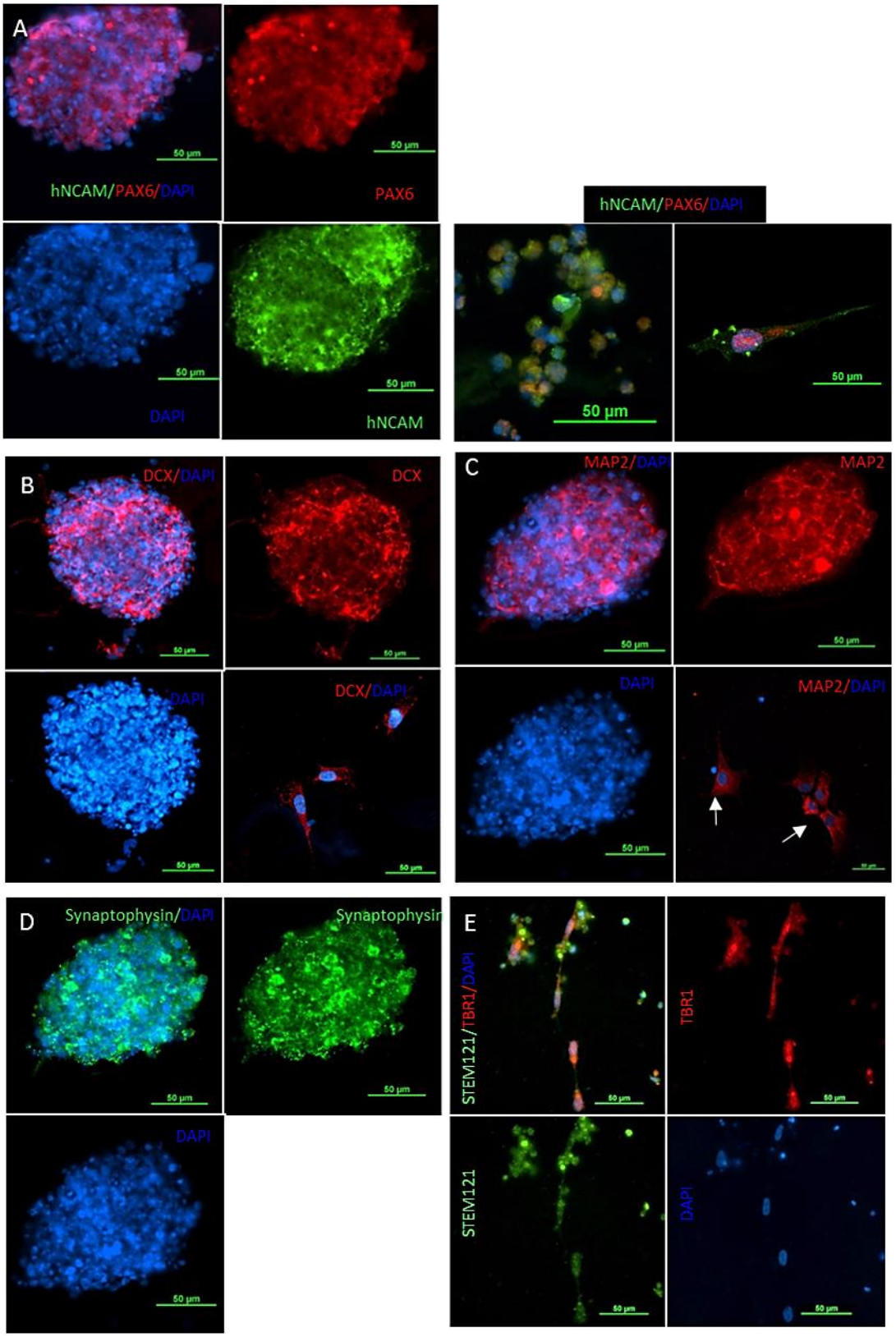
A
hNCAM/PAX6/DAPI
PAX6
DAPI
hNCAM
hNCAM/PAX6/DAPI
50 µm
B
DCX/DAPI
DCX
DAPI
DCX/DAPI
C
MAP2/DAPI
MAP2
DAPI
MAP2/DAPI
D
Synaptophysin/DAPI
Synaptophysin
DAPI
E
STEM121/TBR1/DAPI
TBR1
STEM121
DAPI

**Figure 5.3. Immunofluorescence of NSCs in 2D culture 17 days after spontaneous differentiation *in vitro*.**

(A) Both hNCAM+ (green), and a few PAX6+ (red) cells were observed dispersed within spherical clumps of cells. Also, few single cells co-expressed the cytoplasmic human marker hNCAM (green) and PAX6+ (red). (B) Some NSCs differentiated into the immature neurons that expressed DCX both in spheroid and as single cells (red). (C) NSCs differentiated into MAP2+ neurons in NSCs sphere and as single cells (red). (D) The neural synaptic vesicle marker synaptophysin in the NSCs sphere. (E) NSCs co-expressed the cytoplasmic human marker STEM121 (green), and the nuclear post-mitotic neuron marker in the cortex TBR1 (yellow). Cells were counterstained with the fluorescent nuclear marker DAPI (blue).

**3D NSCs culture**

NSCs in 3D culture were fixed and immunostained at four time points: 10, 14, 17 and 43 days after initiation of differentiation. Many DCX+ immature neurons presented in the 3D culture after ten days (Figure 5.4A). Although only a few neural progenitor cells immunopositive for PAX6 were noted after fourteen days of differentiation (Figure 5.4B), many DCX and Beta-III-Tubulin (β-TUB) positive immature neurons were observed extending long processes through the gel that were over 200µm in length and connected to each other (Figure 5.4C-E). Similarly, MAP2 immunopositive pyramidal neurons extended long processes over 50µm in length in the 3D culture (Figure 5.4F). Interestingly, the neural synaptic vesicle marker synaptophysin was expressed highly around some neuronal cell bodies that could be synaptic terminals around the small cell body, suggesting synaptogenesis as shown in Figure 5.4G.

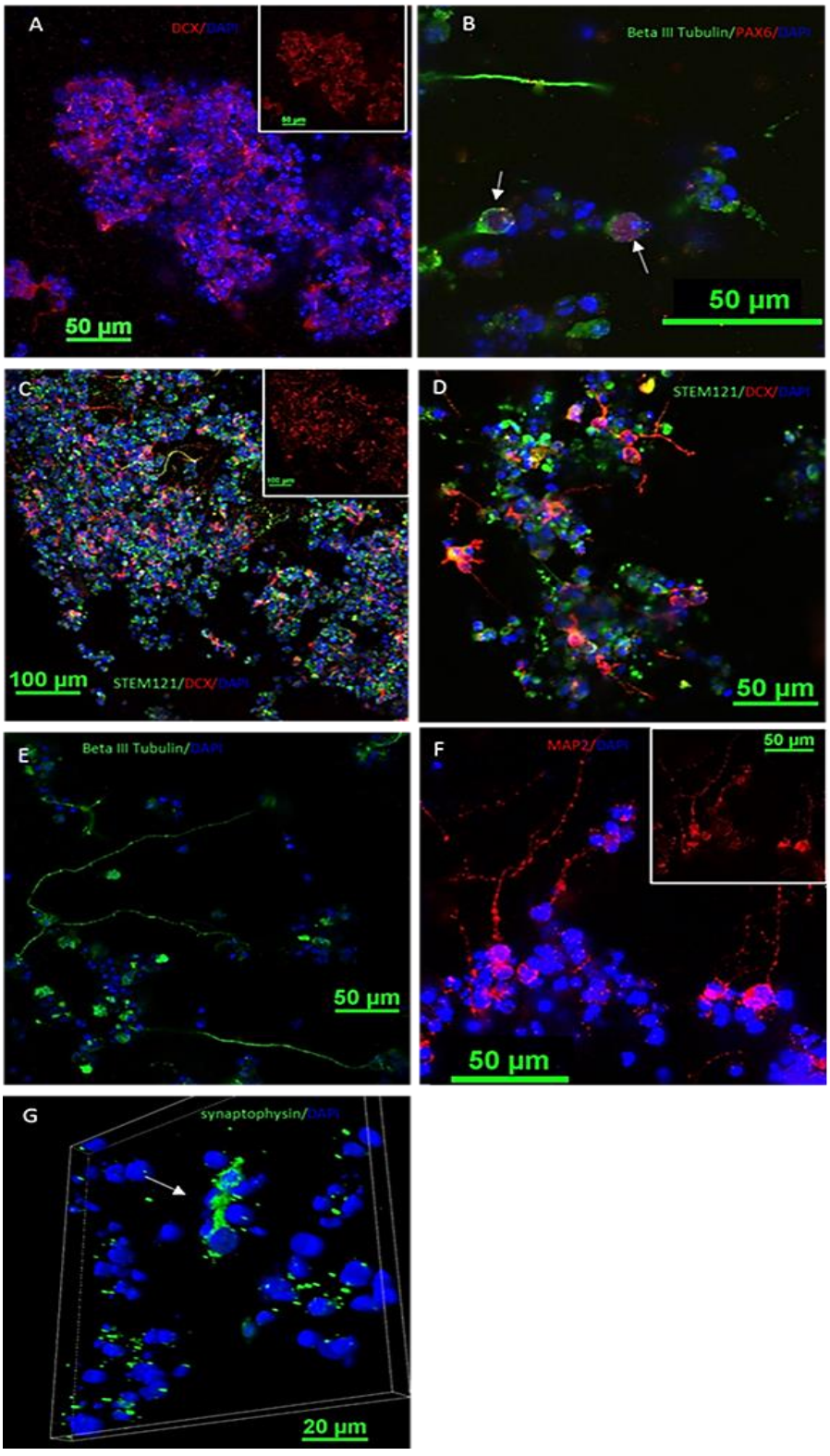
A
DCX/DAPI
50 µm
B
Beta III Tubulin/PAX6/DAPI
50 µm
C
100 µm
STEM121/DCX/DAPI
D
STEM121/DCX/DAPI
50 µm
E
Beta III Tubulin/DAPI
50 µm
F
MAP2/DAPI
50 µm
50 µm
G
synaptophysin/DAPI
20 µm

**Figure 5.4. Immunofluorescence of NSCs in 3D culture 10 and 14 days after spontaneous differentiation *in vitro*.**

After ten days, (A) many NSCs expressed DCX (red) with short processes. After 14 days, (B) few PAX6 positive cells still existed (red) (arrows) and (C) more DCX+ immature neurons generated and (D) connected to each other. (E) Long processes of β-TUB + neurons and their somata in the 3D culture (F).NSCs differentiated into MAP2+ neurons and extended their dendrites. (G) Some of the DAPI+ nuclei (blue) were surrounded by synaptophysin immunopositivity (green). Cells are counterstained with the fluorescent nuclear marker DAPI (blue).

In the 3D NSCs culture, neurons existed at different neuronal maturation stages. At 17 days, DCX stained the long processes and the somata of immature neurons that were distributed throughout the semi-synthetic ECM (Figure 5.5A). Fewer MAP2 immunopositive neurons were present (Figure 5.5B). Later on, after 43 days, few DCX+ immature neurons were observed (Figure 5.5C) while more MAP2+ maturing neurons that extended neurites and appeared connected to each other were present (Figure 5.5D). Only a few NSCs differentiated into astrocytes through all time points. Figure 5.5E, shows that few cells expressed GFAP after 17 days of differentiation.

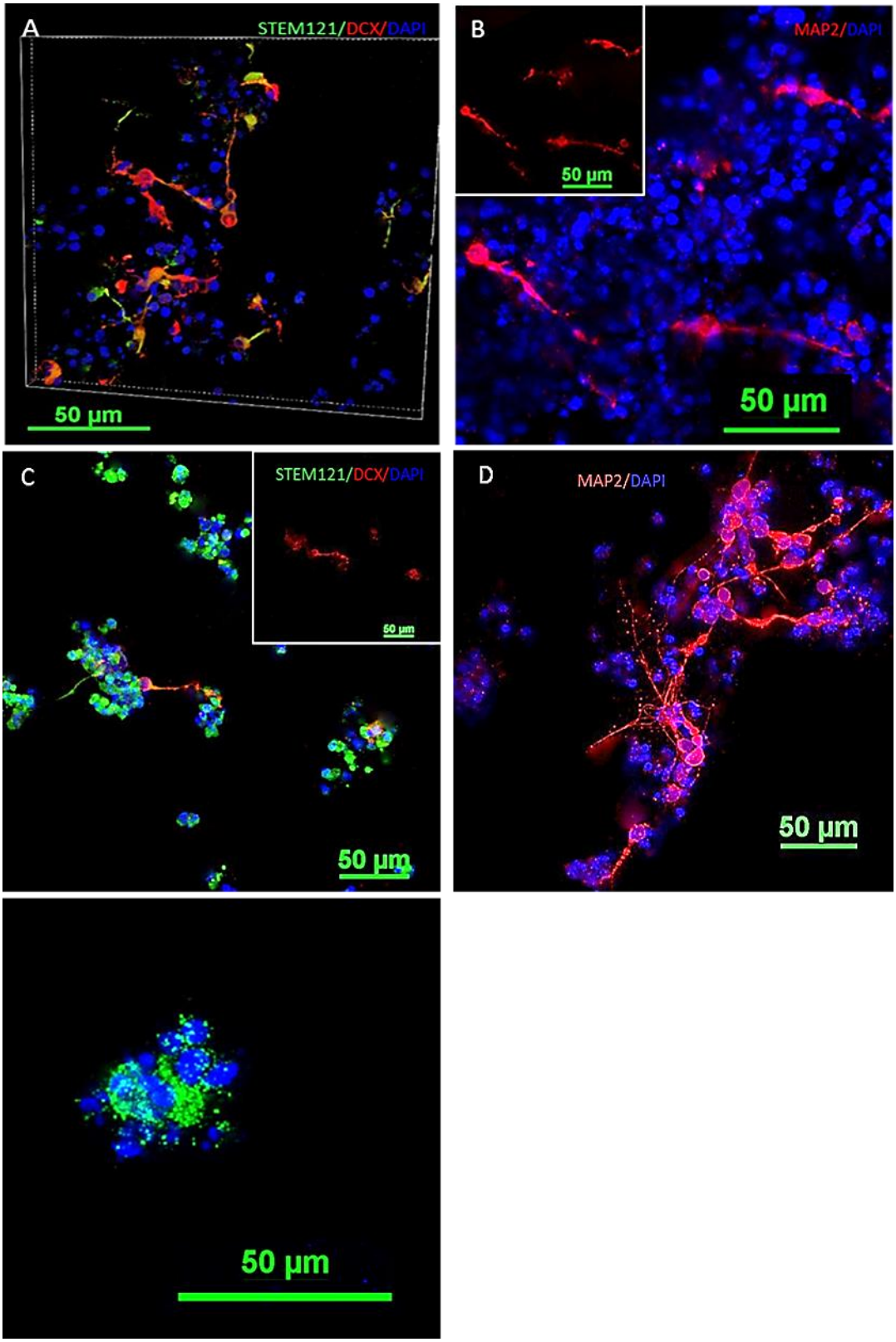
A
STEM121/DCX/DAPI
50 µm
B
MAP2/DAPI
50 µm
50 µm
C
STEM121/DCX/DAPI
50 µm
50 µm
D
MAP2/DAPI
50 µm
50 µm

**Figure 5.5. Immunofluorescence of NSCs in 3D culture 17 and 43 days after spontaneous differentiation *in vitro*.**

After ten days, (A) Three-dimensional image obtained from confocal microscope shows DCX+ neurons with long processes, (B) more mature neurons expressed MAP2 strongly. After 43 days, (C) fewer DCX+ neurons in the 3D culture and more (D) MAP2+ neurons extended processes through the ECM. (E) Few cells were immunopositive for GFAP (green). Cells were counterstained with the fluorescent nuclear marker DAPI (blue). Images are at maximum intensity projection and obtained from confocal microscope.

### *5.2.3 In vivo experiment*

Two main experimental groups were compared; hNSCs/ECM and ECM-only transplants to the PIS model, at one week, one month and three months post-transplantation. The grafting site was investigated by IHC on brain sections.

Endothelial cells and microglia were identified by labelling with biotinylated wisteria floribunda lectin visualised with streptavidin peroxidase histochemistry. IHC was carried out with antibodies to: PAX6 (NPCs proliferation and corticogenesis marker ); human astrocytes (STEM123); DCX (migrating neuroblasts and neurogenesis marker) ; GFAP (astrocyte marker) ; IBA1 (activated microglia); neuron-specific marker Beta-III-Tubulin (TUJ1); MAP2 (dendrite and soma neuron-specific marker); Parvalbumin (calcium-binding protein and inhibitory interneuron marker) ; CTIP2 (deep layer cortical neuron marker) ; synaptophysin (neural synaptic vesicle marker) . Sections were counterstained with the fluorescent nuclear marker DAPI.

Antibodies to hNCAM, a nuclear protein of human cells (STEM101) and cytoplasmic protein of human cells (STEM121) were used to test the presence of the transplanted hNSCs. Also, anti-STEM 101 and STEM121 were used to validate hNCAM immunoreactivity in presumptive hNSCs.

The following figures show examples of the human cell marker immunostaining one month post-transplantation. Figure 5.6A demonstrates that, after one month, anti-hNCAM successfully immunostained the transplanted complex of artificial ECM and cells. Similarly anti-STEM121 stained hNSCs/ECM in adjacent sections of the same brain (Figure 5.6B). Also, anti-hNCAM and STEM101 labelled the same mass of hNSCs in the same brain (Figure 5.6C and D).

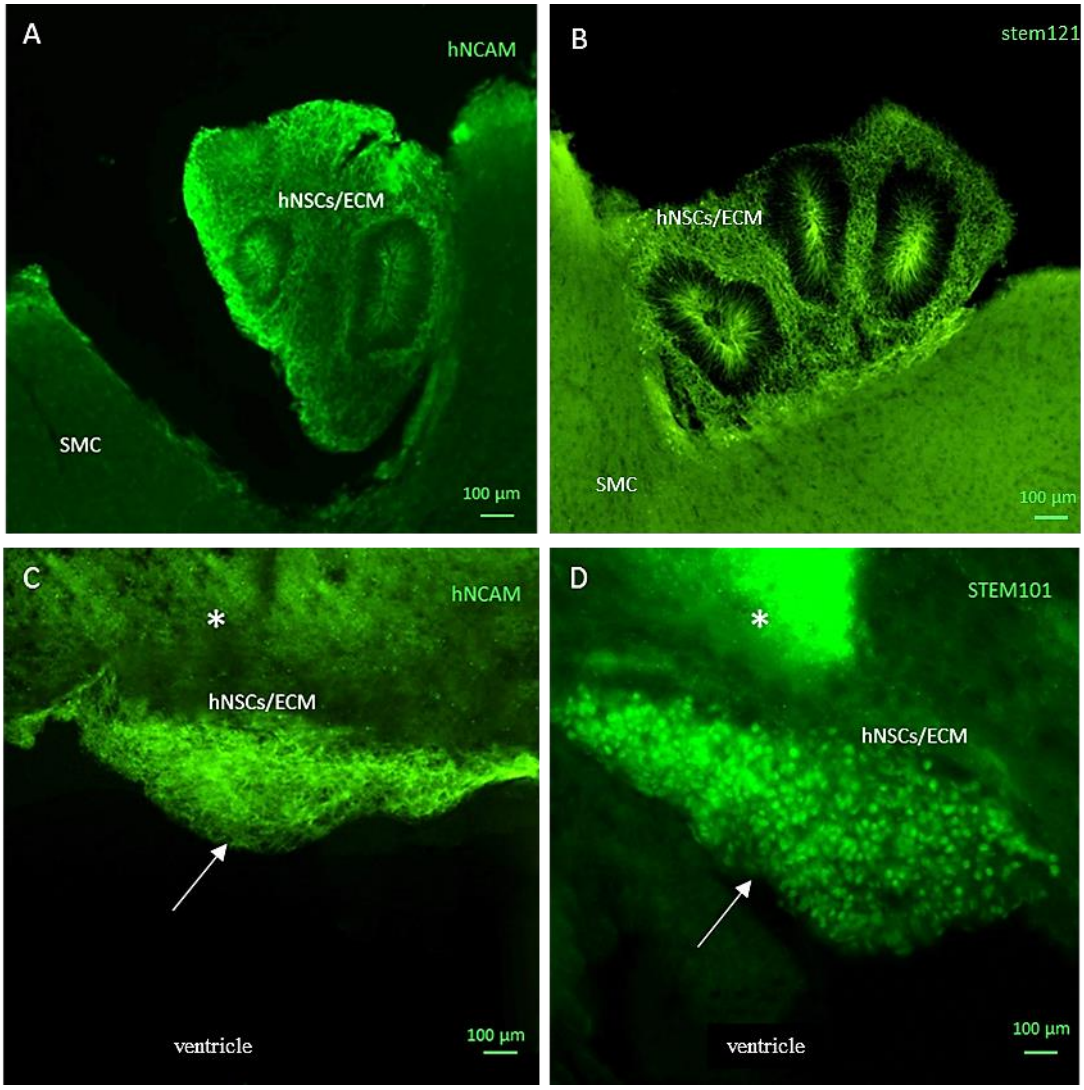


**Figure 5.6. Immunofluorescence of transplanted human cell markers after one month.** Cytoplasmic cell markers (A) hNCAM and (B) STEM121. (C) Cytoplasmic cell marker hNCAM (arrow and asterisk). (D) Nuclear cell marker STEM101 (arrow and asterisk).

Immunoreactivity for transplanted cell markers either appeared as small discs using the nuclear marker STEM 101 or as a meshwork of processes using the cytoplasmic markers STEM 121 and hNCAM. Thus, it could be concluded that the antibodies we used are valid for identifying the injected hNSC cells.

**One week post-transplantation**

Immunostaining of the transplanted hNSCs/ECM was studied one week post grafting. Transplanted hNSCs in the gel scaffold exhibited a labyrinthine morphology which appeared similar to an early stage of cerebral organoid formation (Qian et al., 2016) . This structure had thin layers of PAX6 positive cells which co-expressed hNCAM (Figure 5.7A). The generated cell formation expressed markers of human radial glial cells demonstrated by co-localization of PAX6/ hNCAM+ (Figure 5.7B). Also, some host PAX6+ but hNCAM- cells surrounded the graft (Figure 5.7B). Human grafted cells expressing hNCAM but not PAX6 were also found in the graft site (Figure 5.7C).

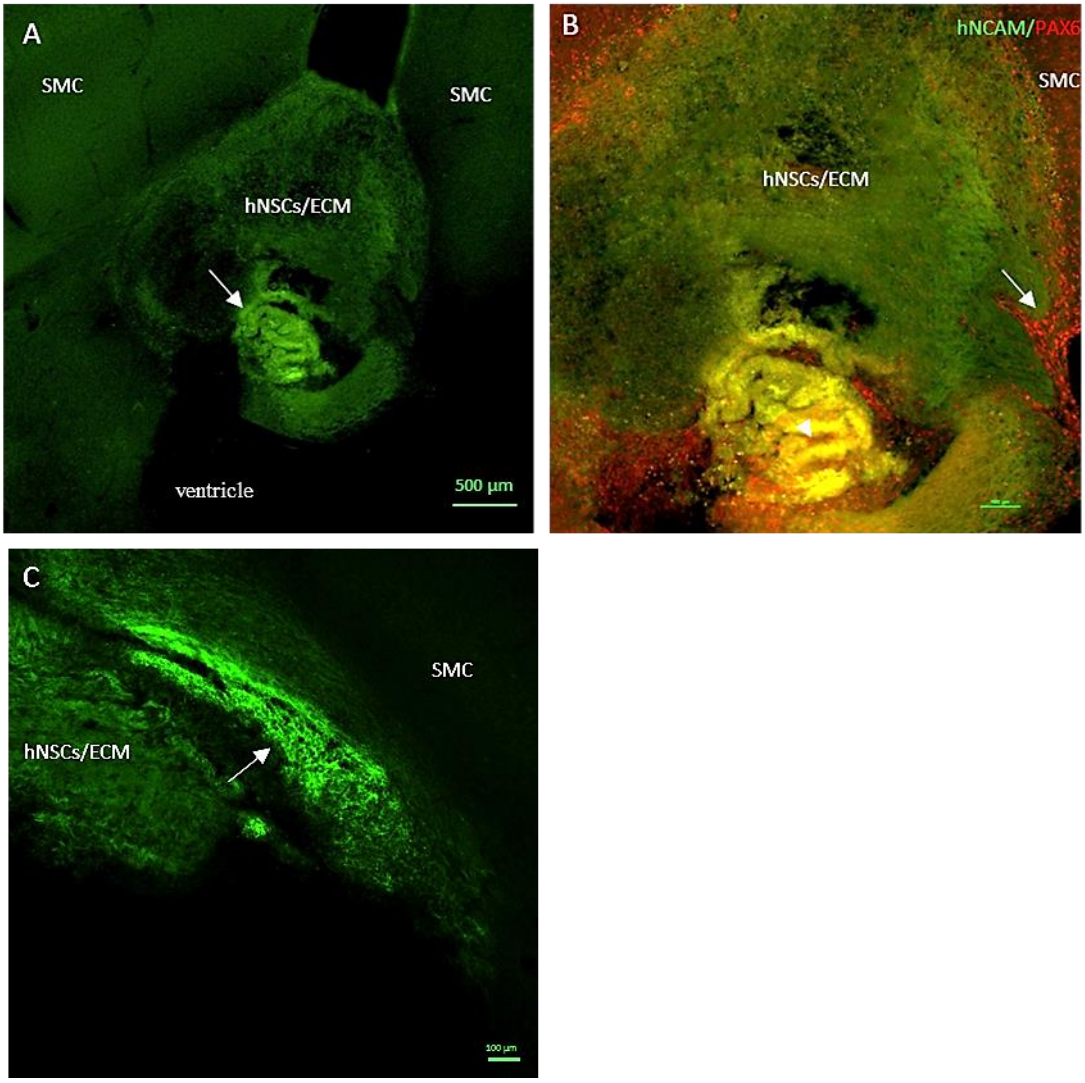


**Figure 5.7. Morphological features of the grafted hNSCs/ECM after one week detected by IHC.**

The graft had an early organoid formation that expressed both (A) hNCAM+ (green) and (B) PAX6+ (red) in the labyrinthine formation (arrowhead) and around the graft (arrow). (C) hNCAM+ cells in the graft were adjacent to host cortex.

As early as one week, transplanted cells appeared to be present away from the xenograft. Figure 5.8A shows hNCAM expressing cells in the striatum. Human astrocytes were detected by anti-STEM123 IHC and had small somata and a few thin processes, both within the transplant site and away from it (Figure 5.8B). Furthermore, we found some cells immunopositive for hNCAM located away from the graft close to the contralateral hemisphere of the brain. Newly host generated migrating neuroblasts expressed DCX in their somata and leading processes are likely to be attracted toward the transplant and invade it (Figure 5.8C and D).

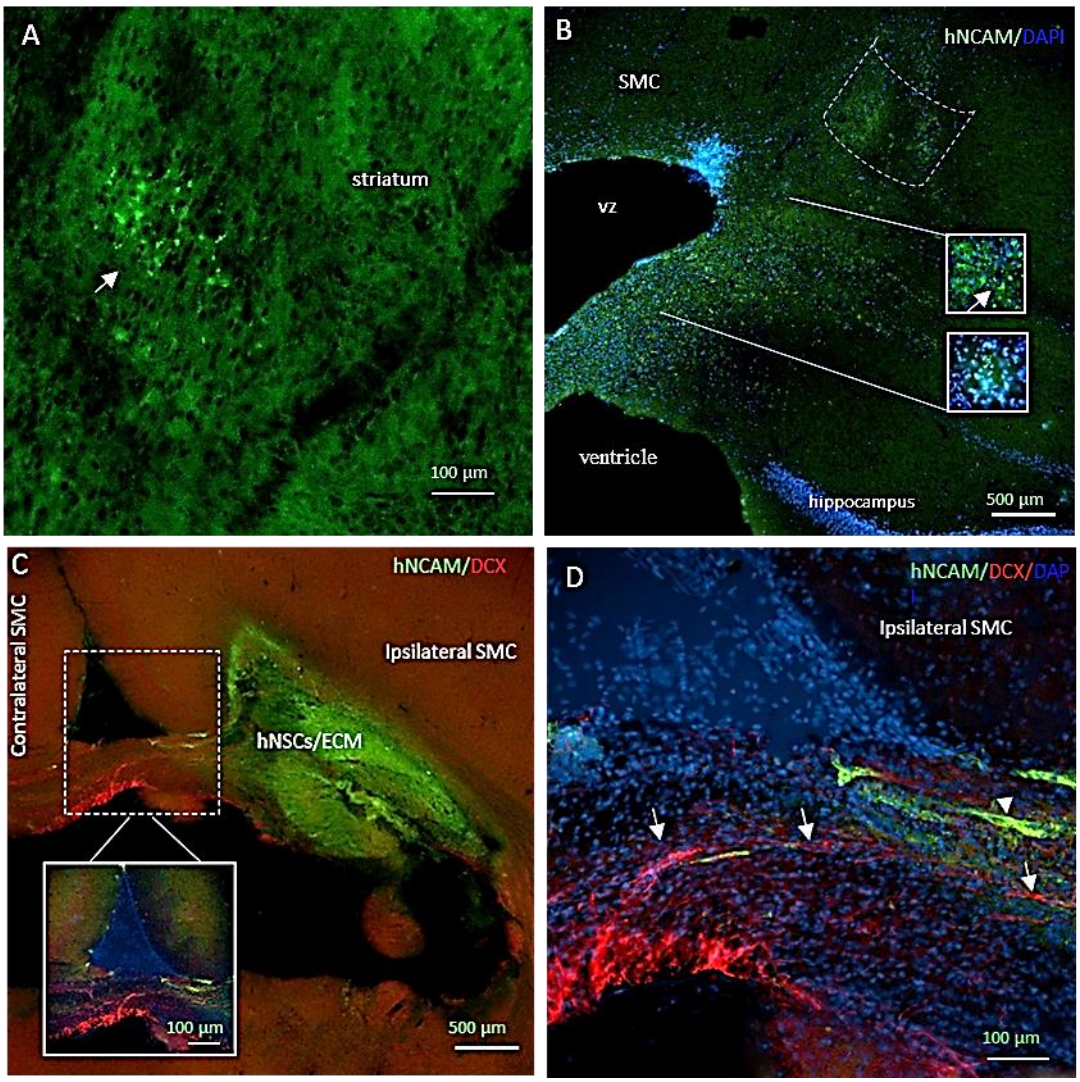


**Figure 5.8. Placement of the grafted hNSCs/ECM after one week detected by IHC.**
Human cells (A) expressed hNCAM+ (arrow) in the striatum. Human astrocytes (B) expressed STEM123+ (green) at the posterior end of the transplant site (dashed rectangle) and in the subcortical region at higher magnification (two squares). DAPI (blue) is nuclear counter staining. In the hippocampus (C) DCX-/ hNCAM+ (green) and DCX+/ hNCAM- (red) cells located between the graft and contralateral hemisphere (in the square). (D) hNCAM+ cells (arrowhead) and DCX+ (arrows) in the hippocampus at higher magnification. (C and D) sections were counter stained with the fluorescence nuclear marker DAPI (blue).

Using immunofluorescence labelling, we found host cells with other phenotypes had surrounded and infiltrated the xenograft. First, GFAP+ but hNCAM- host astrocytes surrounded the graft and extended their long processes toward the centre of the xenograft with some appearing to have started to migrate toward the centre (Figure 5.9A). Similarly, abundant microglia accumulated at the boundary of the graft and a few blood vessels invaded the transplant, as indicated by wisteria floribunda lectin labelling (Figure 5.9B). Figure 5.9C shows activated microglia with an ameboid morphology, (bulbar shape) and immunopositive for IBA1 present within the transplant. Another type of cell that invaded the gel expressed MAP2, they had a more rounded shape than the elongated MAP2 positive pyramidal neurons found in the host cortex (Figure 5.9C and D).

Host cells that infiltrated the transplanted gel in the ECM-only group were tested as a control group using similar immunolabeling protocols. We found that astrocytes immunoreactive for GFAP surrounded and invaded the gel but with fewer of them having long processes in contrast to the astrocytes in the hNSCs/ECM group (Figure 5.10A). Also, a few host DCX immunoreactive neuroblasts presented in both the subventricular zone (SVZ) of the lateral ventricles and the xenograft (Figure 5.10B). DCX+ cells presented in the SVZ of the lateral ventricles in both hemispheres (Figure 5.10C). Figure 5.10D demonstrates that more microglia and fewer blood vessels were present in the ECM-only transplants, as indicated by anti-lectin histochemistry. Interestingly, parvalbumin (PV) expressing cells were also found in the ECM transplant (Figure 5.10E and F).

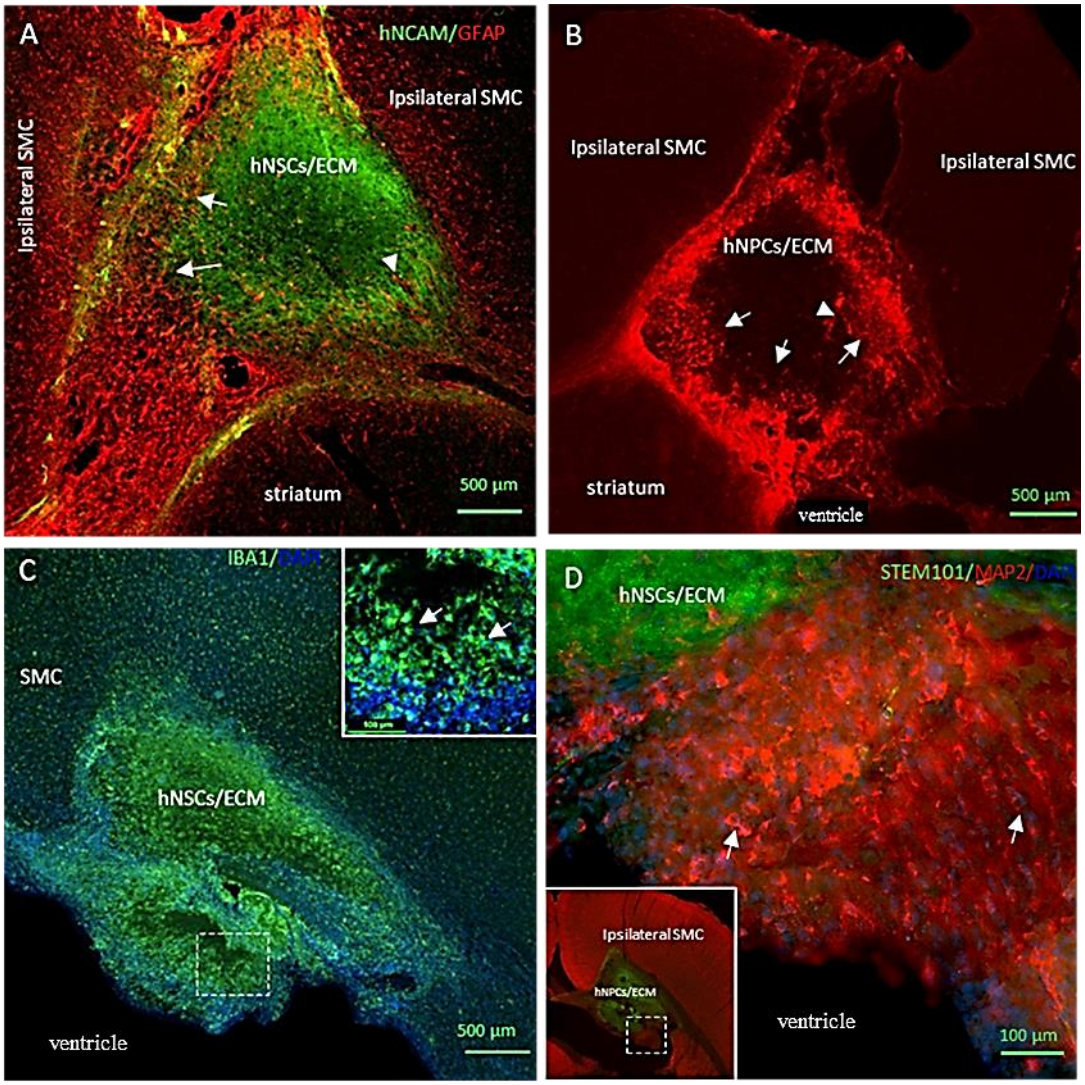


**Figure 5.9. Host cells phenotype that infiltrated the hNSCs/ECM transplant detected by IHC.**

(A) Host GFAP+ cells around the transplant (arrows), and within the transplant (arrowhead). DAPI (blue) is a nuclear counter stain. (B) Using histochemistry for anti-lectin, host lectin+ microglia were found located around the transplant and host blood vessels within the transplant (arrowhead). (C) Bulbar morphology of microglia within the xenograft and resting microglia in SMC. (D) Magnification of the dashed box in the bottom left corner shows host MAP2+/STEM101 presumptive neurons within the transplant (arrows) with short processes and small somata.

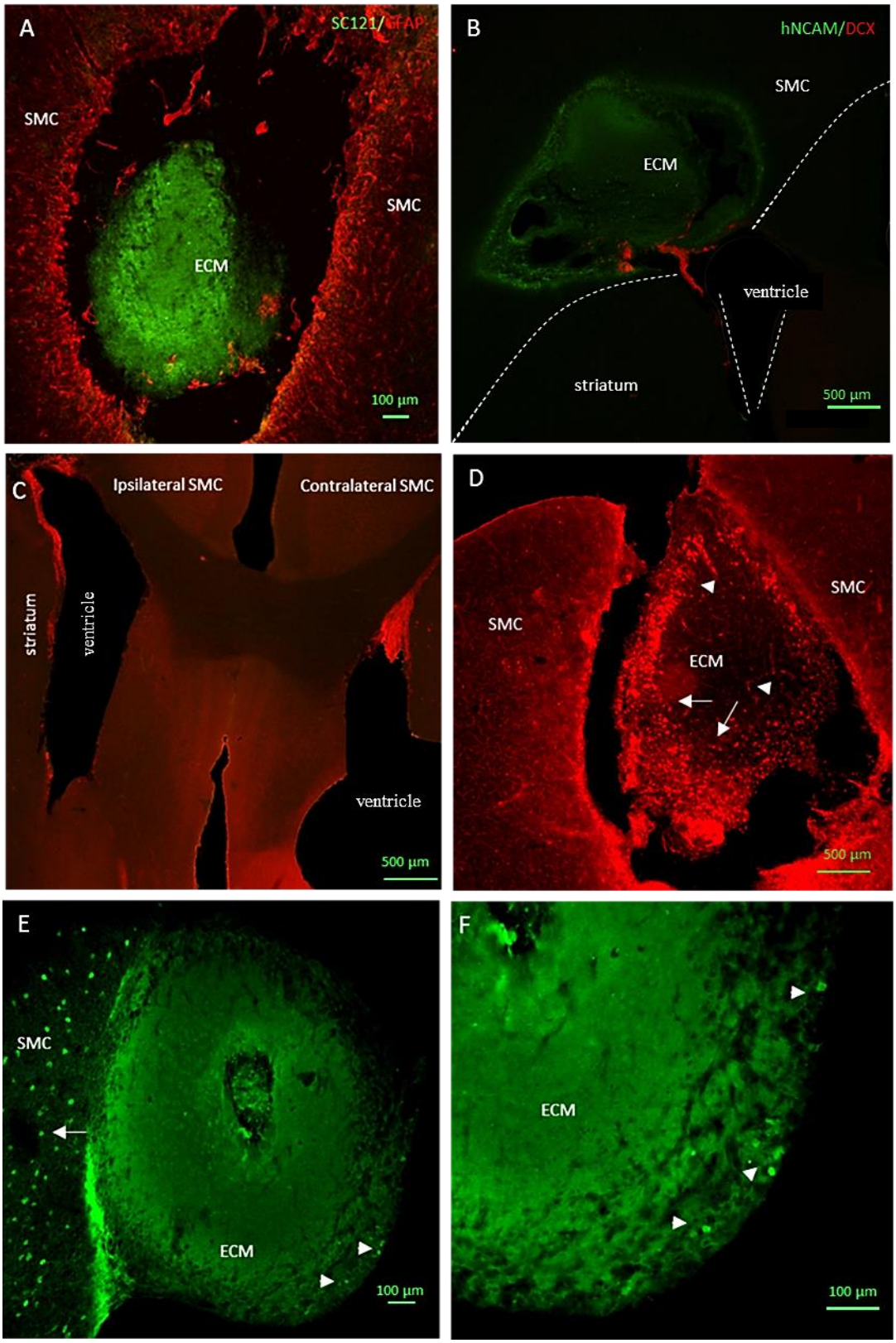
A
SC121/GFAP
SMC
SMC
ECM
100 µm
B
hNCAM/DCX
SMC
ECM
ventricle
striatum
500 µm
C
Ipsilateral SMC
Contralateral SMC
striatum
ventricle
ventricle
500 µm
D
SMC
SMC
ECM
500 µm
E
SMC
ECM
100 µm
F
ECM
100 µm

**Figure 5.10. Phenotype of cells that infiltrated the ECM-only transplant detected by IHC.**

Host (A) GFAP+ cells (red) around the gel transplant, DAPI (blue) is a nuclear counter stain. (B) Host DCX+ cells (red) in the gel transplant and(C) in the ventricular zone in both hemisphere. (D) Host lectin+ microglia (arrow) around the transplant and many small host blood vessels within the transplant (arrowhead), using histochemistry for anti-lectin. (E-F) host cells expressing PV+ in the cortex (E), and invading the gel transplant (F).

**One month post-transplantation**

In 5 brains out of 6, transplanted hNSCs formed neural tube-like rosettes with a morphology resembling cerebral organoids observed to form from NSCs in culture (reference to cerebral organoid formation) while the 6th brain lost its transplant mechanically during brain sectioning. In all 6 brains, the phenotype of a variety of host cells that infiltrated the xenograft was tested by immunofluorescence. Although hNCAM was highly expressed in human cells at the injection site, only a few of these human cells were observed away from the transplant one month post grafting (Figure 5.11).

First, we examined human cell markers for co-expression with the following markers; PAX6, DCX, β-TUB, hGFAP, and the forebrain-specific cortical layer V neuron marker CTIP2.

The transplanted hNSCs expanded in number to form both NPCs that were immunopositive for PAX6 and hNCAM and post-mitotic immature neurons which co-expressed DCX and hNCAM. Figure 5.12A shows columns of tightly packed NPCs uniformly expressing PAX6 in rosette structures. These progenitor cells surrounded an empty space "Lumen" that resembled the neural tube or ventricle of a developing brain (Figure 5.12A and B). PAX6+ cells at the ventricular surface only expressed low levels of hNCAM, which is a cell-adhesion molecule and may form intercellular junctions holding the structure together (Figure 5.12C). This also indicates that these cells were of transplant origin. No other post-mitotic markers for neurons or neuroblasts were expressed by these PAX6+ cells.

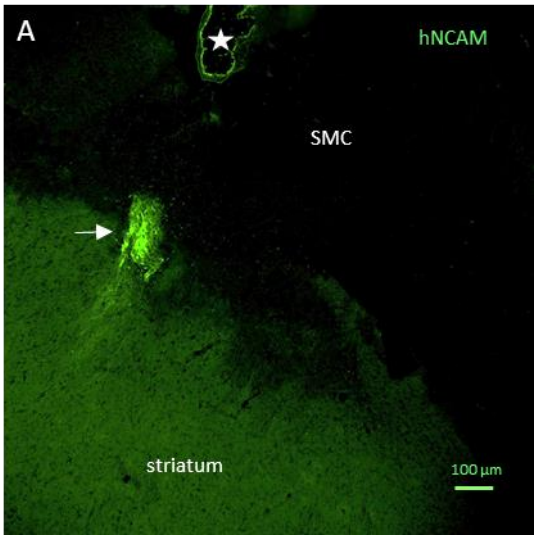


**Figure 5.11.Transplanted human cells located away from the graft site.**

(A) hNCAM+ cells (arrow) presented inferior to the transplantation site (star) detected by IHC for anti-hNCAM antibody.

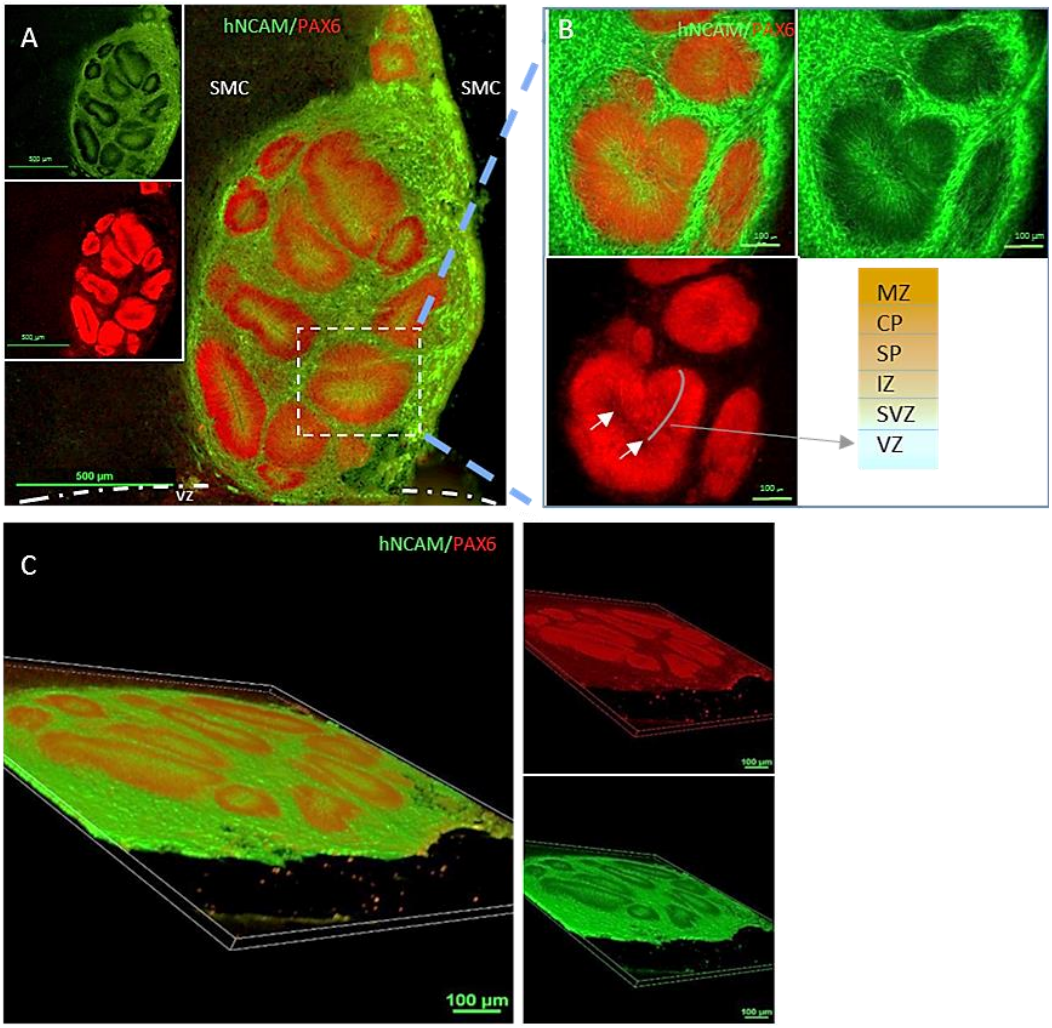


**Figure 5.12. Human progenitor cells in the cerebral organoid formation after one month *in vivo*.**

Immunofluorescent double labelling for PAX6 (red) and hNCAM (green). (A) Shows dense layers of radial arrangements of columnar PAX6+/hNCAM+ cells were around a space resembling the neural tube or ventricle of a developing brain (arrows). (B) Layers of PAX6+/hNCAM+ cells of a magnified inset from image A "Progenitor cellular layer (PCL)" resembled VZ in the human developing brain cortical layers. (C) Three-dimensional reconstructed confocal images of transplanted PAX6+/hNCAM+ human progenitor cells.

Around this “PCL” existed a looser network of heterogeneously distributed cells that were positive for immature neuron markers including doublecortin and β-TUB “Neural cellular layer (NCL)” (Figure 5.13A). These markers were co-expressed with hNCAM indicating that these cells were of human origin. DCX+/hNCAM+ (Figure 5.13A-C) β-TUB +/hNCAM+ (Figure 5.13D) immature neurons occupied the space surrounding the tightly packed PAX6+ cells. It is noteworthy that DAPI was strongly expressed by tightly packed cells (Figure 5.13E) that were positive for progenitor cell marker PAX6 as shown previously (Figure 5.12).

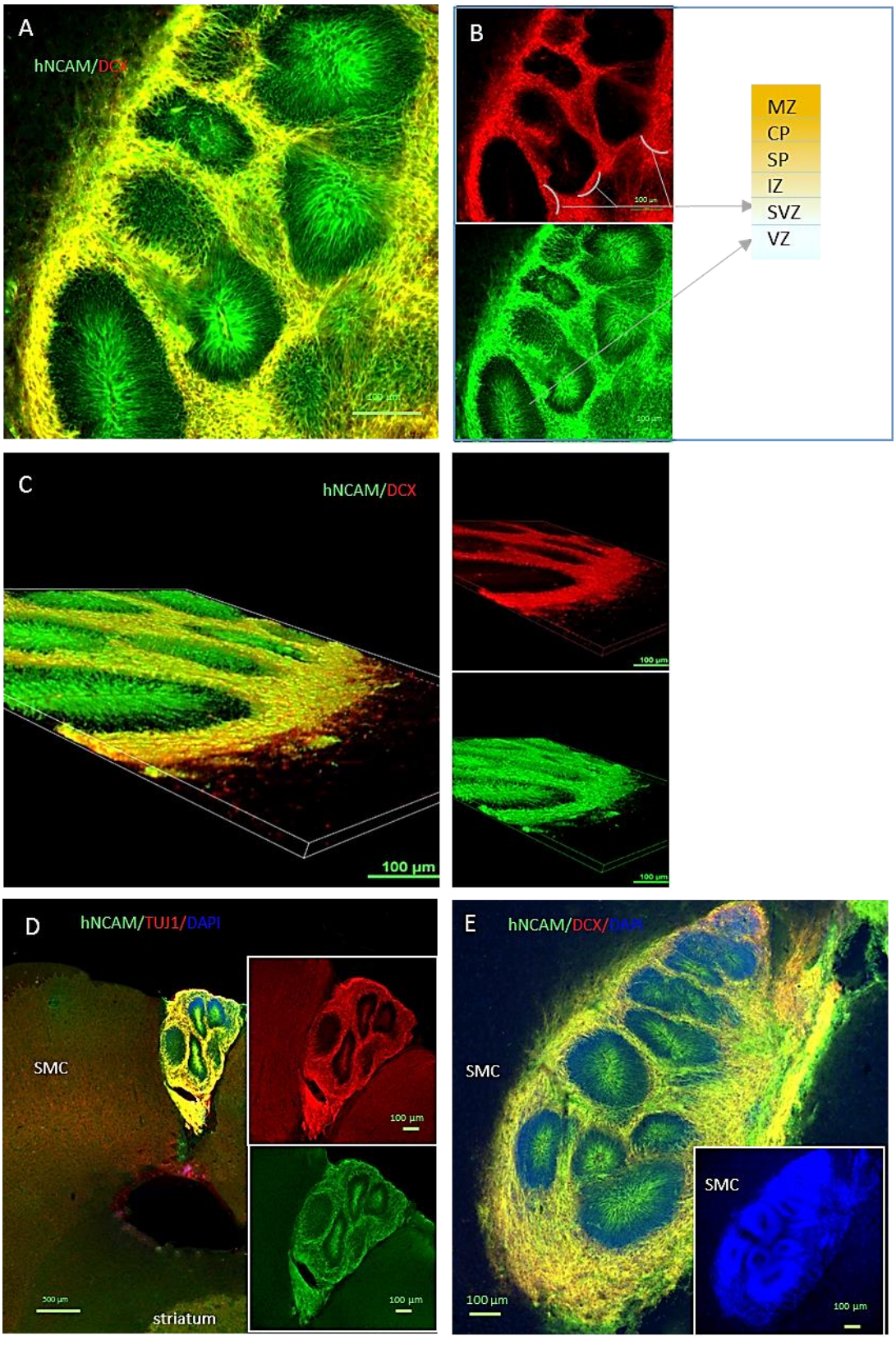
A
hNCAM/DCX
B
MZ
CP
SP
IZ
SVZ
VZ
C
hNCAM/DCX
100 µm
D
hNCAM/TUJ1/DAPI
SMC
striatum
E
hNCAM/DCX/DAPI
SMC
SMC
100 µm

**Figure 5.13. Human immature neurons in the cerebral organoid formation after one month *in vivo***

Immunofluorescent double labelling for DCX (red) and hNCAM (green). (A) Demonstrates loose layers of DCX+/hNCAM+ cell markers (yellow) in the graft. (B) Shows layers of DCX+/hNCAM+ cells in the space of "NCL" resembling the SVZ layer in the developing human brain. (C) Three-dimensional reconstructed images were obtained with a confocal microscope. (D) Demonstrates loose layers of co-localized β-TUB +/hNCAM+ cell markers (yellow). (E) Shows dense layers of DAPI within the PCL area

Moreover, cells in these organoids expressed CTIP2. Transplanted cells were immunopositive for CTIP2/STEM121 in the organoid formation, accumulating in the zone of the immature neurons (Figure 5.14A and B). A few of the transplanted cells differentiated into astrocytes detected by anti- STEM123 IHC and located in the neuronal layer close to the PCL (Figure 5.14C). Strong MAP2 expression was noted in the cytoplasm around the human nuclear marker STEM101 in cells of the organoid formation, with a weak MAP2 expression of host neurons adjacent to the transplanted human cells (Figure 5.14D).

Second, we examined some of the host cell phenotypes that infiltrated the graft of the cerebral organoid structures and were positive for the following markers; IBA1, GFAP, and PV. Angiogenesis was detected by anti-lectin histochemistry staining which labels endothelial and microglial cells. Host blood vessels, detected by lectin staining, were uniformly distributed through the organoids. lectin staining also showed reactive microglia around the graft but not inside it (Figure 5.15A and B). Figure 5.15B demonstrates that blood vessels vascularized the deep layers of the organoids of containing closely packed DAPI + cells.

Host microglia, either ramified or in the resting bipolar form that was immunopositive for IBA1 exhibited a distribution within the cerebral organoid in a similar way to the host cortex, however, a much higher density of expression of IBA1 from amoeboid microglia appeared around and in the gel adjacent to the organoids (Figure 5.15C, and D). Similarly, a dense layer of endogenous cells expressing the astrocyte marker GFAP+ but STEM121- were nested at the boundary between the organoids and the host cortex. They infiltrated the graft and extended their long processes toward the centre of the xenograft with some appearing to have started to migrate toward the centre (Figure 5.15E). It is noteworthy that reactive astrocytes immunopositive for GFAP, and activated microglia immunopositive for IBA1, did not completely surround all the graft boundaries. This suggests that the graft was not totally isolated from the host cortex and trajectories for cells to exchange between the graft and host cortex existed. Finally, a few cells immunopositive for PV entered the periphery of the organoid structures (Figure 5.15F).

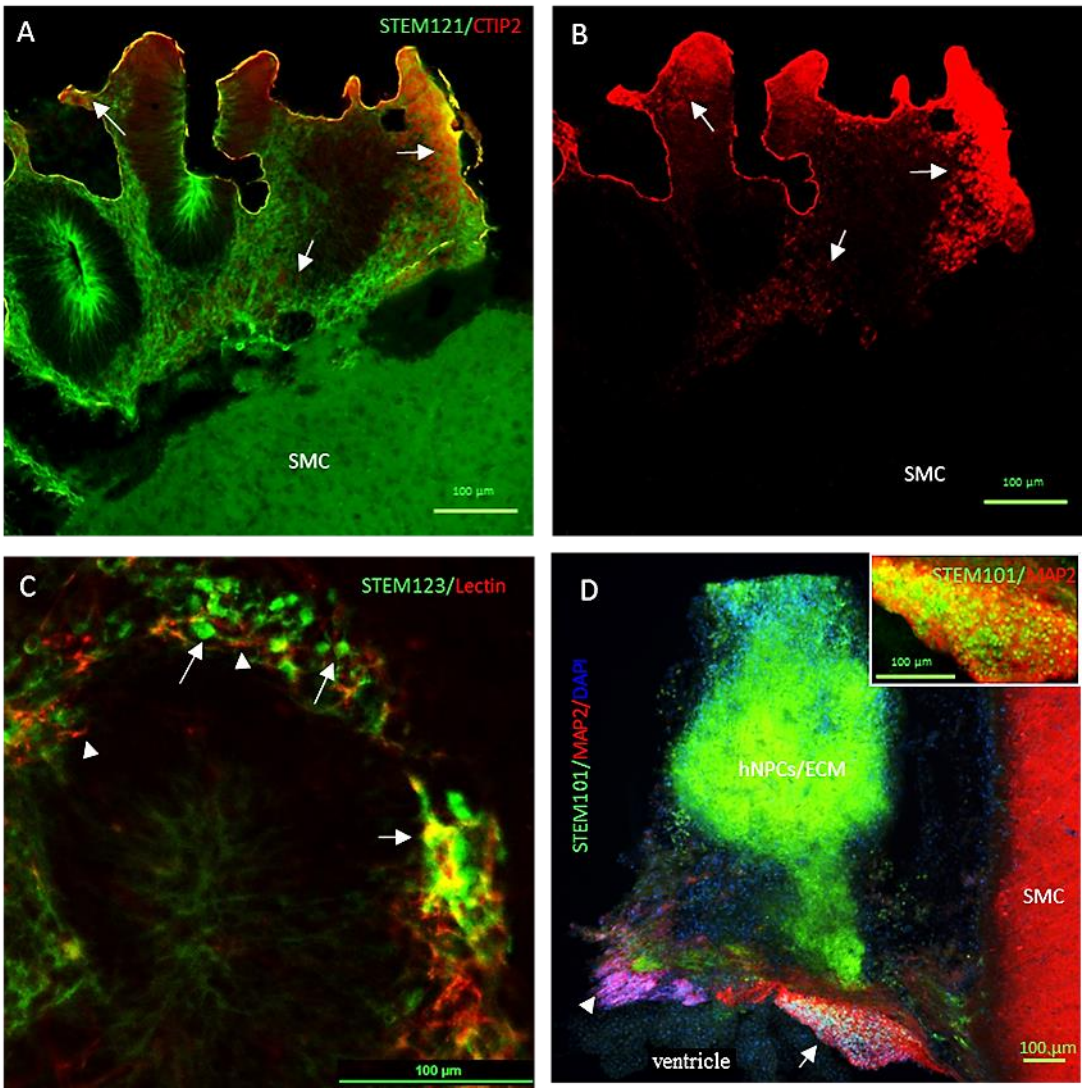


**Figure 5.14. Transplanted hNSCs in the cerebral organoid formation after one month detected by IHC *in vivo*.**

Immunofluorescent double labelling for transplanted cells. (A) CTIP2+/STEM121+ (arrows) cells around the "lumen" space called PCL, (B) CTP2+ cells (red) that resembled the deep layer SVZ in developing the mammalian brain. (C) Transplanted human cells differentiated into STEM123+ astrocytes (green) adjacent to lectin+ host blood vessels (red), using histochemistry for anti-lectin. (D) Shows a mixture of weak expression of MAP2+ (red) only on the left (arrowhead) and strong MAP2+ (red)/ STEM101+ (green) on the right bottom corner (arrow) and in the magnified white rectangular.

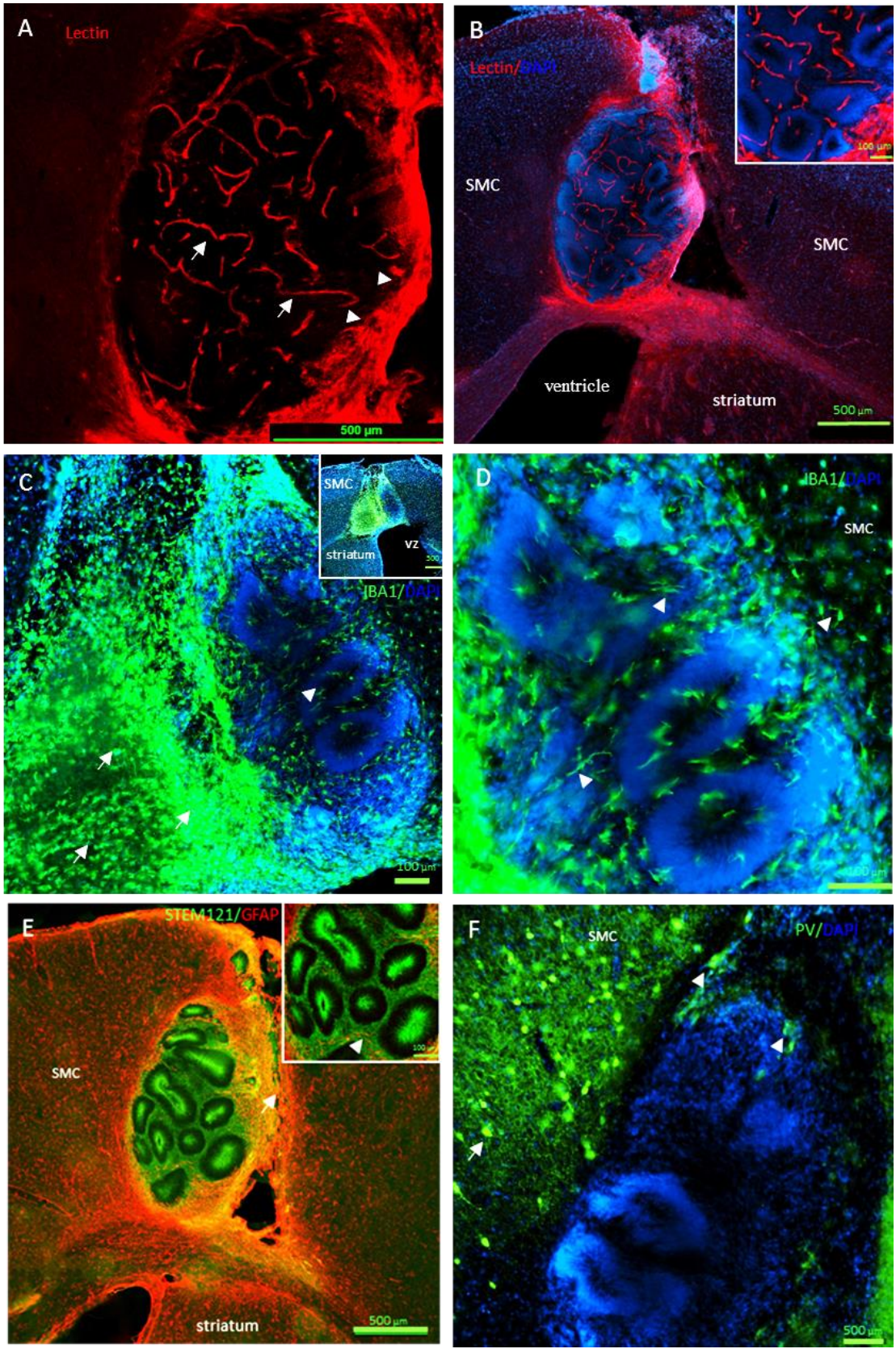
A
Lectin
500 μm
B
Lectin/DAPI
SMC
SMC
ventricle
striatum
500 μm
C
SMC
striatum
VZ
IBA1/DAPI
100 μm
D
IBA1/DAPI
SMC
E
STEM121/GFAP
SMC
striatum
500 μm
F
SMC
PV/DAPI
500 μm

**Figure 5.15. Endogenous cells and angiogenesis in the cerebral organoid formation after one month detected by IHC *in vivo*.**

(A) The host blood vessels penetrated (arrows) the xenograft surrounding the dense DAPI+ cells (B) of the organoids (lectin histochemistry). (C) host resting microglia (arrowhead) invaded the organoid structures and had a similar density as the host resting microglia in the cortex (small box on the top right corner), and host ramified microglia predominantly located in the gel regions of the transplant (arrows). (D) a magnified inset from image C, the resting microglia in the organoid structures (arrowhead) had similar morphology and distribution as the host cortical microglia.(E) some host reactive GFAP+ (red) astrocytes with swollen cell bodies accumulated at one side (arrow) of the graft while some (in the magnified white rectangular) had long processes nested between the organoids. (F) Host cortical PV+ cells (arrow) in the cortex and in the graft with smaller cell bodies (arrowhead).

Third, we examined some of the endogenous cell phenotypes that infiltrated the graft, but not the cerebral organoid structures, and were immunopositive for the following markers; DCX, MAP2, β-TUB, PAX6, GFAP, and PV and positive for lectin histochemistry staining.

Endogenous DCX immunoreactivity was found in three regions of the frontal cortex. First, in the SVZ of the lateral ventricles in both hemispheres, second, between the graft and the xenograft site and third around and inside the transplant. Host neuroblasts immunoreactive for DCX but not hNCAM were located in the lateral SVZ of both hemispheres and along a migratory trajectory between the SVZ and the xenograft, (Figure 5.16A). Also, DCX positive cells were found between the corpus callosum and the graft (Figure 5.16B).

The DCX+ cells surrounded the transplant and intermingled with hNCAM immunopositive transplanted neurons. DCX positive neuroblasts surrounded the transplant and formed a dense network at the inferior boundary where it contacted the SVZ (Figure 5.16C). Some of these cells had an elongated cell body and extended long processes that reached the xenograft and intermingled with hNCAM positive transplanted neurons (Figure 5.16C). Similarly, extended long processes were seen in the bottom border of the ECM-only transplant yet fewer immature neurons with shorter processes invaded the ECM (Figure 5.16D).

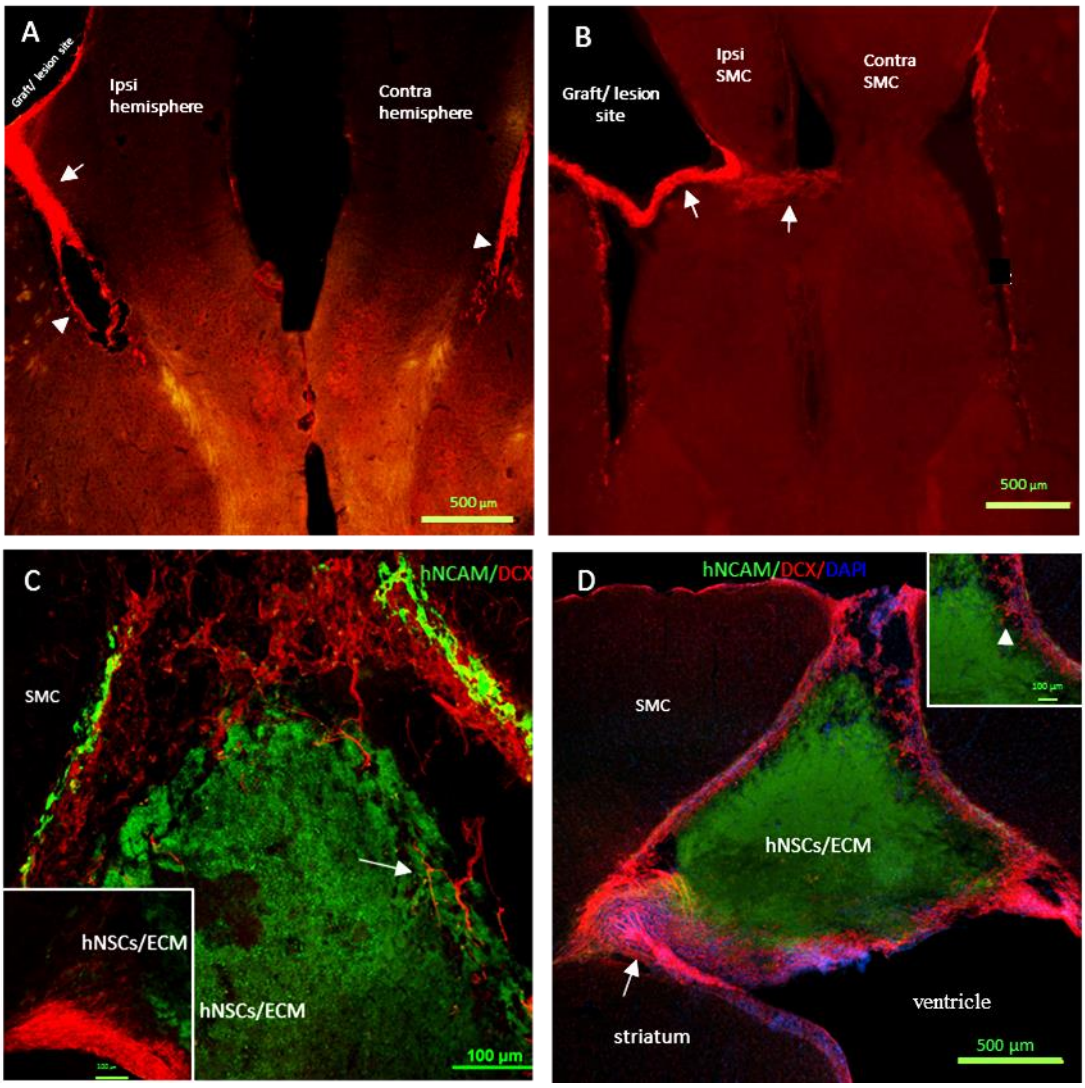


**Figure 5.16. Endogenous immature neurons in the hNSCs/ECM and ECM-only transplants one month after *in vivo* xenograft.**

In non-cerebral organoid regions of the hNSCs/ECM xenografts: (A) endogenous newly formed neuroblasts expressed DCX in their soma, their leading process in the SVZ (arrowhead) and toward the graft/lesion site (arrows) and (B) in the corpus callosum toward the contralateral hemisphere, while (C) maximum intensity projection image of confocal microscope shows some DCX+/hNCAM- cells surrounded and infiltrated the graft with long thin processes (arrow), and more dense DCX expression in the SVZ with migrating neurons into the graft (rectangle).(D) Host DCX+ cells with an elongated morphology surrounded the ECM-only graft, yet only a few with short processes infiltrated the ECM.

Transplanted cells gave rise to MAP2+ and β-TUB + neurons. Rodent cortical neurons that were immunopositive for MAP2 (Figure 5.17A and B) and β-TUB (Figure 5.17C), but not for the human cell markers STEM101 and hNCAM, entered the xenograft and preserved their elongated shape (Figure 5.17A and B). Neurones that were β-TUB + but hNCAM- were located between the cortex and the graft as shown in (Figure 5.17C) suggesting they were migrating toward the graft. In ECM-only groups, MAP2+ but STEM101- neurons surrounded the graft but failed to invade it (Figure 5.17D).

Progenitor cells that were immunoreactive to PAX6 but not hNCAM were found around and inside the transplant, in the SVZ of both lateral ventricles, and along a migratory pathway between the xenograft and the SVZ (Figure 5.18).

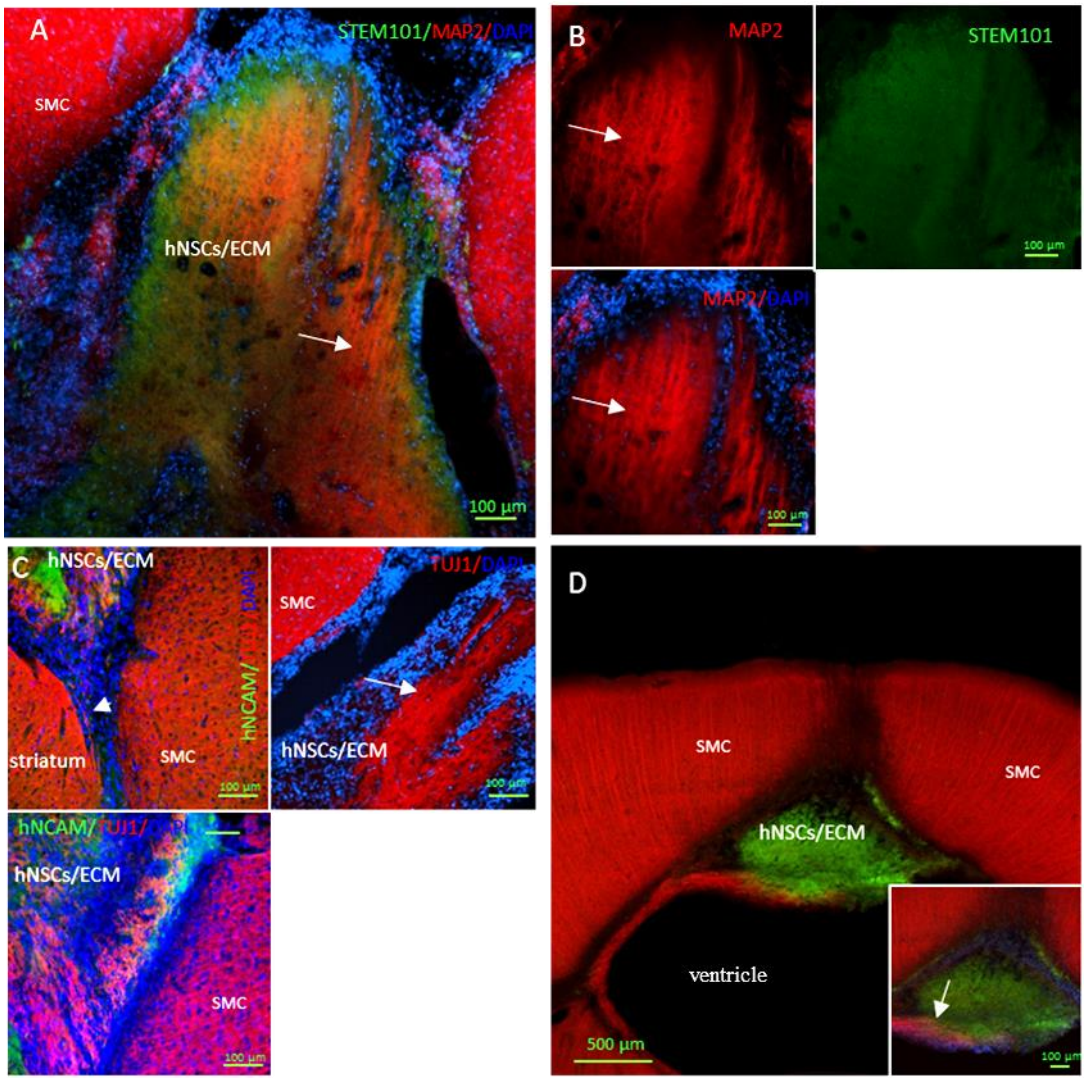


**Figure 5.17. Endogenous neurons in the hNSCs/ECM and ECM-only transplants one month after *in vivo* xenograft.**

Immunofluorescent double labelling for MAP2 (red) and STEM101 or hNCAM (green). (A) Demonstrates MAP2+/STEM101- dendrites of host neurons in the graft (arrow). (B) A magnified inset from image A, demonstrating the absence of the human nuclear marker STEM101 in the MAP2+ cells. (C) Shows host MAP2+/hNCAM- cells in the corpus callosum (arrowhead), the periphery of the graft, and in graft centre (arrow). (D) Shows MAP2+/hNCAM- only in the inferior margin of the ECM-only graft

.

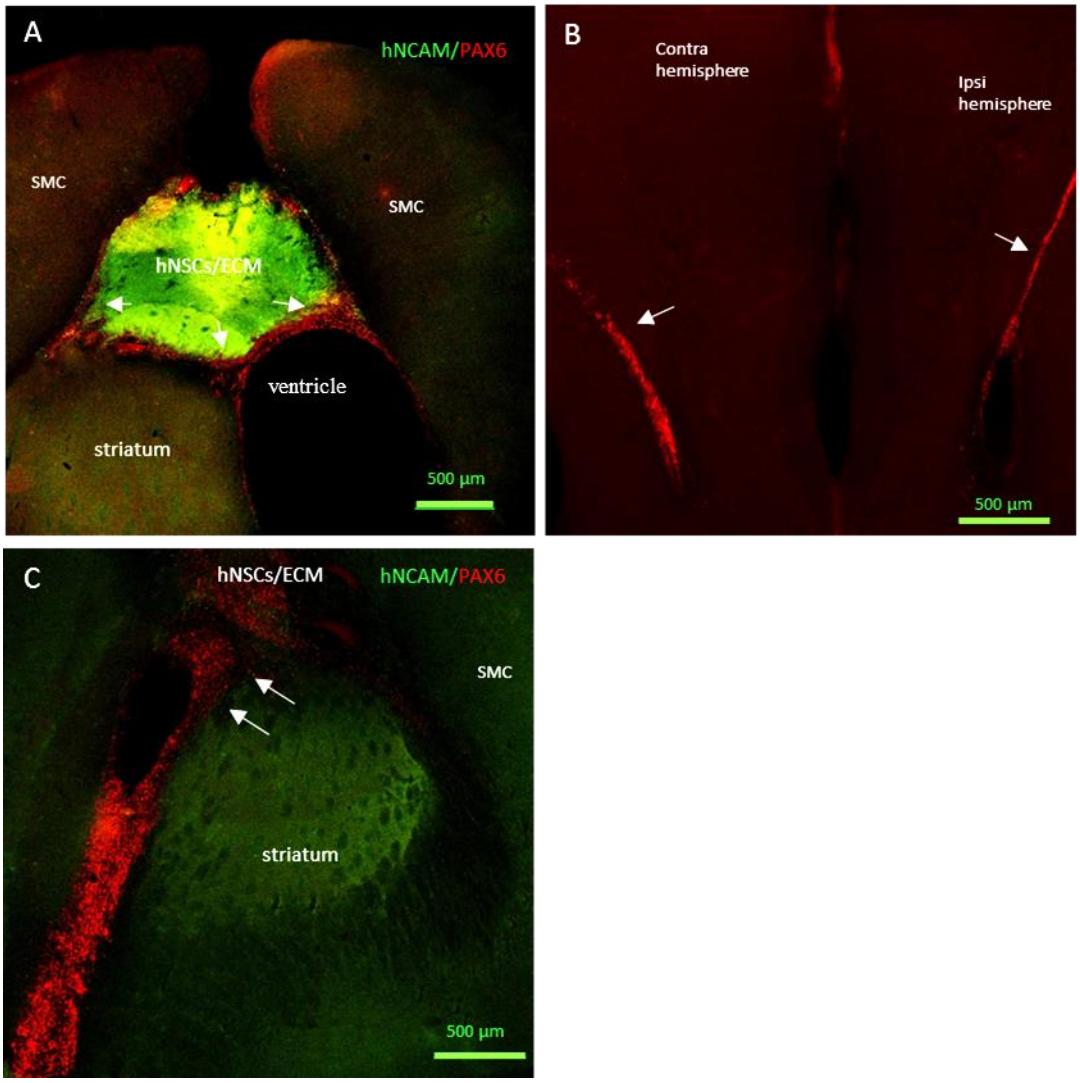


**Figure 5.18. Endogenous progenitor cells in the hNSCs/ECM after one month detected by IHC *in vivo***

Immunofluorescent double labelling for PAX6 (red) and hNCAM (green). (A) Shows endogenous PAX6+/hNCAM- around the graft (arrowhead) (B) around the VZ (arrows) and (C) between the SVZ and the transplant site, host progenitor cells expressed PAX6+ marker (arrows).

Denser GFAP immunoreactivity was observed around the hNSCs/ECM transplant (Figure 5.19A) than what was observed around the hNSCs/ECM transplant containing cerebral organoids (Figure 5.15E). Figure 5.19A shows host astrocytes predominantly nested around the xenograft region that had no cerebral organoids. Figure 5.19B demonstrates that astrocytes highly expressed GFAP and were characterised by a variety of shapes; long, short, or multiple processed. While some astrocytes had a stellate morphology, only a few had enlarged cell bodies and thick processes suggesting that they were reactive astrocytes. Some of these GFAP immunopositive cells invaded and reached to the core of the xenograft and some of them extended processes that surrounded blood vessels (Figure 18B). Interestingly, a similar host astrocyte distribution was seen when an ECM-only graft was made. Figure 5.19C shows strong GFAP immunoreactivity around the ECM-only transplant.

In an additional investigation, in brains with no transplant of either kind, we found that only reactive astrocytes and microglia were present and that they expressed high levels of GFAP and lectin around the ischemic infarction. Also, a small number of blood vessels were located around but not inside the lesion cavity (Figure 5.19D).

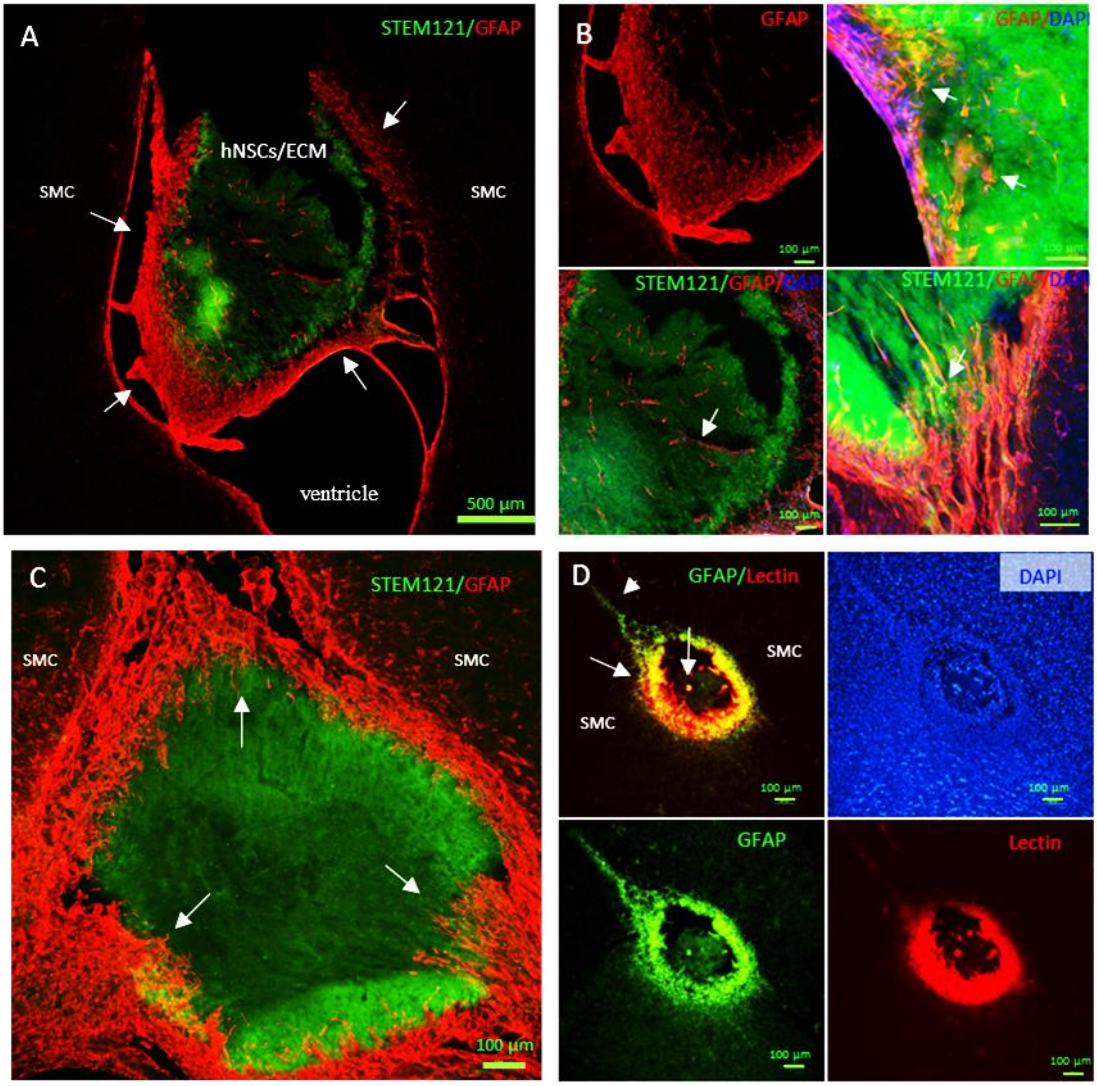


**Figure 5.19. Endogenous astrocytes in the hNSCs/ECM transplant after one month detected by IHC *in vivo***

Immunofluorescent double labelling for GFAP (red) and hNCAM or STEM121 (green). (A) Shows GFAP+ cells present around the transplant (arrows). (B) GFAP+ astrocytes in the graft exhibiting stellate, bulbar, or long processes morphology. (C) Demonstrates GFAP+ cells around but not within the ECM-only graft, the ECM gives a faint green signal as background. (D) Shows high levels of GFAP+ reactive astrocytes (green) and lectin+ ameboid microglia (red) expression in only lesioned brain around the infarction site, using histochemistry for anti-lectin. DAPI (blue) is nuclear counter staining.

Moreover, more blood vessels infiltrated the graft and fewer microglia were observed one month (Figure 5.20A) compared to one week post grafting of hNSCs/ECM using anti-lectin histochemistry (Figure 5.20B). Intriguingly, a large blood vessel could be seen running vertically in the middle of the graft (Figure 5.20A). As was found at the one week time point, a few cells that were immunopositive for PV appeared within the transplant at this time point (Figure 5.20B) which displayed a more elongated somata morphology. Similarly, PV immunopositive cells were seen within the transplanted ECM-only (Figure 5.20C), but we failed to detect any in the infarction site in the ET-1 model with no transplant (Figure 5.20D).

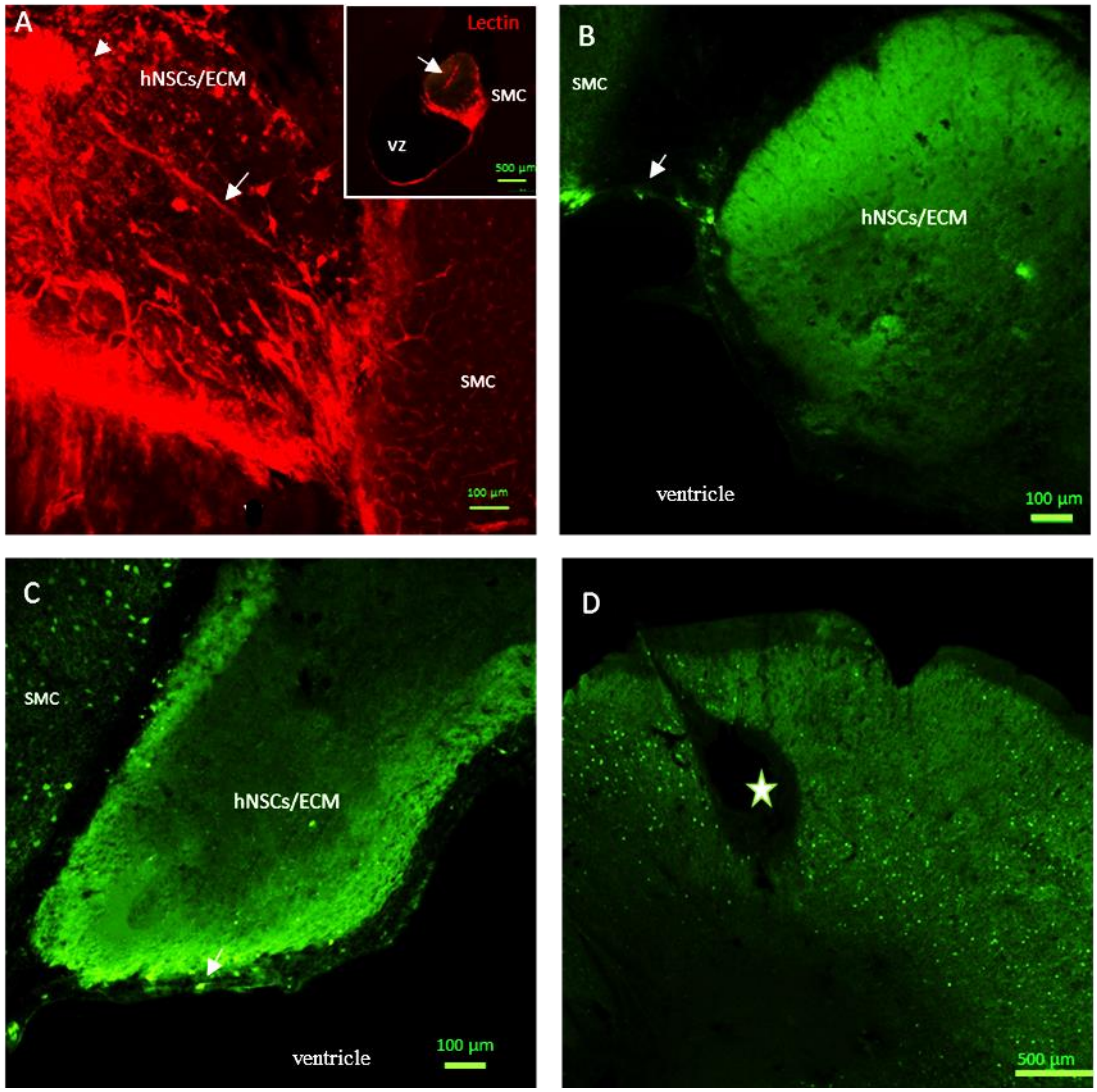


**Figure 5.20. Endogenous cells in the hNSCs/ECM after one month *in vivo*.**

Using histochemistry staining for anti-lectin (A) the host vascularized (arrows) the xenograft and host microglia (arrowhead) invaded the transplant as well. The small box shows large vertical blood vessels inside the xenograft. Using IHC, (B) And (C) shows migrating host PV+ cells from the cortex to the graft (arrow), while (D) demonstrates no PV+ cells inside the infarction in lesioned brain with no transplant

### Three months post-transplantation

Most of the transplanted human cells were seen within the xenograft. Only a few of human cells were observed away from the transplant at this time point post grafting. We observed few human cells in the ipsilateral lateral ventricle (Figure 5.21A) immunopositive for STEM121 and with long processes. Also, we found a clump of cells ventral to the transplant (Figure 5.21B and C).

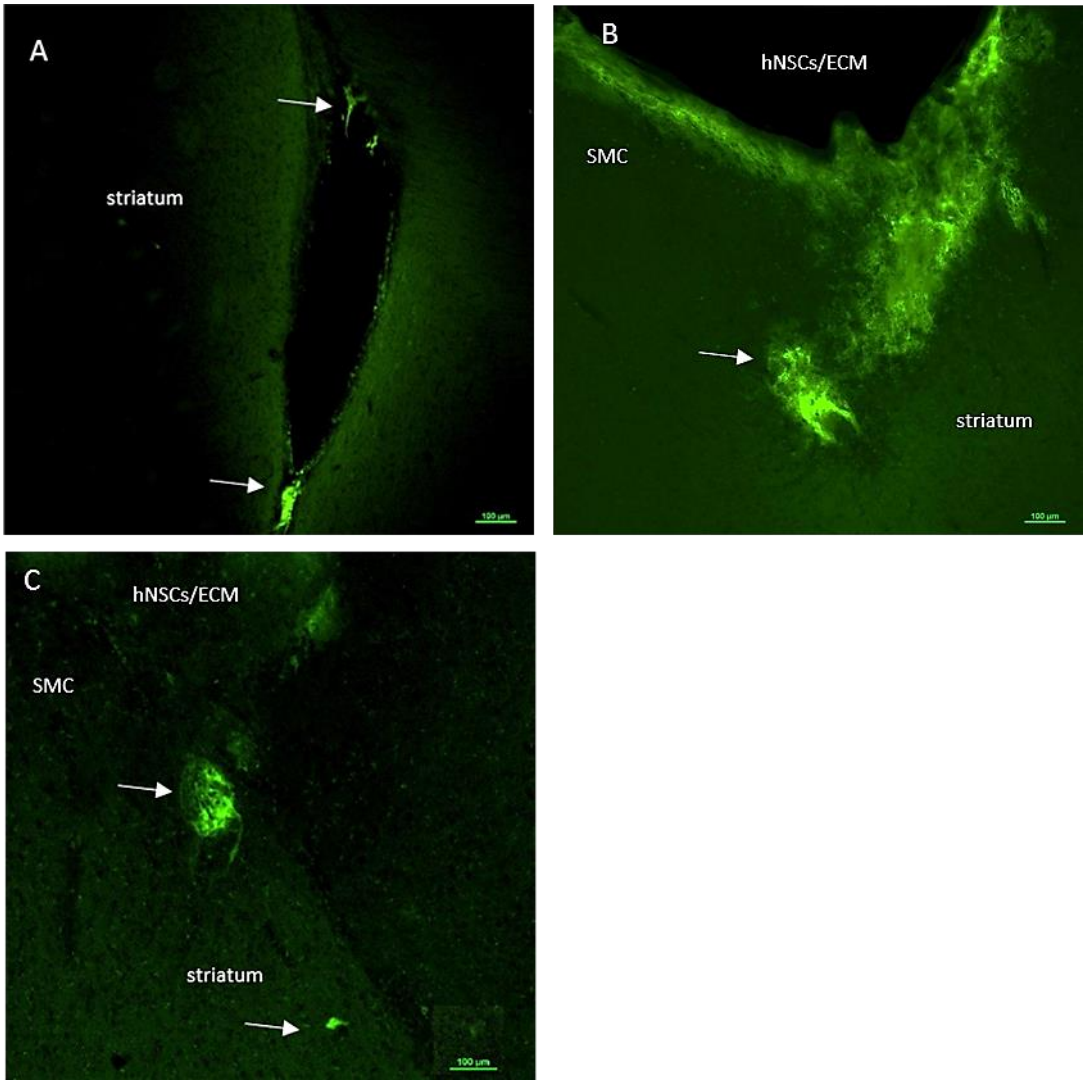


**Figure 5.21. Human cells located away from the graft site three months post-transplantation.**

Immunofluorescent labelling for cytoplasmic markers STEM121 and hNCAM. STEM121+ cells (green) presented in the lateral ventricle of the ipsilateral hemisphere (A) and inferior to the transplantation site in the striatum. (B, C) Another human cell clump was found inferior to the graft detected by IHC for anti-hNCAM antibody (green).

The host brain continued to produce new neurons in the SVZ. These neuroblasts continued migrate toward the xenograft. Figure 5.22A shows endogenous neuroblasts immunopositive for DCX located in the SVZ of the lateral ventricles in both hemispheres. These host immature neurons were strongly immunoreactive for DCX and located in the migratory trajectory between the VZ and the graft site in the ipsilateral hemisphere (Figure 5.22B).

Transplanted and host neuroblasts were distributed through the graft but fewer of them surrounded the xenograft, compared to one week and one month. Neuroblasts, either host or human, were distributed throughout the graft reaching the centre of it. Moreover, the DCX + cells were connected to each other and exhibited elongated processes (Figure 5.22C).

Host neuroblasts exhibited regenerative activity at the graft/ infarction observed three months post-grafting. Endogenous neuroblasts, expressing strong anti-DCX labelling of neurites, started to rebuild the conical bottom of the lesion/graft site (Figure 5.22D). Also, these DCX+ cells connected the upper ends of the infarction margins in some brains while in others they started to fill the ventral region of the lesion/graft site (Figure 5.22D). No MAP2 immunolabeling was observed within the transplant site suggesting no mature neurons of either host or graft origin were present (Figure 5.22E).

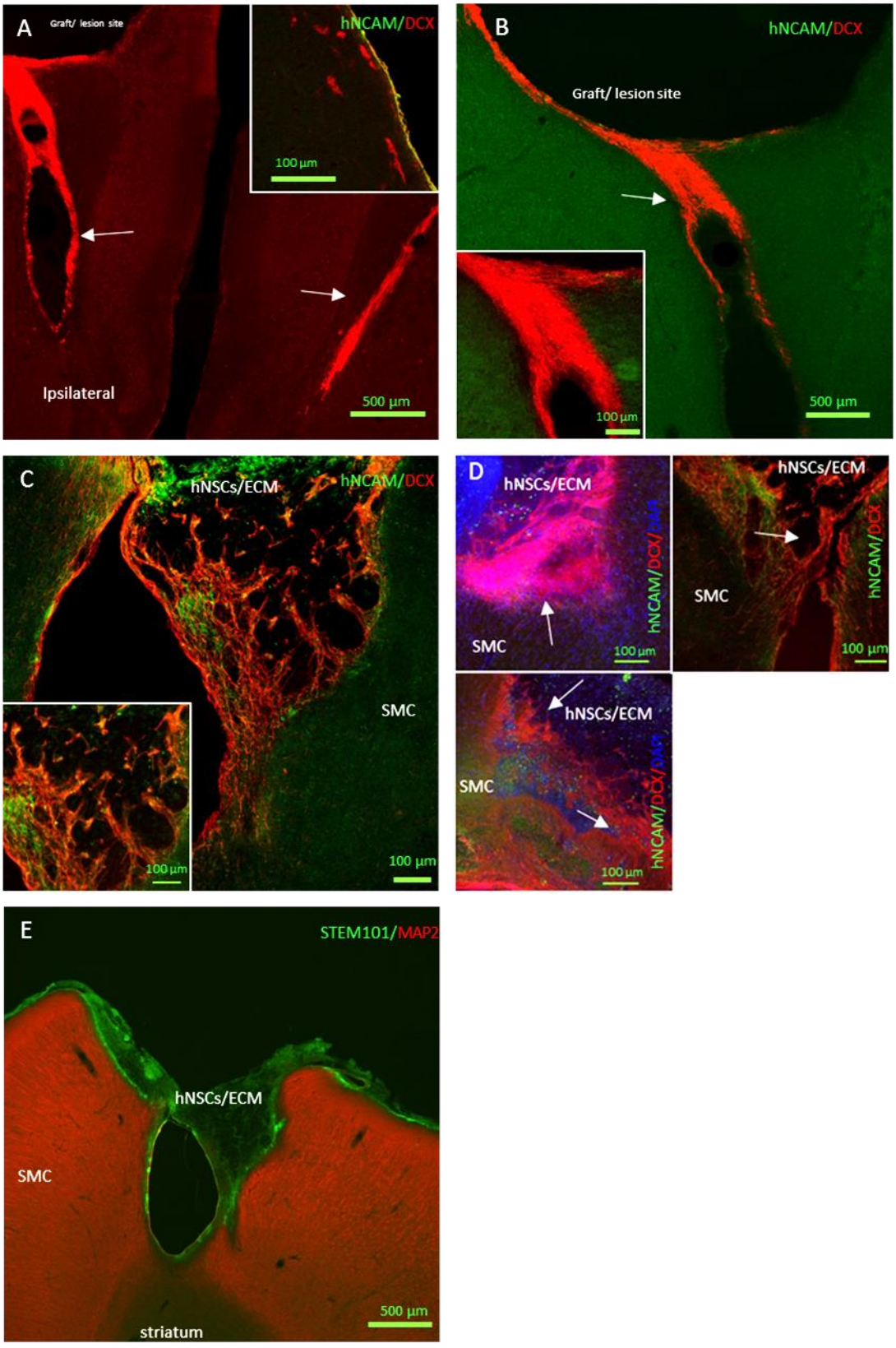
A
Graft/ lesion site
hNCAM/DCX
100 µm
Ipsilateral
500 µm
B
hNCAM/DCX
Graft/ lesion site
100 µm
500 µm
C
hNSCs/ECM
hNCAM/DCX
SMC
100 µm
100 µm
D
hNSCs/ECM
hNCAM/DCX/DAPI
SMC
100 µm
hNSCs/ECM
SMC
hNCAM/DCX
100 µm
hNSCs/ECM
SMC
hNCAM/DCX/DAPI
100 µm
E
STEM101/MAP2
hNSCs/ECM
SMC
500 µm
striatum

**Figure 5.22. Immature neurons in the hNSCs/ECM three months post-transplantation *in vivo*.**

Immunofluorescent double labelling for DCX (red) and hNCAM (green). (A) Shows endogenous newly formed neuroblasts expressed DCX in their somata and leading processes in the SVZ (rectangle) and around both lateral ventricles (arrows) and (B) toward the graft/lesion site. In (C) DCX+ host cells have migrated towards the transplantation site and intermingled with hNCAM+ cells (green) some of which are also positive for DCX (yellow). (D) Examples of cortical regeneration by host DCX+ cells, the arrows show DCX+ neurons filling some regions of the gaps in the lesion/graft site. (E) Shows no host MAP2+ or human STEM101/MAP2+ neurons within the xenograft.

Similar to DCX, the host brain continued producing progenitor cells that were immunopositive for PAX6 around both lateral ventricles. Figure 5.23A demonstrates PAX6+ but not hNCAM cells presented in the trajectory between the SVZ and the graft site. Within the graft, cells immunopositive for PAX6 and hNCAM spread sparsely and connected to the host cortex and each other in a similar way to DCX+ cells. Also, some PAX6/hNCAM+ cells attached to the cortex at the upper boundary of the transplant (Figure 5.23B).

We observed that few hNSCs differentiated into astrocytes detected by anti- STEM123 IHC (Figure 5.24A). Host astrocytes immunopositive for GFAP but not for STEM101 reached the centre of the transplant. Compared to one week and one month post-grafting, fewer host reactive and resting astrocytes with elongated processes were found around and in the graft (Figure 5.24B). Furthermore, a few host amoeboid and resting microglia immunopositive for IBA1 surrounded and infiltrated the graft (Figure 5.24C). Finally, we found some cells within the xenograft stained with anti-synaptophysin (Figure 5.24D) indicating the functionality of the differentiated neurons within the graft.

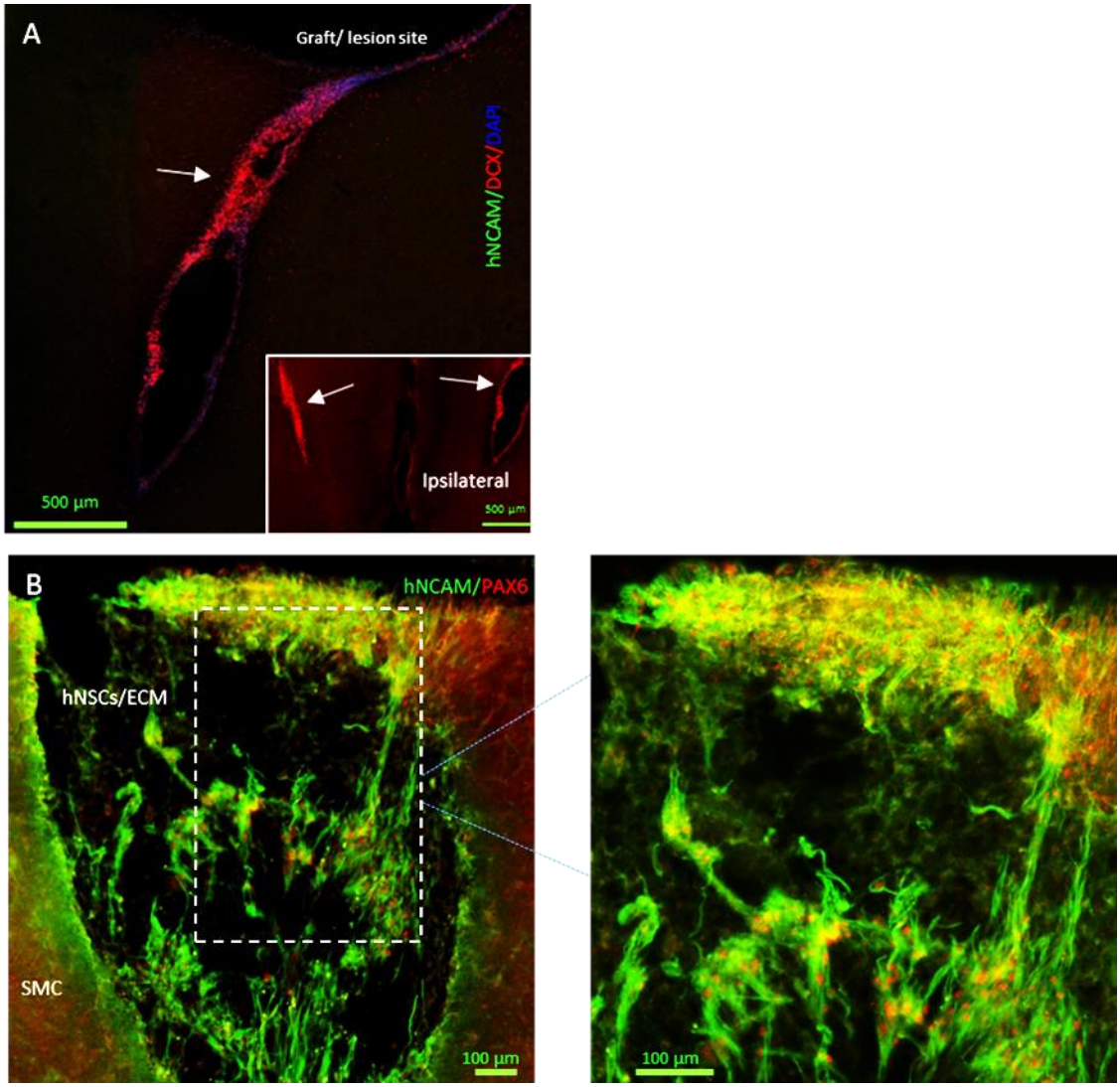


**Figure 5.23. Neural progenitor cells in the hNSCs/ECM three months post-transplantation *in vivo*.**

Immunofluorescent double labelling for PAX6 (red) and hNCAM (green). (A) Shows endogenous PAX6+/hNCAM- cells between the SVZ and the graft/lesion site, and in both lateral ventricles (arrows in the box). (B) Shows PAX6+/ hNCAM + cells within the transplant and at the superior margin of the xenograft.

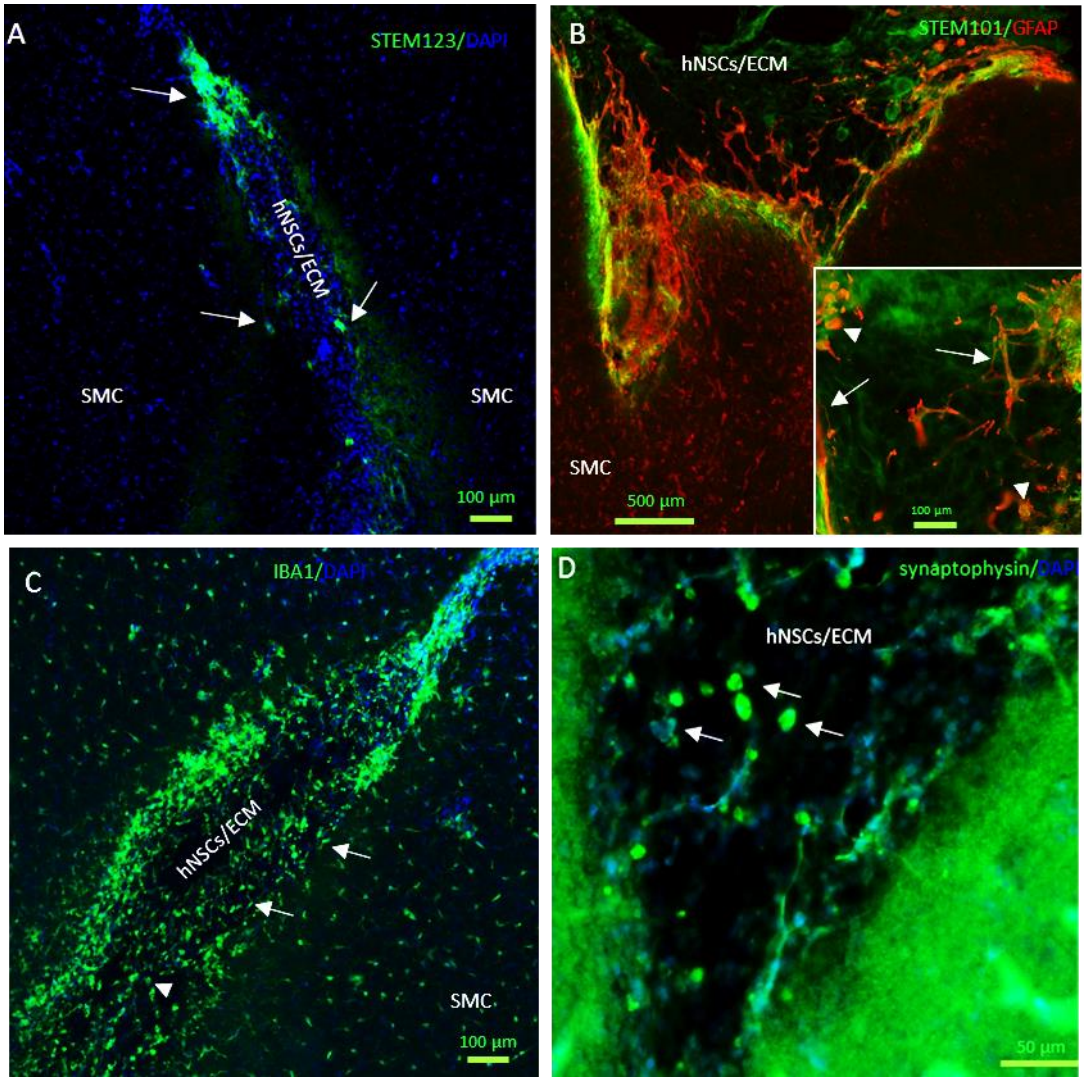


**Figure 5.24. Immunofluorescence for cells in the hNSCs/ECM three months post-transplantation *in vivo*.**

(A) A few STEM123+ (green) human astrocytes (arrows) were around the graft. (B) Immunofluorescent double labelling for GFAP (red) and STEM101 (green) shows GFAP+ only cells within the transplant exhibited bulbar morphology (arrowhead), or extended processes in space and around blood vessels (arrow). (C) shows host resting microglia (arrows) surrounded and invaded the organoid structures, and host ramified microglia (arrowhead) located in and around some boundaries of the xenograft. (D) Synaptophysin expression (green) within the transplant.

## 5.3 Discussion

### *5.3.1 In vitro experiment*

The aim of this study was to make qualitative observations, using double-label immunofluorescence with light and confocal microscopy, of the ability of human induced pluripotent stem cells (hiPSCs) derived NSCs cultured in a 2D monolayer or in a 3D semi-synthetic ECM to spontaneously differentiate into neuronal lineages. The starting cells of the hiPSCs derived NSCs were originally from a umbilical cord blood (UCB) CD34+. Umbilical cord blood cells would make an excellent source of cells for transplantation in perinatal stroke as they could be derived from the umbilical cord of the babies that suffered stroke allowing an autologous transplant.

In the 2D NSCs culture, we found some neural progenitors as well as early and late post-mitotic neurons detected by the antibodies to PAX6 (neural progenitors) DCX (post-mitotic neuroblasts) and TBR1 (post-mitotic neurons) at the following time points: 10, 14, and 17 days after the beginning of differentiation. Over the period of the 3-time points, we noticed more PAX6+ neural progenitors in the early stages and more DCX+ and TBR1+ post-mitotic neurons toward the later stages. Similarly (Ali et al., 2012) found a significant increase in post-mitotic neuron number on day 24 in culture when compared to 10 days in the 2D *in vitro* culture while PAX6+ progenitors were 45% of all cells on day ten decreasing to 15% on day 24. This difference in marker expression followed the expressed marker pattern during human cortical neurogenesis s in which PAX6 was expressed first by neural progenitors, followed by TBR2 then TBR1 at 12 postconceptional weeks (PCW) (Ali et al., 2012, Bayatti et al., 2008).

We reported a clump of cells at the last time point. It had heterogeneous mixture of cells positive for PAX6 and DCX and we also found them immunopositive for synaptophysin. After the last time point in our 2D in vitro experiment, cells started to show the very limited life span of post-mitotic cells in 2D culture.

After we confirmed the differentiation ability of NSCs in the 2D culture, we aimed to conduct qualitative observations of the NSCs differentiation ability in a 3D culture over 4-time points; 10, 14, 17, and 43 days using the same ECM, HyStem-C hydrogel we planned to incorporate the cells into for in vivo grafting. The most prominent difference between the 2D and the 3D culture results was that the NSCs in the 3D culture survived for more than 2.5 fold longer than

in 2D culture. This increase in survival rate supports the finding that the hydrogel we used increased NSCs survival in vitro in a previous study (Zhong et al., 2010). Interestingly, in our study, cells in the 3D culture seem to be able to survive beyond the last time point indicating that the 3D culture promotes NSCs survival and differentiation more than the 2D culture. Likewise, (Liang et al., 2013) found that culturing NSCs in hydrogel scaffold improved the survival rate significantly suggesting that the hydrogel component has a crucial rule in the increased NSCs viability.

In addition to the fewer pre-mitotic radial glial cells and many post-mitotic immature and mature neurons at later time points of the 3D culture, we demonstrated longer neuronal neurites than in the 2D culture that reflected a complicated networking pattern between cells which might have occurred due to the extra space provided by the 3D scaffold (Lam et al., 2014). Unlike the differentiated NSCs in the 2D culture that had short processes, the NSCs in the 3D culture in our study differentiated into immature neurons with around 50µm processes in length as early as ten days in culture and over 200µm after 14 days. We also observed fewer immature neurons and more mature neurons that were immunopositive for MAP2 with more than 50µm of dendritic length with complicated morphology and connections than earlier time points. Similarly, shown in the study by(Carlson et al., 2016) the 3D in vitro culture promoted the differentiation of neural cells with marked expression of MAP2 and β-TUB and complex neurite outgrowth after 12 days, while radial glia that expressed PAX6 were hardly observed at day 14 and diminished at the later time points. Thus, our NSCs in the 3D culture had more division activity into neural progenitors at earlier time point and more post-mitotic neurons with complicated neurites at the later stages. This finding suggests that the NSCs in the 3D culture were differentiating toward mature neurons over time.

Our result is consistent with a study that cultured differentiated NSCs in 2D and 3D culture and found that neurons in the 3D culture had longer processes than in the 2D culture. They found that the axonal process outgrowth was 200 µm and 250 µm at week one and two respectively post culturing(Stevanato et al., 2015). Indeed the use of 3D culture provided a scaffold for the cultured NSCs to survive and differentiate (Carlson et al., 2016, Wu et al., 2017) demonstrated that the 3D scaffold guided neurite growth of the human induced neuronal cells derived from hiPSCs and improved their survival rate.

In our study, NSCs in 3D and 2D culture had potentially functional neurons as we detected expression of the neural synaptic vesicle marker synaptophysin which is similar to a recent study that reported that synaptophysin was robustly expressed on day 28 in the 3D culture(Carlson et al., 2016). Moreover, a recent study demonstrated that the 3D culture enhanced the differentiated NSCs to form a functional synaptic network indicated by the presence of synaptophysin (Smith et al., 2017a).

Only a few cells in the ECM were stained by the GFAP marker suggesting that our NSCs cultured *in vitro* were dedicated to produce more neurons than astrocytes in both 2D and 3D cultures. A similar *in vitro* study showed only a few astrocytes after culturing NSCs with nerve growth factor (NGF) (Arien-Zakay et al., 2011). This may be due to the type of ECM (Thonhoff et al., 2008) or the NSCs origin (Brannvall et al., 2007). Different ECM types have various effects on the neural fate of the cultured cells. For instance, human foetal cells cultured in Matrigel, an ECM protein in a solubilized basement membrane extracted from sarcoma in mice (Hughes et al., 2010), differentiated into GFAP+ astrocytes while when they cultured in Puramax they gave rise into 17% β-TUB+ cells and 27%GFAP+ cells (Thonhoff et al., 2008).

Thus, similar to the recent review that reported the advantages of the 3D *in vitro* culture over the 2D on the neuronal cell expansion and differentiation(Murphy et al., 2017b), we found that the 3D culture of NSCs in 3D hydrogel culture in our study showed advantages over the conventional 2D monolayer culture which make the NSCs suspended in ECM a better choice for our *in vivo* NSCs transplantation.

### *5.3.2 In vivo experiment*

After we confirmed the ability of the NSCs derived from hiPSCs to survive and differentiate in the vitro 3D culture using the semi-synthetic ECM, HyStem-C hydrogel, we aimed to transplant NSCs/ECM complex into the lesioned SMC of the PIS model at postnatal age (P) 14 and study the development and survival of NSCs qualitatively at 3 time points: 1, 4, and 10 weeks post transplantation.

**Cerebral organoid formation in vivo**

The most prominent result in our *in vivo* experiment one month after transplantation in the PIS model was the formation of cerebral organoids. A cerebral organoid is a specific patterning of cells into a neural rosette formation that mimics the features of the neural tube in the developing

human foetal brain during the fourth week of development (Murphy et al., 2017b). The laminar phenotypes of our resultant cerebral organoids were as follows: first the central space (lumen) in each rosette formation resembled the ventricle of a developing brain, surrounded by a layer of condensed hiPSCs derived NPCsimmunopositive for PAX6, resembling the VZ of certain regions of the developing

central nervous system (CNS) including the cerebral cortex which we named "PCL" , and finally an outer layer that contained proliferating cells and post-mitotic human neurons that were immunopositive for DCX and β-TUB which we named "NCL", four weeks after transplantation.

In addition to DCX and β-TUB+ neuroblasts, transplanted cells gave rise to more mature MAP2+ neurons. We found more mature post-mitotic neurons which stained with MAP2 in the organoid formation, however, we could not specify at what layer due to technical difficulties. In a previous study, transplanted NSCs derived from human ESC with Matrigel differentiated into MAP2+ cells three weeks after inducing focal cerebral ischemia in adult rats (Jin et al., 2010). This might highlight one of the advantages of the use of the ECM as a vehicle for *in vivo* transplantation in promoting cell differentiation.

To our knowledge, our transplantation method is the first that was able to generate such formations recapitulating some of the characteristics of the developing cortex in the human brain *in vivo*. Thus, our results are not comparable to any previous study. However, two aspects could be compared to our cerebral organoids. Firstly, the features of the neural tube in the developing human brain, and secondly, the features of the cerebral organoids generated *in vitro* in previous studies.

The neural tube can be defined as "a single layer of proliferating columnar neuroepithelial cells that eventually give rise to the CNS (brain and spinal cord)". In mammalian brain formation, neuroepithelial progenitors are located around the inner surface of the neural tube called the ventricular zone (VZ). These human progenitors divide symmetrically generating radial glial cells that later divide asymmetrically producing daughter progenitors (McConnell, 1995) immunopositive for PAX6 in the VZ (mainly) although some of them translocate to the SVZ (Britz et al., 2006, Miyata et al., 2004, Rakic, 1988, Tan and Shi, 2013) and either neurons or intermediate progenitor cells that can divide further to give neurons. In mammalian

corticogenesis, newborn neurons migrate towards the pial surface forming the layers of neurons observed in the adult cerebral cortex. Each cortical layer shares a laminar phenotype (Stiles and Jernigan, 2010) with the deepest layer generated first and the superficial ones formed subsequently (McConnell, 1995, Tan and Shi, 2013). Corticogenesis in human starts with the formation of cortical plate (CP) at 8 at PCW and the cortical progenitor layer at 12.5 PCW (Bayatti et al., 2008). In rodents, cortical generation starts on day 10 and finishes on day 18 (Levers et al., 2001), and the cell cycle is five times shorter than in human and non-human primates (Kornack and Rakic, 1998).

Likewise, similar morphology and organisation of PCL and NCL layers occurred in our organoids. We found a significant amount of neural progenitors with PAX6 gene expression around the central lumen of the generated cerebral organoids. Furthermore, DCX immunoreactive neuroblasts were found in a layer surrounding these progenitors suggesting that they were post-mitotic daughters of the asymmetric division of the progenitor cells (Luskin et al., 1988).

Cerebral organoids were generated recently for the first time from pluripotent stem cells *in vitro* (Lancaster et al., 2013) and called "cerebral or whole brain organoids" and "Brain in a dish". More recent advances have been achieved improving the methods for generating these organoids *in vitro* (Mason and Price, 2016, Qian et al., 2016).

To generate these organoids *in vitro*, researchers used Matrigel as a scaffold in a 3D culture within rotating vessels to enhance nutrients and oxygen reaching the core of the organoid avoiding necrosis and growth size limitation (Lancaster et al., 2013). Since then, the number of studies has expanded in this area of research giving better results than with simple *in vitro* protocols (Qian et al., 2016). This achievement has had a significant impact especially in modelling disease and introducing drugs *in vitro* without the need for animal models (Lancaster et al., 2013, Mason and Price, 2016, Qian et al., 2016). All these factors are crucial to generate *in vitro* cerebral organoids however in our *in vitro* experiment we did not propose to produce cerebral organoids, but we intended to test the NSCs ability to differentiate in hydrogel before we transplanted them. As a result, cerebral organoids were absent in our *in vitro* experiments due to the lack of some essential procedures such as the spinning vessels.

Contrary to the organoids generated *in vitro* in previous studies that have shown variability and heterogeneity (Lancaster et al., 2013), our organoids were consistent in their morphology. All the cerebral organoids that resulted from our experiments shared similar patterns of gene and protein expression with mammalian developing cortical layers (Noctor et al., 2004). We identified PAX6 gene expression in the inner layer and DCX protein expression in the outer layer in all generated organoids. Researchers have been able to generate brain organoids *in vitro* that have the PCL (Lui et al., 2011) and the NCL which is important in cerebral cortex development (Mariani et al., 2012, Qian et al., 2016).

Recently (Qian et al., 2016) have developed a protocol that produces organoids containing neural progenitors in the PCL and more maturing cells in the NCL and even the CP-like layer where the deep layer cortical neuron marker CTIP2 is expressed at day 70. In At the 4 week time point, our cerebral organoids were homogenous and robustly generated the cerebral-specific progenitor markers PAX6 exclusively in the PCL and the immature neuronal marker DCX in the NCL. Also, we observed some CTIP2+ cells in the outer part of the organoid after four weeks post-grafting, similar to (Renner et al., 2017) who found CTIP2+ cells in this location *in vitro*.

The timing of our cerebral organoids formation was consistent with studies of *in vitro* generated organoids. Cerebral organoids have been formed 20-30 days after encapsulating hiPSCs in Matrigel, an ECM protein derived from tumours in mice (Hughes et al., 2010), in an *in vitro* study (Lancaster et al., 2013). In our study, fully formed cerebral organoids were found 4 weeks after transplantation.

It is noteworthy to report that we found that one week after the transplantation the transplant formed a labyrinthine structure that was similar to what (Qian et al., 2016) observed in their *in vitro* cerebral organoids one week after the transplantation. This structure could be the beginning of the cerebral organoid formation detected by immunopositivity for the gene marker PAX6. We did not detect any mature neurons with a MAP2+ marker at this early time point.

Several factors probably contribute to the resultant cerebral organoids 4 weeks post grafting in our study. Our *in vitro* protocol to prepare cells was different from the previous *in vivo* transplantation study protocols (Lam et al., 2014, Nih et al., 2017, Zhong et al., 2010). We directly grafted the NSCs *in vivo* instead of passaging cells *in vitro* to transform the NSCs into

NPCs because it has been shown that the intrinsic environment in the brain and the transplanted ECM will act together to provide the growth factors to the grafted NSCs to differentiate into NPCs and neurons (Park et al., 2014).

Also, we transplanted NSCs with hydrogel as a vehicle and this combination had not been utilised before this study. The ECM mimics the brain niche and provides a scaffold that might support the transplanted cells physically to organise themselves into organoid structures (Gjorevski et al., 2014). Beside the mechanical support, it has been demonstrated that the hydrogel 3D scaffold is an important factor in providing a beneficial environment for the NSCs. For instance, when UCB and NSCs were cultured *in vitro* with hydrogel, the hydrogel enhanced the UCB provided beneficial environment for the NSCs by enhancing the secretion of neurotrophic factors such as NGF, brain-derived neurotrophic factor (BDNF) and promoting cell differentiation and metabolic activities (Park et al., 2014).

*In vitro*, studies have suggested that organoid formations are self-dependent (Elkabetz et al., 2008, Lancaster et al., 2013). However, the underlying mechanism of self-organising of organoids *in vitro* is not yet fully understood, given the fact that the generation of the cerebral organoids *in vitro* is a recent finding. The developing embryonic human brain has different signalling centres that secrete morphogens patterning the neural tube. These centres are the anterior neural ridge, cortical hem, and the antihem for the telencephalic portion of the neural tube. When no extrinsic patterning cues are available in the 3D *in vitro* culture, human embryonic stem cell -derived NSCs organoids will be committed to being anterior neural ectoderm (Elkabetz et al., 2008, Renner et al., 2017).

A recent *in vitro* study has indicated that the generated cerebral organoids themselves contain some of the signalling centres that have been found in the developing foetal forebrain (Renner et al., 2017). These are the cortical hem and the antihem centres that are patterning the dorsal brain in Telencephalic vesicles of the foetal brain (Camp et al., 2015, Renner et al., 2017). However, it still unknown when they are active, and how long is their life span. Indeed further investigation must be done to understand the underlying mechanism of how grafted cells self-organise into organoid formations *in vivo*.

We found that our transplanted NSCs survived, proliferated, and differentiated at the four week time point. One possible reason behind this result is the use of the hydrogel, HyStem-C, as an

ECM. This hydrogel has three components; hyaluronic acid (HA), gelatin, and the cross linker Polyethylene (glycol) Diacrylate (PEGDA), which promoted transplanted human cell survival and proliferation in stroke models previously (Liang et al., 2013). The high molecular weight of the HA that we used enhances the survival of the cells and mitigates the host inflammatory response *in vivo*. A previous study has shown that the use of this hydrogel supported the transplanted human cells in term of surviving and proliferating in stroke model in rodents(Liang 2013) which could be as a result of the ability of the high molecular HA in reducing the cell apoptosis activity (Jiang et al., 2005, Liang et al., 2013).

Moreover, the molar ratio of this component that we used ( HA, gelatin, and PEGDA = 2:2:1) and the injection timing protocol that was just prior to the gelling time of the hydrogel (20 minutes) were demonstrated to produce the perfect environment *in vivo* at least for 12 days post grafting in normal mice in a previous study (Liang et al., 2013). This molar proportion yielded a sponge-like ECM with mild stiffness that gave the transplanted cells more room to exchange the essential surviving factors such as nutrients and oxygen by avoiding the grafted cells accumulating along the injection needle trajectory (Liang et al., 2013). Furthermore, the mechanical properties of the hydrogel may contribute to the transplanted cell differentiation. (Seidlits et al., 2010) have found that the soft hydrogel which comparable to neonatal brain promoted rodent NPCs to differentiate into post-mitotic β-TUB+ neurons while they mainly differentiated astrocyte when cultured with stiffer hydrogel.

The underlying mechanism of cell survival and division in organoids has been studied previously *in vitro*. Researchers have explored active notch signalling, which is a cell to cell signalling pathway that is crucial to maintain the grafted NSCs derived from rosette formation, and found that this enhances NSCs division (Elkabetz et al., 2008, Shen et al., 2004) and decreases cell death (Androutsellis-Theotokis et al., 2006) *in vivo*.

It seems that our NSCs rarely differentiate into astrocytes when transplanted with ECM in PIS model. In our study, we did not see any astrocytes stained for human specific GFAP, except for 4 or 5 cells on one occasion. Consistent with our results, studies that have transplanted a similar cell source to ours in neonate rodents, but not suspended in a gel, have produced no or few astrocytes immunopositive for GFAP. Transplanted NSCs had not differentiated into GFAP positive cells five weeks post grafting (Jablonska et al., 2010). Furthermore, when NSCs were

grafted with ECM intracerebrally into the striatum of ischemic model (MCAO) of adult rats, no differentiated astrocytes were seen (Bible et al., 2012).

On the other hand, astrocytes were presented in some *in vivo* neonatal rat studies that grafted different stem cell than ours without ECM for instance after grafting human embryonic stem cells into a normal P2 rat neonate(Denham et al., 2012) and mesenchymal stem cells into a neonatal rat model of hypoxic ischemic brain (Xia et al., 2010), resulted in differentiation into mature glial cells expressing GFAP, particularly ten weeks post grafting in normal rats (Denham et al., 2012, Xia et al., 2010). These conflicting results might be due to the different cell type, different animal models, or histology assessment timing. For example, in focal ischemic adult rats, (Zhong et al., 2010) found that NSCs from human embryonic cortex can survive and differentiate into astrocytes and a few DCX neurons by two weeks from the grafting while the NSCs from human embryonic stem neural progenitor cells remain undifferentiated with a lower survival rate.

Another surprising result we found was the even vascularization of the cerebral organoids from the adjacent cortical tissue of the host brain. Anti-lectin histochemistry showed many host blood vessels invading the *in vivo* organoids in a well-distributed manner. *In vitro*, a spinning culture vessel is required to promote organoid survival, by forcing the oxygen and the fluid to reach the centre of the organoids physically (Lancaster et al., 2013, Qian et al., 2016). However, our *in vivo* experiment it appears that the cerebral organoids overcame the limitation in oxygen and nutrient supply by permitting ingrowth of vessels from the host tissue. Angiogenesis in our experiments provided a natural alternative to the rotating vessels for the *in vitro* organoids to keep them nourished at least for four weeks.

Previous *in vivo* studies have shown that angiogenesis occurred at the pre-lesion area after inducing stroke (Krupinski et al., 1993, Senior, 2001) but not in the transplant as in our results. This angiogenesis could happen due to a limited development of scar tissue at the infarction site because of the use of hydrogel. Although some studies used hydrogels, including the one we used, as a vehicle for *in vivo* transplantation, they have not stimulated angiogenesis (Bible et al., 2012, Zhong et al., 2010). However, other researchers have considered that hydrogels enhanced vascularization (Ju et al., 2014, Peattie et al., 2004). One explanation of the angiogenesis is the transplant itself. A study has reported that grafted cells secrete a vascular

endothelial growth factor that stimulates vessel formation (Horie et al., 2011) suggesting our cells enhanced neovascularization into the graft.

An important question is whether the cerebral organoids in our study survived or evolved into more defined cortical layers at ten weeks post grafting. To answer this question, we examined the graft histologically 75 days from grafting. Although we noticed regenerative activity by the endogenous cells, unexpectedly we could find barely any human cells either within the graft or away from it. An *in vitro* study had similarly generated organoids to ours which survived more than 84 days and exhibited the PCL and NCL layers of the developing human cortex. Then, after 100 days from the onset of cerebral organoids, the progenitor cells in the PCL depleted and the CP layer, which is a cortical layer containing CTIP2+ neurons located above the PCL and NCL, expanded (Qian et al., 2016). In our study, at the four week time point, we saw a few CTIP2+ neurons were located around the PCL and NCL suggesting the beginning of forming the CP layer.

At the ten week time point, we noticed graft regression occurred alongside a lack of ECM at the graft site. The survival rate of the transplanted cells was similar to a previous study transplanting stem cells into rodent neonate lesioned brain in which grafted human cells survived for five weeks with no ECM before they diminished (Jablonska et al., 2010). There are two possible explanations behind this ECM-related observation. First, the fast degradability of the thiolated hydrogel used in our ECM (Hahn et al., 2007, Prestwich et al., 2012) and second, the transplanted cells themselves or the host infiltrating cells might contribute to hydrogel dissolution (Moshayedi et al., 2016) have reported that the grafted hydrogel degraded faster when mixed with 100,000 NSCs than when it was grafted alone *in vivo*. The resultant delayed gelling time allows grafted cells to settle down in the graft rather than being distributed evenly within the ECM (Martens et al. 2009) *in vivo* and subsequently results in low survival rate as demonstrated in a previous study (Zhong et al. 2010).

Moreover, possible unbalanced intrinsic cues of the host brain and the cues needed by the graft might contribute to organoid degeneration. First, the xenograft transplantation method might result in a lack of the needed trophic factors to keep the grafted human cells alive in the rat brain as shown in a previous study (Glover et al., 2009). Second, the mismatch between rodent (host) and grafted human cells in the cell cycle timing could be another reason. The cell cycle duration affects the cortical layer phenotype (Dehay and Kennedy, 2007, Pilaz et al.), and in

our study we transplanted human cells into rodent brains while the human cell cycle is 5 times longer and needs an over 7 times longer period than rodents to produce the CP (Bayatti et al., 2008, Kornack and Rakic, 1998). Together, these are some of the possible reasons behind the regression of the cerebral organoids at ten week time point from transplantation in our study.

Finally, we found that at ten weeks human cells that were still immunopositive for DCX, β-TUB and PAX6 but not for MAP2+ suggesting a decreased number of maturing cells survived.

Now that we have discussed in detail the generation of cerebral organoids *in vivo* we can move on to the second interesting result which is the innate immune response by host cells toward the graft and endogenous brain regeneration in response to the NSCs/ECM transplantation.

**Host Immune Response to the Transplant**

We found that astrocytes and microglia infiltrated the cerebral organoids but they mainly displayed resting morphology and there was no evidence of harm to the organoids at the 4 week time point. This suggests that the host brain did not initially recognise the graft as a foreign body. In the same way, when hydrogel and NSCs were grafted intracerebrally in adult rodents, few inflammatory cells invaded the graft (Zhong et al., 2010) suggesting that the hydrogel worked as a shield to protect the transplanted cells. Thus, our result provided an *in vivo* cerebral organoid that not only mimicked the developing brain but also did not trigger the host innate immune system.

The immediate reaction of microglia serves as the first line in defence against the transplant (Glezer et al., 2007). We did not use immunosuppression to ameliorate the immune reaction as some studies have argued that using immunosuppression will prevent neural repair, or lead to deterioration in the underlying disorder and prevent the beneficial role of microglia in the repair of the lesioned brain tissue (Glezer et al., 2007, Kulbatski, 2010). Furthermore, the immune system is too immature and less able to mount an immunogenic response to xenogeneic transplants in neonate rodents (Coenen et al., 2005, Englund et al., 2002, Jablonska et al., 2010).

Although we transplanted the NSCs/ECM into immature rodents at age P14, we found that reactive microglia surrounded and invaded the ECM which semi-surrounded the organoids and the ECM-only brain group at the one and 4 week time points. Likewise in other intracerebral transplantation studies (Bible et al., 2012, Liang et al., 2013, Zhong et al., 2010), graft areas with ECM alone have been easily detected by the brain to be attacked suggesting that grafted

ECM trigger the immune system of the host. The mechanical properties of ECM are believed to trigger the innate immune system of the host (Lam et al., 2014).

Grafting hydrogel can cause an inflammatory reaction because of its mechanical properties, but still less than the reaction resulting from our stroke model which is similar to previous studies (Lam et al., 2014, Zhong et al., 2010). Furthermore, this was consistent with the previous study that used the exact same hydrogel as we used (Liang et al., 2013) suggesting that the stiffness of the hydrogel, Hystem-C, will mitigate the inflammatory reaction at the insult site. The hydrogel component HA, which we used in our study, is a high molecular weight polymer and previously has been demonstrated to be an excellent support for the transplanted human cells in terms of surviving and proliferating following grafting to a stroke model in rodents (Liang et al., 2013) unlike the low-molecular weight polymer which enhances inflammatory gene expression (Jiang et al., 2005).

**Endogenous brain regeneration**

In our study host neuroblasts and neural progenitors were located in the SVZ of the lateral ventricles in both hemispheres and along a migratory pathway between the SVZ and the xenograft in the ipsilateral hemisphere at all three time points. In a similar study that transplanted hydrogel and NSCs in focal ischemic stroke model, the host neuroblasts migrated to the graft two weeks after transplantation whether the grafted cells had been injected with or without hydrogel (Zhong et al., 2010).

Neurogenesis and migration of host neuroblasts after inducing stroke occurs at several sites including the adult SVZ around the lateral ventricle (Kadam et al., 2008, Kokaia and Lindvall, 2003, Ohab and Carmichael, 2008). Studies have shown that a NSCs xenograft in MCAO stroke model in adult rats enhanced neurogenesis in the SVZ and vascularization in the pre-infarcted area (Zhang et al., 2011b). It has been demonstrated that after inducing stroke the generated neovessels promoted host neurogenesis in the SVZ by secreting trophic factors (Mine et al., 2013). However, this neurogenesis occurred in the first week then decreased significantly (Arvidsson et al., 2002, Ohab et al., 2006, Zhang et al., 2001).

At the 4 week time point, we found that the host neural progenitors and immature neurons surrounded the graft and intermingled with the human grafted neurons at the periphery of, but not centre of, the cerebral organoids. A similar cellular distribution was observed in the ECM-

only transplant but with fewer cells with shorter processes invading the ECM. Rodent cortical neurons, which were immunopositive for MAP2 and β-TUB, infiltrated parts of the ECM which were not populated with human cells, yet we did not see this in the ECM-only group. At ten weeks, the host neuroblasts exhibited regenerative activity at the graft/ infarction, , and started to rebuild the conical bottom of the lesion/graft site connecting the upper ends of the infarction margins in some brains. This suggests that transplanted ECM and NSCs activated the host endogenous regeneration activity.

Studies have shown that transplanted stem cells enhance endogenous axonal sprouting and dendritic branching (Horie et al., 2015). The suggested underlying mechanism is that the grafted cells travel along the host vessels showing the crucial role of neovascularization in the cellular exchange between the host and the graft (Horie et al., 2015).

It has been previously shown that after ischemic insult in the rodent brain, neurogenesis took place in different brain regions including the SZV and there was migration of new cells to the lesion site. However, these cells died within a week (Jin et al., 2001, Nakagomi et al., 2009). In our study, the host DCX+ neurons were capable of being produced, migrating and surviving through all the three time points; 9, 32, 77 days after inducing the insult.

It is noteworthy to report that we observed positive PV+ cells in the organoid area as well as in other areas of the graft at both the one and four week time points. Moreover, we observed PV immunopositive cells within the transplanted ECM-only, but none presented at the infarction site in the ET-1 model. Interestingly, a study has reported for the first time that neuroepithelial stem cells differentiated into an inhibitory cortical interneuron PV+ cells *in vitro* but not when transplanted in neonate mouse *in vivo* (Zhu et al., 2016). Thus, our study is the first to report PV+ cells within the graft. Although they were reported to be in the ECM and the graft and looked as though they migrated from the cortex, whether they were host or human will be addressed in future studies.

Since synaptogenesis is an advanced form of plasticity leading to restoration of neural circuit function in the lesioned brain, we tested our graft for anti-synaptophysin immunoreactivity, and we found that transplanting NSCs with ECM enhanced synaptogenesis. Likewise, studies of transplanting stem cells after ischemic lesions recorded some synaptogenic activity using electronic microscopy (Daadi et al., 2009, Ding et al., 2013). Also, synaptophysin

immunoreactivity has been demonstrated previously in ischemic rats after human umbilical tissue-derived cell transplantation at four weeks (Zhang et al., 2011a).

Overall, this experiment was primarily intended to address the challenges of transplanted cells survival and integration in the host brain. Our data suggest that when the IPSC derived NSCs that were originally from a UCB CD34+ were suspended in hydrogel and transplanted immediately into ischemic SMC of P14 rats, they will be capable of producing cerebral organoids and respond to the intrinsic cues of the rat developing brain at least for 4 weeks as long as the ECM is not degraded.

## 5.4 Conclusion

This chapter has demonstrated that:

1. NSCs cultured in 3D hydrogel *in vitro* showed a higher survival rate and denser pre and post-mitotic marker expression with longer and more complex morphology of neuronal processes than NSCs in the 2D culture.
2. NSCs grafted with hydrogel *in vivo* into the SMC of the PIS model at P14 resulted in cerebral organoid formation, neovascularization, host cell migration toward the graft and infiltration with milder inflammatory reaction than in the PIS model but did not extend axons to towards internal capsule or migrate into host cortex, and 4 weeks post transplantation.
3. NSCs grafted with hydrogel *in vivo* into the SMC of the PIS model at P14 resulted in stroke cavity reduction and neurogenesis by the host cells, but by 6 weeks post transplantation however the ECM degraded.

# Chapter 6 . General Discussion, Limitation and Future Work

## 6.1 Modelling perinatal stroke in the rat: middle cerebral artery occlusion versus Endothelin-1 injection to the sensorimotor cortex

In human neonates, perinatal ischemic stroke (PIS) is a significant cause of hemiplegic cerebral palsy, and the incidence of stroke is higher perinatally compared to any other time of life (Benders et al., 2008). As was reviewed in Chapter One, a suitable animal model is needed to test early intervention therapies.

In this research, we first compared middle cerebral artery occlusion (MCAO), performed via electroligation, with direct intracerebral injection of reversible vasoconstrictor Endothelin-1 (ET-1) into the sensorimotor cortex (SMC). This was done during the developmental stage, at postnatal day 12 (P12), which is comparable to birth in humans, to model human PIS. Either the left middle cerebral artery was exposed by craniotomy (temporal bone) or electro-coagulated, or 400 Picomole (Pmol) of ET-1 was unilaterally injected into three sites in the SMC (Chapter Two).

The results presented in Chapter Three showed that the MCAO model did not primarily affect the SMC, a major site of damage in human neonates. Expression of Hypoxia inducible transcription factor and activation of microglia at 2-5 days following lesioning was restricted to the lateral cortex close to the occlusion site at the barrel field somatosensory cortex (bfSSC). At one month post lesion, cellular immunoreactivity assessments revealed a cortical ischemic lesion present mainly in the bfSSC. Furthermore, no significant behavioural deficits were detected in this model at P45. ET-1 intracerebral injection, on the other hand produced a more appropriate model, including immunoreactivity for hypoxia inducible transcription factor and activated microglia immunoreactivity more dorsally in the limb sensorimotor cortex (lSMC). However, although we found some evidence of functional disabilities in the ET-1 group compared to sham animals at P45, these differences, again, were not statistically significant. It is possible that the induced SMC lesion had recovered by P45 due to high plasticity during development. Alternatively, the behavioural test used to measure the behavioural defects after SMC lesioning in P12 rat neonates might not be sensitive enough for our model (Clowry et al., 2014). However, the low mortality rate observed using ET-1 to produce PIS is an advantage of this method.

Loss of corticospinal tract (CST) neurons in the SMC was investigated by injecting Fluorogold, a retrograde tracer, into the contralateral cervical spinal cord to trace the CST (Chapter Two). The results presented in Chapter Four showed a small loss of corticospinal neurons at the ET-1 induced lesion site, but an increase in labelled corticospinal neurons in the contralateral cortex, compared to sham animals. Evidence has been found that surviving aberrant corticospinal projections from the contralateral hemisphere to the lesion could be related to positive behavioural outcomes in the lesioned animals (Jansen and Low, 1996). Thus, we suggest that in our ET-1 injection PIS model, corticospinal plasticity during development might have overcome the behavioural disability and led to only limited behavioural dysfunction that did not reach statistical significance at one month after insult.

Although there was no measurable behavioural deficit, there was loss of corticospinal neurons in response to the ET-1 lesion so, in Chapter Five, we tested the potential therapeutic effect of intracerebrally injecting human neural stem cells (hNSCs) derived from human induced pluripotent stem cells (hiPSCs) and suspended in semi-synthetic extracellular matrix (ECM) into the ET-1 PIS model perinatal rat brain. The aim was to replace missing corticospinal neurons with new neurons derived from the graft. Prior to the in vivo experiment, we differentiated the hNSCs into 2 and 3 dimensions (2D and 3D) in in vitro culture in order to compare it with the grafted cells in vivo.

## 6.2 hNSCs-ECM organise into cerebral organoids after transplantation into stroke-lesioned perinatal rat brain.

In this experiment, we compared the survival and development hNSCs-ECM in vitro and following grafting into a rodent model of perinatal infarction damaging the SMC. The prediction was that grafted stem cells would develop into cortical neurons and replace neurons killed by the infarction. To test this hypothesis, ET-1 PIS model surgery was performed at P12, following our previous ET-1 protocol. Two days following the lesion surgery, 100,000 hNSCs were transplanted directly into the sensorimotor cortex. Cells were suspended in ECM as a transplantation vehicle. Also, a sham group that was injected only with ECM during the ET-1 surgery protocol, was assigned to be compared with the intervention group and a control group that received only ET-1 surgery followed by craniectomy. Another hNPC cell line was cultured in vitro to be tested for differentiation (chapter two).

A mixture of cell types was tested for *in vitro* by immunocytochemistry (ICC), including PAX6-positive neural progenitor cells and doublecortin-positive neuroblasts in 2D *in vitro* culture after starting the differentiation protocol for hNSCs-ECM described in Chapter Five. In the 3D culture, however, the hNSCs in ECM survived longer than cells in the 2D culture, and were composed of neurons in various states of maturity that expressed doublecortin, beta-tubulin, and MAP2 in addition to the PAX6-positive neural progenitor cells. Cells in 3D culture also extended long neurites, and synaptophysin was observed at the contacts between neurites.

The results in Chapter Five led us to hypothesize that transplanting hNSCs along with ECM possibly results in cortical regeneration via the development and integration of cortical neurons. Surprisingly, transplanted hNSCs formed neural tube-like rosettes with a morphology resembling the cerebral organoids one month after transplantation previously only observed in 3D in vitro neural stem cell culture using special culture conditions not employed in our 3D study. To our knowledge, our transplantation method is the first to be able to generate formations that recapitulate the characteristics of the developing cortex in the human brain in vivo. Immunofluorescent double labelling showed dense layers of radially arranged columns of PAX6-positive cells around a lumen resembling the neural tube, or a ventricle with PAX6-positive cells bordering the lumen, which were also expressing human neural cell adhesion molecule (hNCAM), a marker of exclusively human neural cells. PAX6 is a marker for neural progenitor cells of the ventricular zone of the developing cerebral cortex. Double labelling for DCX/hNCAM revealed an outer layer of post-mitotic neurons that also expressed other markers for neurons, including CTIP2 characteristic of corticofugal neurons. The organoid structures remained largely self-contained, however, with few grafted cells or axons integrating with the surrounding host tissue. Host cells also penetrated the grafts – principally blood vessels, microglia and astrocytes, but also a few neurons. Three months post-grafting, the organoid structures had broken down and grafted cells had largely disappeared.

As discussed in Chapter Five, the most prominent result was the formation of cerebral organoids within the mature cerebral cortex but not *in vitro*. These organoids have previously been generated *in vitro* (Qian et al., 2016, Mason and Price, 2016, Lancaster et al., 2013), suggesting that some factors are produced in the host brain that induce this behaviour.

To conclude, we were able to provide reproducible PIS model by injecting ET- intracerebrally into the SMC of P12 rat neonates. Then, we were able to produce for the first time structures

which are “cerebral organoids like” that was formed after injecting hNSCs suspended in 3D hydrogel into the resulted ischemic infarction in the SMC. Furthermore, the stem cell intervention we applied, enhanced neurogenesis, neovascularization, and integration by invading the cortical infarction in the host brain (Figure 6.1).

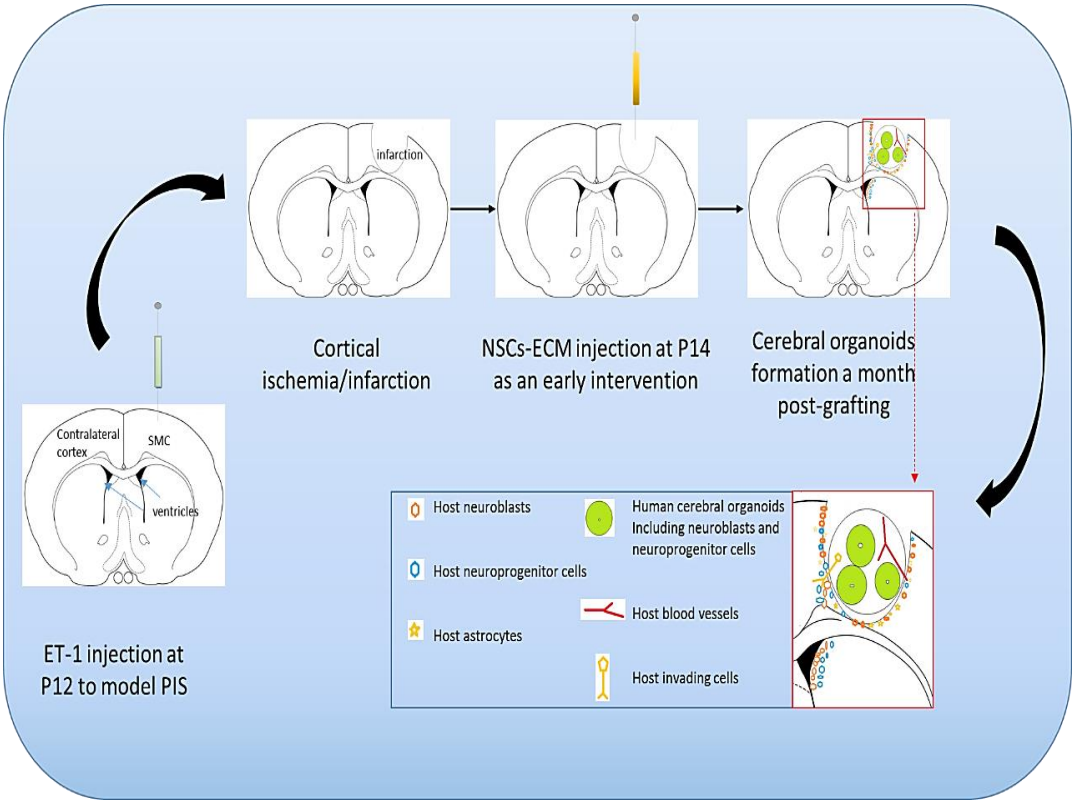


**Figure 6.1 overview of the main results in the research project presented in cartoon drawings of brain coronal sections.**

## 6.3 Moving toward clinical trials

A recent review indicated the promising nature of stem cell therapy, as shown in neonatal experimental studies, and highlighted its application in clinical settings (Wagenaar et al., 2017). In our study, we utilized human neural stem cells derived from induced pluripotent stem cells that were suspended in semi-synthetic extracellular matrix (hNSCs-ECM) and injected intracerebrally into P14 PIS rat model. The source of the induced pluripotent stem cells was umbilical cord blood cells; this has been shown to be a safe and feasible stem cell source for treating human neonates (Sun et al., 2015, Cotten et al., 2014). The umbilical cord blood derived cells have been reported to be safe for clinical use, unlike other NSC sources. For example, NSCs derived from embryonic cells resulted in teratoma formation (Elkabetz et al., 2008, Blum et al., 2009). Also, there are no ethical conflicts with using umbilical cord blood derived cells in the clinic. Moreover, there is a non-invasive collection protocol that could be autologous (Singh and Kashyap, 2016). These advantages have allowed umbilical cord blood derived cells to reach Phase I clinical trials for PIS (ClinicalTrials.gov Identifier NCT01700166) and neonatal encephalopathy (ClinicalTrials.gov Identifier NCT01506258) (Basu, 2014).

ECM has long been used *in vivo* in other fields, such as a filler in dermatology clinics (Zarembinski et al., 2011). Our study showed that grafted ECM causes no adverse reactions in animals that receive only ECM. We believe that ECM helps the grafted cells organise themselves in particular pattern, forming the *in vivo* cerebral organoids. Indeed future optimization to enhance the survival of these organoids *in vivo* and to help them continue differentiate into cortical neurons.

It is unpredictable how NSCs/ECM will integrate to the host cortex or establish connections to the ascending pathways in the long term. Myelination of the new generated neurons post grafting will be another challenge. However, a recent study has shown that applying ontogenetic electrical stimulation on the premotor cortex in awake mice results in adaptive myelination for neurons through promoting the local oligodendrogenesis (Gibson et al., 2014). Thus, preclinical trails combining our method with other therapeutic methods such as the electrical stimulation are needed to enhance the long term differentiation and integration abilities of the NSCs/ECM in vivo before reaching clinic trails.

## 6.4 Limitations and future work

The MCAO model of PIS has some weaknesses compared with the ET-1 model. Firstly, the degree of brain injury is fixed and cannot be increased or decreased in this model. Secondly, MCAO mainly lesions the bfSSC, while it is the SMC region responsible for limb movement is a more clinically relevant target. Thirdly, at P12, the cerebral arteries are small and the brain tissue beneath the occluded MCA can be easily burned by the tip of the electroligation device.

All these limitations are overcome in the ET-1 model. However, the ET-1 model has high variability in infarction volume, even with the use of a precise injection protocol. This variability can be reduced by using laser Doppler flowmetry to verify cerebral ischemia during ET-1 infusion.

In both the MCAO and ET-1 models, the underlying brain tissue can be injured mechanically by the craniotomy. We knew that this could be avoided by performing small intracortical injections (Windle et al., 2006), yet the use of a drill or even the tip of a needle to form holes in the skull could press the underlying brain tissue underneath due to the soft skull bone of rat neonates at P12. Thus, we performed the craniectomy with care rather than making skull holes for the intracortical injections.

The advantages of using ET-1 intracerebral injection at P12 to model PIS include the simple procedure, the focal localization of lSMC lesion and 100% long-term survival rate, enabling neuropathological examination in the chronic stage. However, we were not able to determine whether the non-significant behavioural deficits reflect a poor choice of behavioural tests or nervous system plasticity. The type of behavioural assessments used after lesioning might be not sensitive enough for our model (Zhang et al., 2002, Clowry et al., 2014), although they have been found to be sensitive for use in adult stroke models (Stroemer et al., 1995, Schallert et al., 2000). Also, the number of animals analysed after injecting the retrograde tracer was very low. This was due to the difficulty of avoiding spread of tracer across the spinal cord midline during injection, which resulted in the exclusion of many animals from the assessment of corticospinal cell count. Thus, more sensitive behavioural tests need to be developed, or electrophysiological assessment must be used for future work.

The generation of neurons in the last cortical layer in the in vitro cerebral organoids has been shown to peak at day 60 from the start of differentiation (Qian et al., 2016). Thus, we recommend adding more time points for immunohistochemistry (IHC) with shorter intervals. For example, further investigation about the cell phenotype within the resultant cerebral organoids can also be done by using additional cellular markers, such as a marker for cortical neurons that are differentiating from the neural progenitor (TBR1) (Zhu et al., 2016), as well as the upper-layer cortical neuron marker SATB2, which localises close to the pial surface of the generated *in vitro* cerebral organoids (Qian et al., 2016).

Furthermore, more advanced assessment methods, such as Magnetic resonance imaging (MRI), are recommended in order to study the pathology occurring after ET-1 injection and the formation of cerebral organoids after transplantation of the NSCs-ECM complex. In our study, utilizing such equipment was beyond the research budget.

It was disappointing that the resulting *in vivo* organoids disappeared by the time the rats reached 3 months of age. Undoubtedly, the hydrogel used should be modified to further support the long-term survival of the grafted cells. In addition, it may be necessary in future experiments to maintain the survival of the grafts by providing immunosuppression. Although there are no FDA-approved hydrogels for stem cell therapy, the hydrogel we used, HyStem-C, is one of the matrices that can be used for clinical applications (Zarembinski et al., 2011).

ECM has long been used in vivo in other fields, such as a filler in dermatology clinics (Zarembinski et al., 2011). Our study showed that grafted ECM causes no adverse reactions in animals that receive only ECM. We believe that ECM helps the grafted cells organise themselves in particular pattern, forming the in vivo cerebral organoids. In our future studies, we need to optimize a protocol for ECM to enhance the survival of these organoids in vivo and to help them continue differentiate into cortical neurons.

Also in our future studies, we will combine additional factors that can enhance neuronal integration with the host neighbor tissue. It is unpredictable how NSCs/ECM will integrate to the host cortex or establish connections to the ascending pathways in the long term. Myelination of the new generated neurons post grafting will be another challenge. However, a recent study has shown that applying ontogenetic electrical stimulation on the premotor cortex in awake mice results in adaptive myelination for neurons through promoting local

oligodendrogenesis (Gibson et al., 2014). Thus, preclinical trails combining our method with other therapeutic methods such as electrical stimulation are needed to enhance the long term differentiation and integration abilities of the NSCs/ECM in vivo before reaching clinic trails.

Finally, the success of generating a 3D construction of cerebral organoids that somewhat mimics the developing brain in the neonatal ischemic brain model in vivo is significant. It is the first step toward a new prospective stem cell therapy that is initiated by forming two main cortical layers of the developing brain. Further improvements to our protocol that will ensure long-term cellular survival, followed by integration of the neurons into the host circuitry including extension of axons to sub-cortical targets; outcomes that are needed in order to move toward clinical application.

# References


Adkins, D. L., Voorhies, A. C. & Jones, T. A. 2004. Behavioral and neuroplastic effects of focal endothelin-1 induced sensorimotor cortex lesions. *Neuroscience,* 128**,** 473-486.

Alaverdashvili, M. & Whishaw, I. Q. 2008. Motor cortex stroke impairs individual digit movement in skilled reaching by the rat. *European Journal of Neuroscience,* 28**,** 311-322.

Ali, H., Forraz, N., Mcguckin, C. P., Jurga, M., Lindsay, S., Ip, B. K., Trevelyan, A., Basford, C., Habibollah, S., Ahmad, S., Clowry, G. J. & Bayatti, N. 2012. In vitro modelling of cortical neurogenesis by sequential induction of human umbilical cord blood stem cells. *Stem Cell Rev,* 8**,** 210-23.

Ali, H., Jurga, M., Kurgonaite, K., Forraz, N. & Mcguckin, C. 2009. Defined serum-free culturing conditions for neural tissue engineering of human cord blood stem cells. *Acta neurobiologiae experimentalis,* 69**,** 12-23.

Allred, R. P., Adkins, D. L., Woodlee, M. T., Husbands, L. C., Maldonado, M. A., Kane, J. R., Schallert, T. & Jones, T. A. 2008. The vermicelli handling test: a simple quantitative measure of dexterous forepaw function in rats. *Journal of neuroscience methods,* 170**,** 229-244.

Alvarez-Buylla, A. & Temple, S. 1998. Stem cells in the developing and adult nervous system. *Journal of neurobiology,* 36**,** 105-110.

Androutsellis-Theotokis, A., Leker, R. R., Soldner, F., Hoeppner, D. J., Ravin, R., Poser, S. W., Rueger, M. A., Bae, S. K., Kittappa, R. & Mckay, R. D. 2006. Notch signalling regulates stem cell numbers in vitro and in vivo. *Nature,* 442**,** 823-6.

Annunziato, L., Boscia, F. & Pignataro, G. 2013. Ionic transporter activity in astrocytes, microglia, and oligodendrocytes during brain ischemia. *J Cereb Blood Flow Metab,* 33**,** 969-82.

Ansari, S., Azari, H., Mcconnell, D. J., Afzal, A. & Mocco, J. 2011. Intraluminal middle cerebral artery occlusion (MCAO) model for ischemic stroke with laser doppler flowmetry guidance in mice. *J Vis Exp*.

Araki, T., Kato, H., Liu, X. H., Kogure, K., Kato, K. & Itoyama, Y. 1994. An immunohistochemical study of parvalbumin containing interneurons in the gerbil hippocampus after cerebral ischemia. *Metabolic brain disease,* 9**,** 225-234.

Arien-Zakay, H., Lecht, S., Nagler, A. & Lazarovici, P. 2011. Neuroprotection by human umbilical cord blood-derived progenitors in ischemic brain injuries. *Arch Ital Biol,* 149**,** 233-45.

Armand, J. 1982. The origin, course and terminations of corticospinal fibers in various mammals. *Prog Brain Res,* 57**,** 329-60.

Arvidsson, A., Collin, T., Kirik, D., Kokaia, Z. & Lindvall, O. 2002. Neuronal replacement from endogenous precursors in the adult brain after stroke. *Nat Med,* 8**,** 963-70.

Ashwal, S., Cole, D. J., Osborne, S., Osborne, T. N. & Pearce, W. J. 1995. A new model of neonatal stroke: reversible middle cerebral artery occlusion in the rat pup. *Pediatr Neurol,* 12**,** 191-6.

Ashwal, S., Tone, B., Tian, H. R., Chong, S. & Obenaus, A. 2007. Comparison of two neonatal ischemic injury models using magnetic resonance imaging. *Pediatr Res,* 61**,** 9-14.

Aurand, E. R., Lampe, K. J. & Bjugstad, K. B. 2012. Defining and designing polymers and hydrogels for neural tissue engineering. *Neuroscience research,* 72**,** 199-213.

Baeten, K. M. & Akassoglou, K. 2011. Extracellular matrix and matrix receptors in blood–brain barrier formation and stroke. *Developmental neurobiology,* 71**,** 1018-1039.

Bakshi, A., Keck, C. A., Koshkin, V. S., Lebold, D. G., Siman, R., Snyder, E. Y. & Mcintosh, T. K. 2005. Caspase-mediated cell death predominates following engraftment of neural progenitor cells into traumatically injured rat brain. *Brain research,* 1065**,** 8-19.

Ban, H., Nishishita, N., Fusaki, N., Tabata, T., Saeki, K., Shikamura, M., Takada, N., Inoue, M., Hasegawa, M. & Kawamata, S. 2011. Efficient generation of transgene-free human induced pluripotent stem cells (iPSCs) by temperature-sensitive Sendai virus vectors. *Proceedings of the National Academy of Sciences,* 108**,** 14234-14239.

Bareyre, F. M., Kerschensteiner, M., Misgeld, T. & Sanes, J. R. 2005. Transgenic labeling of the corticospinal tract for monitoring axonal responses to spinal cord injury. *Nat Med,* 11**,** 1355-60.

Barth, T. M. & Stanfield, B. B. 1990. The recovery of forelimb-placing behavior in rats with neonatal unilateral cortical damage involves the remaining hemisphere. *J Neurosci,* 10**,** 3449-59.

Basu, A. P. 2014. Early intervention after perinatal stroke: opportunities and challenges. *Developmental Medicine & Child Neurology,* 56**,** 516-521.

Bayatti, N., Moss, J. A., Sun, L., Ambrose, P., Ward, J. F., Lindsay, S. & Clowry, G. J. 2008. A molecular neuroanatomical study of the developing human neocortex from 8 to 17 postconceptional weeks revealing the early differentiation of the subplate and subventricular zone. *Cereb Cortex,* 18**,** 1536-48.

Bederson, J. B., Pitts, L. H., Tsuji, M., Nishimura, M. C., Davis, R. L. & Bartkowski, H. 1986. Rat middle cerebral artery occlusion: evaluation of the model and development of a neurologic examination. *Stroke,* 17**,** 472-476.

Belayev, L., Endres, M. & Prinz, V. 2010. Focal Cerebral Ischemia in the Mouse and Rat Using the Intraluminal Suture–Filament Model. 47**,** 29-40.

Benders, M. J., Groenendaal, F., Uiterwaal, C. S. & De Vries, L. S. 2008. Perinatal arterial stroke in the preterm infant. *Semin Perinatol,* 32**,** 344-9.

Benton, R. L., Maddie, M. A., Minnillo, D. R., Hagg, T. & Whittemore, S. R. 2008. Griffonia simplicifolia isolectin B4 identifies a specific subpopulation of angiogenic blood vessels following contusive spinal cord injury in the adult mouse. *Journal of Comparative Neurology,* 507**,** 1031-1052.

Bible, E., Dell'acqua, F., Solanky, B., Balducci, A., Crapo, P. M., Badylak, S. F., Ahrens, E. T. & Modo, M. 2012. Non-invasive imaging of transplanted human neural stem cells and ECM scaffold remodeling in the stroke-damaged rat brain by (19)F- and diffusion-MRI. *Biomaterials,* 33**,** 2858-71.

Bliss, T., Guzman, R., Daadi, M. & Steinberg, G. K. 2007. Cell transplantation therapy for stroke. *Stroke,* 38**,** 817-826.

Blum, B., Bar-Nur, O., Golan-Lev, T. & Benvenisty, N. 2009. The anti-apoptotic gene survivin contributes to teratoma formation by human embryonic stem cells. *Nature biotechnology,* 27**,** 281-287.

Bonnin, P., Leger, P. L., Deroide, N., Fau, S., Baud, O., Pocard, M., Charriaut-Marlangue, C. & Renolleau, S. 2011. Impact of intracranial blood-flow redistribution on stroke size during ischemia-reperfusion in 7-day-old rats. *J Neurosci Methods,* 198**,** 103-9.

Bouet, V., Freret, T., Ankri, S., Bezault, M., Renolleau, S., Boulouard, M., Jacotot, E., Chauvier, D. & Schumann-Bard, P. 2010. Predicting sensorimotor and memory deficits after neonatal ischemic stroke with reperfusion in the rat. *Behav Brain Res,* 212**,** 56-63.

Brannvall, K., Bergman, K., Wallenquist, U., Svahn, S., Bowden, T., Hilborn, J. & Forsberg-Nilsson, K. 2007. Enhanced neuronal differentiation in a three-dimensional collagen-hyaluronan matrix. *J Neurosci Res,* 85**,** 2138-46.

Brima, T., Mikulecka, A. & Otahal, J. 2013. Impacts of perinatal induced photothrombotic stroke on sensorimotor performance in adult rats. *Physiol Res,* 62**,** 85-94.

Britz, O., Mattar, P., Nguyen, L., Langevin, L. M., Zimmer, C., Alam, S., Guillemot, F. & Schuurmans, C. 2006. A role for proneural genes in the maturation of cortical progenitor cells. *Cereb Cortex,* 16 Suppl 1**,** i138-51.

Burdick, J. A. & Prestwich, G. D. 2011. Hyaluronic acid hydrogels for biomedical applications. *Adv Mater,* 23**,** H41-56.

Burdjalov, V. F., Baumgart, S. & Spitzer, A. R. 2003. Cerebral Function Monitoring: A New Scoring System for the Evaluation of Brain Maturation in Neonates. *Pediatrics,* 112**,** 855-861.

Burtrum, D. & Silverstein, F. S. 1994. Hypoxic-ischemic brain injury stimulates glial fibrillary acidic protein mRNA and protein expression in neonatal rats. *Experimental neurology,* 126**,** 112-118.

Bużańska, L., Machaj, E. K., Zabłocka, B., Pojda, Z. & Domańska-Janik, K. 2002. Human cord blood-derived cells attain neuronal and glial features in vitro. *Journal of cell science,* 115**,** 2131-2138.

Camp, J. G., Badsha, F., Florio, M., Kanton, S., Gerber, T., Wilsch-Brauninger, M., Lewitus, E., Sykes, A., Hevers, W., Lancaster, M., Knoblich, J. A., Lachmann, R., Paabo, S., Huttner, W. B. & Treutlein, B. 2015. Human cerebral organoids recapitulate gene expression programs of fetal neocortex development. *Proc Natl Acad Sci U S A,* 112**,** 15672-7.

Carlson, A. L., Bennett, N. K., Francis, N. L., Halikere, A., Clarke, S., Moore, J. C., Hart, R. P., Paradiso, K., Wernig, M., Kohn, J. & Pang, Z. P. 2016. Generation and transplantation of reprogrammed human neurons in the brain using 3D microtopographic scaffolds. 7**,** 10862.

Carmichael, S. T. 2006. Cellular and molecular mechanisms of neural repair after stroke: making waves. *Annals of neurology,* 59**,** 735-742.

Castillo-Melendez, M., Yawno, T., Jenkin, G. & Miller, S. L. 2013. Stem cell therapy to protect and repair the developing brain: a review of mechanisms of action of cord blood and amnion epithelial derived cells. *Front Neurosci,* 7**,** 194.

Chen, A., Siow, B., Blamire, A. M., Lako, M. & Clowry, G. J. 2010.

. *Stem Cell Res,* 5**,** 255-66.

Chen, H., Burris, M., Fajilan, A., Spagnoli, F., Zhang, J. H. & Tang, J. 2011. Prolonged exposure to isoflurane ameliorates infarction severity in the rat pup model of neonatal hypoxia-ischemia. *Translational stroke research,* 2**,** 382-390.

Chen, J., Magavi, S. S. & Macklis, J. D. 2004. Neurogenesis of corticospinal motor neurons extending spinal projections in adult mice. *Proc Natl Acad Sci U S A,* 101**,** 16357-62.

Choi, J. T., Vining, E. P., Mori, S. & Bastian, A. J. 2010. Sensorimotor function and sensorimotor tracts after hemispherectomy. *Neuropsychologia,* 48**,** 1192-9.

Clowry, G. J. 2007. The dependence of spinal cord development on corticospinal input and its significance in understanding and treating spastic cerebral palsy. *Neurosci Biobehav Rev,* 31**,** 1114-24.

Clowry, G. J., Basuodan, R. & Chan, F. 2014. What are the Best Animal Models for Testing Early Intervention in Cerebral Palsy? *Front Neurol,* 5**,** 258.

Clowry, G. J., Davies, B. M., Upile, N. S., Gibson, C. L. & Bradley, P. M. 2004. Spinal cord plasticity in response to unilateral inhibition of the rat motor cortex during development: changes to gene expression, muscle afferents and the ipsilateral corticospinal projection. *Eur J Neurosci,* 20**,** 2555-66.

Clowry, G. J., Fallah, Z. & Arnott, G. 1997. Developmental expression of parvalbumin by rat lower cervical spinal cord neurones and the effect of early lesions to the motor cortex. *Developmental brain research,* 102**,** 197-208.

Coenen, M., Kogler, G., Wernet, P. & Brustle, O. 2005. Transplantation of human umbilical cord blood-derived adherent progenitors into the developing rodent brain. *J Neuropathol Exp Neurol,* 64**,** 681-8.

Comi, A. M., Cho, E., Mulholland, J. D., Hooper, A., Li, Q., Qu, Y., Gary, D. S., Mcdonald, J. W. & Johnston, M. V. 2008. Neural stem cells reduce brain injury after unilateral carotid ligation. *Pediatr Neurol,* 38**,** 86-92.

Comi, A. M., Johnston, M. V. & Wilson, M. A. 2005. Strain variability, injury distribution, and seizure onset in a mouse model of stroke in the immature brain. *Dev Neurosci,* 27**,** 127-33.

Cotten, C. M., Murtha, A. P., Goldberg, R. N., Grotegut, C. A., Smith, P. B., Goldstein, R. F., Fisher, K. A., Gustafson, K. E., Waters-Pick, B., Swamy, G. K., Rattray, B., Tan, S. & Kurtzberg, J. 2014. Feasibility of autologous cord blood cells for infants with hypoxic-ischemic encephalopathy. *J Pediatr,* 164**,** 973-979.e1.

Coyle, P. 1982. Middle cerebral artery occlusion in the young rat. *Stroke,* 13**,** 855-859.

Daadi, M. M., Lee, S. H., Arac, A., Grueter, B. A., Bhatnagar, R., Maag, A. L., Schaar, B., Malenka, R. C., Palmer, T. D. & Steinberg, G. K. 2009. Functional engraftment of the medial ganglionic eminence cells in experimental stroke model. *Cell Transplant,* 18**,** 815-26.

Dallison, A. & Kolb, B. 2003. Recovery from infant medial frontal cortical lesions in rats is reversed by cortical lesions in adulthood. *Behavioural brain research,* 146**,** 57-63.

Day, S. M., Strauss, D. J., Vachon, P. J., Rosenbloom, L., Shavelle, R. M. & Wu, Y. W. 2007. Growth patterns in a population of children and adolescents with cerebral palsy. *Developmental Medicine & Child Neurology,* 49**,** 167-171.

Dehay, C. & Kennedy, H. 2007. Cell-cycle control and cortical development. *Nat Rev Neurosci,* 8**,** 438-50.

Denes, A., Vidyasagar, R., Feng, J., Narvainen, J., Mccoll, B. W., Kauppinen, R. A. & Allan, S. M. 2007. Proliferating resident microglia after focal cerebral ischaemia in mice. *J Cereb Blood Flow Metab,* 27**,** 1941-53.

Denham, M., Parish, C. L., Leaw, B., Wright, J., Reid, C. A., Petrou, S., Dottori, M. & Thompson, L. H. 2012. Neurons derived from human embryonic stem cells extend long-distance axonal projections through growth along host white matter tracts after intra-cerebral transplantation. *Front Cell Neurosci,* 6**,** 11.

Derugin, N., Ferriero, D. M. & Vexler, Z. S. 1998. Neonatal reversible focal cerebral ischemia: a new model. *Neurosci Res,* 32**,** 349-53.

Derugin, N., Wendland, M., Muramatsu, K., Roberts, T. P. L., Gregory, G., Ferriero, D. M., Vexler, Z. S. & Dietrich, W. D. 2000. Evolution of Brain Injury After Transient Middle Cerebral Artery Occlusion in Neonatal Rats Editorial Comment. *Stroke,* 31**,** 1752-1761.

Detante, O., Moisan, A., Dimastromatteo, J., Richard, M.-J., Riou, L., Grillon, E., Barbier, E., Desruet, M.-D., De Fraipont, F. & Segebarth, C. 2009. Intravenous administration of 99mTc-HMPAO-labeled human mesenchymal stem cells after stroke: in vivo imaging and biodistribution. *Cell transplantation,* 18**,** 1369-1379.

Ding, X., Li, Y., Liu, Z., Zhang, J., Cui, Y., Chen, X. & Chopp, M. 2013. The sonic hedgehog pathway mediates brain plasticity and subsequent functional recovery after bone marrow stromal cell treatment of stroke in mice. *J Cereb Blood Flow Metab,* 33**,** 1015-24.

Dirnagl, U. 2010. Complexities, Confounders, and Challenges in Experimental Stroke Research: A Checklist for Researchers and Reviewers. 47**,** 263-277.

Dreifuss, J. J., Kelly, J. S. & Krnjevic, K. 1969. Cortical inhibition and gamma-aminobutyric acid. *Exp Brain Res,* 9**,** 137-54.

Elkabetz, Y., Panagiotakos, G., Al Shamy, G., Socci, N. D., Tabar, V. & Studer, L. 2008. Human ES cell-derived neural rosettes reveal a functionally distinct early neural stem cell stage. *Genes & development,* 22**,** 152-165.

Englund, U., Fricker-Gates, R. A., Lundberg, C., Bjorklund, A. & Wictorin, K. 2002. Transplantation of human neural progenitor cells into the neonatal rat brain: extensive migration and differentiation with long-distance axonal projections. *Exp Neurol,* 173**,** 1-21.

Ethell, I. M. & Ethell, D. W. 2007. Matrix metalloproteinases in brain development and remodeling: synaptic functions and targets. *Journal of neuroscience research,* 85**,** 2813-2823.

Eyre, J. A. 2007. Corticospinal tract development and its plasticity after perinatal injury. *Neurosci Biobehav Rev,* 31**,** 1136-49.

Eyre, J. A., Smith, M., Dabydeen, L., Clowry, G. J., Petacchi, E., Battini, R., Guzzetta, A. & Cioni, G. 2007. Is hemiplegic cerebral palsy equivalent to amblyopia of the corticospinal system? *Ann Neurol,* 62**,** 493-503.

Eyre, J. A., Taylor, J. P., Villagra, F., Smith, M. & Miller, S. 2001. Evidence of activity-dependent withdrawal of corticospinal projections during human development. *Neurology,* 57**,** 1543-54.

Fagel, D. M., Ganat, Y., Cheng, E., Silbereis, J., Ohkubo, Y., Ment, L. R. & Vaccarino, F. M. 2009. Fgfr1 is required for cortical regeneration and repair after perinatal hypoxia. *Journal of Neuroscience,* 29**,** 1202-1211.

Faustino, J. V., Wang, X., Johnson, C. E., Klibanov, A., Derugin, N., Wendland, M. F. & Vexler, Z. S. 2011. Microglial cells contribute to endogenous brain defenses after acute neonatal focal stroke. *Journal of Neuroscience,* 31**,** 12992-13001.

Fernandez-Lopez, D., Natarajan, N., Ashwal, S. & Vexler, Z. S. 2014. Mechanisms of perinatal arterial ischemic stroke. *J Cereb Blood Flow Metab,* 34**,** 921-32.

Fraser, J. R. E., Laurent, T. C. & Laurent, U. B. G. 1997. Hyaluronan: its nature, distribution, functions and turnover. *Journal of internal medicine,* 242**,** 27-33.

Frost, S. B., Barbay, S., Mumert, M. L., Stowe, A. M. & Nudo, R. J. 2006. An animal model of capsular infarct: endothelin-1 injections in the rat. *Behav Brain Res,* 169**,** 206-11.

Fuxe, K., Kurosawa, N., Cintra, A., Hallstrom, A., Goiny, M., Rosen, L., Agnati, L. F. & Ungerstedt, U. 1992. Involvement of local ischemia in endothelin-1 induced lesions of the neostriatum of the anaesthetized rat. *Exp Brain Res,* 88**,** 131-9.

Genade, T. & Lang, D. M. 2011. Antibody markers for studying neurodegeneration in the Nothobranchius central nervous system. *J Cytol Histol,* 2**,** 120.

Gennaro, M., Mattiello, A., Mazziotti, R., Antonelli, C., Gherardini, L., Guzzetta, A., Berardi, N., Cioni, G. & Pizzorusso, T. 2017. Focal Stroke in the Developing Rat Motor Cortex Induces Age- and Experience-Dependent Maladaptive Plasticity of Corticospinal System. *Front Neural Circuits,* 11**,** 47.

Gibson, C. L., Arnott, G. A. & Clowry, G. J. 2000a. Plasticity in the rat spinal cord seen in response to lesions to the motor cortex during development but not to lesions in maturity. *Experimental neurology,* 166**,** 422-434.

Gibson, C. L., Arnott, G. A. & Clowry, G. J. 2000b. Plasticity in the rat spinal cord seen in response to lesions to the motor cortex during development but not to lesions in maturity. *Exp Neurol,* 166**,** 422-34.

Gibson, E. M., Purger, D., Mount, C. W., Goldstein, A. K., Lin, G. L., Wood, L. S., Inema, I., Miller, S. E., Bieri, G., Zuchero, J. B., Barres, B. A., Woo, P. J., Vogel, H. & Monje, M. 2014. Neuronal activity promotes oligodendrogenesis and adaptive myelination in the mammalian brain. *Science,* 344**,** 1252304.

Gilmour, G., Iversen, S. D., O'neill, M. F. & Bannerman, D. M. 2004. The effects of intracortical endothelin-1 injections on skilled forelimb use: implications for modelling recovery of function after stroke. *Behav Brain Res,* 150**,** 171-83.

Gjorevski, N., Ranga, A. & Lutolf, M. P. 2014. Bioengineering approaches to guide stem cell-based organogenesis. *Development,* 141**,** 1794-1804.

Glezer, I., Simard, A. R. & Rivest, S. 2007. Neuroprotective role of the innate immune system by microglia. *Neuroscience,* 147**,** 867-83.

Glover, J. C., Boulland, J. L., Halasi, G. & Kasumacic, N. 2009. Chimeric animal models in human stem cell biology. *Ilar j,* 51**,** 62-73.

Gold, E. M., Su, D., López-Velázquez, L., Haus, D. L., Perez, H., Lacuesta, G. A., Anderson, A. J. & Cummings, B. J. 2013. Functional assessment of long-term deficits in rodent models of traumatic brain injury. *Regenerative medicine,* 8**,** 483-516.

Golomb, M. R., Garg, B. P., Saha, C., Azzouz, F. & Williams, L. S. 2008. Cerebral palsy after perinatal arterial ischemic stroke. *J Child Neurol,* 23**,** 279-86.

Gonzales-Portillo, G. S., Sanberg, P. R., Franzblau, M., Gonzales-Portillo, C., Diamandis, T., Staples, M., Sanberg, C. D. & Borlongan, C. V. 2014. Mannitol-Enhanced Delivery of Stem Cells and Their Growth Factors Across the Blood‐Brain Barrier. *Cell transplantation,* 23**,** 531-539.

Govaert, P., Matthys, E., Zecic, A., Roelens, F., Oostra, A. & Vanzieleghem, B. 2000. Perinatal cortical infarction within middle cerebral artery trunks. *Arch Dis Child Fetal Neonatal Ed,* 82**,** F59-63.

Grow, J. L., Liu, Y. Q. & Barks, J. D. E. 2003. Can lateralizing sensorimotor deficits be identified after neonatal cerebral hypoxia-ischemia in rats? *Developmental neuroscience,* 25**,** 394-402.

Gruen, L. & Grabel, L. 2006. Concise review: scientific and ethical roadblocks to human embryonic stem cell therapy. *Stem Cells,* 24**,** 2162-9.

Gu, Z. & Kalambogias, J. 2017. Control of species-dependent cortico-motoneuronal connections underlying manual dexterity. 357**,** 400-404.

Guzman, R., Uchida, N., Bliss, T. M., He, D., Christopherson, K. K., Stellwagen, D., Capela, A., Greve, J., Malenka, R. C. & Moseley, M. E. 2007. Long-term monitoring of transplanted human neural stem cells in developmental and pathological contexts with MRI. *Proceedings of the National Academy of Sciences,* 104**,** 10211-10216.

Hagberg, H., Bona, E., Gilland, E. & Puka-Sundvall, M. 1997. Hypoxia-ischaemia model in the 7-day-old rat: possibilities and shortcomings. *Acta Paediatr Suppl,* 422**,** 85-8.

Hagberg, H., Peebles, D. & Mallard, C. 2002. Models of white matter injury: comparison of infectious, hypoxic-ischemic, and excitotoxic insults. *Ment Retard Dev Disabil Res Rev,* 8**,** 30-8.

Hahn, S. K., Park, J. K., Tomimatsu, T. & Shimoboji, T. 2007. Synthesis and degradation test of hyaluronic acid hydrogels. *Int J Biol Macromol,* 40**,** 374-80.

Hess, P. G. 2009. Risk of tumorigenesis in first-in-human trials of embryonic stem cell neural derivatives: Ethics in the face of long-term uncertainty. *Account Res,* 16**,** 175-98.

Hicks, S. P. & D'amato, C. J. 1970. Motor-sensory and visual behavior after hemispherectomy in newborn and mature rats. *Exp Neurol,* 29**,** 416-38.

Hicks, S. P. & D'amato, C. J. 1977. Locating corticospinal neurons by retrograde axonal transport of horseradish peroxidase. *Exp Neurol,* 56**,** 410-20.

Horie, N., Hiu, T. & Nagata, I. 2015. Stem cell transplantation enhances endogenous brain repair after experimental stroke. *Neurol Med Chir (Tokyo),* 55**,** 107-12.

Horie, N., Maag, A. L., Hamilton, S. A., Shichinohe, H., Bliss, T. M. & Steinberg, G. K. 2008. Mouse model of focal cerebral ischemia using endothelin-1. *J Neurosci Methods,* 173**,** 286-90.

Horie, N., Pereira, M. P., Niizuma, K., Sun, G., Keren-Gill, H., Encarnacion, A., Shamloo, M., Hamilton, S. A., Jiang, K., Huhn, S., Palmer, T. D., Bliss, T. M. & Steinberg, G. K. 2011. Transplanted stem cell-secreted vascular endothelial growth factor effects poststroke recovery, inflammation, and vascular repair. *Stem Cells,* 29**,** 274-85.

Hou, S., Xu, Q., Tian, W., Cui, F., Cai, Q., Ma, J. & Lee, I.-S. 2005. The repair of brain lesion by implantation of hyaluronic acid hydrogels modified with laminin. *Journal of neuroscience methods,* 148**,** 60-70.

Hsu, C. Y. 1993. Criteria for valid preclinical trials using animal stroke models. *Stroke,* 24**,** 633-636.

Hsu, J. E. & Jones, T. A. 2005. Time-sensitive enhancement of motor learning with the less-affected forelimb after unilateral sensorimotor cortex lesions in rats. *Eur J Neurosci,* 22**,** 2069-80.

Hu, B. R., Liu, C. L., Ouyang, Y., Blomgren, K. & Siesjo, B. K. 2000. Involvement of caspase-3 in cell death after hypoxia-ischemia declines during brain maturation. *J Cereb Blood Flow Metab,* 20**,** 1294-300.

Hughes, C. S., Postovit, L. M. & Lajoie, G. A. 2010. Matrigel: a complex protein mixture required for optimal growth of cell culture. *Proteomics,* 10**,** 1886-90.

Husson, B., Hertz-Pannier, L., Renaud, C., Allard, D., Presles, E., Landrieu, P. & Chabrier, S. 2010. Motor outcomes after neonatal arterial ischemic stroke related to early MRI data in a prospective study. *Pediatrics,* 126**,** 912-8.

Ip, B. K., Bayatti, N., Howard, N. J., Lindsay, S. & Clowry, G. J. 2011. The corticofugal neuron-associated genes ROBO1, SRGAP1, and CTIP2 exhibit an anterior to posterior gradient of expression in early fetal human neocortex development. *Cereb Cortex,* 21**,** 1395-407.

Ito, D., Imai, Y., Ohsawa, K., Nakajima, K., Fukuuchi, Y. & Kohsaka, S. 1998. Microglia-specific localisation of a novel calcium binding protein, Iba1. *Brain Res Mol Brain Res,* 57**,** 1-9.

Jablonska, A., Kozlowska, H., Markiewicz, I., Domanska-Janik, K. & Lukomska, B. 2010. Transplantation of neural stem cells derived from human cord blood to the brain of adult and neonatal rats. *Acta Neurobiol Exp (Wars),* 70**,** 337-50.

Jacobs, S. E., Berg, M., Hunt, R., Tarnow-Mordi, W. O., Inder, T. E. & Davis, P. G. 2013. Cooling for newborns with hypoxic ischaemic encephalopathy. *Cochrane Database Syst Rev***,** Cd003311.

Jansen, E. M. & Low, W. C. 1996. Quantitative analysis of contralateral hemisphere hypertrophy and sensorimotor performance in adult rats following unilateral neonatal ischemic-hypoxic brain injury. *Brain Res,* 708**,** 93-9.

Järlestedt, K., Rousset, C. I., Faiz, M., Wilhelmsson, U., Ståhlberg, A., Sourkova, H., Pekna, M., Mallard, C., Hagberg, H. & Pekny, M. 2010. Attenuation of reactive gliosis does not affect infarct volume in neonatal hypoxic-ischemic brain injury in mice. *PLoS One,* 5**,** e10397.

Jendelová, P., Kubinová, Š., Sandvig, I., Erceg, S., Sandvig, A. & Syková, E. 2016. Current developments in cell-and biomaterial-based approaches for stroke repair. *Expert opinion on biological therapy,* 16**,** 43-56.

Jiang, D., Liang, J., Fan, J., Yu, S., Chen, S., Luo, Y., Prestwich, G. D., Mascarenhas, M. M., Garg, H. G., Quinn, D. A., Homer, R. J., Goldstein, D. R., Bucala, R., Lee, P. J., Medzhitov, R. & Noble, P. W. 2005. Regulation of lung injury and repair by Toll-like receptors and hyaluronan. *Nat Med,* 11**,** 1173-9.

Jin, K., Mao, X., Xie, L., Galvan, V., Lai, B., Wang, Y., Gorostiza, O., Wang, X. & Greenberg, D. A. 2010. Transplantation of human neural precursor cells in Matrigel scaffolding improves outcome from focal cerebral ischemia after delayed postischemic treatment in rats. *J Cereb Blood Flow Metab,* 30**,** 534-44.

Jin, K., Minami, M., Lan, J. Q., Mao, X. O., Batteur, S., Simon, R. P. & Greenberg, D. A. 2001. Neurogenesis in dentate subgranular zone and rostral subventricular zone after focal cerebral ischemia in the rat. *Proc Natl Acad Sci U S A,* 98**,** 4710-5.

Joosten, E. A., Schuitman, R. L., Vermelis, M. E. & Dederen, P. J. 1992. Postnatal development of the ipsilateral corticospinal component in rat spinal cord: a light and electron microscopic anterograde HRP study. *J Comp Neurol,* 326**,** 133-46.

Ju, R., Wen, Y., Gou, R., Wang, Y. & Xu, Q. 2014. The experimental therapy on brain ischemia by improvement of local angiogenesis with tissue engineering in the mouse. *Cell Transplant,* 23 Suppl 1**,** S83-95.

Kadam, S. D., Mulholland, J. D., Mcdonald, J. W. & Comi, A. M. 2008. Neurogenesis and neuronal commitment following ischemia in a new mouse model for neonatal stroke. *Brain Res,* 1208**,** 35-45.

Kahvecİ, N., Alkan, T., Korfali, E. & Özlük, K. Middle Cerebral Artery Occlusion of Rats: Pathological and Neurological Evaluation of the Model.

Kai, D., Prabhakaran, M. P., Stahl, B., Eblenkamp, M., Wintermantel, E. & Ramakrishna, S. 2012. Mechanical properties and in vitro behavior of nanofiber–hydrogel composites for tissue engineering applications. *Nanotechnology,* 23**,** 095705.

Kartje-Tillotson, G., Neafsey, E. J. & Castro, A. J. 1985. Electrophysiological analysis of motor cortical plasticity after cortical lesions in newborn rats. *Brain Res,* 332**,** 103-11.

Kartje-Tillotson, G., Neafsey, E. J. & Castro, A. J. 1986. Topography of corticopontine remodelling after cortical lesions in newborn rats. *J Comp Neurol,* 250**,** 206-14.

Kartje-Tillotson, G., O'donoghue, D. L., Dauzvardis, M. F. & Castro, A. J. 1987. Pyramidotomy abolishes the abnormal movements evoked by intracortical microstimulation in adult rats that sustained neonatal cortical lesions. *Brain Res,* 415**,** 172-7.

Kawano, H., Kimura-Kuroda, J., Komuta, Y., Yoshioka, N., Li, H. P., Kawamura, K., Li, Y. & Raisman, G. 2012. Role of the lesion scar in the response to damage and repair of the central nervous system. *Cell and tissue research,* 349**,** 169-180.

Kelsom, C. & Lu, W. 2013. Development and specification of GABAergic cortical interneurons. *Cell Biosci,* 3**,** 19.

Kennard, M. A. 1938. Reorganization of motor function in the cerebral cortex of monkeys deprived of motor and premotor areas in infancy. *Journal of Neurophysiology*.

Kiasatdolatabadi, A., Lotfibakhshaiesh, N., Yazdankhah, M., Ebrahimi-Barough, S., Jafarabadi, M., Ai, A., Sadroddiny, E. & Ai, J. 2017. The Role of Stem Cells in the Treatment of Cerebral Palsy: a Review. *Mol Neurobiol,* 54**,** 4963-4972.

Kim, D., Kim, C.-H., Moon, J.-I., Chung, Y.-G., Chang, M.-Y., Han, B.-S., Ko, S., Yang, E., Cha, K. Y. & Lanza, R. 2009. Generation of human induced pluripotent stem cells by direct delivery of reprogramming proteins. *Cell stem cell,* 4**,** 472.

Kirton, A., Armstrong-Wells, J., Chang, T., Deveber, G., Rivkin, M. J., Hernandez, M., Carpenter, J., Yager, J. Y., Lynch, J. K., Ferriero, D. M. & International Pediatric Stroke Study, I. 2011. Symptomatic neonatal arterial ischemic stroke: the International Pediatric Stroke Study. *Pediatrics,* 128**,** e1402-10.

Kirton, A. & Deveber, G. 2013. Life after perinatal stroke. *Stroke,* 44**,** 3265-71.

Kögler, G., Sensken, S., Airey, J. A., Trapp, T., Müschen, M., Feldhahn, N., Liedtke, S., Sorg, R. V., Fischer, J. & Rosenbaum, C. 2004. A new human somatic stem cell from placental cord blood with intrinsic pluripotent differentiation potential. *Journal of Experimental Medicine,* 200**,** 123-135.

Koizumi, J. 1986. Experimental studies of ischemic brain edema. 1. A new experimental model of cerebral embolism in rats in which recirculation can be introduced in the ischemic area. *Jpn. J. Stroke.,* 8**,** 1-8.

Kokaia, Z. & Lindvall, O. 2003. Neurogenesis after ischaemic brain insults. *Curr Opin Neurobiol,* 13**,** 127-32.

Kolb, B. & Gibb, R. 2007. Brain plasticity and recovery from early cortical injury. *Dev Psychobiol,* 49**,** 107-18.

Kornack, D. R. & Rakic, P. 1998. Changes in cell-cycle kinetics during the development and evolution of primate neocortex. *Proc Natl Acad Sci U S A,* 95**,** 1242-6.

Krick, J., Murphy-Miller, P., Zeger, S. & Weight, E. 1996. Pattern of growth in children with cerebral palsy. *Journal of the American Dietetic Association,* 96**,** 680-685.

Krupinski, J., Kaluza, J., Kumar, P., Wang, M. & Kumar, S. 1993. Prognostic value of blood vessel density in ischaemic stroke. *Lancet,* 342**,** 742.

Kulbatski, I. 2010. Stem/precursor cell-based CNS therapy: the importance of circumventing immune suppression by transplanting autologous cells. *Stem Cell Rev,* 6**,** 405-10.

Kuluz, J. W., Prado, R., He, D., Zhao, W., Dietrich, W. D. & Watson, B. 2007. New pediatric model of ischemic stroke in infant piglets by photothrombosis: acute changes in cerebral blood flow, microvasculature, and early histopathology. *Stroke,* 38**,** 1932-7.

Kuypers, H. 1981. Anatomy of the descending pathways. *Comprehensive Physiology*.

Kwok, J. C. F., Dick, G., Wang, D. & Fawcett, J. W. 2011. Extracellular matrix and perineuronal nets in CNS repair. *Developmental neurobiology,* 71**,** 1073-1089.

Lai, J. C., White, B. K., Buerstatte, C. R., Haddad, G. G., Novotny, E. J., Jr. & Behar, K. L. 2003. Chronic hypoxia in development selectively alters the activities of key enzymes of glucose oxidative metabolism in brain regions. *Neurochem Res,* 28**,** 933-40.

Lam, J., Lowry, W. E., Carmichael, S. T. & Segura, T. 2014. Delivery of iPS-NPCs to the Stroke Cavity within a Hyaluronic Acid Matrix Promotes the Differentiation of Transplanted Cells. *Adv Funct Mater,* 24**,** 7053-7062.

Lancaster, M. A., Renner, M., Martin, C.-A., Wenzel, D., Bicknell, L. S., Hurles, M. E., Homfray, T., Penninger, J. M., Jackson, A. P. & Knoblich, J. A. 2013. Cerebral organoids model human brain development and microcephaly. *Nature,* 501**,** 373-379.

Lanciego, J. L. & Wouterlood, F. G. 2011. A half century of experimental neuroanatomical tracing. *Journal of chemical neuroanatomy,* 42**,** 157-183.

Larpthaveesarp, A. & Gonzalez, F. F. 2017. Transient Middle Cerebral Artery Occlusion Model of Neonatal Stroke in P10 Rats. *J Vis Exp*.

Lee, J., Croen, L. A., Backstrand, K. H., Yoshida, C. K., Henning, L. H., Lindan, C., Ferriero, D. M., Fullerton, H. J., Barkovich, A. J. & Wu, Y. W. 2005a. Maternal and infant characteristics associated with perinatal arterial stroke in the infant. *Jama,* 293**,** 723-9.

Lee, J., Croen, L. A., Lindan, C., Nash, K. B., Yoshida, C. K., Ferriero, D. M., Barkovich, A. J. & Wu, Y. W. 2005b. Predictors of outcome in perinatal arterial stroke: a population-based study. *Ann Neurol,* 58**,** 303-8.

Lemon, R. N. 2008. Descending pathways in motor control. *Annu Rev Neurosci,* 31**,** 195-218.

Lepore, A. C., Neuhuber, B., Connors, T. M., Han, S. S., Liu, Y., Daniels, M. P., Rao, M. S. & Fischer, I. 2006. Long-term fate of neural precursor cells following transplantation into developing and adult CNS. *Neuroscience,* 142**,** 287-304.

Levers, T. E., Edgar, J. M. & Price, D. J. 2001. The fates of cells generated at the end of neurogenesis in developing mouse cortex. *J Neurobiol,* 48**,** 265-77.

Li, F., Omae, T., Fisher, M., Dietrich, W. D. & Kuluz, J. W. 1999. Spontaneous Hyperthermia and its Mechanism in the Intraluminal Suture Middle Cerebral Artery Occlusion Model of Rats Editorial Comment. *Stroke,* 30**,** 2464-2471.

Li, L., Lundkvist, A., Andersson, D., Wilhelmsson, U., Nagai, N., Pardo, A. C., Nodin, C., Ståhlberg, A., Aprico, K. & Larsson, K. 2008. Protective role of reactive astrocytes in brain ischemia. *Journal of Cerebral Blood Flow & Metabolism,* 28**,** 468-481.

Liang, Y., Walczak, P. & Bulte, J. W. 2013. The survival of engrafted neural stem cells within hyaluronic acid hydrogels. *Biomaterials,* 34**,** 5521-9.

Liebeskind, D. S. 2003. Collateral circulation. *Stroke,* 34**,** 2279-84.

Lin, C.-M., Lin, J.-W., Chen, Y.-C., Shen, H.-H., Wei, L., Yeh, Y.-S., Chiang, Y.-H., Shih, R., Chiu, P.-L. & Hung, K.-S. 2009. Hyaluronic acid inhibits the glial scar formation after brain damage with tissue loss in rats. *Surgical neurology,* 72**,** S50-S54.

Lo, B. & Parham, L. 2009. Ethical issues in stem cell research. *Endocrine reviews,* 30**,** 204-213.

Low, C. B., Liou, Y. C. & Tang, B. L. 2008. Neural differentiation and potential use of stem cells from the human umbilical cord for central nervous system transplantation therapy. *J Neurosci Res,* 86**,** 1670-9.

Lui, J. H., Hansen, D. V. & Kriegstein, A. R. 2011. Development and Evolution of the Human Neocortex. *Cell,* 146**,** 18-36.

Luskin, M. B., Pearlman, A. L. & Sanes, J. R. 1988. Cell lineage in the cerebral cortex of the mouse studied in vivo and in vitro with a recombinant retrovirus. *Neuron,* 1**,** 635-47.

Lynch, J. K. 2009. Epidemiology and classification of perinatal stroke. *Semin Fetal Neonatal Med,* 14**,** 245-9.

Macrae, I. M. 2010. Focal Ischemia Models: Middle Cerebral Artery Occlusion Induced by Electrocoagulation, Occluding Devices, and Endothelin-1. 47**,** 41-53.

Manabat, C., Han, B. H., Wendland, M., Derugin, N., Fox, C. K., Choi, J., Holtzman, D. M., Ferriero, D. M. & Vexler, Z. S. 2003. Reperfusion differentially induces caspase-3 activation in ischemic core and penumbra after stroke in immature brain. *Stroke,* 34**,** 207-13.

Mariani, J., Simonini, M. V., Palejev, D., Tomasini, L., Coppola, G., Szekely, A. M., Horvath, T. L. & Vaccarino, F. M. 2012. Modeling human cortical development in vitro using induced pluripotent stem cells. *Proc Natl Acad Sci U S A,* 109**,** 12770-5.

Martin, J. H. 2005. The corticospinal system: from development to motor control. *Neuroscientist,* 11**,** 161-73.

Martin, J. H., Donarummo, L. & Hacking, A. 2000. Impairments in prehension produced by early postnatal sensory motor cortex activity blockade. *Journal of Neurophysiology,* 83**,** 895-906.

Mason, J. O. & Price, D. J. 2016. Building brains in a dish: Prospects for growing cerebral organoids from stem cells. *Neuroscience,* 334**,** 105-118.

Mateffyova, A., Otahal, J., Tsenov, G., Mares, P. & Kubova, H. 2006. Intrahippocampal injection of endothelin-1 in immature rats results in neuronal death, development of epilepsy and behavioral abnormalities later in life. *Eur J Neurosci,* 24**,** 351-60.

Mcconnell, S. K. 1995. Constructing the cerebral cortex: neurogenesis and fate determination. *Neuron,* 15**,** 761-8.

Mcguckin, C. P., Forraz, N., Allouard, Q. & Pettengell, R. 2004. Umbilical cord blood stem cells can expand hematopoietic and neuroglial progenitors in vitro. *Experimental cell research,* 295**,** 350-359.

Merigo, F., Mucignat-Caretta, C. & Zancanaro, C. 2005. Timing of neuronal intermediate filament proteins expression in the mouse vomeronasal organ during pre-and postnatal development. An immunohistochemical study. *Chemical senses,* 30**,** 707-717.

Mine, Y., Tatarishvili, J., Oki, K., Monni, E., Kokaia, Z. & Lindvall, O. 2013. Grafted human neural stem cells enhance several steps of endogenous neurogenesis and improve behavioral recovery after middle cerebral artery occlusion in rats. *Neurobiol Dis,* 52**,** 191-203.

Miyata, T., Kawaguchi, A., Saito, K., Kawano, M., Muto, T. & Ogawa, M. 2004. Asymmetric production of surface-dividing and non-surface-dividing cortical progenitor cells. *Development,* 131**,** 3133-45.

Moshayedi, P., Nih, L. R., Llorente, I. L., Berg, A. R., Cinkornpumin, J., Lowry, W. E., Segura, T. & Carmichael, S. T. 2016. Systematic optimization of an engineered hydrogel allows for selective control of human neural stem cell survival and differentiation after transplantation in the stroke brain. *Biomaterials,* 105**,** 145-55.

Mu, D., Jiang, X., Sheldon, R. A., Fox, C. K., Hamrick, S. E., Vexler, Z. S. & Ferriero, D. M. 2003. Regulation of hypoxia-inducible factor 1alpha and induction of vascular endothelial growth factor in a rat neonatal stroke model. *Neurobiol Dis,* 14**,** 524-34.

Murphy, A. R., Laslett, A., O'brien, C. M. & Cameron, N. R. 2017a. Scaffolds for 3D In Vitro Culture of Neural Lineage Cells. *Acta Biomaterialia*.

Murphy, A. R., Laslett, A., O'brien, C. M. & Cameron, N. R. 2017b. Scaffolds for 3D in vitro culture of neural lineage cells. *Acta Biomater,* 54**,** 1-20.

Nakagomi, T., Taguchi, A., Fujimori, Y., Saino, O., Nakano-Doi, A., Kubo, S., Gotoh, A., Soma, T., Yoshikawa, H., Nishizaki, T., Nakagomi, N., Stern, D. M. & Matsuyama, T. 2009. Isolation and characterization of neural stem/progenitor cells from post-stroke cerebral cortex in mice. *Eur J Neurosci,* 29**,** 1842-52.

Nathan, P. W. 1994. Effects on movement of surgical incisions into the human spinal cord. *Brain,* 117 ( Pt 2)**,** 337-46.

Nehlig, A., Pereira De Vasconcelos, A. & Boyet, S. 1989. Postnatal changes in local cerebral blood flow measured by the quantitative autoradiographic [14C]iodoantipyrine technique in freely moving rats. *J Cereb Blood Flow Metab,* 9**,** 579-88.

Nieuwenhuys, R., Hans, J. & Nicholson, C. 2014. *The central nervous system of vertebrates,* Springer.

Nih, L. R., Moshayedi, P., Llorente, I. L., Berg, A. R., Cinkornpumin, J., Lowry, W. E., Segura, T. & Carmichael, S. T. 2017. Engineered HA hydrogel for stem cell transplantation in the brain: Biocompatibility data using a design of experiment approach. *Data Brief,* 10**,** 202-209.

Noctor, S. C., Martinez-Cerdeno, V., Ivic, L. & Kriegstein, A. R. 2004. Cortical neurons arise in symmetric and asymmetric division zones and migrate through specific phases. *Nat Neurosci,* 7**,** 136-44.

Nodari, L. R., Ferrari, D., Giani, F., Bossi, M., Rodriguez-Menendez, V., Tredici, G., Delia, D., Vescovi, A. L. & De Filippis, L. 2010. Long-term survival of human neural stem cells in the ischemic rat brain upon transient immunosuppression. *PLoS One,* 5**,** e14035.

Northington, F. J., Chavez-Valdez, R. & Martin, L. J. 2011. Neuronal cell death in neonatal hypoxia-ischemia. *Ann Neurol,* 69**,** 743-58.

Nowicka, D., Rogozinska, K., Aleksy, M., Witte, O. W. & Skangiel-Kramska, J. 2008. Spatiotemporal dynamics of astroglial and microglial responses after photothrombotic stroke in the rat brain. *Acta Neurobiol Exp (Wars),* 68**,** 155-68.

Ohab, J. J. & Carmichael, S. T. 2008. Poststroke neurogenesis: emerging principles of migration and localization of immature neurons. *Neuroscientist,* 14**,** 369-80.

Ohab, J. J., Fleming, S., Blesch, A. & Carmichael, S. T. 2006. A neurovascular niche for neurogenesis after stroke. *J Neurosci,* 26**,** 13007-16.

Pakulska, M. M., Ballios, B. G. & Shoichet, M. S. 2012. Injectable hydrogels for central nervous system therapy. *Biomedical materials,* 7**,** 024101.

Park, J. W., Kang, Y. D., Kim, J. S., Lee, J. H. & Kim, H. W. 2014. 3D microenvironment of collagen hydrogel enhances the release of neurotrophic factors from human umbilical cord blood cells and stimulates the neurite outgrowth of human neural precursor cells. *Biochem Biophys Res Commun,* 447**,** 400-6.

Paxinos, G. & Watson, C. 1998. A stereotaxic atlas of the rat brain. *New York: Academic*.

Peattie, R. A., Nayate, A. P., Firpo, M. A., Shelby, J., Fisher, R. J. & Prestwich, G. D. 2004. Stimulation of in vivo angiogenesis by cytokine-loaded hyaluronic acid hydrogel implants. *Biomaterials,* 25**,** 2789-98.

Pilaz, L.-J., Mcmahon, John J., Miller, Emily E., Lennox, Ashley L., Suzuki, A., Salmon, E. & Silver, Debra L. Prolonged Mitosis of Neural Progenitors Alters Cell Fate in the Developing Brain. *Neuron,* 89**,** 83-99.

Prestwich, G. D., Erickson, I. E., Zarembinski, T. I., West, M. & Tew, W. P. 2012. The translational imperative: Making cell therapy simple and effective (). *Acta biomaterialia,* 8**,** 4200-4207.

Qian, X., Nguyen, H. N., Song, M. M., Hadiono, C., Ogden, S. C., Hammack, C., Yao, B., Hamersky, G. R., Jacob, F., Zhong, C., Yoon, K. J., Jeang, W., Lin, L., Li, Y., Thakor, J., Berg, D. A., Zhang, C., Kang, E., Chickering, M., Nauen, D., Ho, C. Y., Wen, Z., Christian, K. M., Shi, P. Y., Maher, B. J., Wu, H., Jin, P., Tang, H., Song, H. & Ming, G. L. 2016. Brain-Region-Specific Organoids Using Mini-bioreactors for Modeling ZIKV Exposure. *Cell,* 165**,** 1238-54.

Raivich, G., Bohatschek, M., Kloss, C. U., Werner, A., Jones, L. L. & Kreutzberg, G. W. 1999. Neuroglial activation repertoire in the injured brain: graded response, molecular mechanisms and cues to physiological function. *Brain Res Brain Res Rev,* 30**,** 77-105.

Raju, T. N., Nelson, K. B., Ferriero, D., Lynch, J. K. & Participants, N.-N. P. S. W. 2007. Ischemic perinatal stroke: summary of a workshop sponsored by the National Institute of Child Health and Human Development and the National Institute of Neurological Disorders and Stroke. *Pediatrics,* 120**,** 609-16.

Rakic, P. 1988. Specification of cerebral cortical areas. *Science,* 241**,** 170-6.
Rauch, U., Hirakawa, S., Oohashi, T., Kappler, J. & Roos, G. 2004. Cartilage link protein interacts with neurocan, which shows hyaluronan binding characteristics different from CD44 and TSG-6. *Matrix biology,* 22**,** 629-639.
Renner, M., Lancaster, M. A., Bian, S. & Choi, H. 2017. Self-organized developmental patterning and differentiation in cerebral organoids.
Renolleau, S., Aggoun-Zouaoui, D., Ben-Ari, Y., Charriaut-Marlangue, C. & Traystman, R. J. 1998. A Model of Transient Unilateral Focal Ischemia With Reperfusion in the P7 Neonatal Rat : Morphological Changes Indicative of Apoptosis Editorial Comment: Morphological Changes Indicative of Apoptosis. *Stroke,* 29**,** 1454-1461.
Rice, J. E., 3rd, Vannucci, R. C. & Brierley, J. B. 1981. The influence of immaturity on hypoxic-ischemic brain damage in the rat. *Ann Neurol,* 9**,** 131-41.
Robinson, M. J., Macrae, I. M., Todd, M., Reid, J. L. & Mcculloch, J. 1990. Reduction of local cerebral blood flow to pathological levels by endothelin-1 applied to the middle cerebral artery in the rat. *Neurosci Lett,* 118**,** 269-72.
Rogers, D. C., Campbell, C. A., Stretton, J. L. & Mackay, K. B. 1997. Correlation between motor impairment and infarct volume after permanent and transient middle cerebral artery occlusion in the rat. *Stroke,* 28**,** 2060-5; discussion 2066.
Romijn, H. J., Hofman, M. A. & Gramsbergen, A. 1991. At what age is the developing cerebral cortex of the rat comparable to that of the full-term newborn human baby? *Early Hum Dev,* 26**,** 61-7.
Rouiller, E. M., Liang, F. Y., Moret, V. & Wiesendanger, M. 1991. Trajectory of redirected corticospinal axons after unilateral lesion of the sensorimotor cortex in neonatal rat; a phaseolus vulgaris-leucoagglutinin (PHA-L) tracing study. *Exp Neurol,* 114**,** 53-65.
Saggu, R. 2013. Characterisation of endothelin-1-induced intrastriatal lesions within the juvenile and adult rat brain using MRI and 31P MRS. *Transl Stroke Res,* 4**,** 351-67.
Sanchez-Ramos, J. R., Song, S., Kamath, S. G., Zigova, T., Willing, A., Cardozo-Pelaez, F., Stedeford, T., Chopp, M. & Sanberg, P. R. 2001. Expression of neural markers in human umbilical cord blood. *Experimental neurology,* 171**,** 109-115.
Sareen, D., Gowing, G., Sahabian, A., Staggenborg, K., Paradis, R., Avalos, P., Latter, J., Ornelas, L., Garcia, L. & Svendsen, C. N. 2014. Human neural progenitor cells generated from induced pluripotent stem cells can survive, migrate, and integrate in the rodent spinal cord. *The Journal of comparative neurology,* 522**,** 2707.
Sarkar, S., Raymick, J. & Schmued, L. C. 2014. The Use of Recently Developed Histochemical Markers for Localizing Neurotoxicant Induced Regional Brain Pathologies. *Toxins,* 6**,** 1453-1470.
Scales, D. A. & Collins, G. H. 1972. Cerebral degeneration with hypertrophy of the contralateral pyramid. *Archives of Neurology,* 26**,** 186-190.
Schaar, K. L., Brenneman, M. M. & Savitz, S. I. 2010. Functional assessments in the rodent stroke model. *Exp Transl Stroke Med,* 2**,** 13.
Schallert, T. 2006. Behavioral tests for preclinical intervention assessment. *NeuroRx,* 3**,** 497-504.
Schallert, T., Fleming, S. M., Leasure, J. L., Tillerson, J. L. & Bland, S. T. 2000. CNS plasticity and assessment of forelimb sensorimotor outcome in unilateral rat models of stroke, cortical ablation, parkinsonism and spinal cord injury. *Neuropharmacology,* 39**,** 777-787.
Schallert, T. & Woodlee, M. T. 2005a. The behavior of the laboratory rat: a handbook with tests.

Schallert, T. & Woodlee, M. T. 2005b. Orienting and placing. *The behavior of the laboratory rat: a handbook with tests***,** 129-140.

Schulzke, S., Weber, P., Luetschg, J. & Fahnenstich, H. 2005. Incidence and diagnosis of unilateral arterial cerebral infarction in newborn infants. *J Perinat Med,* 33**,** 170-5.

Seidlits, S. K., Khaing, Z. Z., Petersen, R. R., Nickels, J. D., Vanscoy, J. E., Shear, J. B. & Schmidt, C. E. 2010. The effects of hyaluronic acid hydrogels with tunable mechanical properties on neural progenitor cell differentiation. *Biomaterials,* 31**,** 3930-40.

Senior, K. 2001. Angiogenesis and functional recovery demonstrated after minor stroke. *Lancet*, 358**,** 817.

Sharkey, J. & Butcher, S. P. 1995. Characterisation of an experimental model of stroke produced by intracerebral microinjection of endothelin-1 adjacent to the rat middle cerebral artery. *J Neurosci Methods,* 60**,** 125-31.

Sharkey, J., Butcher, S. P. & Kelly, J. S. 1994. Endothelin-1 induced middle cerebral artery occlusion: pathological consequences and neuroprotective effects of MK801. *J Auton Nerv Syst,* 49 Suppl**,** S177-85.

Sharp, F. R., Bergeron, M. & Bernaudin, M. 2001. Hypoxia-inducible factor in brain. *Hypoxia.* Springer.

Shen, Q., Goderie, S. K., Jin, L., Karanth, N., Sun, Y., Abramova, N., Vincent, P., Pumiglia, K. & Temple, S. 2004. Endothelial cells stimulate self-renewal and expand neurogenesis of neural stem cells. *Science,* 304**,** 1338-40.

Singh, A. K. & Kashyap, M. P. 2016. An Overview on Human Umbilical Cord Blood Stem Cell-Based Alternative In Vitro Models for Developmental Neurotoxicity Assessment. *Molecular neurobiology,* 53**,** 3216-3226.

Skop, N. B., Calderon, F., Cho, C. H., Gandhi, C. D. & Levison, S. W. 2014. Improvements in biomaterial matrices for neural precursor cell transplantation. *Molecular and cellular therapies,* 2**,** 19.

Smith, I., Silveirinha, V., Stein, J. L., De La Torre-Ubieta, L., Farrimond, J. A., Williamson, E. M. & Whalley, B. J. 2017a. Human neural stem cell-derived cultures in three-dimensional substrates form spontaneously functional neuronal networks. *J Tissue Eng Regen Med,* 11**,** 1022-1033.

Smith, I., Silveirinha, V., Stein, J. L., Torre‐Ubieta, L., Farrimond, J. A., Williamson, E. M. & Whalley, B. J. 2017b. Human neural stem cell‐derived cultures in three‐dimensional substrates form spontaneously functional neuronal networks. *Journal of tissue engineering and regenerative medicine,* 11**,** 1022-1033.

Solbach, S. & Celio, M. R. 1991. Ontogeny of the calcium binding protein parvalbumin in the rat nervous system. *Anatomy and embryology,* 184**,** 103-124.

Soleman, S., Yip, P., Leasure, J. L. & Moon, L. 2010. Sustained sensorimotor impairments after endothelin-1 induced focal cerebral ischemia (stroke) in aged rats. *Exp Neurol,* 222**,** 13-24.

Souvenir, R., Doycheva, D., Zhang, J. H. & Tang, J. 2015. Erythropoietin in stroke therapy: friend or foe. *Curr Med Chem,* 22**,** 1205-13.

Staudt, M., Gerloff, C., Grodd, W., Holthausen, H., Niemann, G. & Krägeloh-Mann, I. 2004. Reorganization in congenital hemiparesis acquired at different gestational ages. *Annals of Neurology,* 56**,** 854-863.

Stevanato, L., Hicks, C. & Sinden, J. D. 2015. Differentiation of a Human Neural Stem Cell Line on Three Dimensional Cultures, Analysis of MicroRNA and Putative Target Genes. *J Vis Exp*.

Stiles, J. & Jernigan, T. L. 2010. The basics of brain development. *Neuropsychol Rev,* 20**,** 327-48.

Stroemer, R. P., Kent, T. A. & Hulsebosch, C. E. 1995. Neocortical neural sprouting, synaptogenesis, and behavioral recovery after neocortical infarction in rats. *Stroke,* 26**,** 2135-2144.

Stüttgen, M. C. & Schwarz, C. 2010. Integration of vibrotactile signals for whisker-related perception in rats is governed by short time constants: comparison of neurometric and psychometric detection performance. *Journal of Neuroscience,* 30**,** 2060-2069.

Sun, J. M., Grant, G. A., Mclaughlin, C., Allison, J., Fitzgerald, A., Waters-Pick, B. & Kurtzberg, J. 2015. Repeated autologous umbilical cord blood infusions are feasible and had no acute safety issues in young babies with congenital hydrocephalus. *Pediatr Res,* 78**,** 712-6.

Taguchi, A., Kasahara, Y., Nakagomi, T., Stern, D. M., Fukunaga, M., Ishikawa, M. & Matsuyama, T. 2010. A Reproducible and Simple Model of Permanent Cerebral Ischemia in CB-17 and SCID Mice. *J Exp Stroke Transl Med,* 3**,** 28-33.

Takahashi, K., Tanabe, K., Ohnuki, M., Narita, M., Ichisaka, T., Tomoda, K. & Yamanaka, S. 2007. Induction of pluripotent stem cells from adult human fibroblasts by defined factors. *cell,* 131**,** 861-872.

Takahashi, M., Vattanajun, A., Umeda, T., Isa, K. & Isa, T. 2009. Large-scale reorganization of corticofugal fibers after neonatal hemidecortication for functional restoration of forelimb movements. *European Journal of Neuroscience,* 30**,** 1878-1887.

Tan, X. & Shi, S. H. 2013. Neocortical neurogenesis and neuronal migration. *Wiley Interdiscip Rev Dev Biol,* 2**,** 443-59.

Thonhoff, J. R., Lou, D. I., Jordan, P. M., Zhao, X. & Wu, P. 2008. Compatibility of human fetal neural stem cells with hydrogel biomaterials in vitro. *Brain Res,* 1187**,** 42-51.

Tornero, D., Wattananit, S., Grønning Madsen, M., Koch, P., Wood, J., Tatarishvili, J., Mine, Y., Ge, R., Monni, E. & Devaraju, K. 2013. Human induced pluripotent stem cell-derived cortical neurons integrate in stroke-injured cortex and improve functional recovery. *Brain,* 136**,** 3561-3577.

Tsenov, G., Vondrakova, K., Otahal, J., Burchfiel, J. & Kubova, H. 2015. Activation of either the ETA or the ETB receptors is involved in the development of electrographic seizures following intrahippocampal infusion of the endothelin-1 in immature rats. *Exp Neurol,* 265**,** 40-7.

Tsuji, M., Ohshima, M., Taguchi, A., Kasahara, Y., Ikeda, T. & Matsuyama, T. 2013. A novel reproducible model of neonatal stroke in mice: comparison with a hypoxia-ischemia model. *Exp Neurol,* 247**,** 218-25.

Tucker, A. M., Aquilina, K., Chakkarapani, E., Hobbs, C. E. & Thoresen, M. 2009. Development of amplitude-integrated electroencephalography and interburst interval in the rat. *Pediatr Res,* 65**,** 62-6.

Uematsu, J., Ono, K., Yamano, T. & Shimada, M. 1996. Development of corticospinal tract fibers and their plasticity. II. Neonatal unilateral cortical damage and subsequent development of the corticospinal tract in mice. *Brain Dev,* 18**,** 173-8.

Umeda, T., Takahashi, M., Isa, K. & Isa, T. 2010. Formation of descending pathways mediating cortical command to forelimb motoneurons in neonatally hemidecorticated rats. *J Neurophysiol,* 104**,** 1707-16.

Van Der Worp, H. B., Sena, E. S., Donnan, G. A., Howells, D. W. & Macleod, M. R. 2007. Hypothermia in animal models of acute ischaemic stroke: a systematic review and meta-analysis. *Brain,* 130**,** 3063-74.

Van Zelst, B. R., Miller, M. D., Russo, R. N., Murchland, S. & Crotty, M. 2006. Activities of daily living in children with hemiplegic cerebral palsy: a cross-sectional evaluation using the Assessment of Motor and Process Skills. *Dev Med Child Neurol,* 48**,** 723-7.

Wagenaar, N., Nijboer, C. H. & Van Bel, F. 2017. Repair of neonatal brain injury: bringing stem cell-based therapy into clinical practice. *Dev Med Child Neurol*.

Wang, J., Yang, W., Xie, H., Song, Y., Li, Y. & Wang, L. 2014. Ischemic stroke and repair: current trends in research and tissue engineering treatments. *Regenerative medicine research,* 2**,** 3.

Wang, Y., Jin, K. & Greenberg, D. A. 2007. Neurogenesis associated with endothelin-induced cortical infarction in the mouse. *Brain Res,* 1167**,** 118-22.

Watson, B. D., Dietrich, W. D., Busto, R., Wachtel, M. S. & Ginsberg, M. D. 1985. Induction of reproducible brain infarction by photochemically initiated thrombosis. *Annals of neurology,* 17**,** 497-504.

Wen, T. C., Rogido, M., Gressens, P. & Sola, A. 2004. A reproducible experimental model of focal cerebral ischemia in the neonatal rat. *Brain Res Brain Res Protoc,* 13**,** 76-83.

Whishaw, I. Q. & Coles, B. L. K. 1996. Varieties of paw and digit movement during spontaneous food handling in rats: postures, bimanual coordination, preferences, and the effect of forelimb cortex lesions. *Behavioural brain research,* 77**,** 135-148.

Whishaw, I. Q. & Kolb, B. 2004. *The behavior of the laboratory rat: a handbook with tests*, Oxford University Press.

Willenberg, R. & Steward, O. 2015. Nonspecific labeling limits the utility of Cre‐Lox bred CST‐YFP mice for studies of corticospinal tract regeneration. *Journal of Comparative Neurology,* 523**,** 2665-2682.

Windle, V., Szymanska, A., Granter-Button, S., White, C., Buist, R., Peeling, J. & Corbett, D. 2006. An analysis of four different methods of producing focal cerebral ischemia with endothelin-1 in the rat. *Experimental neurology,* 201**,** 324-334.

Witte, O. W. 2010. Photochemical and Endothelin Models of Focal Brain Ischemia. 47**,** 71-83.

Woo, M. S., Wang, X., Faustino, J. V., Derugin, N., Wendland, M. F., Zhou, P., Iadecola, C. & Vexler, Z. S. 2012. Genetic deletion of CD36 enhances injury after acute neonatal stroke. *Ann Neurol,* 72**,** 961-70.

Wu, S., Xu, R., Duan, B. & Jiang, P. 2017. Three-Dimensional Hyaluronic Acid Hydrogel-Based Models for In Vitro Human iPSC-Derived NPC Culture and Differentiation. *J Mater Chem B Mater Biol Med,* 5**,** 3870-3878.

Xia, G., Hong, X., Chen, X., Lan, F., Zhang, G. & Liao, L. 2010. Intracerebral transplantation of mesenchymal stem cells derived from human umbilical cord blood alleviates hypoxic ischemic brain injury in rat neonates. *J Perinat Med,* 38**,** 215-21.

Xiong, T., Qu, Y., Mu, D. & Ferriero, D. 2011. Erythropoietin for neonatal brain injury: opportunity and challenge. *Int J Dev Neurosci,* 29**,** 583-91.

Yager, J. Y., Wright, S., Armstrong, E. A., Jahraus, C. M. & Saucier, D. M. 2006. The influence of aging on recovery following ischemic brain damage. *Behav Brain Res,* 173**,** 171-80.

Yang, Z. & Wang, K. K. W. 2015. Glial fibrillary acidic protein: from intermediate filament assembly and gliosis to neurobiomarker. *Trends in neurosciences,* 38**,** 364-374.

Yoshikawa, A., Atobe, Y., Takeda, A., Kamiya, Y., Takiguchi, M. & Funakoshi, K. 2011. A retrograde tracing study of compensatory corticospinal projections in rats with neonatal hemidecortication. *Dev Neurosci,* 33**,** 539-47.

Yu, H., Cao, B., Feng, M., Zhou, Q., Sun, X., Wu, S., Jin, S., Liu, H. & Lianhong, J. 2010. Combinated transplantation of neural stem cells and collagen type I promote functional recovery after cerebral ischemia in rats. *The Anatomical Record,* 293**,** 911-917.

Z'graggen, W. J., Fouad, K., Raineteau, O., Metz, G. A., Schwab, M. E. & Kartje, G. L. 2000. Compensatory sprouting and impulse rerouting after unilateral pyramidal tract lesion in neonatal rats. *J Neurosci,* 20**,** 6561-9.

Zarembinski, T. I., Tew, W. P. & Atzet, S. K. 2011. The use of a hydrogel matrix as a cellular delivery vehicle in future cell-based therapies: biological and non-biological considerations. *Regenerative Medicine and Tissue Engineering-Cells and Biomaterials.* InTech.

Zewdie, E., Damji, O., Ciechanski, P., Seeger, T., Barlow, K. & Kirton, A. 2017. P034 Lesioned motor cortex neurophysiology in children with perinatal stroke. *Clinical Neurophysiology,* 128**,** e25.

Zhang, L., Li, Y., Zhang, C., Chopp, M., Gosiewska, A. & Hong, K. 2011a. Delayed administration of human umbilical tissue-derived cells improved neurological functional recovery in a rodent model of focal ischemia. *Stroke,* 42**,** 1437-44.

Zhang, L., Schallert, T., Zhang, Z. G., Jiang, Q., Arniego, P., Li, Q., Lu, M. & Chopp, M. 2002. A test for detecting long-term sensorimotor dysfunction in the mouse after focal cerebral ischemia. *Journal of neuroscience methods,* 117**,** 207-214.

Zhang, P., Li, J., Liu, Y., Chen, X., Lu, H., Kang, Q., Li, W. & Gao, M. 2011b. Human embryonic neural stem cell transplantation increases subventricular zone cell proliferation and promotes peri-infarct angiogenesis after focal cerebral ischemia. *Neuropathology,* 31**,** 384-91.

Zhang, R. L., Zhang, Z. G., Zhang, L. & Chopp, M. 2001. Proliferation and differentiation of progenitor cells in the cortex and the subventricular zone in the adult rat after focal cerebral ischemia. *Neuroscience,* 105**,** 33-41.

Zhong, J., Chan, A., Morad, L., Kornblum, H. I., Fan, G. & Carmichael, S. T. 2010. Hydrogel matrix to support stem cell survival after brain transplantation in stroke. *Neurorehabil Neural Repair,* 24**,** 636-44.

Zhu, X., Ai, Z., Hu, X. & Li, T. 2016. Efficient Generation of Corticofugal Projection Neurons from Human Embryonic Stem Cells. *Scientific Reports,* 6**,** 28572.